Development of cardiac patches using medium chain length polyhydroxyalkanoates for cardiac tissue engineering

Dubey, P.

Development of cardiac patches using medium chain length polyhydroxyalkanoates for cardiac tissue engineering

Prachi Dubey

A thesis submitted to the University of Westminster in candidature for the award of the degree of Doctor of Philosophy

January 2017

AUTHOR'S DECLARATION

I declare that the present work was carried out in accordance with the Guidelines and Regulations of the University of Westminster. The work is original except where indicated by special reference in the text.

The submission as a whole or part is not substantially the same as any that I previously or am currently making, whether in published or unpublished form, for a degree, diploma or similar qualification at any university or similar institution.

Until the outcome of the current application to the University of Westminster is known, the work will not be submitted for any such qualification at another university or similar institution. Any views expressed in this work are those of the author and in no way represent those of the University of Westminster.

Signed: Prachi Dubey   Date: January, 2017

ACKNOWLEDGEMENTS

ABSTRACT

Medium chain length-PHAs (MCL-PHAs) have properties that make them exceptional for applications in cardiac tissue engineering. Cardiovascular diseases (CVD) are a major cause of death worldwide. Cardiac patches aim to facilitate the normal functioning of the heart muscle by providing repair and support to the infarcted tissue post myocardial infarction. In this project, two MCL-PHAs, poly(3-hydroxyoctanoate) (P(3HO) homopolymer and poly(3-hydroxynonanoate-co-3-hydroxyheptanoate) P(3HN-co-3HHP) were produced from *Pseudomonas mendocina CH50* using sodium octanoate and sodium nonanoate respectively as the carbon source and the growth profiles were monitored for 48 h. The polymers were characterised to confirm the chemical structure of the polymers. Different types of scaffolds were fabricated like plain films, random fibres and aligned fibres, using different ratios of P(3HO) and P(3HN-co-3HHP) which were 100:0 (P(3HO)), 20:80 (P(3HO):P(3HN-co-3HHP), 50:50 (P(3HO):P(3HN-co-3HHP), 80:20 (P(3HO):P(3HN-co-3HHP) and 0:100 P(3HN-co-3HHP). The mechanical and thermal properties of the films were analysed along with the wettability of all the scaffolds. *In vitro* cytocompatibility studies were also conducted on all the different scaffolds (films, random and aligned fibres) by growing human induced pluripotent stem cell derived cardiomyocytes (hiPSC-CM) on them. The cells were found to be viable and healthy with comparable beating rates and calcium transients to that measured on gelatin which was used as the positive control. The cell alignment quantification on the aligned fibres indicated around 50% of the cells were aligned in one direction. Porous 5 wt% 2D scaffolds and porous 20 wt% 3D structure were fabricated using P(3HO) and different concentrations of the porogen, sucrose and NaCl respectively, to obtain pores in the size range of 250-300 µm which exhibited decreased hydrophobicity compared to the neat scaffolds. *In vitro* cell culture with C2C12 exhibited higher cell proliferation rate on the porous P(3HO) structures as compared to the neat P(3HO) film. The P(3HO) and PANI (polyaniline) blend scaffolds were fabricated to introduce electrical conductivity and they were analysed for their material characteristics. The effect of the addition of PANI on cardiomyocyte proliferation was studied using neonatal ventricular rat myocardial cells (NVRM). A one step method involving the use of poly(ethylene oxide-stat-propylene oxide) with isocyanate end groups (NCO-sP(EO-stat-PO) was used for the incorporation of RGD, YIGSR peptides and the vascular endothelial growth factor (VEGF) on the surface of P(3HO)/P(3HN-co-3HHP) (80:20) electrospun fibres and enhanced cell viability was studied using NVRMs.

TABLE OF CONTENTS

List of Figures

List of Tables

List of Abbreviations

%WA: Water uptake

%WL: Weight loss%

(NCO-sP(EO-stat-PO) : poly(ethylene oxide-stat -propylene oxide) with isocyanate end groups

3HB: R)-3-hydroxybutyric acid

A band: Anisotropic band

ACP: Acyl carrier protein

ADMSC: adipose-derived mesenchymal stem cells

ANGs: Angiopoietins

BSA: Bovine serum albumin

CaKII: Ca^{2+}/calmodulin–dependent kinase II

CDI: Cellular Dynamics International

CHF: Congestive heart failure

CICR: Calcium-induced calcium release

CNT: Carbon nanotubes

CP: Conducting polymers

CVD: Cardiovascular diseases

Dcw: Dry cell weight

DMEM: Dulbecco's modified Eagle medium

DSC: Differential Scanning Calorimetry

EBL: Electron beam lithography

E-C coupling: excitation– contraction coupling

ePTFE: Polytetrafluoroethylene

ESC: Embryonic stem cells

f_1/f_0 : normalised fluorescent amplitude

FIBL: Focused ion beam lithography

FTIR: Fourier Transform Infrared Spectroscopy

GelMA: gelatin methacryloyl

GRGDS: Glycine-arginine-glycine-aspartate-serine

HA: hyaluronic acid

HCN: Hyperpolarization-activated, Cyclic Nucleotide gated channels

hiPSC-CM: Human induced pluripotent stem cell derived cardiomyocytes

HN: P(3HN-co-3HHP)

HO: P(3HO)

HO:HN (20:80) : P(3HO):P(3HN-co-3HHP) (20:80)

HO:HN (50:50): P(3HO):P(3HN-co-3HHP) (50:50)

HO:HN(80:20): P(3HO):P(3HN-co-3HHP) (80:20)

I band: Isotropic band

$I_{Ca,L}$: L-type calcium current

I_f : Hyperpolarisation-activated pacemaker

$I_{K1:}$ Inward rectifier potassium

LV: left ventricular modelling

LVH: Left Ventricular Hypertrophy

MCL-PHAs: Medium-chain-length PHAs

MHC: Myosin heavy chain

MI: Myocardial infarction

Micro CT : Micro computed tomography

MSC: mesenchymal stem cells

MTT: 3-(4,5-Dimethylthiazol-2-yl)-2,5-diphenyltetrazolium bromide)

NCIMB 10541: National Collection of Industrial and Marine Bacteria

NCX: Sodium calcium exchanger

NFAT: Nuclear factor of activated T cells

NMR: Nuclear Magnetic Resonance

NVRM: Neonatal ventricular rat myocytes

P(3HB): Poly(3-hydroxybutyrate)

P(3HB-co-3HHx): Poly(3-hydroxybutyrate-co-3-hydroxyhexanoate)

P(3HB-co-3HV): Poly (3-hydroxybutyrate-co-3-hydroxyvalerate).

P(3HN-co-3HHP): Poly(3-hydroxynonanoate-co-3-hydroxyheptanoate)

P(3HO): Poly(3-hydroxyoctanoate)

P(4HB): Poly-4-hydroxybutyrate

PANI: Polyaniline

PBS: Phosphate buffered saline

PCL: Poly-ε-caprolactone

PDGF: platelet-derived growth factor

PEDOT: Poly(3,4-ethylenedioxythiophene)

PEO: Poly(ethylene oxide)

PET: Polyethylene terephthalate

PGA: Polyglycolic acid

PGS: Poly(glycerol sebacate)

PHA: Polyhyroxyalkanoates

PLGA: Poly-lactic-co-glycolic acid

PLLA: Poly(L-lactic acid)

PP2B: calcium/calmodulin-activated protein phosphatase calcineurin

PPy: Polypyrrole

PT: Polythiophenes

PVA: Poly(vinyl alcohol)

rBM-MSCs : rat bone marrow mesenchymal stem cells

RGD: Arginine-glycine-aspartate

RyR: Ryanodine channels

SA node: Sinusoidal node

SCL-PHAs: Short-chain-length PHAs

SEM: Scanning Electron Microscopy

SF: Silk Fibroin

T_{50} : time to 50% decay

T_{90} : time to 90% decay

TE: Trace element

T_g: Glass transition temperature

TGF-β: Transforming growth factor beta

T_m: Melting temperature

T_p : time to peak

VEGF: Vascular endothelial growth factor

YIGSR: Tyrosine-isoleucine-glycine-serine-arginine

CHAPTER 1

Introduction

1.1. Heart Anatomy

The heart is an important organ of the body responsible for pumping blood to the different organs. Figure 1.1 depicts a typical mammalian heart. As depicted in Figure 1.2, the heart wall is comprised of three layers, the pericardium, endocardium and the myocardium (Kierszenbaum *et al*., 2015). The two layer membrane of the pericardium, called the fibrous pericardium and parietal layer of serous pericardium covers and protects the heart. The epicardium, within the pericardium also called the visceral layer of serous pericardium is the outermost layer of the heart wall is mainly composed of connective tissue. The endocardium is the innermost layer and is comprised of a thin endothelial layer along with connective tissue that line the various chambers of the heart. The myocardium forms the functional layer of the heart. This region is responsible for the various contraction and relaxation cycles of the heart for blood circulation which is initiated by the electrical impulses. This region is formed of cardiomyocytes, extracellular matrix and blood vessels. The cardiomyocytes are terminally differentiated muscular cells which are connected via gap junctions and are responsible for the contractile activity of the heart. The extracellular matrix is mainly composed of Type I and Type III collagen, and provides a framework that couples and aligns adjacent myocytes to optimize and distribute force development in the ventricular walls and avoids deformation (Sutton and Sharpe, 2000).

The human heart is divided into four chambers. The two lower thick walled muscular chambers are the ventricles (right ventricle and left ventricle) and the two upper chambers, are the atria (right atria and left atria). The upper atrial chambers receive the blood coming from all parts of the body and the lower chambers, i.e. ventricles pump blood out of the heart to the rest of the body. The right atrium and ventricle are responsible for pumping blood to and from the pulmonary region and the left atrium and ventricle are responsible for the peripheral circulation. Oxygenation of the blood takes place in the lungs and is pumped to the heart via the pulmonary veins to the left atrium and is then passed to the left ventricle via the bicuspid valve which is then circulated to the different organs through the aorta. The deoxygenated blood from the rest of the body is pumped to the right atrium via the vena cava, which then flows into the right ventricle through the tricuspid valves and is circulated to the lungs via the pulmonary artery. Thus the heart controls the circulation and oxygenation of the blood in conjunction with the lungs (Laizzo *et al.*, 2009).
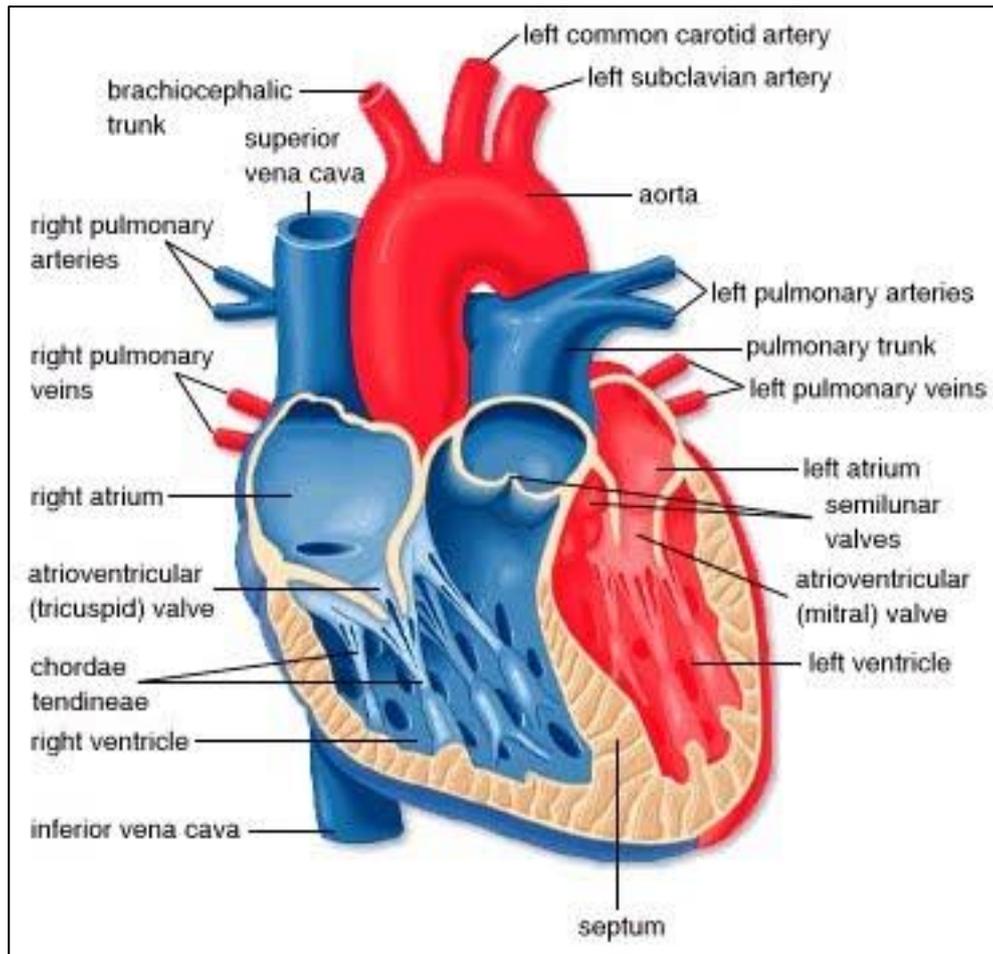
Figure1.1: *The structure of a mammalian heart showing the various chambers, blood vessels. (http://www.rbch.nhs.uk)*
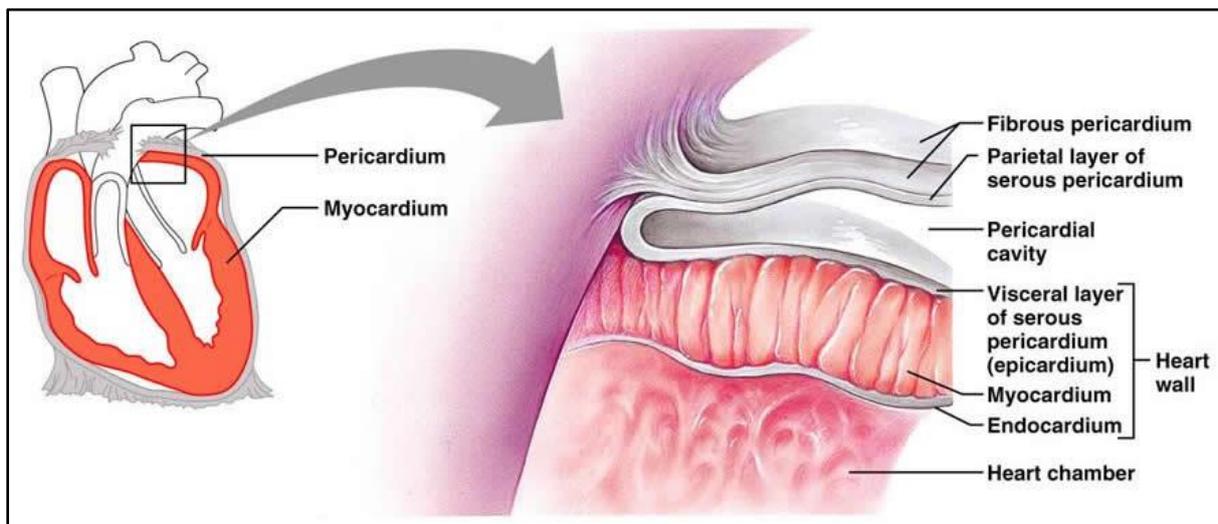
Figure 1.2: *Diagram depicting the different layers of heart wall including pericardium, epicardium, myocardium and endocardium (http://anatomyandphysiologyi.com)*

1.2. Heart Physiology and contraction

The cardiac muscle is a highly organised tissue and converts chemical energy to physical energy, and uses this energy to pump blood to the whole body. The cardiac muscle comprises of muscle fibres that are surrounded by numerous elongated mitochondria as the heart needs continuous energy supply. These fibres branch and are parallel to each other and at the end of each fibres are extensive folds of cell membrane called intercalated discs. They provide strong bond between the fibres and help in cell cohesion. The heart muscle thus acts as a syncytium i.e. a multinucleated mass. Therefore when one of the cells is excited, the action potential spreads from cell to cell through the latticework interconnections fast and the syncytium as a whole contracts. The sarcoplasmic reticulum is an important store of Ca^{2+} and also participates in muscle metabolism (Figure 1.4). The mechanical properties of human myocardial tissue have been measured. This included a Young's modulus value of 0.2- 0.5 MPa, elongation at break 100-300% and tensile strength 3-15 KPa. (Watanabe *et al.*, 2006).

The ultrastructure of a cardiomyocyte comprises of sarcomeres which are the basic contractile units consisting of a dark anisotropic myosin rich central band (A band) and two actin rich light isotropic bands (I band). The region where the A band and I band overlap and provide support to the contractile proteins is called the Z-line (Figure 1.3) (Hanson *et al.,* 1953, Huxley *et al.,* 1953). The cardiomyocytes are connected via specialized structures known as the intercalated discs, which are present at the Z line of the sarcomere. There are gap junctions between the intercalated discs which is essential for the rapid conductance of electrical stimulus in the cardiac muscle. The T system of transverse tubules is located at the Z line, which is continuous with the sarcolemma of the muscle fiber, forms a grid perforated by the individual muscle fibrils. It provides a path for the rapid transmission of the action potential from the cell membrane to all the fibrils in the muscle. The cardiomyocytes are mononucleated cells, ~120 µm in length, and contain centrally located nuclei. These cells remain mononucleated during all stages of human heart development. Collagen I is the main extracellular matrix protein produced by the cardiac fibroblasts which were considered to be the dominant cell type until recently (Bergmann *et al*., 2015). In recent studies endothelial cells were observed to be in abundance in the human adult ventricles representing 45-55% of total cell count (compared to ~30% cardiomyocytes and ~15% fibroblasts) (Pinto *et al.,* 2016; Shadrin *et al*., 2016). Figure 1.5 depicts the interrelation of fibroblasts with the cardiomyocytes in a cardiac tissue.
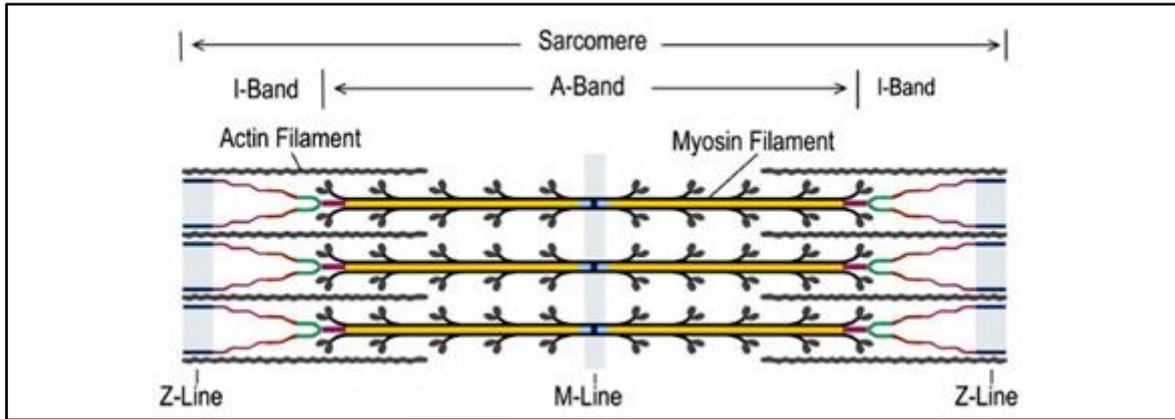
Figure 1.3: Ultrastructure of a sarcomere showing the A band, I band and Z line. (Taken from Castro-Ferreira et al., 2010)
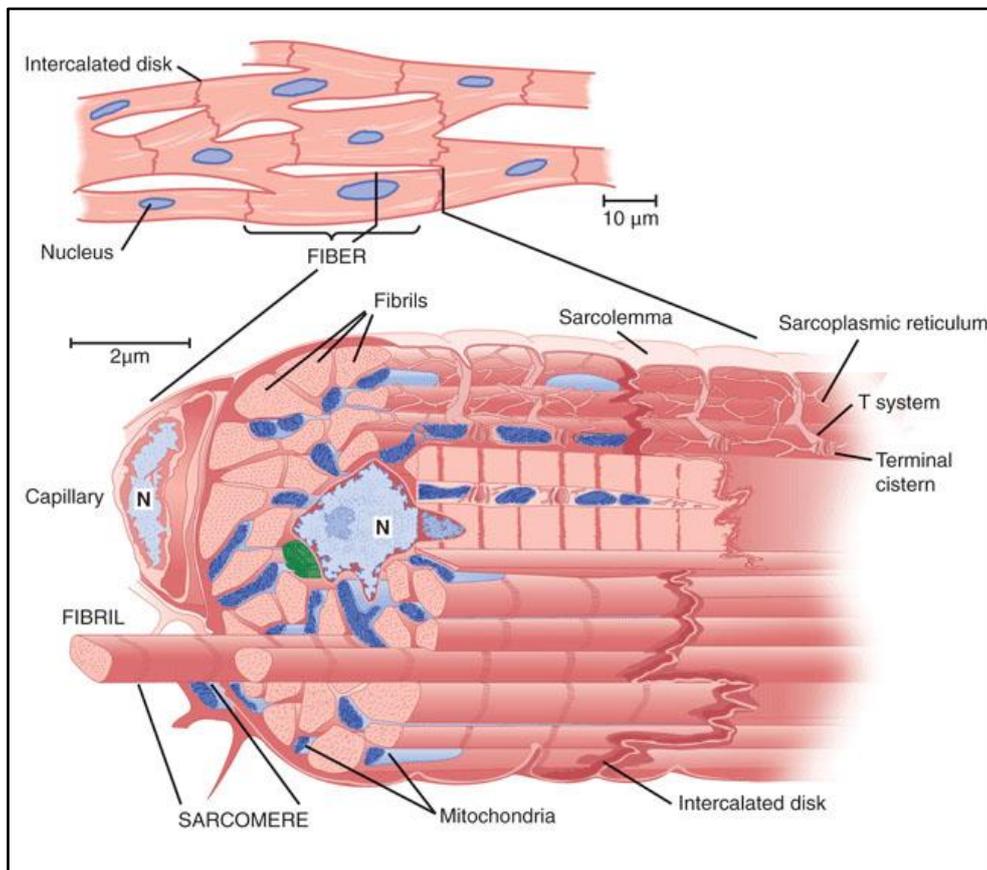
Figure 1.4: Microstructure of a cardiac tissue (Taken from http://www.medicinehack.com)
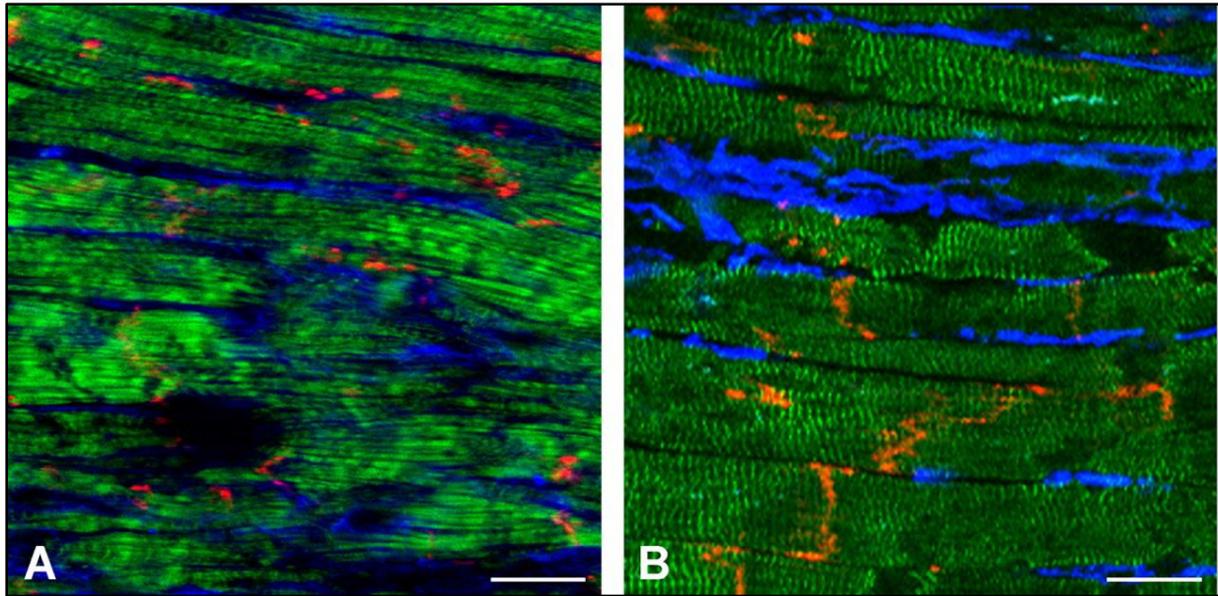
Figure 1.5: *Immunostaining showing the interrelation of fibroblasts and cardiomyocytes in cardiac tissue. (A) Fibroblasts labelled with anti-DDR2 (blue) separate phalloidin-labelled myocytes (green) in mouse ventricular tissue (red label: connexin43). (B) Fibroblasts labelled with anti-vimentin (blue) form layers between anti-myomesin labelled myocytes (green) in sheep ventricular tissue (red: connexin43). Scale bar: 20 µm (Taken from Camelliti et al., 2005)*

The electrical conductance in the heart that causes the cardiac contractions is controlled by a specialised conduction system comprised of the sinoatrial node (SA node), atrioventricular node (AV node) and Purkinje fibres. The SA node is the pacemaker of the heart and generates electrical impulses in the heart. It consists of a cluster of cells that are situated in the upper part of the wall of the right atrium. The Purkinje fibres are located in the inner ventricular walls of the heart and are responsible for the synchronised contractions of the ventricles. The atrioventricular (AV) node is located at the lower back of the interatrial septum and conducts the electrical impulses from the atria to the ventricles. There is a special mechanism and coordination between the SA node, AV node and Purkinje fibres for transmission of the electrical impulse. The initiation of the heartbeat occurs in the SA node which acts as a pacemaker and the impulse is rapidly conducted to the heart through the AV node and the branches of Purkinje fibres (Hall *et al.,* 2016). This process thus synchronises the heart contraction and optimizes the ejection fraction of the heart. The conduction system comprises of excitatory cells having the pacemaker channels (I_f) on the membranes. These channels belong to the HCN (Hyperpolarization-activated, Cyclic Nucleotide gated channels) family channels and are responsible for the generation of an electrical gradient across the cardiac cell membrane. The maintenance of the electrical gradient is due to various ion pumps and

exchange mechanisms, which use ATP to pump ions against their electrochemical gradient, some of which include the Na^+-K^+ ion exchange pump, the Na^+-Ca^{+2} exchanger current and the I_{K1} inwardly rectifying K^+ current. The electrical conductance is a vital process in the body and dysfunctional pacing results in life threatening arrhythmias which can be cured using electronic pacemakers. The dependence of the electronic pacemakers on batteries and electronic control systems indicate potential advantages of biological and bioelectronic approaches to cardiac pacing including genetic engineering and cell implantation (Capulli *et al.*, 2016).

The cardiomyocyte excitation-contraction cycle initiates when the K^+ ions enter through the connexin channels of the cell membrane from the adjacent cardiomyocytes and renders it in a depolarized state. This depolarisation triggers the Na^+ ions to enter the cell through the voltage gated-sodium channels. Rapid depolarization of the membrane inactivates the Na^+ channels and activates the K^+ and Ca^{+2} channels. This triggers the influx of Ca^{+2} ions into the cells which in turn causes the release of Ca^{+2} ions from the sarcoplasmic reticulum through the ryanodine channels (RyR) into the cytoplasm via a process called calcium-induced calcium release (CICR). This raises the Ca^{+2} concentration inside the cell, which binds to the troponin complex and activates the contractile system. The cardiomyocyte cell relaxation occurs when there is a drop in the Ca^{+2} ion concentration due to the activation of the Ca^{+2}-uptake pump from the cytosol to the sarcoplasmic reticulum pump called SERCA and by the exchange of Na^+ with Ca^{+2} ions with the extracellular fluid through the sodium pump called sodium calcium exchanger (NCX) on the cell membrane (Bedada *et al.,* 2016). The intracellular Na^+ equilibrium is maintained by the Na^+/ K^+ pump on the cell membrane (Bedada *et al.,* 2016, Knollmann *et al.*, 2008). This is explained in detail in Figure 1.6. The Ca^{+2} ion transients thus plays a crucial role in the contraction process of the heart. The rapid fluctuations in the intracellular Ca^{+2} concentration regulates the electrical and mechanical activity of the heart and hence control the other major processes in the body such as hormonal responses, physiological interventions and disease conditions (Lee *et al.,* 1987).
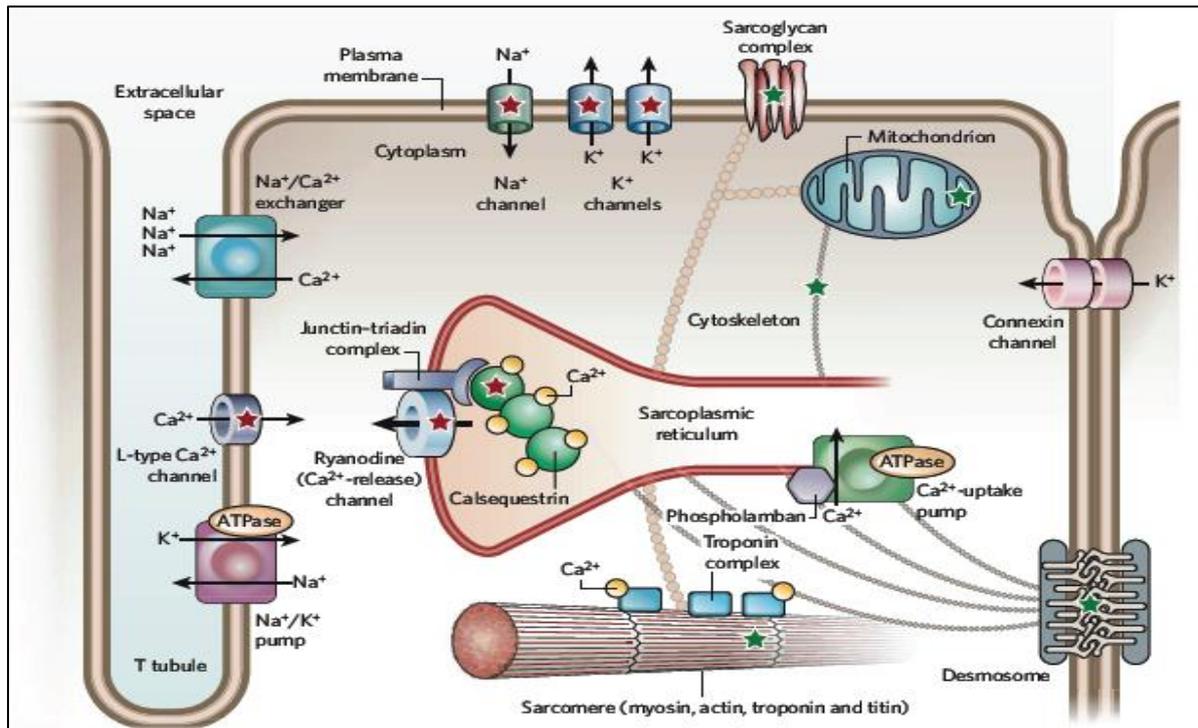
Figure 1.6: *A schematic representation of the mechanism of calcium transients through the tubules of a myocyte during cardiac contraction (Adapted from Knollmann et al., 2008)*

1.3. Cardiovascular Diseases

Cardiovascular diseases (CVD) are one of the major causes of death in the world. Approximately 2.5 million deaths and 1.8 million deaths are reported in the US and UK respectively every year caused by cardiovascular diseases. Major CVDs include coronary heart disease, hypertension, peripheral artery disease, rheumatic heart disease and congenital heart disease and many others are caused due to abnormalities in the cardiac tissue and their blood vessels (Chen *et al.,* 2008, Zimmermann *et al*., 2003, Robinson *et al*., 2005). Myocardial infarction (MI) and congestive heart failure (CHF) account for around 40% of the annual mortality rate in the major developing countries of the world. The necrotic tissue produced due to myocardial infarction causes inflammation, apoptosis of the adjoining tissues and results in decreased pumping efficiency which finally leads to heart failure. There is also evident weakening of the extracellular collagen which causes the thinning of the heart wall and ventricular dilation. These events result in a damaged heart wall and permanent loss of the regenerative property of the heart tissue (Vacanti *et al.,* 2006; Young *et al*. 2004). A cascade of cell signals which trigger ventricular dilation causes the structural and functional changes in the ventricles called ventricular remodelling. This can be divided into two phases: early remodelling and late remodelling. The early remodelling includes physical changes involving

the formation, thinning and elongation of the necrotic scar which causes stress on the diastolic and systolic wall. As a result of the rise in wall stress the tissue enters the late remodelling stage which is characterized by myocyte hypertrophy and production of interstitial collagen with an increased wall mass and chamber enlargement. Heart failure results in the release and activation of various toxic humoral factors, such as catechol amines, angiotensin-converting enzyme and aldosterone. Hence, myocardial infarction may lead to an irregularity in the systolic and diastolic function of the heart and may give rise to arrhythmia and other long term complications. Various clinical and preclinical studies are being conducted to restore the damaged myocardium which include cell delivery to the heart, cardiac tissue engineering and angiogenic therapies (Pons *et al.*, 2009; Liu *et al.*, 2016). Cell suspension injections have been injected into the blood circulation or directly onto the myocardium, but there is a disadvantage of cell loss in the process.

The heart is a dynamic organ and is capable of modulating itself depending on various external and internal stimuli including work load or injury. The development of heart failure is a cascade effect of a sequence of events that may involve multiple causes and may affect several organs. Hemodynamic stress or neuroendocrine signalling associated with myocardial infarction, hypertension, aortic stenosis, and valvular dysfunction initiate a pathologic remodelling response through the activation of intracellular signalling pathways and transcriptional mediators in cardiomyocytes. There are many reasons which are responsible for causing the different cardiac pathologies including heart failure (Weber *et al.*, 1991). Cardiac remodelling involves molecular, cellular changes in the heart which eventually bring about change in size, shape and function of heart after stress stimulation or injury. Cardiac hypertrophy is a common type of cardiac modelling which involves the enlargement of the heart and individual cardiomyocytes as a means to reduce the stress on the ventricular and septal wall when under influence of increased workload or injury. Left Ventricular Hypertrophy (LVH) is the major risk factor associated with the myocardial failure. Severe hypertension can lead to pronounced LV hypertrophy, which in some cases can gradually transform into a picture of dilated cardiomyopathy. Likewise, valvular heart disease, congenital heart disease can all lead to the syndrome of congestive heart failure (CHF) (Kehat *et al.,* 2010). From a morphological point of view in LVH, there is an increased collagen production as compared to its degradations, thus causing an accumulation of myocardial mass and wall. The fibroblasts which contain the messenger RNA for the synthesis of type I and type III collagens, the major fibrillar collagens of the myocardium that constitute the normal structural proteins are responsible for the

production. There is also a noted increase in the cardiomyocyte cell width and/or length which increases the myocardial thickness thus contributing to the cellular hypertrophy. In addition to ventricular and cellular hypertrophy, pathologic hypertrophy involves molecular remodelling re-expression of fetal genes, alterations in the expression of proteins involved in excitation–contraction (E-C) coupling, and changes in the energetic and metabolic state of the myocyte which ultimately lead to cell death caused by necrosis or apoptosis (Francis *et al.*, 2001). There are several pathologic hypertrophic signalling pathways which also assist in the response of heart failure. One such pathway is mediated by the calcium/calmodulin-activated protein phosphatase calcineurin (PP2B). Calcineurin is activated by sustained elevations in intracellular calcium, which facilitates binding to its primary downstream effector, nuclear factor of activated T cells (NFAT). It was observed that the activation of the calcineurin-NFAT pathway in the heart of transgenic mice overexpressing an activated mutant of calcineurin, causes a dramatic increase in heart size (Molkentin *et al.*, 1998). Another molecule that plays an important role in the pathological hypertrophy response in heart is Ca^{2+}/calmodulin–dependent kinase II (CaMKII). CaMKII expression and activity are observed to increase in failing human myocardium and in many animal models of cardiac hypertrophy and heart failure. Transgenic mice that overexpress CaMKII developed significant cardiac dilation with reduced function, cardiomyocyte enlargement, and fibrosis, suggesting that CaMKII is involved in the pathological response to stress (Zhang *et al.,* 2003).

1.4. Cardiac tissue engineering

The main aim of tissue engineering is to combine biomaterials, cells, growth factors, drugs and active molecules to restore the biological function. In recent times, different fields such as cell biology, chemistry, material science, nanotechnology, micro and nanofabrication are being integrated towards the development of a suitable scaffold for tissue engineering.

Cardiac tissue engineering is based on regeneration of cardiac tissue by implanting biocompatible and biodegradable scaffolds cultured with cells that are capable of forming cardiomyocytes in the infarcted region of the heart (Figure 1.7) (Dubey *et al*., 2014). In addition to providing a source of healthy cardiomyocytes, the scaffold further replaces the infarcted myocardium and provides temporary support to the infarct region, thus acting like a cardiac patch (Dubey *et al*., 2014). A complete understanding of the scaffold and cardiomyocyte interaction is essential for myocardial regeneration. The cardiomyocytes are composed of

aligned intracellular cytoskeleton and anisotropic contraction. Hence, simple seeding of the cardiomyocytes on 2-dimensional scaffolds is not sufficient to recover the lost myocardial structure and function. The major challenge in myocardial regeneration is to provide a scaffold which helps in the formation of highly aligned myofibres, which are essential to provide the strength and flexibility, characteristic of the myocardium (Coulombe *et al.*, 2014). To fulfil these requirements, micro and nanofabrication technologies have been employed for the production of scaffolds capable of replacing the infarcted myocardium and recreating the topography of the cardiac microenvironment.
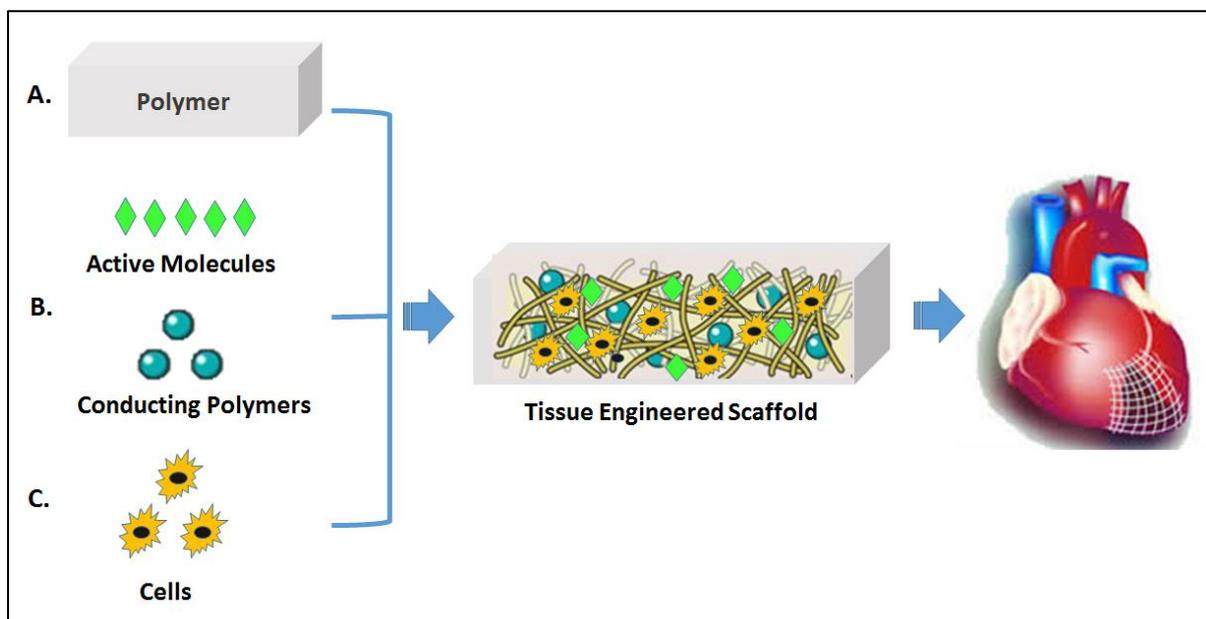
Figure 1.7: *Schematic representation of Cardiac Tissue Engineering*

There are various methods that can be used to achieve the main goals mentioned above to restore myocardial activity. Techniques such as electrospinning, micromoulding, microablation, photolithography, microcontact printing are few of the techniques which when combined or used individually could provide a scaffold which could mimic the functional requirements of the cardiac muscle. Guillemette *et al.*(2010) combined micromoulding and microablation of poly(glycerol sebacate) to form a scaffold which could provide the required alignment and orientation to the seeded mouse myoblast cell line, C2C12 cells. Salick *et al.* (2014) combined the high resolution photolithography and microcontact printing of Matrigel (which consists of 60% laminin, 30% collagen IV, and 8% entactin) and fibronectin to fabricate a two dimensional micropatterned structure of various geometries. The seeded cardiomyocytes showed high degree of alignment, and features with widths between 30 and 80 μm resulted in a dramatic increase in sarcomere alignment relative to the long axis of the pattern. Aligned

conductive fibres were electrospun by Hsiao *et al*. using PLGA and polyaniline and used as a scaffold for cardiomyocyte adhesion and electrical stimulation (Hsiao *et al.*, 2013). Fibrous scaffolds were also fabricated using electrospinning of poly(glycerol sebacate) and gelatin and were tested for stiffness and anisotropy. Cardiomyocytes seeded on the aligned scaffolds were shown to have an anisotropically organised structure along with synchronised beating of the cells (Kharaziha *et al*., 2014).

1.4.1. Biomaterials used in myocardial tissue engineering

The material used for the development of a scaffold is one of the most important aspects to be considered before its fabrication. There are specific criteria which should be considered before selecting a material. Firstly, the material should be biodegradable. Secondly, the *in vivo* degradation rate of the material should match with the rate of tissue regeneration. The material should be able to deliver cells and promote cell attachment, growth and differentiation. Thirdly, the scaffold should be able to provide mechanical support to the cells and surrounding tissues until new extracellular matrix is synthesised by the cells. Fourthly, there should be inherent porosity in the structure which would promote vascularisation and exchange of nutrients and gases within the scaffold. In addition, the material should be processable and amenable to the fabrication of a desired structure to match the defect to be repaired. Finally, the synthesis and fabrication of the material should be relatively easy to commercialise and introduce to the clinic (Chen *et al.,* 2008). Presently, the most widely used surgical solutions for repairing damaged cardiac tissue are the synthetic patch materials Dacron (polyethylene terephthalate, PET) and Gore-Tex (expanded polytetrafluoroethylene or ePTFE), or naturally occurring materials such as autologous, allogeneic, and xenogeneic pericardium. There are several limitations to the use of these materials. Despite of the low immunogenicity of these materials, they provide limited support to the damaged tissue, do not promote cell regeneration and do not remodel with the changes in the native tissue. Hence, various researchers are focused on modulating the material for the provision of more efficient functional support to the heart (Chu *et al*., 2002).

Natural and synthetic non-conducting polymers

Many synthetic and naturally occurring biomaterials pre-seeded with different cell sources have been implanted in the necrotic heart tissue for the regeneration of the myocardium. Natural protein-based matrices (e.g. collagen, alginate and fibrin), synthetic polymers including poly(L-lactic acid) acid (PLLA) and synthetic polymers (e.g. polyglycolic acid (PGA), poly lactic-co-glycolic acid (PLGA) and poly ε-caprolactone (PCL) are the most

common biomaterials used to fabricate 3D scaffolds for tissue engineering applications. In addition, biological biomaterials such as autologous muscle and decellularized biological matrices seeded with adult stem cells or cell sheets have also been used (Leor *et al.,* 2005; Leor and Cohen, 2004).

Natural polymer-based biomaterials have also been widely used in cardiac regeneration through cardiac patches. Natural polymers mainly comprise of polysaccharide and protein based matrices which are made of biomolecules that mimic and interact with the components in the extracellular matrix (ECM). This helps in a better interaction of the scaffold with the internal tissue environment. It promotes cell adhesion and proliferation and hence does not induce any immunogenic response. Unlike the synthetic biodegradable polymers, the natural polymers are degraded into biomolecules which are completely non-toxic to the tissue and get easily resorbed in the body (Contu *et al*., 2009). These characteristics hence offer better cell delivery and enhance the improvement of heart function for which scaffolds are implanted during early stage of MI**.** Collagen, a natural biopolymer, is an abundant protein found in the human body and has been extensively used in cardiac applications (Silva *et al*., 2016). In a study by Kofidis *et al*., neonatal rat cardiomyocytes were seeded *in vivo* onto a commercially available collagen matrix and the cellular engraftment was observed and examined for a period of 2 weeks. The results showed that the embedded cardiomyocytes were evenly distributed in the matrix with good cell attachment and contraction (Kofidis *et al*., 2002). But there were many drawbacks observed due to inadequate geometry, weak mechanical properties, low biocompatibility and high production costs. In another study, 3D porous alginate scaffolds were seeded with foetal cardiac cells and the constructs were implanted *in vivo* onto the injured rat myocardium. This resulted in better heart functioning and attenuation of the left ventricular dilation. However, macrophages and lymphocyte infiltration was observed indicating a mild inflammatory response of the tissue towards the scaffold (Leor *et al*., 2000). In another study, a core/shell poly(glycerol sebacate) (PGS)/fibrinogen fibre scaffold was fabricated by Ravichandran *et al*., where PGS formed the core and provided suitable mechanical support and fibrinogen formed the shell and enhanced the cell-scaffold attachment. Neonatal cardiomyocytes were seeded on to these scaffolds and a significantly higher cell proliferation rate was observed as compared to the fibrinogen scaffold, confirming the structure to be suitable for cardiac applications (Ravichandran *et al*., 2014). Yang *et al*. fabricated a hybrid cardiac patch using silk fibrion (SF) with polysaccharide microparticles of chitosan or hyaluronic acid (HA) and rat bone marrow mesenchymal stem cells (rBM-MSCs) were seeded

on these scaffolds. It was observed that the hybrid scaffolds of SF/chitosan and SF/chitosan-hyaluronic acid demonstrated higher cell growth and higher expression of cardiac genes and proteins when compared to induced rBM-MSCs cultured on SF patches alone. The higher growth rate and expression on the hybrid scaffolds can be explained by the fact that the combination of proteins and polysaccharides mimic the cellular environment and enhance the interaction of the cells with the infarct cardiac tissue (Yang *et al.,* 2009).

Many synthetic materials have also been used for cardiac tissue engineering as they have predictable and reproducible mechanical and physical properties (e.g., tensile strength, elastic modulus, and degradation rate), and they can be manufactured with great precision. However, there are shortcomings with the use of some synthetic polymers where the degradation products induce an inflammatory response in the tissue, or the material is unable to integrate with the host tissue. Among them, aliphatic polyesters (PLA, PGA and PCL) have been widely applied as scaffolding materials for 3D tissue engineering constructs. A few non-degradable synthetic polymers, including polytetrafluoroethylene (PTFE) and polyethylene (PE), have also been investigated for certain tissue engineering approaches, such as congenital heart disease, especially in the context of vascular tissue engineering. A scaffold constructed using PTFE, polylactide mesh, and type I and IV collagen hydrogel resulted in minimal inflammation without aneurysmal dilatation. Successful transplantation and differentiation of mesenchymal progenitor cells was accomplished using this scaffold. No ventricular arrhythmias was observed from the infarcted tissue *in vivo* (Krupnick *et al.,* 2002*)*. Ozawa *et al*. studied a non-biodegradable PTFE, a biodegradable non-woven PGA mesh, a biodegradable poly-L-lactide knitted fabric, and a 50% ε-caprolactone and 50% L-lactide spongy polymer (PCLA). These were used to transplant the right ventricular outflow tract. The unique structure of the PCLA patch with a spongy matrix favoured *in vivo* cell colonization relative to other patches (Ozawa *et al*., 2002). Jin *et al*. also studied poly(lactide-co-ε-caprolactone) scaffolds which served as a replacement of the ECM. These were seeded with bone marrow MSCs, which survived, differentiated into CMs, ultimately regenerating the myocardium and improving cardiac function (Jin *et al*., 2009). In another work, scaffolds were prepared consisting of 50% polylactic acid (PLA) and 50% polyglycolic acid (PGA) and were used as myocardial grafts by seeding bone marrow mesenchymal stem cells on them, *in vivo*, in rats. It was observed that the PLGA constructs could resemble the function and structure of the heart and hence revive the scarred tissue. However, long term analysis was required to determine the capability of the construct to support and revive the myocardial infarcted tissue (Xing *et al*., 2012). Additionally,

due to the cyclic and constant beating of the myocardial tissue, a plastic deformation and failure might occur when thermoplastic polymers such as PGA, PLA, PCL and their copolymers are exposed to long term cyclic strain. This aspect also needs to be studied in depth.

Synthetic Conducting polymers

Conducting polymers (CPs) are polymers with conducting properties similar to that of metals and inorganic semi-conductors. They can be easily synthesised and processed and hence due to their unique properties have various applications in the microelectronics industry, including battery technology, photovoltaic devices, light emitting diodes, and most recently in biomedical applications (Bendrea *et al.,* 2011). The human body is a system which responds to electrical impulses which are generated within many organs in the body. The key tissues which are electrically responsive are brain, heart and skeletal muscles. The introduction of CPs in the biomedical applications brings about a unique coupling of the conducting materials with human tissue, generating a therapeutic-body interface. Most CPs have various advantages for biomedical applications since their electrical, chemical and other inherent properties can be altered to suit requirements of the particular tissue under consideration. These unique characteristics are useful in many biomedical applications, such as biosensors, tissue engineering scaffolds, neural probes and drug-delivery devices (Guimard *et al.,* 2007). Conductivity in CPs arise due to the presence of conjugated double and single bonds between the carbon atoms along the backbone of the polymer structure. Every bond in the backbone contains a localized 'sigma' (σ) bond, which forms a strong chemical bond and every double bond also contains a less strongly localized 'pi' (π) bond (Wise *et al*. 1998; Heeger *et al*. 2000). The introduction of a dopant ion in the structure carries the charge in the form of an electron across the backbone of the polymer, thus rendering it conductive. On application of a potential across the film, a flux of ions enters in or out of the film, dependent on the dopant charge and motility, resulting in the passage of charge through the polymer film. Several CPs used in tissue engineering include polypyrrole (PPy), polyaniline (PANI), polythiophenes (PT) and poly(3,4-ethylenedioxythiophene) (PEDOT) (Ravichandran *et al*., 2010).

Polyaniline (PANI) is an intrinsically conductive polymer which can potentially have extensive applications in cardiac tissue regeneration (Humpolicek. *et al.,* 2012). PANI has been of interest as a suitable conducting polymer because of several reasons. The polymerisation process of PANI is inexpensive (low cost of aniline) and straightforward with a high yield. The conducting form has good chemical stability combined with relatively high levels of electrical

conductivity. PANI also exhibits properties such as biocompatibility, conductivity, high level of cellular adhesion, which are all required for cardiac tissue engineering (Kai *et al.,* 2011). Due to its low solubility in organic solvents it is difficult to process the polymer. However, PANI can be processed by blending with some conventional polymers without altering its structure and retaining the properties of both PANI (electrical conductivity) and the matrix polymer (Narkis *et al.,* 2000). The cells grown on such conductive scaffolds receive electrical signals directly from the substrate rather than from the culture medium (Meng *et al.,* 2005). Polyaniline exists in three different states, reduced leucoemeraldine base, the completely oxidised pernigraniline base and the emeraldine base consisting of alternating oxidized and reduced repeat units in its structure. The emeraldine base form is inherently non-conductive and can be converted into conductive emeraldine salt form by doping using proton donors such as acids (Figure 1.8).
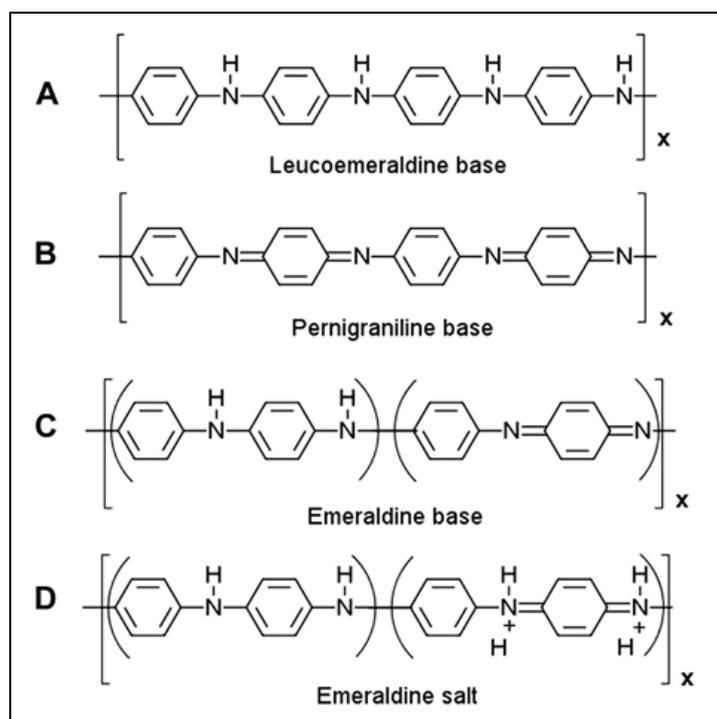
Figure 1.8: *Chemical structures of the different forms of polyaniline (Adapted from Qazi et al., 2014)*

1.4.2. Active molecules involved in cardiac tissue engineering

Growth factors play an important role in the formation of a capillary network near the infarct region. The growth factors thus promote angiogenesis. Vascular Endothelial Growth Factor (VEGF), fibroblast growth factor (FGFs) and Notch signalling control the endothelial cell

activation, behaviour and selection. This promotes the differentiation of perivascular cells and smooth muscle cells to enhance vessel tightness and stabilisation which is regulated by the platelet-derived growth factor (PDGF) and transforming growth factor-beta (TGF-β). Finally, angiopoietins (ANGs) regulate vessel tightness, endothelial cell sprouting and angiogenesis. VEGF, FGFs, Notch, and ANGs also play key roles during coronary vasculature development. Thus these factors are used as novel additives for revascularisation in the infarcted myocardium (Olivey and Svensson, 2010). The VEGF receptors are expressed in the epicardium and sub epicardium, suggesting that this growth factor family is involved in myocardial-epicardial signalling. The introduction of these growth factors in the polymer material allows localised release of the factors along with the control on the rate of release by altering the polymer degradation rates (Patra *et al.,* 2015). These factors can be added to the tissue engineered scaffold in three different ways. The first approach is to mix the growth factor with the polymer solution before the fabrication of the construct. The second approach is by pre encapsulating the growth factor in polymer microspheres and then incorporating these microspheres in the final construct (Richardson *et al.,* 2001). The last and final approach involves surface functionalisation with growth factors immobilised on the scaffold.

An important aspect of the engineered construct involves the interaction of the scaffold with the cells. This is an essential requirement as it can otherwise lead to rejection of the construct, foreign body reactions, thrombosis and embolization (Thull *et al.,* 2001). For this purpose various cell-adhesion mediating proteins or peptide sequences can be either physically adsorbed or covalently attached onto the scaffold surface to have a controlled positive interaction between the cells and the material. There have been many peptides which have proven to be efficient in promoting cell adhesion and proliferation. Some of these are the glycine-arginine-glycine-aspartate-serine peptide (GRGDS), arginine-glycine-aspartate tripeptide (RGD) which promote cell attachment and proliferation and tyrosine-isoleucine-glycine-serine-arginine peptide (YIGSR) which inhibits metastasis and tumour formation (Hersel *et al.,* 2003, Ota *et al*., 2005, Yoon *et al*., 2004; Hirano *et al.*, 1993). Due to the widespread distribution of the RGD peptide, it is used in a range of organisms and due to its high biological effect on cell adhesion, cell behaviour and cell survival, the RGD sequence is one of the most effective active molecules used in tissue engineering (Hersel *et al*., 2003). For example, the effect of neonatal rat cardiac cells were analysed on the RGD-immobilised alginate and unmodified alginate scaffolds. It was observed that cell adherence on the RGD immobilised constructs was higher as compared to the unmodified alginate scaffolds and

enhanced cardiac tissue regeneration was observed on the RGD-immobilised alginate scaffolds, (Shachar *et al.,* 2011). Bagdadi *et al.,* immobilised RGD and VEGF growth factors on P(3HO) films and studied the cell proliferation rates. A significant increase in cell proliferation was observed when VEGF and RGD were incorporated into the P(3HO) cardiac patches. A synergistic effect was observed when both VEGF and RGD were incorporated together, showing a highly significant effect on cell proliferation (Bagdadi *et al*., 2016).

Although several strategies have been used by researchers for the covalent attachment of different peptide motifs onto the polymer scaffold surface, these methods have been typically time consuming and involve several activation and coupling steps. An alternative method which involves combination of the material with a star shaped additive poly(ethylene oxide-stat-propylene oxide) with isocyanate (NCO) end groups, NCO-sP(EO-stat-PO) and the peptide motif can be used to functionalise the outer surface of electrospun fibres in a single step, as described by Grafahrend *et al*., 2010. The peptide is found on the surface of the fibres, attached to the NCO sequences of the NCO-sP(EO-stat-PO), forming urethane bridges (Figure 1.9). The electrospun fibres of PLGA with NCO-sP(EO-stat-PO) and GRGDS were fabricated and seeded with human dermal fibroblasts. The modified fibres showed a much higher cellular adhesion on the GRGDS containing constructs as compared to the fibres with no peptide immobilisation (Grafahrend *et al.,* 2010).
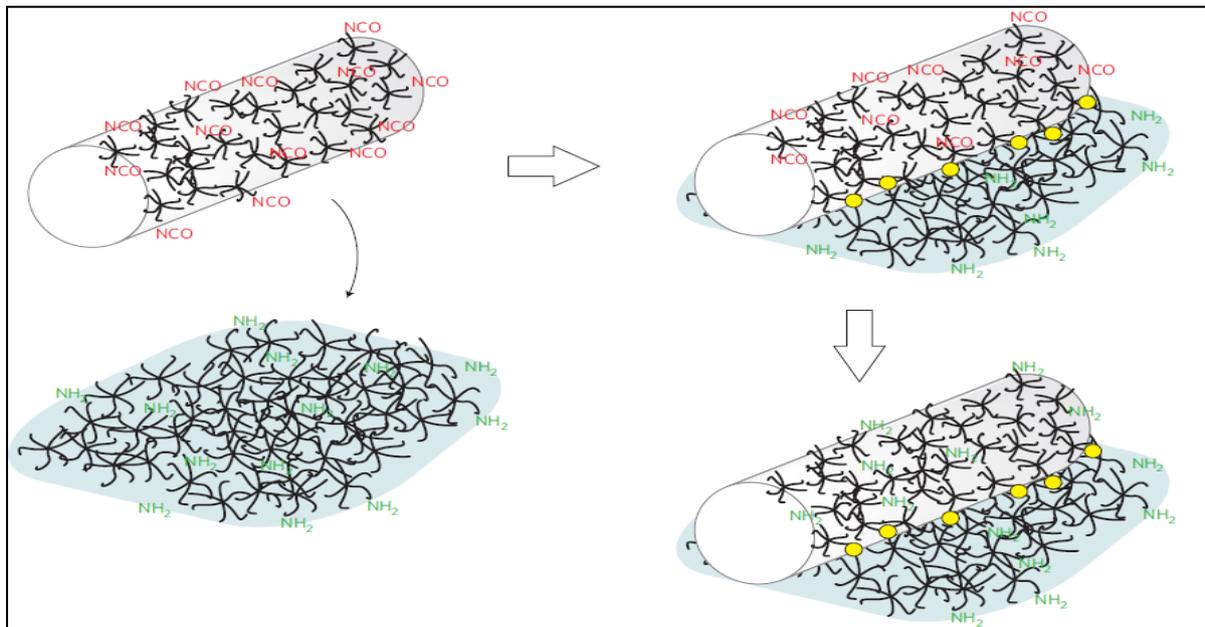
Figure 1.9*: A schematic representation of NCO-sP(EO-stat-PO) on the surface of PLGA/ NCO-sP(EO-stat-PO) fibres. The NCO groups (red) on the fibre surface covalently bind to the amino groups on the peptide, GRGDS (green), resulting in urethane bridges (schematically highlighted as yellow dots). Taken from(Grafahrend et al., 2010).*

1.4.3. Cells used in cardiac tissue engineering

During myocardial infarction the heart tissue gets damaged and the tissue loses its capability to regenerate and hence there is a need to transplant specific stem cells/primary cells with the biomaterial in order to help repair the necrotic area and resume its functioning. The typical type of cell source for a myocardial patch needs to be one that is easy to harvest, has high cell proliferative property, is non-immunogenic and has the ability to mature and differentiate into adult cardiomyoctes. These cells can be categorised as autologous (from the same body), allogenic (different body, same species) and xenogenic (animal origin), depending on the origin of the cells. Out of these, autologous cells do not induce any immunogenic response due to the source being from the same body as the patient, but it is difficult to harvest and culture these cells. Allogenic and xenogenic donor cells can potentially trigger an immunogenic response when transplanted due to their origin but they are comparatively easier to harvest and maintain (Chen *et al.,* 2008). Various cell types including mesenchymal stem cells (MSCs), embryonic stem cells (ESCs), adipose-derived mesenchymal stem cells (ADMSCs) have been clinically tried and delivered to the cardiac injury site to restore tissue functionality (Wang *et al.,* 2010). There are a variety of cell models which are under investigation. Depending on the stage of differentiation of the cells they can be divided into three different cell types, (1) somatic muscle cells, such as foetal or neonatal cardiomyocytes, (2) myocardium-generating cells, such as embryonic stem cells which include bone marrow-derived mesenchymal stem cells, adipose stem cells and induced pluripotent stem cells; and (3) angiogenesis-stimulating cells, including fibroblasts and endothelial progenitor cells.

The two major stem cell types used for myocardial tissue engineering are the embryonic stem cells (ESC) which are differentiated into cardiaomyocytes and human induced pluripotent stem cell derived cardiomyocytes (hiPSC-CMs). Recently human induced pluripotent stem cell derived cardiomyocytes (hiPSC-CMs) have gained a lot of attention and are being considered as one of the main potential cell source. Human induced pluripotent stem cells (hiPSC)s can be generated from somatic cells such as fibroblasts via delivery and ectopic expression of the Yamanaka factors (Oct4, Sox2, Klf4, and c-Myc), also known as OKSM. Recent studies have also demonstrated the successful derivation of iPSCs from other sources, including amniotic fluid, human blood, and keratinocytes. This is ground breaking research which has given rise to a completely new area of stem cell research and avoids many of the ethical problems associated with human embryonic stem cells (hESC)s. Once pluripotency is established,

hiPSCs can be differentiated using various methods into CMs and are termed as human induced pluripotent stem cell derived cardiomyocytes (hiPSC-CM)s (Mordwinkin *et al*., 2013). Recent studies showed that hiPSCs can differentiate into cardiomyocytes with cardiomyocyte-like molecular, structural, and functional properties (Zwi *et al.,* 2009). Nelson *et al*. observed that intramyocardial delivery of iPSCs into infarcted murine hearts restored contractile performance and ventricular wall thickness. This was a result of the iPSCs differentiating into cardiac, smooth muscle and endothelial cells (Nelson *et al.,* 2009). Another advantage of hiPSC-CMs are their ready availability from different companies, Cellular Dynamics International (CDI), Axiogenesis and Pluriomics. HiPSC-CMs express most, if not all, structural and regulatory elements present in a human cardiomyocyte, display a cross-striated ultrastructure, contract spontaneously and show basic functional properties of the human heart, including typical responses to drugs. However, some characteristics of the hiPSC-CMs differ from the adult cardiomyoctes such as, hiPSC-CMs beat spontaneously, show a low degree of ultrastructure organisation and have no T-tubules. Hence extensive research is currently being pursued in order to validate and improve the maturation and function of these cells (Eder *et al.,* 2016).

1.5. Technologies used for scaffold fabrication of cardiac patches

There are different ways to fabricate biocompatible structural materials which fulfil the requirements of restoring the damaged tissue in cardiac tissue engineering applications. The main aim of these scaffolds is to bio-mimic, restore and revive the necrotic tissue and to resynthesize the original tissue (Langer *et al*., 1993). There are several microfabrication techniques such as micromachining, photolithography, metal deposition, electrospinning, wet and dry etching, thin-film growth, and 3D printing which have been used to create scaffolds with micro and nano scale features using a range of different materials (Limongi *et al*., 2016).

1.5.1. Solvent casting technology

The solvent casting technology is one of the most common and easily achievable techniques that is widely used for the fabrication of porous and non-porous 2D scaffolds. This technique is simple and can be used to incorporate porous structures with controlled pore sizes (Figure 1.10). It involves the use of a water soluble porogen which is added to the polymer solution in an organic solvent, followed by casting of the scaffold in a mould. The porogen is finally removed using water (Siemann *et. al*., 2005; Ikada *et al*., 2011).This is a simple and cheap process and can be used for a range of different polymers. The major advantage of the solvent

cast method is that the scaffold with a specific and controlled pore size can be fabricated while the disadvantage lies in the uncertainty of the interconnectivity of the pores.
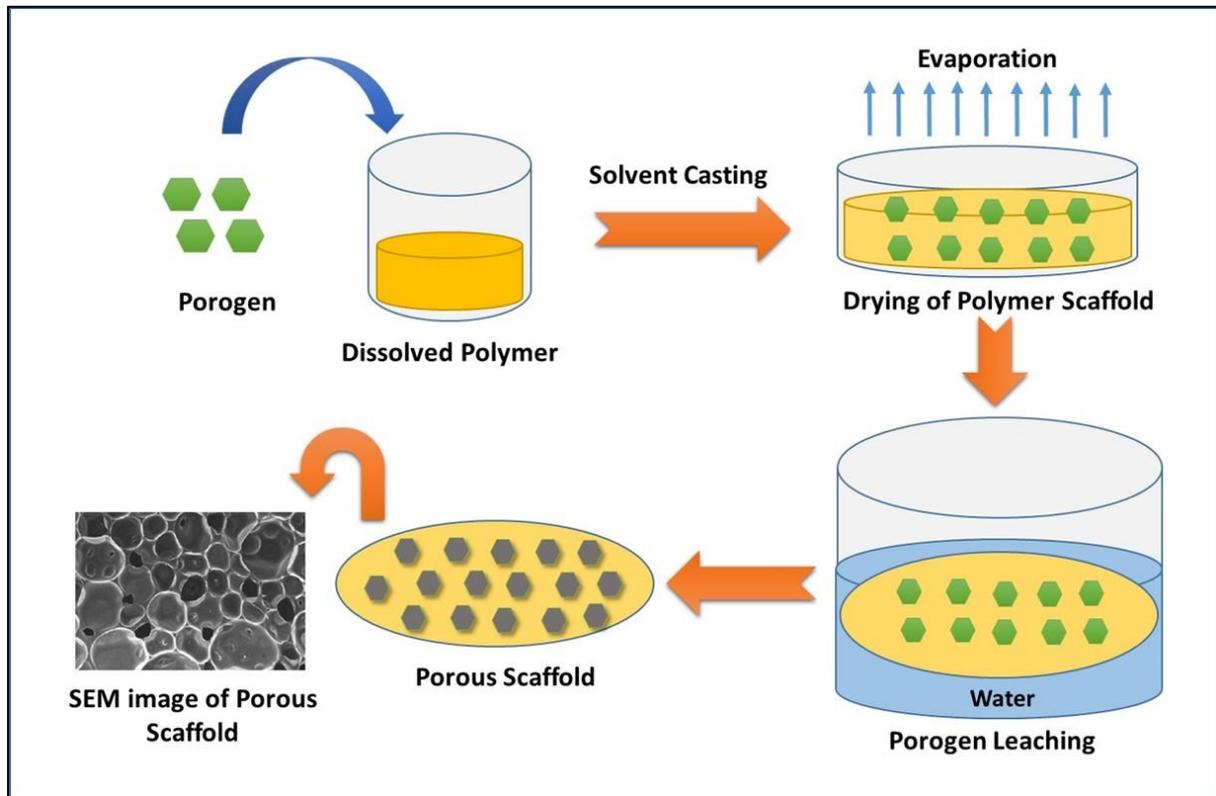
Figure 1.10: *A schematic representation of the solvent casting technology used for the production of porous 2D polymer scaffolds*

1.5.2. Electrospinning

Electrospinning is a versatile technique which produces ultrathin fibres ranging from microns to nanometers in diameter which are either nonwoven or aligned and provide the required nanotopography found in the cardiac ECM (Figure1.11). These fibres have high porosity and high interconnectivity which allow efficient exchange of nutrients and gases within the structure. In addition, the fibre alignment and incorporation of the conducting polymers in the electrospun fibres can be easily modulated to mimic the cardiac tissue microenvironment (Orlova *et al.,* 2011). Electrospinning helps to fabricate polymeric scaffolds with specific mechanical and biological properties similar to native ectracellular matrix (ECM) in order to modulate cellular behaviour (Pham *et al.,* 2006). These are some of the advantages of this technique. Major disadvantage of this technique is that there could be fibre breakage if the speed of the rotating drum collector is too high. The common problem with the electrospun scaffolds is the smaller pore size which inhibits tissue ingrowth due to lack of cellular

21

infiltration and cell accommodation in the pores. Various electrospinning techniques and post electrospinning modifications are taking place to overcome this limitation while maintaining the fibre morphology and pore interconnectivity (Rnjak-Kovacina *et al*., 2011).

In this technique, a polymer solution is loaded and pumped through a syringe fitted with a nozzle connected to a voltage source. The suspended droplet created by either gravity or mechanical pumping at the tip of the nozzle, is electrically charged creating a repulsion force against the mechanical force provided by the pump. As the intensity of the electric field is increased, the surface of the droplet elongates to form a conical shape called the Taylor cone (Taylor 1969). When the electric charges overcome the surface tension of the droplet, a charged jet is ejected from the tip of the Taylor cone. As the jet is ejected from the droplet and travels through air, the solvent evaporates and fibres are deposited on the collector. There are various factors which affect the size and shape of the electrospun fibres. The properties of the polymer solution affecting the fibre parameter are its viscosity, conductivity and surface tension. On the other hand, the controlled variables include electric potential, the distance between the nozzle tip and the collector and speed of the rotating collector (for aligned fibres). Finally, the environmental parameters including temperature, humidity and air velocity also have significant effect on the fabricated fibres. Different non-woven, nano- or micro-scaled, porous, aligned or random fibres can be fabricated with different synthetic or natural materials, by adjusting one or more of the above parameters (Smith *et al.,* 2009).

Electrospinning has been extensively used on various synthetic and natural materials including PLGA, PLLA, poly(vinyl alcohol) (PVA), poly(ethylene oxide) (PEO), poly(caprolactone) (PCL), PHAs, collagen, gelatin, dextran, silk protein and fibrinogen and various conductive polymers and blends (Pham *et al.*, 2006). The composite mesh of polyaniline/poly(lactic-co-glycolic acid) (PLGA) was electro-spun and it offered to mimic the anisotropic environment of the cardiac tissue and provided a better electrical conductance across the scaffold (Hsiao *et al.*, 2013). In a study conducted on P(3HO) electro-spun fibres of different diameters, the highest cell proliferation rate of 196.8±16.0 was observed on the C2C12 cells grown on the 750 nm diameter P(3HO) fibres. This indicated high biocompatibility of the P(3HO) fibres with C2C12 cells (Bagdadi *et al.,* 2016)
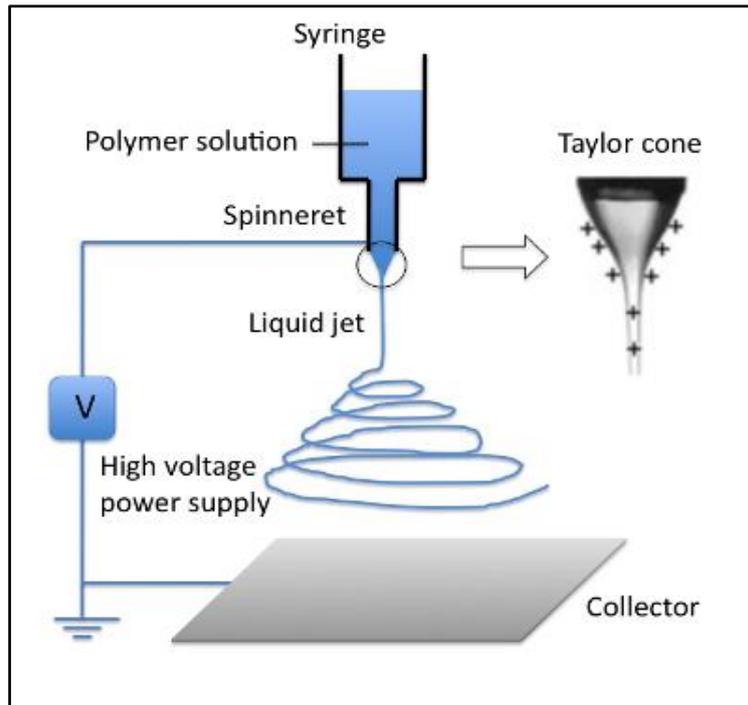
Figure 1.11*: A schematic diagram of the electrospinning setup. (Taken from Athira et al., 2014)*

1.5.3. 3D Printing

3D-Bioprinting is one of the promising new techniques that is used in the fabrication of 3D constructs through controlled deposition of biomaterials and cells. Most of the experiments conducted involve the use of sacrificial bioprinting where the bioink is printed inside the hydrogel and after drying, the ink is washed off leaving a hollow vessel mimicking structure. The bioprinted scaffold is then seeded with different cells to impart a biological function to the scaffold (Kolesky *et al.*, 2014, ; Lee *et al.*, 2014). This is a complex process and hence the size, morphology and functionality of these scaffolds can be limited. However, due to some recent advancements, this process has become more achievable and convenient and methods that are easy to bioprint desirable scaffolds using a single method have been successfully developed (Jia *et al.*, 2016).

Hot pressing or compression moulding can also be achieved by using a hot press, where the biomaterial can be moulded depending on the structural parameters required for the scaffold. The final structure can be controlled by changing the temperature of the press and the force applied on the biomaterial by the press.

1.5.4. Electron beam (EBL) and Focused ion beam (FIBL) Lithography

EBL and FIBL are the latest direct-write technologies that are able to create nanometric patterning on the biomaterial by the use of focused accelerated particle beams to scan the surface of the scaffold. This technology is used to make grooves ranging from 20-1000 nm widths. EBL has been used to fabricate nanopillared moulds which were then used to emboss PCL surfaces with nanometric topology.

FIBL uses electrostatic and magnetic fields to focus on a low energy ion beam to create a topography of around 50 nm. FIBL is generally used in hard biomaterials such as silicon but it has also been used in biomedical tasks involving tuning the morphology and modulus of hydrogels. Unique nanoscale pore parameters were achieved by this technique which could be changed by the angle of the incident ion beam (Limongi *et al*., 2016).

1.5.5. Plasma etching

Plasma etching is a surface treatment technique, which helps to modify the surface properties without changing the bulk properties of different biomaterials. This is useful in enhancing the biocompatibility of the scaffold with the cells. It also helps in areas required to monitor wear, friction and roughness of the scaffold and thus changes the topography of the interacting surface of the biomaterial with the cells (Chu *et al*., 2002). Nano textured biocompatible PCL films were fabricated on silicon wafer by using plasma etching by Cesca *et al.*(2014). These scaffolds could then be peeled off the silicon wafer and used for cell culture. Due to increased roughness these PCL scaffolds provided high cellular adhesion.

1.6. Polyhydroxyalkanoates (PHAs)

Polyhyroxyalkanoates (PHAs) are natural polymers which have a great potential to be used in cardiac tissue engineering. They are well known biopolyesters of 3-, 4-, 5- and 6-hydroxyalkanoic acids (Figure 1.12 (A) and (B)). They are synthesized by a wide range of bacteria such as *Bacillus cereus, Pseudomonas putida, Pseudomonas oleovorans* as an intracellular energy source, under nutrient limiting conditions. An essential nutrient such as nitrogen, phosphorus, sulphur or magnesium is provided in limiting conditions along with excess of carbon. These elements play a vital role and are constituents of essential cellular components such as amino acids (nitrogen), nucleotides (phosphorous), enzymes, coenzymes or act as a cofactors for vital enzymes (magnesium). These limiting conditions hinder cell

growth and division and switch on the biosynthetic pathway of the PHAs (Valappil *et al*., 2007, 2008; Hyakutake *et al*., 2011). Hence, bacteria including *Cuprivadus necator, Alcaligenes latus, Pseudomonas mendocina* accumulate these polyesters as insoluble inclusions in the cytoplasm that provide an intracellular carbon and energy source under limiting nutrient conditions. These water insoluble polymers are biodegradable, thermoplastic, exhibit high molecular weight. The molecular weight of the PHAs range from 2×10^5 to 3×10^6 Daltons depending on the microorganism used and the growth conditions provided during polymer production (Byrom *et al.,* 1994). They are being considered for several applications in the packaging industry, medicine, pharmacy, agriculture and food industry, or as raw materials for the synthesis of enantiomerically pure chemicals and the production of paints (Halami *et al.*, 2008). In addition, these polymers are highly biocompatible and hence have several medical applications.

The physical properties of PHAs are greatly influenced by the length of the side chain. Hence, PHAs can be divided into two main classes: Short-chain-length PHAs (SCL-PHAs), that have monomers consisting of 3-5 carbons, are partially crystalline, thermoplastic in nature. They generally lack toughness and hence are brittle polymers and have high melting points. Medium-chain-length PHAs (MCL-PHAs) have monomers consisting of 6–14 carbons and these polymers are elastomeric in nature with low crystallinity, low tensile strength, low melting point and high elongation at break (Nomura *et al.,* 2007). Both SCL-PHAs and MCL-PHAs have been extensively explored in various medical and industrial applications (Shishatskaya *et al.,* 2002; Witholt *et al.,* 1999). SCL-PHAs are produced by numerous bacteria such as *Cuprivadus necator, Alcaligenes latus, Bacillus megaterium* and *Bacillus cereus* while MCL-PHAs are synthesized by bacteria such as *Pseudomonas putida, Pseudomonas mendocina* and *Pseudomonas oleovorans*. Examples of SCL-PHAs include poly(3-hydroxybutyrate) (P(3HB)), poly-4-hydroxybutyrate (P(4HB)) and poly(3-hydroxybutyrate-co-3-hydroxyvalerate) (P(3HB-co-3HV)). Examples of MCL-PHAs include polyhydroxyundecenoate (PHU) and Poly(3-hydroxyoctanoate) (P(3HO)) (Dufresne *et al.,* 2000; Rai *et al.*, 2011). The P(3HO) described in Rai *et al.*, (2011) is completely different from the P(3HO) described in Dufresne *et al* (2000). The former is a unique homopolymer produced using *P. mendocina*, whereas the other P(3HO)s are copolymers containing monomers 3-hydroxyhexanoate and 3-hydroxydecanoate with the dominant monomer being 3-hydroxyoctanoate (86%).
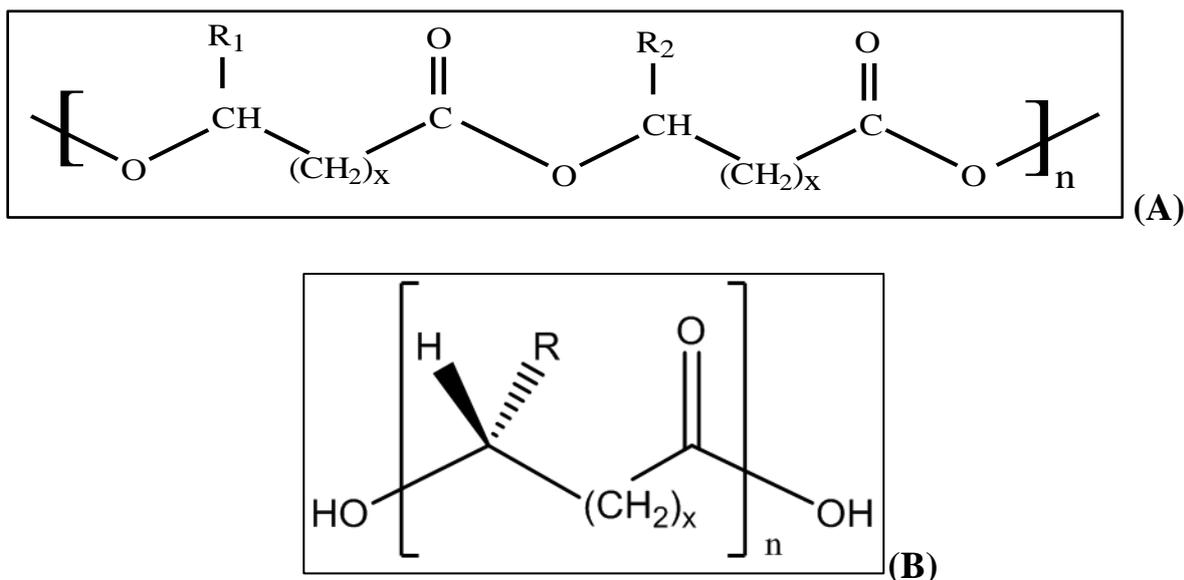
Figure 1.12: *(A) The general structure of polyhydroxyalkanoates (x = 1, 2, 3; n = 100-30000; R₁, R₂ = alkyl groups, C1-C13 units) (B) The chiral general structure of polyhydroxyalkanoates exhibiting the R- stereo-regular configuration.*

PHAs have many advantages over the synthetic polymers in the context of biomedical applications. These are natural polymers, and hence do not have remnants of chemical catalysts, leading to lower cytotoxicity. PHAs degrade by surface erosion rather than bulk erosion as observed for PLA and PLGA, hence leading to longer term structural stability of the scaffolds. The degradation products of PHAs (hydroxyacids) have lower acidity as compared to the degradation products of PLA (lactic acid) which leads to low immunogenicity. The length of the side chain and its functional group also has a direct effect on the polymer's physical properties such as flexibility, crystallinity, melting point and glass transition temperature (Volvoa *et al.*, 2004). Hence, another very important advantage of PHAs is that their material properties and degradation rates can be controlled and changed by varying the polymer production conditions including the bacterial strain, carbon source, media composition and fermentation conditions (Rai *et al.,* 2011). In particular, medium chain length PHAs (MCL-PHAs) exhibit a larger structural diversity including C6-C14 containing monomer units and provide a huge range of polymer types. Hence, their mechanical properties can be modified as per the requirement of specific application (Philip *et al.*, 2007). These polymers being elastomeric in nature can be used in soft tissue engineering, cardiovascular applications (cardiac patch, valve), cartilage tissue engineering and wound healing (Kim *et al.*, 2007). In

spite of having a wide range of applications, due to the lack of availability of these polymers in large quantities, there are limited studies on MCL-PHAs (Rai *et al.,* 2011).

1.6.1. Biosynthesis of PHAs

Over 300 different species of Gram positive and Gram negative bacteria have been reported to produce different types of PHAs. The bacteria store the polymer in the form of an energy reserve in the cytoplasm. Based on the conditions required for production, bacteria can be categorised into two groups. The first group requires the limitation of an essential nutrient such as phosphorous, nitrogen, sulphur or magnesium with an excess of carbon during its production process such as *Pseudomonas mendocina*, *Protomonas extorquens* and *Protomonas oleovorans* (Chen *et al.,* 2010). The second group of bacteria do not require any nutrient limiting condition and generally include mutants (*Azotobacter vinelandii*) or recombinant strains of *E.coli.* There are various wild type and recombinant species of bacteria that are used for the production of PHAs. Some of them include *Cupriavidus necator, Azotobacter sp.*, *Bacillus sp.*, *Pseudomonas sp., Burkholderia sp.*, *Halomonas sp.*, *Haloferax sp., Aeromonas sp.* and recombinant *E.coli* to name a few (Akaraonye *et al.,* 2011; De Smet *et al.,* 1983; Haywood *et al.,* 1989; Rai *et al.*, 2011; Povolo *et al.,* 2010). In a study conducted with *B. subtilis 1604-pha*C1 recombinant strain showed a higher PHA accumulation of 32% dcw when compared to *B. subtilis* wild type and *B. subtilis* containing the vector with no insert, which showed a PHA accumulation of 3% dcw (Bagdadi *et al.*, 2013). A wide range of carbon sources have been used for the production of PHAs including cheap carbon sources for economical production. Some of them include sodium octanoate, glucose, glycerol, fats; oils; industrial byproducts such as sugarcane molasses; agricultural wastes such as soyabean/sunflower cake, corn steep liquor; some household wastes including waste potato starch, waste cooking oil, sesame oil; waste water and fatty acids. Specialized carbon sources like 4-hydroxybutyric acid, γ-butyrolactone and 1,4-butanediol give rise to 4HB monomers along with 3HB monomer.

PHA biosynthesis can take place via three different pathways (Figure 1.12). The biosynthetic pathway for the production of PHAs involves the combination of enzymes present in the cytoplasm of the bacterial cell. Pathway I is observed in *Cupriavidus necator* and it best explains PHA biosynthesis using sugar as the carbon source. In this pathway, condensation of two acetyl CoA molecules leads to the generation of 3HB monomers which further forms acetoacetyl-CoA with the help of the enzyme β-ketothiolase. The acetoacetyl-CoA reductase then acts on the acetoacetyl-CoA molecule to form 3-hydroxybutyryl-CoA. In the end,

esterification of 3-hydroxybutyryl-CoA into poly(3-hydroxybutyrate) (P(3HB)) takes place, which is the key polymerisation reaction catalysed by the PHA synthase. This pathway can also be utilised for the synthesis of P(3HB-co-3HV). Pathway II and III are involved in fatty acid oxidation and biosynthesis respectively which eventually lead to the formation of the corresponding hydroxyalkanoate monomer depending on the carbon source used. Pathways II and III are mainly found in bacteria producing medium chain length PHAs (mcl-PHAs). Pathway II is the fatty acid β-oxidation pathway which involves the production of the hydroxyacyl substrate related to the fatty acids used as the carbon source. This substrate can be polymerised by the PHA synthases of *Pseudomonads* belonging to the ribosomal RNA-homology group I and are mainly found in organisms such as *Pseudomonas aeruginosa* (Kabilan *et al.*, 2012). As shown in the Figure 1.13, the PHA synthase catalyses the polymerization of the hydroxyacyl substrates into PHA. Pathway III is the fatty acid *de novo* synthetic pathway which is used by the organisms when grown on sugars such as glucose as the carbon source. The (R)-3-hydroxyacyl intermediates from the fatty acid biosynthetic pathway are converted from the acyl carrier protein (ACP) form to the CoA form by the enzyme acyl-ACP-CoA transacylase (encoded by *phaG*). Therefore, this enzyme is the key link between the fatty acid biosynthetic pathway and PHA biosynthesis (Rehm *et al.*, 2003).
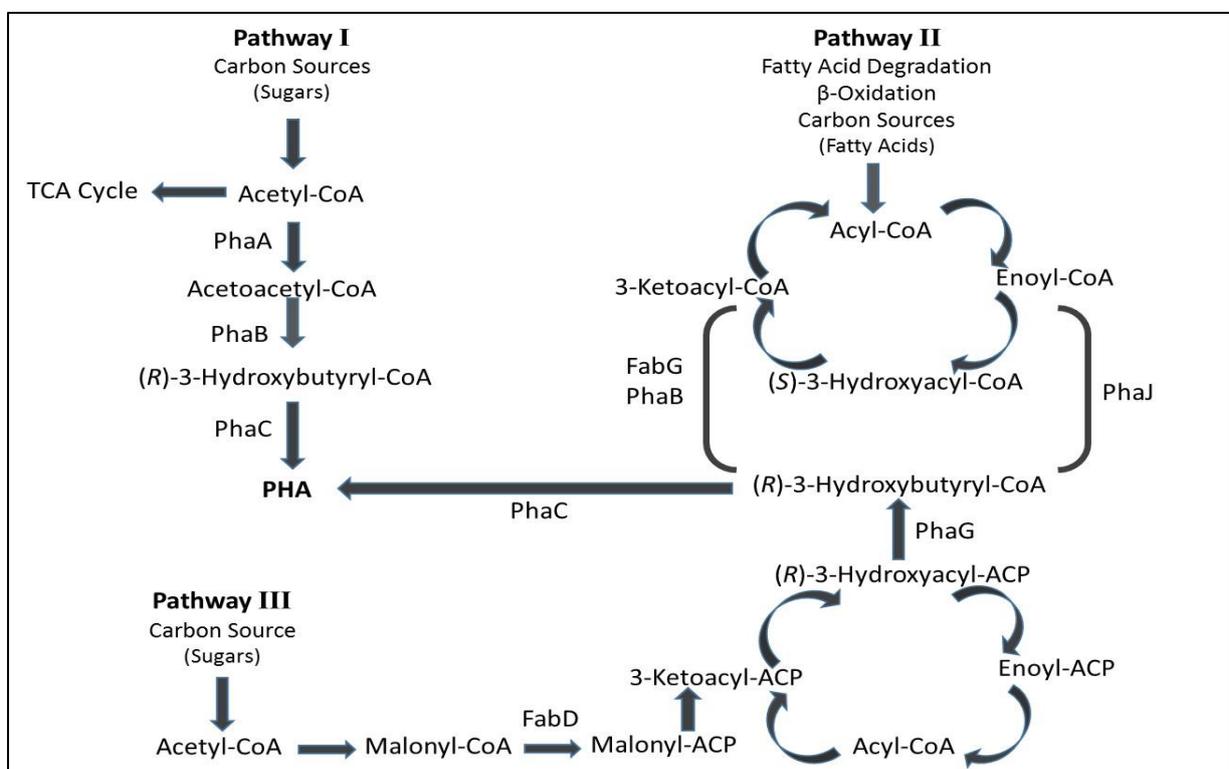
Figure 1.13: *The three main PHA biosynthetic pathways used by different organisms for the production of PHAs.*

PHA synthases are the key enzymes of PHA biosynthesis. They catalyse the conversion of 3-hydroxyacyl-CoA substrates to PHAs, accompanying the release of CoA. PHA synthases are classified into 4 classes on the basis of their activities toward substrates with different carbon chain lengths and their subunit compositions (Table 1.1). Class I and II have a similar type of subunit, PhaC, whereas the Class III enzyme comprises of the PhaEC complex including subunits PhaC and PhaE and Class IV enzymes have a PhaRC complex comprising of PhaR (molecular mass of approx. 22 kDa) and PhaC. Class I, III and IV synthases polymerise short chain length (SCL) monomers (C_3-C_5), whereas Class II synthases polymerise medium chain length (MCL) monomers (C_6-C_{14}). The PHA synthases of *Ralstonia eutropha, Pseudomonas aeruginosa* and *Allochromatium vinosum* and *Bacillus megaterium* represent Classes I, II, III, and IV respectively.

Table 1.1: *Classes of PHA synthases showing different subunits.*

Class	Subunits	Size	Substrate	Species
I	PhaC	(60-73 KDa)	$3HA_{SCL}$	*C. necator*
II	PhaC	(60-65 KDa)	$3HA_{MCL}$	*P. aeruginosa*
III	PhaC PhaE	(40 KDa)/(40KDa)	$3HA_{SCL}$	*A. caviae*
IV	PhaC PhaR	(40 KDa)/(22KDa)	$3HA_{SCL}$	*B. cereus SPV*

1.6.2. Biodegradability / Bioresorbability of Polyhydroxyalkanoates

Biodegradability or Bioresorbability is an important property of PHAs which makes them suitable for their use in a range of medical applications. Within the biological tissue PHAs are subject to degradation by the action of lipases, esterases and other hydrolytic enzymes (Wu *et al*., 2009; Williams *et al.,* 1999). Wu *et al*. studied *in vivo* degradation of P(3HB-co-4HB) and observed that the polymer degraded into its monomeric units, i.e. 3- and 4- hydroxybutyric acid (Wu *et al*., 2009). There are many factors which affect the biodegradability of PHAs including stereochemistry of the polymeric units, molecular weight, monomeric composition, chemical structure (which affects the interaction of the functional groups with the enzymes and the wettability), presence of an ordered structure in the polymer like crystallinity, orientation,

morphological properties and exposure of the polymer surface to the degrading enzymes. The effect of alkyl side chain length on the biodegradability of PHAs was studied by Quinteros *et al*., (1999), showing an increment in the degradation rates with the change in proportion of the side chain repeating units in the PHA. They also observed that polymers with high crystallinity had lower degradation rates. As polymer with low melting temperatures, will melt sooner and so have low crystallinity. So the higher melting temperature (T_m) of the crystalline phase of the polymer, there is a decrease in the degradation rate of the polymer. Thus, the MCL-PHAs with low crystallinity and low melting temperature are more prone to degradation as compared to the SCL-PHAs with higher crystallinity and Tm (Wang *et al., 2005*).

In the context of tissue engineering, it is important that the rate of degradation of the polymer should match the rate of regeneration of the tissue. Various *in vitro* and *in vivo* degradation studies have been conducted with PHA scaffolds. One of the studies was conducted *in vivo* where P(3HO-co-3HHx) subcutaneous implants in mice showed a decrease in M_w to 65,000 from an initial implantation weight of 137,000 in 40 weeks (Williams *et al.,* 1999). Further to this experiment, Wang *et al.,* 2005 blended P(3HO-co-3HHx) with gelatin and found a higher degradation rate of the scaffold as compared to the neat P(3HO-co-3HHx). After 2 months, there was about 15% weight loss in P(3HO-co-3HHx) blending with 30% gelatin. Blending with gelatin increased the hydrophilicity, porosity and decreased the crystallinity of the scaffold. Hence, the hydrolytic enzymes were able to access a higher surface area of the polymer leading to a faster degradation rate. The *in vitro* degradation behaviour was also studied on P(3HO) homopolymer films by Rai *et al.*, 2011. They showed 15% degradation after 3 months in DMEM media. This could be explained due to the semi crystalline nature of the material. In a study carried out by Tepha Inc., monofilament fibres were prepared by melt spinning of Poly-4-hydroxybutyrate (P(4HB) "PHA4400". *In vitro* and *in vivo* degradation studies were studied in Dulbecco's phosphate buffered saline and rabbit respectively. It was observed after 26 weeks of the study that the M_w of the implanted sutures and the control PHA4400 sutures *in vitro* decreased to approximately 43% of their original M_w implying that the hydrolytic stability of the implanted sample was very similar to the *in vitro* control (Martin *et al.,* 2016).

1.6.3. Biocompatibility of Polyhydroxyalkanoates

Biocompatibility is one of the most important requirements for a material to be suitable for medical applications. Various parameters influence the biocompatibility of PHA scaffolds

which include size, porosity, shape, surface topography, chemical and molecular structure of the material. The material composition and the degradation products are also an important parameter which affect the biocompatibility of PHAs. The absence of any non-toxic compound produced during polymer degradation along with it being non-immunogenic are essential requirements for the acceptance of the scaffold by the body (Zhao *et al.*, 2003; Zheng *et al.*, 2005). The monomer for P(3HB), (R)-3-hydroxybutyric acid (3HB) is present at concentrations of 3-10 mg per 100 ml blood in healthy adults and is a normal metabolite found in human blood. There are various lipoproteins found in the body where presence of low molecular weight P(3HB) have been detected (Hocking and Marchessault, 1994; Williams *et al.*, 1999). Hence, P(3HB) is expected to be highly biocompatible. The effect of PHA degradation products was established by Sun *et al.*, where cellular responses of the mouse fibroblast cell line L929 were studied in the presence of PHA degradation products. It was observed that MCL-PHAs are even more biocompatible than the SCL-PHAs (Sun *et al.*, 2007). It is also important for the biomaterial implants which are in contact with blood for a long term application, to not have any antigenic responses, nor induce thrombosis or embolism and should not cause destruction of plasma proteins. *In vivo* studies conducted on P(3HB-co-3HHx) as a blood contact graft material showed that it reduced thrombogenicity and attachment of blood platelets as compared to gelatin coated films, thus promoting haemocompatibility (Qu *et al.*, 2006). Sevastianov *et al.,* 2003 used purified P(3HB) and P(3HB-co-3HV) films for haemocompatibility studies and it was observed that the films did not cause any blood coagulation or thrombosis and were suitable to be used in contact with blood. The *in vivo* response of the cells towards the biomaterial used is important to decide whether the material is suitable for medical applications. The cytotoxicity of P(3HB) and P(3HB-co-HV) fibres were analysed by implanting them in Wistar rats for a period of 6 months. There was no adverse effect reported in their physiological and biochemical processes, confirming the biocompatibility of the polymers (Shishatskaya *et al.*, 2002). In a study conducted on a subcutaneous poly(3-hydroxyoctanoate-co-3-hydroxyhexanoate) (P(3HO-co-HHx)), the scaffolds were implanted in mice for 40 days. There was a thin layer of fibroblast growth on the implant with no macrophage infiltration and no significant inflammatory response observed at the end of the experiment (Williams *et al.*, 1999). Chen *et al.* observed that poly(3-hydroxybutyrate-co-3-hydroxyhexanoate) scaffolds initiated far less inflammatory response as compared to the polylactides, attributing this to a slower degradation rate and less acidic nature of the degradation products and hence lower inflammatory response.

In a study conducted on P(3HB-co-3HHx) seeded with mice-iPSCs, it was observed there was a higher cell activity and adhesion on the PHA construct as compared to the tissue culture plastic. Hence, P(3HB-co-3HHx) was found to be highly biocompatible enabling growth, proliferation and myocardial cell differentiation of the mice-iPSCs (Shijun *et al.,* 2016). In another study it was observed that the inoculated chondrocyte cells grew and proliferated well on the P(3HB)-co-(3HHx)/ PHB blend scaffold. After an incubation of 14 days, the outside layer of P(3HB)-co-(3HHx)/ PHB blend scaffold was covered with proliferated cells and the cells merged on some of the scaffold surfaces to form cell layers confirming the biocompatibility of the polymers (Zhao *et al.,* 2003). Saito *et al*. also reported no inflammatory reaction on the chorioallantoic membrane of the developing egg with the interaction of P(3HB) sheets, thus confirming it to be a biocompatible material (Saito *et al.,* 1991). Furthermore, Tepha Inc. have fabricated surgical sutures using poly-4-hydroxybutyrate P(4HB) in 2007 and FDA has approved its use for clinical applications. This was an important achievement and confirmed the biocompatible nature of PHAs (Martin *et al.,* 2012).

1.6.4. Applications of Polyhydroxyalkanoates

PHAs are an emerging group of polymers which are now being used in various industrial and medical applications due to their unique properties. As discussed above, the material characteristics of PHAs can be varied from being highly rigid to highly elastomeric in nature. They are optically active molecules, piezoelectric in nature and water insoluble materials. These features of PHAs make them highly suitable for a variety of applications.

Industrial applications

PHAs have been used in various industrial applications. They have a wide range of applications due to their novel features. Biopol is one of the commercial products which is a copolymer of poly (3-hydroxybutyrate-co-3-hydroxyvalerate). It is a thermoplastic and has a melting point of 140-180 ℃. It can also be injection moulded and vacuum formed. Hence it has its applications in packaging, shampoo bottles, disposable razors, disposable cups, surgical stitches, surgical pins, disposable knives and forks, woven medical patches and nappy linings. Nodax is another PHA copolymer consisting of 3-hydroxybutyrate and three MCL units which include 3-hydroxyhexanoate, 3-hydroxyoctanoate and 3-hydroxydecanoate. Procter and Gamble have developed this polymer and it is available as foams, fibres or nonwovens, films and latex among others. Biogreen is another product which is P(3HB) produced from methanol.

It is produced by a Japan based company Mitsubishi Gas Chemicals. Due to its piezoelectric nature, PHAs can be used for making pressure sensors for keyboards, stretch and acceleration measuring instruments, material testing, shockwave sensors, lighters, gas lighters; acoustics: microphone, ultra-sonic detectors, sound pressure measuring instruments, oscillators, headphones, loudspeakers, for ultrasonic therapy and atomization of liquids. The gas barrier property of P(3HB-3HV) is useful for applications in food packaging and for making plastic beverage bottles. For agricultural purposes, PHAs have been used as mulch films, herbicides, insecticides, bacterial inoculants used to enhance nitrogen fixation in plants.

Medical applications

PHAs are natural biomaterials that have a potential to be used in medical applications due to their natural source, biocompatibility, biodegradability, non-toxic nature, their ability to provide mechanical support to the injured region and to promote cell growth and proliferation (Valappil *et al.,* 2006). A large number of PHAs are currently under investigation and need to be researched and evaluated as a potential material for medical applications. These include P(3HB) (Basnett *et al.*, 2013; Akaraonye *et al.,* 2016), P(3HB-co-3HV), poly-4-hydroxybutyrate, P(4HB), poly(3-hydroxybutyrate-co-3-hydroxyhexanoate), P(3HB-co-3HHx), and P(3HO) (Bagdadi *et al.,* 2016; Rai *et al.*, 2011; Byrom, 1992, Chen *et al*., 2001, Hrabak, 1992). They are used as bone plates, osteosynthetic materials, surgical sutures, dusting powders, wound dressings, nerve conduits, soft tissue repair, dental and maxillofacial treatment and cardiovascular implants (patches and heart valves) (Chen *et al*., 2005). They can also be utilized in the slow release of drugs and hormones in the affected tissue. One such example includes, P(3HB) which is used in the synthesis of Merck's anti-glaucoma drug "Truspot" due to its ability to hydrolyze instantly to R-3-hydroxybutyric acid. A monofilament suture was fabricated using P(3HB) and P(3HB-co-3HV) and was implanted intramuscularly in Wister rats. These sutures did not cause any acute vascular reactions at the site of implantation or any adverse effects such as inflammation, necrosis, and calcification of fibrous capsule or malignant tumour formation after a period of 1 year of implantation (Shishatskaya *et al*., 2004). An *in vivo* study was conducted by implantation of a composite which was fabricated using hydroxyapatite (HA) and polyhydroxybutyrate/polyhydroxyvalerate. Lamellar bone was formed at the interface, which replaced the degrading polymer matrix, while engulfing HA filler particles. Osteoblasts and osteocytes were identified throughout the interface region. The thickness of the newly formed bone also increased significantly. These materials were thus found to be suitable for bone replacement therapies (Luklinska et al., 2003).

Cardiovascular applications

One of the greatest contribution of PHAs to medicine have been in the cardiovascular area (pericardial and atrial septal repair patches, scaffolds for regeneration of arterial tissues, vascular grafts, cardiovascular stents and heart valves). There are different PHAs which have been used for these applications. MCL-PHAs due to their elastomeric properties and flexible nature have been commercially used in cardiac tissue engineering especially in heart valve development. Poly(4-hydroxybutyrate) (P(4HB)), an SCL-PHA, also has elastomeric properties and has been found to be useful in cardiac tissue applications (Chen and Wu, 2005). Tepha Inc. has produced commercially available P(4HB) TephaFLEX® for various applications including heart valve development. Sodian *et al*. (2000), fabricated a biodegradable, biocompatible and porous trileaflet heart valve using P(3HO) produced by Tepha Inc., and seeded vascular cells from sheep carotid arteries *in vitro*. The P(3HO) valve was monitored for 120 days and was found to be functional and suitable to be implanted in pulmonary valve position in the pulmonary artery in the lambs. The valve also showed cell proliferation and accumulation which confirmed it to be a suitable material for valve development (Chen and Qiong, 2005). P(4HB) and poly(3-hydroxyoctanoate-co-3-hydroxyhexanoate) (PHOH) produced by Tepha Inc. were used to fabricate a trileaflet valve scaffold using stereolithography. This valve had an advantage that it could be moulded without the need for suturing to the tissue (Sodian *et al*., 2002). In another study, P(3HO-co-3HHx) produced by Metabolix Inc. was used as a copolymer of polyglycolic acid (PGA) for the fabrication of a two component tubular vascular graft which was seeded with autologous cells where PGA formed the inner layer and P(3HO-co-3HHx) formed the outer layer of the conduit. This construct was implanted in the aortic tissue of the lambs. An increased cell density, collagen formation was observed along with insignificant inflammatory response (Shum-Tim *et al.,* 1999). A P(3HO) polymer patch was also fabricated and was implanted in the pulmonary artery of sheep. The scaffold was seeded with autologous ovine cells. It was observed that at the end of 24 weeks there was an organised viable accumulation of cells on the graft containing endothelial cell lining. There was no stenosis or thrombosis reported at the end of the experiment (Stock *et al*., 2000). In an *in vivo* study conducted using P(3HB-co-3HHx), it was observed that a coating of the polymer on the decellularised porcine aortic valves, decreased calcification and promoted cell proliferation and migration on the engineered valve (Wu *et al.,* 2007). Another PHA used in cardiac applications is poly(3-hydroxybutyrate-co-3-hydroxyvalerate) P(3HB-co-3HV). A 3D microfibrous scaffold was electrospun using a blend of poly(3-hydroxybutyrate-co-3-hydroxyvalerate) (P(3HB)-co-(3HV), poly(L-D,L-lactic acid)

(P(L-D,L)LA) and poly(glycerol sebacate) (PGS). The scaffolds were seeded with mesenchymal stem cells (MSCs) which were developed from human umbilical cord matrix (Wharton's Jelly) cells. These were found to align in parallel to each other, mimicking the native myocardium (Kenar *et al*., 2010).

1.7. AIMS OF PROJECT

The main aim of this project was the development of a "cardiac patch" involving the use of novel biodegradable materials, MCL-PHAs particularly, poly(3-hydroxyoctanoate) homopolymer, P(3HO), (as described by Rai *et al.*, 2011 and Bagdadi *et al.,* 2016) and poly(3-hydroxynonanoate-co-3-hydroxyheptanoate) P(3HN-co-3HHP).

The specific aims which led to the fulfilment of the main aim stated above included:

1. Production and characterization of MCL-PHAs including Poly(3-hydroxyoctanoate), P(3HO), and Poly(3-hydroxynonanoate-co-3-hydroxyheptanoate), P(3HN-co-3HHP) using *Pseudomonas mendocina CH50*.
2. Fabrication and characterization of cardiac patches using solvent casting and electrospinning of neat P(3HO), P(3HN-co-3HHP) and their blends.
3. Preparation of 3D porous scaffolds of P(3HO) and their characterization.
4. Production and characterisation of polyaniline/P(3HO) blend scaffolds to introduce electrical conductivity in the scaffolds.
5. Functionalization of the scaffolds using a star PEG mediated incorporation of peptides and growth factors in order to allow efficient host cell recruitment, adhesion, proliferation, differentiation and vascularisation.

CHAPTER 2

Materials and Methods

2.1. Chemicals and Reagents

All the chemicals were purchased from Sigma-Aldrich or BDH Ltd. (Dorset, UK) or VWR (Leicestershire, UK) and TCI, UK. For Nuclear Magnetic Resonance (NMR), chromatography grade reagents were used while for the analytical work, analytical grade reagents were used. Cell culture studies were carried out using cell culture grade media and reagents from Sigma-Aldrich, UK, and Lonza, UK. The primary antibody was bought from abcam and Millipore. The live and dead assay kit and the secondary antibody was purchased from Invitrogen.

2.2. Bacterial strains and cell line

P(3HO) and P(3HN-co-3HHP) was produced using the Gram-negative bacterium *Pseudomonas mendocina CH50* which was obtained from the National Collection of Industrial and Marine Bacteria (NCIMB 10541), Aberdeen, UK. The C2C12 cell line was obtained from Sigma-Aldrich. Cell culture studies were carried out using the human induced pluripotent stem cell derived cardiomyocytes (hiPSC-CM) purchased from Cellular Dynamics International and neonatal ventricular rat myocytes (NVRM) which were isolated from neonatal mice at the National Heart and Lung Institute, Imperial College and provided for this work.

2.3. Production of Poly (3-hydroxyoctanoate) (P(3HO)) and Poly (3-hydroxynonanoate-co-3-hydroxyheptanoate) (P(3HN-co-3HHP))

The production of P(3HO) and P(3HN-co-3HHP) can be divided into four phases as depicted in Figure 2.1.

These include:

- Growth of *P. mendocina* CH50 in nutrient broth; growth in second stage mineral salt medium (MSM) for the production of an inoculum for the final fermentation; finally, the production stage MSM was used for the production of PHAs.

- Harvesting the cells and their lyophilisation by freeze drying.

- Solvent extraction of PHAs from the freeze dried bacterial cells followed by differential precipitation

- Various characterisations and analysis of the PHA produced
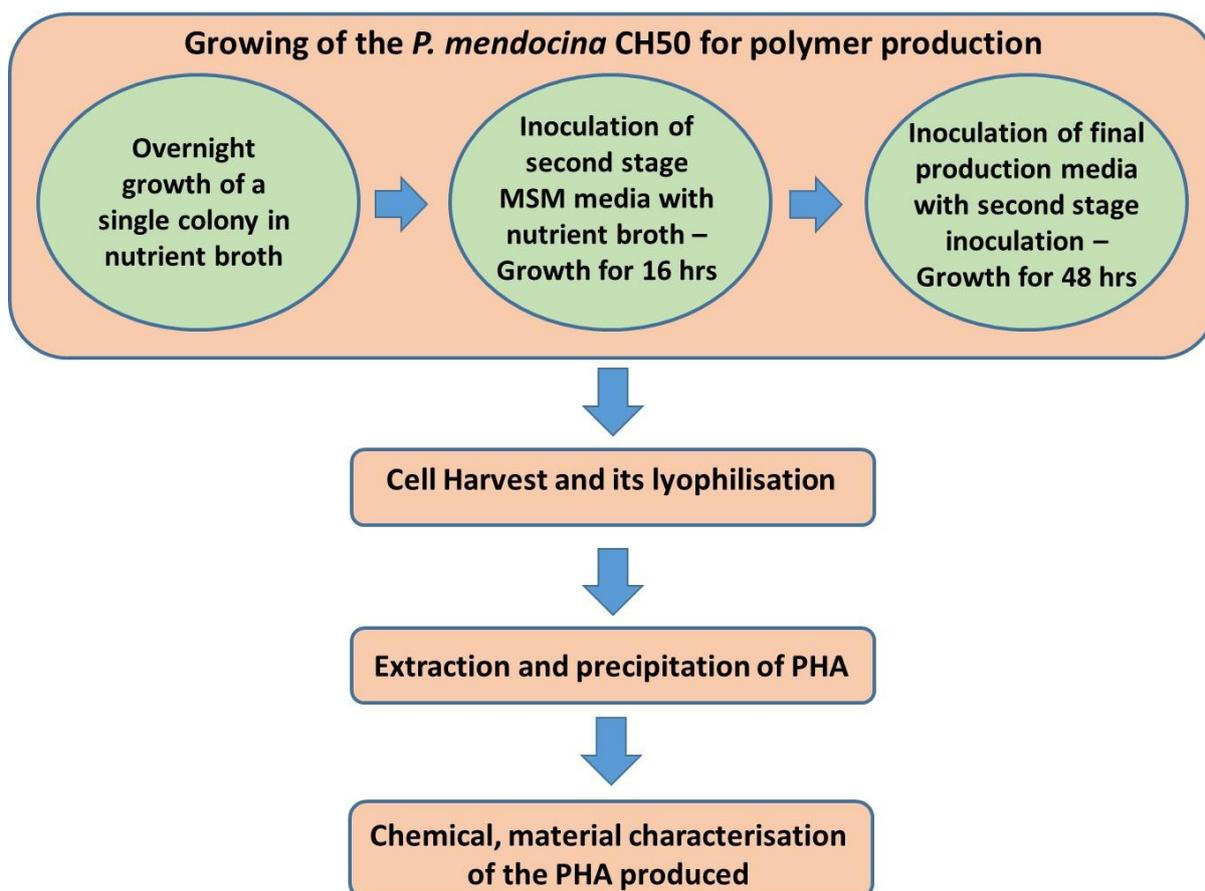
Figure 2.1: *Pictorial representation of the production of P(3HO) and P(3HN-co-3HHP) from P. mendocina CH50*

2.3.1. Media composition

Composition of Nutrient Broth (g/L)

Table 2.1: *Composition of nutrient broth no 2 used in this work, was purchased from Sigma Aldrich*

Meat peptone	4.3
Casein peptone	4.3
Sodium chloride	6.4

The final pH of the media was maintained at 7.5±0.2 and was stored at 25ºC. Fifteen grams of the nutrient broth was dissolved in 1L of distilled water and was used after sterilising it using autoclave at 121°C for 15 minutes.

Composition of the second stage MSM (g/L)

Chemicals Composition (g/L)

Table 2.2: Composition of the second stage MSM (Rai et al., 2011)

$(NH_4)_2SO_4$	0.45
Na_2HPO_4	3.42
KH_2PO_4	2.38
$Mg\ SO_4.7H_20$	0.80
Trace element solution	1 ml/L

Composition of the production stage MSM (g/L)

Chemicals Composition (g/L)

Table 2.3: Composition of the production stage MSM (Tian et al., 2000)

$(NH_4)_2SO_4$	0.50
Na_2HPO_4	3.80
KH_2PO_4	2.65
$Mg\ SO_4.7H_20$	0.80
Trace element solution	1 ml/L

Trace element solution (TE)

Chemicals Composition (g/L)

Table 2.4: *Composition of the trace element solution (Rai et al., 2011)*

$CoCl_2$	0.22
$FeCl_3$	9.70
$CaCl_2$	7.80
$NiCl_3$	0.12
$CrCl_6. H_2O$	0.11
$CuSO_4. 6H_2O$	0.16

The carbon source used for the production of P(3HO) and P(3HN-co-3HHP) were sodium octanoate and sodium nonanoate respectively. The molar ratio of C/N for the two productions were kept as 20 and hence the concentration of sodium octanoate used was 3.32 g/L while that of sodium nonanoate was 3.60 g/L respectively. The salts were sterilised by autoclaving at 121°C for 15 minutes. The carbon sources, sodium octanoate and sodium nonanoate and magnesium sulphate were sterilised separately. Trace element (TE) solution was prepared by dissolving all the chemicals in 1N HCl. The TE solution was filter sterilised before use. The pH of the media, sodium octanoate/sodium nonanoate and magnesium sulphate was adjusted to 7.00 using 1N HCl or 1M NaOH before autoclaving.

2.3.2. Fermentation for the production of P(3HO) and P(3HN-co-3HHP)

Nutrient broth inoculation of *P. mendocina CH50*

A single colony of *P. mendocina CH50* was used to inoculate the nutrient broth. The culture was incubated at 30°C at 200 rpm for 24 hours. This was used as the seed culture.

Second stage inoculation

The seed culture described above was used to inoculate the second stage MSM (section 2.3.1). The bacteria were cultured in this medium for 16 h at 30°C at 200 rpm. This was used as the inoculum in the final fermentation for polymer production.

Production stage MSM inoculation

The second stage culture described above was used to inoculate the production stage MSM (section 2.3.1). Sodium octanoate and sodium nonanoate were used as the carbon source at both stages for the production of P(3HO) and P(3HN-co-3HHP) respectively. The culture was incubated for a period of 48 hours before being harvested (Rai *et al*., 2011). The final production was carried out in 2 L fermenters.

2.3.3. Extraction and purification of the PHA by soxhlet extraction

After 48 h of growth, the cells were harvested by centrifuging the cultures at 4600 rpm for 30 min. The cell pellet obtained was then lyophilised. The dry cells were placed in a thimble and fitted onto the soxhlet apparatus. Methanol was added in the round bottom flask of the set up and the soxhlet was left to reflux for a minimum of 3 h. This dissolved all the impurities from the cells in methanol. The methanol was then discarded and replaced with chloroform. The cells were refluxed with chloroform for 12 h which enabled polymer extraction and dissolution. Later this chloroform layer was evaporated using a rotary evaporator and the polymer was precipitated using an ice cold solution of 50:50 methanol: ethanol.

2.3.4. Analytical studies

Biomass estimation

Estimation of the biomass was carried out by centrifuging 1 ml of the culture sample at 12,000g for 10 min. The cell pellets obtained were freeze dried and weighed.

pH estimation

The supernatant was collected from the above mentioned centrifuged samples and the pH was measured and recorded.

Estimation of nitrogen concentration

The reagents required for this analysis were prepared as follows:

- *Phenol nitroprusside buffer*: Sodium phosphate tribasic (3 g), sodium citrate (3 g) and ethylene tetraacetic acid (EDTA) (0.3 g) were dissolved in HPLC water. pH was adjusted to 12. To this, 6 g of phenol and 20 mg of sodium nitroprusside were added.
- *Alkaline hypochlorite reagent*: This reagent was prepared by mixing 2.5 ml of sodium hypochlorite solution containing 4% chlorine and 40 ml of 1M sodium hydroxide solution.

The estimation of nitrogen in the medium was carried out using the phenol hypochlorite reaction (Rai *et al*., 2011). The sample was prepared by centrifuging the culture at 12,000 g for 10 min. The supernatant obtained was used for analysis by diluting 1:100 times with Millipore water. 1 ml of phenol nitroprusside buffer was added to 2.5 ml of the diluted sample and mixed by swirling. Next, 1.5 ml of the hypochlorite reagent was added rapidly and vortexed. The sample was then incubated for 45 min in the dark. The absorbance was measured at 635 nm.

2.3.5. Processing of PHAs into 2D/3D scaffolds

Scaffold formation- neat P(3HO), P(3HN-co-3HHP) and P(3HO) / P(3HN-co-3HHP) blend 2D film production

The neat P(3HO), P(3HN-co-3HHP), blend P(3HO)/P(3HN-co-3HHP) scaffolds were prepared using solvent casting. Neat and blend scaffolds were prepared by dissolving 0.5 g of the neat polymer or polymer mixture in 10 mL of chloroform and casting into a 6-cm diameter petri dish. The blend films were prepared by mixing P(3HO) and P(3HHN-co-3HP) in the ratio of 80:20, 50:50, 20:80 in wt% respectively. These films were left for air drying for 1 week and in the freeze drier for 3 weeks.

Fibre formation- neat P(3HO), P(3HN-co-3HHP) and P(3HO)/ P(3HN-co-3HHP) blend random and aligned fibre formation using electrospinning

The random and aligned fibres were electrospun using electrospinning technology. For random fibre formation of these polymers, P(3HO), P(3HN-co-3HHP) and the blend of P(3HO) and P(3HN-co-3HHP) in weight ratio of 20:80, 50:50 and 80:20 were dissolved in acetone with a final polymer concentration of 8 wt % and stirred for 12 h. These solutions were electrospun from a 1 ml syringe with a 18G stainless steel needle, at a flow rate of 1.25 ml/h. A high voltage of 14kV was applied when the polymer solution was drawn into fibres and collected on an aluminium foil wrapped collector, kept at a distance of 10 cm from the needle. For collecting aligned fibres, a rotating drum was place at 10 cm and the speed of the rotating disc was set at 3000 rpm. The fibre were collected on 15 mm coverslips. The fibre coated coverslips were dried and used for characterisation and cell culture experiments.

Preparation of porous scaffolds

Fabrication of 2D porous P(3HO) scaffolds using porogen leaching

The scaffolds were prepared using solvent casting. Three different 5 wt% porous P(3HO) scaffolds were prepared. For this, 0.5 g of the polymer was dissolved in 10 ml of chloroform, and 50 mg, 100 mg and 150 mg of sucrose, used as the porogen, with particle size of 250-300 µm was added to cast three different porous films. This solution was poured in a petri dish and left on the bench for 1 week for air drying followed by 3 weeks in a freeze drier. To achieve the required pore size, sucrose was first sieved through a 300 µm sieve followed by sieving through 250 µm pore size sieve. The sucrose particles which remained on the sieve were >250 µm and <300 µm in diameter, and were used for further work.

After the neat and sucrose containing scaffolds were dried, water was added in the petri-dish and left for 2 h. Water was then removed and the scaffolds were peeled off. In the presence of water it was easier to peel off the scaffolds. The sucrose in the porogen containing scaffolds was dissolved by water and the scaffold was also easily removed from the petri-dish, leaving behind a porous scaffold. The scaffolds were then left to air dry on the bench.

Fabrication of 3D porous P(3HO) scaffolds

P(3HO) 3D porous scaffolds were fabricated by the salt leaching method using sodium chloride as a porogen. A mould was prepared using a vial of 1 cm^2 diameter. It was cut into a 2 cm long cylinder. One end of this cylinder was stuck to a slide using a silicon based glue. This set up was left for drying for 24 h.

In this mould, a 1 ml solution of 20% P(3HO) in chloroform was added and 4 g of sodium chloride was added (in excess). The sodium chloride particles were of particle size between 250 µm -300 µm. The scaffold set up was left for air drying for 1 week and was freeze dried for another week. The scaffold set up was then immersed in water and the sodium chloride was washed out. Water was changed every 12 h. This washing with water was carried out for 2 days. The 3D scaffolds were finally removed from the mould and left for air drying.

2.4. Characterisation of the PHAs

Chemical characterisation

Fourier Transform Infrared Spectroscopy (FTIR)

Preliminary confirmation of the polymer structure was determined by FTIR. The conditions under which this analysis was performed were as follows: spectral range 4000 to 600 cm^{-1}; window material, CsI: 10 scans and resolution 4 cm^{-1}. Polymer sample (2 mg) was used to carry out this analysis at the Department of Biomaterials and Tissue Engineering, Eastman Dental Institute, University College London, UK.

Nuclear Magnetic Resonance Spectroscopy (NMR)

The final confirmation and structural characterisation of the polymer produced by *P.mendocina CH50* was carried out using ^{13}C and ^{1}H NMR. For this, 20 mg of the purified polymer was dissolved in 1 mL of deuterated chloroform. These samples were sent to the Department of Chemistry, University College London, UK for NMR analysis. Chemical shifts were referenced against the residual solvent signal (7.26 ppm and 77.0 ppm for ^{1}H and ^{13}C respectively).

Material characterisation of the neat and blend scaffolds

Mechanical testing

Mechanical properties of the films were measured using the Perkin–Elmer Dynamic Mechanical Analyser (DMA) as described in Misra *et al.,* 2008. Polymer film strips (n=5) were cut with dimensions of 23 mm length, 5 mm width. The program for the test was set with a rate of deformation of 10 mm/min. This analysis was carried out to measure the Young's modulus, tensile strength and the elongation at break values.

Thermal property: Differential Scanning Calorimetry (DSC)

Thermal properties of the films such as melting temperature (T_m) and the glass transition temperature (T_g) were measured by DSC using a Perkin Elmer Pyris Diamond (Perkin Elmer Instrument). Film samples were used for the analysis. Prior to the analysis, these samples were encapsulated in the standard aluminium pans and the tests were performed under nitrogen atmosphere. The sample was heated and then cooled and then heated again at the rate of 20°C/min between -50°C to 200 °C.

Wettability analysis

The wettability analysis was carried out by measuring the water contact angle on the film samples (n=9) by using KSV Cam 200 optical contact angle meter (KSV instruments Ltd) as described in Misra *et al.,* 2008. This analysis gave an indication about the hydrophobicity of the sample. This experiment was done at the Department of Biomaterials and Tissue Engineering, Eastman Dental Institute, University College London, UK.

Surface morphology: Scanning Electron Microscopy (SEM)

Surface characterisation of the films was carried out using a JOEL 5610L scanning electron microscope (JOEL). The polymer samples were placed on the 8mm diameter aluminium stubs and gold coated for 2 min using the gold sputtering device (EMITECH-K550). Images were then recorded at different magnifications and acceleration voltages to study the surface topography of the sample (Misra *et al.,* 2008). The operating pressure of 7×10^{-2} bar and deposition current of 20 mA, for 2 min, was used. SEM analysis was carried out at the Department of Biomaterials and Tissue Engineering, Eastman Dental Institute, University College London, UK.

The samples with cells grown were analysed for their surface properties and the cell samples were prepared before viewing under SEM. The cells grown on different scaffolds were fixed in 3% paraformaldehyde for 30 min at room temperature and stored in PBS. Before imaging, the samples were dehydrated in a series of ethanol solutions (50%, 70%, 90% and 100%), incubating 10 minutes in each solution. Samples were air dried, coated and examined under the SEM, as described above in this section.

Porosity measurements

The porosity of the porous films was determined using equation 2.1.

$$\text{Porosity \%} = 1 - \left(\frac{\rho_p}{\rho_n} \right) \times 100 = \left(\frac{\rho_n - \rho_p}{\rho_n} \right) \times 100$$

....2.1

Where ρ_n is density of neat films, ρ_p is density of porous films.

Porosity measurements were made in triplicates.

Micro Computed Tomography (Micro-CT) analysis

Micro-CT analysis was used to analyse the interconnectivity of pores of the 3D scaffold structure. Surface characterisation of the films were carried out using a JOEL 5610Lv scanning electron microscope (JOEL).

Degradation studies

Degradation study was carried out by incubating film samples in phosphate buffered saline solution (PBS) and at 37°C with mild shaking at 80 rpm. Phosphate buffered saline (PBS) is an isotonic solution containing: NaCl 8g/L, KCL 0.2 g/L, Na_2HPO_4 1.44 g/L and KH_2PO_4 0.24g/L. Film samples 25 cm long and 0.5cm long were analysed for water uptake, weight loss and pH change for 3 months. The samples were analysed in triplicates.

The *in vitro* degradation analysis was also conducted on the P(3HO)-PANI films containing 10 vol%, 20 vol% and 30 vol% PANI. The study was conducted for a period of 1 month and different parameters were measured at 3 days, 15 days and 30 days. The samples used were 1cm long and 0.5cm width and were immersed in PBS. These immersed samples were kept in the incubator set at 37° C with mild shaking at 80 rpm. The samples were analysed in triplicates.

Water uptake and Weight loss

Prior to the incubation, the samples were weighed M_o ($M_{o, dry}$ the initial weight of the sample). After this, the samples were immersed in PBS under mild shaking of 80 rpm, at 37^0 C, for a period of one and three months. At the end of the incubation period, the samples were withdrawn from PBS and their weight loss (%WL) and water uptake (%WA) behaviour was analysed as described in Misra *et al.,* 2008. The following equations were used to calculate water uptake and weight loss of the samples:

$$\text{Weight Uptake (\%WA)} = \left(\frac{M_{w,wet} - M_{t,dry}}{M_{t,dry}} \right) \times 100 \quad \text{.......................................2.2}$$

$$\text{Weight Loss (\%WL)} = \left(\frac{M_{o,dry} - M_{t,dry}}{M_{o,dry}} \right) \times 100 \quad \text{.......................................2.3}$$

Where,

$M_{o, dry}$ = the initial weight of the sample.

$M_{w, wet}$ = M_w, the weight of the samples after the immersion in PBS

$M_{t, dry}$ = M_t, the dry weight of the samples after the incubation in PBS followed by drying (Misra *et al.,* 2008).

pH measurements

After the samples were removed from PBS, pH was measured to record change in pH during the given time period.

2.5. *In vitro* biocompatibility studies

2.5.1. Growth of human induced pluripotent stem cell derived cardiomyocytes (hiPSC-CMs) on the scaffolds:

Polymer coated coverslips were prepared using neat P(3HO) and P(3HN-co-3HHP). Coverslips were also coated with the P(3HO)/ P(3HN-co-3HHP) blend polymer solutions and left to dry. The hiPSC-CMs were grown for 14 days, with regular change in media, on the PHAs and gelatin coated coverslips were used as positive controls.

***In vitro* culture of human induced pluripotent stem cell derived cardiomyocytes (hiPSC-CMs)**

Cell culture was carried out under sterile conditions in a Biomat 2 class II microbial safety cabinet and cells were incubated in a CO_2 incubator (Sanyo, MCO-5M) at 37°C and 5% CO_2. *In vitro* culture of the hiPSC-CM were conducted on P(3HO), P(3HN-co-3HHP) and blend (80:20,50:50,20:80) coated coverslips while 0.1% gelatin coated coverslips were used as the positive control. The hiPSC-CM from Cellular Dynamics International, iCell Cardiomyocytes, were thawed in iCell cardiomyocytes plating medium (CMM-100-110-001) as per the guidelines provided by the manufacturer. The scaffolds were placed in a 12-well tissue culture plate and were sterilized with 70% ethanol and further sterilized for 1 h UV light prior to the seeding of cells. After sterilization, 60,000 cells were seeded on the scaffolds as a 100 µl drop and left for a few hours. Later in iCell cardiomyocytes plating medium (CMM-100-110-001) was added to the wells in the culture plate and left for 2 days for the cells to stick on the scaffolds. Two days later the cells were seen to adhere to the scaffolds and the media was changed to the iCell cardiomyocyte maintaining medium (CMM-100-120-001) (CDI 2013).

The cardiomyocytes were left to grow for 14 days and media was changed every 2 days. On day 14 they were used to conduct various biocompatibility experiments.

Live and dead assay

Live and dead assay was conducted on day 14 on the hiPSC-CMs grown on P(3HO), P(3HN-co-3HHP) and P(3HO)/ P(3HN-co-3HHP) scaffolds and gelatin which was used as positive control. A live/ dead cell cytotoxicity assay was used to label the cells. Cells were washed in sterile PBS and a 100 µL of 2 µM calcein AM and 4 µM ethidium homodimer-1 solution was added to each well for 30 min in the dark at room temperature. Following incubation, the samples were mounted in fresh PBS and imaged using an inverted Zeiss LSM-780 confocal microscope. Cells were counted using the Fiji image processing software (ImageJ).

Functional assays for cardiomyocytes

Optical mapping- calcium transients of hiPSC-CMs with fluo-4 AM- The cells were analysed for their calcium transient channels which are the major drivers for the beating of the cells. This work was carried out with assistance from Ms. Eleanor Humphrey, Imperial College London. The scaffolds were placed in a mattik dish and cells were seeded onto them. Cells were loaded with 20 µM fluo-4 AM in DMEM and left in the incubator. After 20 min the DMEM was refreshed and left in the incubator for 20 min.

Recording Calcium Transients- The scaffolds were mounted on the stage of an upright Nikon eclipse FN1 microscope in a glass bottom dish (MatTek Corporation) and observed through a 40x water immersion objective. Throughout the experiment the cells were superfused at 37°C with Normal Tyrode's (NT) solution containing 140 mM NaCl, 4.5 mM KCl, 10 mM glucose, 10 mM HEPES, 1 mM $MgCl_2$, 1.8 mM $CaCl_2$, adjusted to pH 7.4 using 2 M NaOH. The hiPSC-CMs were field stimulated at 0.5, 1 and 1.5 Hz using an external stimulator and upon stimulation the fluorescence signal (excitation wavelength= 300-520 nm and emission wavelength= 480-620 nm) was recorded using a RedShirt CMOS camera (128x 128 pixels, 2 ms frame rate) and dedicated Neuroplex software (IDL, Research Systems Inc.). The fluorescence signal was then analysed using a custom MatLab code®. The transients were analysed to determine four main parameters: normalised amplitude (f_1/f_0) which is the peak transient amplitude divided by the baseline value of the signal; time to peak (T_p) which is the time taken to reach peak amplitude; time to 50% decay (T_{50}) and 90% decay (T_{90}) which are

the time taken for the transient to decrease from T_p to 50% and 90% of the transient amplitude respectively, during the recovery phase of the transient.

Beat rate measurements

hiPSC-CMs were placed on the stage of a Nikon eclipse TE2000-E inverted light microscope at 37 °C and the number of beats per minute counted and recorded using a Nikon digital sight DS-2Mv camera.

Immunofluorescence staining (F-actin, Myosin Heavy Chain (MHC), Nuclei)

Immunofluorescence of the cells was analysed by staining the cells for myosin heavy chain (MHC), F-actin and nuclei. F-actin was stained with phalloidin and nuclei with DAPI. For immunofluorescence, at day 14 the beating cardiomyocyte monolayers were fixed with 4% paraformaldehyde for 20 mins, permeabilised with 0.1% Triton-X-100, and blocked with 4% FBS in PBS for 1 h. Cardiomyocytes were then stained with mouse anti-myosin heavy chain (α/β) primary antibody (Table 2.5) (1:200) for 1 h, washed three times with PBS, and then stained with donkey anti-mouse Alexa 546 secondary antibody (1:400) and FITC-phalloidin (1:200) for 45 min in 3% BSA in PBS. After staining, the cardiomyocytes were washed an additional three times in PBS. They were then mounted in vectashield mounting medium containing DAPI. Immunofluorescence imaging was performed using an inverted Zeiss LSM-780 confocal microscope.

Sarcomere staining

Cells were washed in phosphate buffered saline (PBS), fixed with ice-cold methanol for 5 min and blocked in 1% bovine serum albumin (BSA) (subsequently used for all antibody dilutions) for 1 hour. Cells were stained with a primary antibody overnight at 4°C and then incubated with a secondary antibody for 1 hour at room temperature before mounting in vectashield (Vectalabs) mounting medium containing DAPI (Table 2.5). The cells were imaged using an inverted Zeiss LSM-780 confocal microscope.

Table 2.5: *Different antibodies used for immunoflourescence staining of the sarcomere (α-actinin) and Myosin heavy chain (MHC)*

Immunofluorescence labelling	Primary antibody	Secondary antibody
α-actinin	mouse anti- α actinin antibody (1:1000 dilution) (Sigma)	anti-mouse Cy3 antibody (1:500 dilution) (Millipore)
MHC (α/β)	mouse anti-myosin heavy chain (α/β) primary antibody (abcam) (1:200)	donkey anti-mouse Alexa 546 secondary antibody (1:400) (Invitrogen)

2.5.2. C2C12 myoblast proliferation

The C2C12 myoblast cell line was used to assess cell proliferation in the P(3HO) porous constructs by the MTT (3-(4,5-Dimethylthiazol-2-yl)-2,5-diphenyltetrazolium bromide) colorimetric assay and SEM.

C2C12 cell growth

C2C12 myoblast cells were grown in a DMEM supplemented with 10% of foetal calf serum, 1% w/v penicillin and 1% w/v streptomycin solution and grown in a 75 cm^2 tissue culture flask at 37 ºC with 5% of CO_2. Media was pre-warmed at 37ºC and filter sterilized prior to use. Cell passages were carried out before confluence, every one or two days. For the passages, cells were detached from the flask using 5% trypsin at 37ºC for 2.5 minutes and the reaction was stopped by adding an equal volume of the supplemented DMEM. Samples were centrifuged at 400 g for 10 min and the resulting pellet was dissolved in freshly supplemented DMEM. Cells were seeded in sterile 75cm^2 tissue culture flasks.

C2C12 cell seeding

C2C12 myoblast cells in 70% confluence were used for the cell seeding on the scaffolds. The cells were grown on the scaffolds in a 24 well tissue culture plate. Scaffdex® cell crowns were used to hold the cells on the well's surface on the films. Around 20,000 cells were seeded on the pre-wetted constructs in a 24 well plate. As a positive control, cells were seeded in the wells without films. For the negative control, films were incubated in supplemented DMEM without cells. Plates were incubated at 37ºC with 5% of CO_2 and media was changed every 2 days. Cell proliferation was assessed at 24 hrs.

Cell proliferation study using the MTT assay

The MTT assay was performed on the constructs containing cells at 24hrs. For this, 100 µl of a 5 mg/ml MTT solution in distilled water were added to each well at 24hrs and the plates were incubated for two hours at 37ºC with 5% of CO_2. After this, films were transferred to new 24 well tissue culture plates and 500µl of DMSO were added. After a 5 minute incubation, 100µl of the resulting solution were transferred to 96 well plates and the absorbance at 540nm was measured on a Thermomax® microtitre plate reader. The absorbance of the samples were normalised with respect to the positive control. The difference in the surface areas of the tissue culture plate wells and the films were considered for the calculation of % cell viability on the films.

2.5.3. Growth of neonatal ventricular rat myocytes (NVRM) on the polymers

The biocompatibility of the scaffolds were also analysed by growing NVRMs on the different films. This work was carried out by cell biologists at National Heart and Lung Institute, Imperial College. NRVMs were isolated from Sprague-Dawley rats 0-2 days after birth by excising the hearts and isolating the ventricles. All work was carried out under the Animals (Scientific Procedures) Act 1986 and the EU Directive 2010/63/EU. A Gentle MACs neonatal heart dissociation kit (Miltenyi Biotec) was used to enzymatically digest the ventricles to produce a cell suspension that was pre-plated for 1 hour to remove the fibroblasts. Two hundred thousand (200,000) NRVMs were seeded per P(3HO):PANI constructs, NCO-sP(EO-stat-PO): P(3HO):P(3HHN-co-3HHP) fibres with either one/two or three active molecules (RGD,YIGSR and VEGF) and the collagen construct which was used as a positive control. These cells were grown in NRVM medium: 67% Dulbecco's modified Eagle medium (DMEM), 16% Medium 199, 10% Horse serum (HS) (Gibco), 4% foetal bovine serum (FBS) (Gibco), 2% HEPES (4-(2-hydroxyethyl)-1- piperazineethanesulfonic acid) buffer and 1% penicillin-streptomycin. The live and dead assay was conducted at 3 days post seeding.

Image analysis

Image processing software Fiji (ImageJ) was used for all image analysis. The live, dead cell numbers and nuclei density was quantified using Fiji to count the cells and nuclei, which it recognised by the elliptical shape.

Sarcomere length was measured by viewing the profile plot of a line drawn perpendicular across the α-actinin bands. The distance between each peak on the graph was measured and averaged to give sarcomere length.

Alignment analysis of the cells grown on aligned fibres

The alignment of the cells grown on aligned fibres were quantified by using the angle tool of the Image J software. The nuclei were stained using DAPI and the modulus of the deviation of the individual angles were calculated with respect to the mean angle. The percentage of cells in a given range were plotted for each scaffold which gave a quantification of the cell alignment.

2.6. Development of conductive scaffolds

Production of P(3HO):PANI blends to introduce electrical conductivity in the scaffold.

Polyaniline (PANI) synthesis

PANI-HCl synthesis

Polyaniline-HCl (PANI-HCl) is formed by oxidising aniline hydrochloride with ammonium peroxidisulphate in aqueous medium. For this, 0.2 M aniline hydrochloride and 0.25 M ammonium peroxidisulphate were each kept for dissolving with stirring in 50 ml of distilled water. Both solutions were kept for 1 h at room temperature (~18–24 °C), then mixed in a beaker, briefly stirred, and left undisturbed to polymerize. Next day, the PANI precipitate was collected on a filter, washed with three 100-mL portions of 0.2 M HCl, and similarly with acetone until a clear filtrate was obtained. Polyaniline (emeraldine) hydrochloride powder was dried in air and then in an oven at 60°C (Stejskal *et al.*, 2002).

PANI-base synthesis

The PANI-HCl was dissolved in excess of 3% ammonium hydroxide to convert to blue coloured non-conducting PANI-base. The solution was filtered next day and washed thrice with 200 ml of acetone. The PANI-base pellet was left for air drying followed by drying in an oven at 60°C.

Fabrication of the P(3HO)-PANI blends

Blends of P(3HO) and PANI were prepared by dissolving P(3HO), PANI-base and camphor sulfonic acid (CSA) in chloroform. Camphor sulfonic acid (CSA) was used as a dopant to

convert the non-conducting PANI-base to conducting PANI-CSA. Initially, PANI-base and CSA in the ratio of 0.78:1 were dissolved in 10 ml of chloroform and left for stirring for 2 days. The PANI-doped CSA solution was filtered twice and the filtrate was collected. P(3HO) was added to the PANI filtrate solution and kept for dissolving overnight. Three different solutions were prepared, containing 10 vol%, 20 vol% and 30 vol% of PANI and by dissolving P(3HO) in it. The solutions were cast in Teflon moulds and left for 2 days to form a film. The films were peeled off and various other characterization were carried out with the films.

Electrical conductivity measurement

The electrical conductivity of the films were measured using a 2 probe technique. The films were attached to two probes which in turn were connected with a multimeter and a voltage source in series. The voltage was applied through the films and the current passing through the films was recorded. Using these values, the electrical conductivity was recorded using the following equation:

$$\rho = \frac{V}{I} \times \frac{A}{l}$$

....2.4

Where ρ = electrical resistivity, V = voltage, I = current, and l=length of the sample, A= area of the cross-section. The electrical conductivity was then calculated using the following equation

$$\sigma = \frac{1}{\rho}$$

....2.5

Where σ = electrical conductivity

2.7. Incorporation of growth factors and peptides in the polymer scaffolds for promoting cell adhesion

Growth factors and peptides were incorporated with the P(3HO): P(3HHN-co-3HHP) (80:20) blend fibres by adding a functional amphiphilic macromolecule based on star-shaped poly ethylene oxide (PEO). The additive is a six-armed star-shaped poly(ethylene oxide-stat - propylene oxide) with isocyanate end groups (NCO-sP(EO-stat-PO)) with 80% EO content and a molecular weight of 12 kDa. The molecule was obtained from Dr. Jochen Salber, University

Hospital Knappschaftskrankenhaus, Bochum, Germany. For incorporation of growth factors and peptides, four types of fibres were electrospun. One batch had 2 µg VEGF as an additive along with the 30% polymer solution. Another batch had 2.7 mmoles of RGD and YIGSR as an additive while a third had a combination of 2 µg VEGF and 2.7 mmoles RGD and YIGSR in the 30% polymer solution. The fourth batch was spun without any incorporated peptides or growth factors and acted as a control. The NCO-sP(EO-stat-PO) was dissolved in acetone and 30% polymer solution was prepared by further dissolving P(3HO) and P(3HN-co-3HHP) in 80:20 ratio. The various additives of peptides and VEGF was added to the respective solutions as mentioned above. This solution was immediately used for electrospinning. The polymer was spun at a rate of 1ml/hr, at a speed of 3000 rpm, voltage of 14kV to obtain aligned fibres. The distance between the needle and the collector was 15 cm. The fibres were collected on coverslips.

2.8. Statistical analysis

Data sets have been expressed along with their mean ± standard deviation. The data, where appropriate, were compared using the ANOVA and t-test. The differences were considered significant when *$p < 0.05$, **$p < 0.001$. p value greater than 0.05 ($p > 0.05$) was interpreted as indicating no significant difference.

CHAPTER 3

Production and characterisation of MCL-polymer based cardiac patches

3.1 Introduction

Medium chain length PHAs have been extensively used in soft tissue engineering due to their elastomeric properties and low Young's modulus. These properties are adjustable based on the production conditions and hence can be tailored specifically to match with the properties of the tissue being regenerated. They have been explored for their application in biological implants such as the heart valves, cartilage tissue engineering and in wound healing (Kim *et al*., 2007). In addition to the different properties obtained with different MCL-PHAs, the production of co-polymers, blends and composites further increase their range of applications. However, despite the varied applicability of these polymers, widespread use of the MCL-PHAs remain limited, mainly because of the lack of availability of these materials in large quantities (Rai *et al*., 2011).

This chapter describes the production and characterisation of two MCL-PHAs, P(3HO) and P(3HN-co-3HHP) produced from *Pseudomonas mendocina CH50* using sodium octanoate and sodium nonanoate as the carbon sources respectively. Novel cardiac patches of neat and blend polymers have been fabricated and characterised with respect to their thermal properties, mechanical properties and biocompatibility with respect to human induced pluripotent stem cells derived cardiomyocytes (hiPSC-CM)s and neonatal ventricular rat myocytes (NVRM)s.

3.2. Results

3.2.1. Production of Poly(3-hydroxyoctanoate), P(3HO) and poly (3-hydroxynonanoate - co-3-hydroxyheptanoate), P(3HN-co-3HHP) by bacterial fermentation

Production of Poly(3-hydroxyoctanoate), P(3HO)

Poly(3-hydroxyoctanoate), P(3HO) production by *P. mendocina CH50* using sodium octanoate as the sole carbon source was carried out as described in section 2.3.2. The fermentation was carried out in a 2L fermenter for 48 hr and the growth profile is shown in Figure 3.1. During the fermentation, the OD_{450} increased from 0.21 to 0.88 showing slow growth for the initial 9 hours of fermentation, indicating a lag phase of growth. After this there was a steady increase in growth and the OD value reached a maximum of 5.7. Biomass estimation was carried out by weighing the freeze dried cells. Dry cell weight was also found to show the highest value of 2.8 g/L at 48 h. The initial nitrogen concentration of 0.52 g/L decreased to 0.11 g/L at 12 h, 0.003 g/L at 36 h and continued to decrease until 48 h, which was accompanied by a simultaneous increase in polymer accumulation. The pH of the culture also increased from 7

to a maximum of 7.9. The PHA yield was determined every 9 h. In case of P(3HO), there was no polymer found in the 9 h sample, but a 5.12% dry cell weight (dcw) yield was observed at 18 h. Following that 11.37% dcw and 21.65% dcw polymer yield was obtained at 27 h and 36 h respectively. A maximum polymer yield of 45.76% dcw was obtained at 48 h.
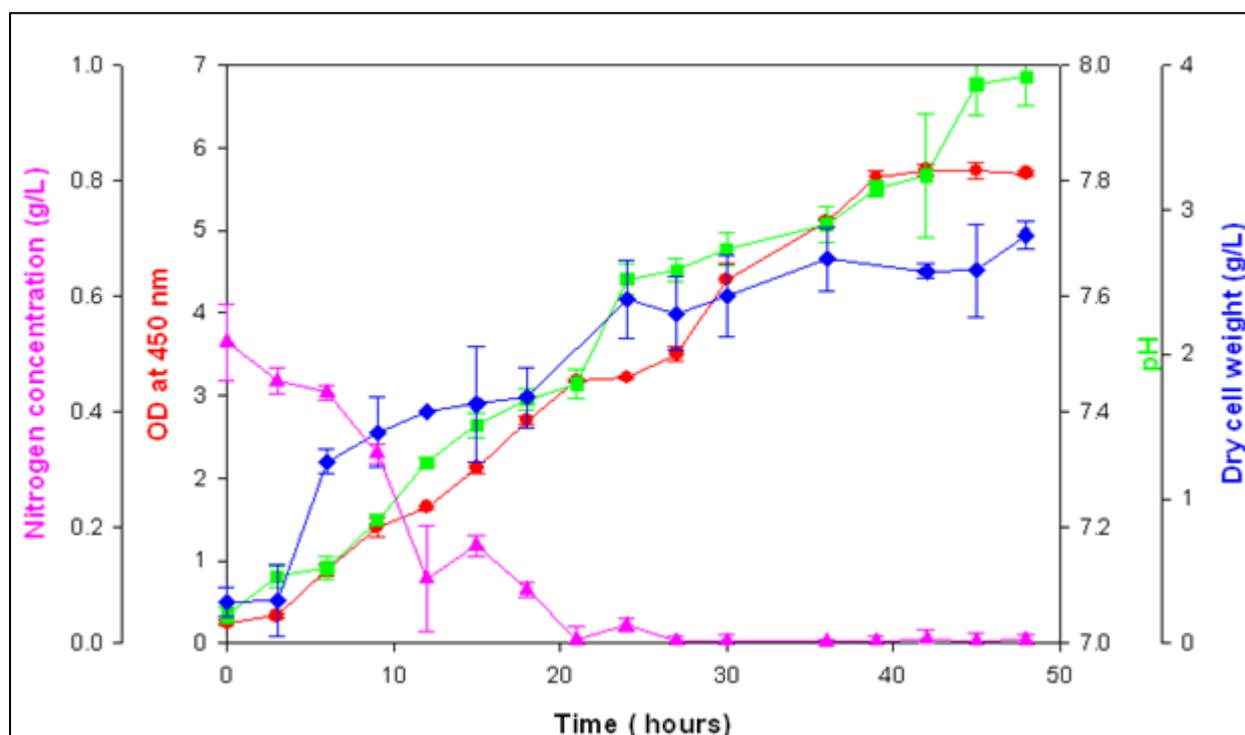
Figure 3.1: *A temporal profile of the fermentation of Pseudomonas mendocina CH50 using sodium octanoate as the carbon source.* ━●━ *OD at 450 nm,* ━■━ *pH,* ━◆━ *Dry cell weight (g/L),* ━▲━ *nitrogen concentration (g/L)*

Production of poly(3-hydroxynonanoate)-co-(3-hydroxyheptanoate), P(3HN-co-3HHP)

P. mendocina CH50 was grown using sodium nonanoate as the sole carbon source as explained in section 2.3.2 for the production of poly(3-hydroxynonanoate)-co-(3-hydroxyheptanoate). The fermentation profile is shown in Figure 3.2. Here too a lag phase was observed in the initial 9 h, with an increase in OD_{450} from 0.164 to 0.280. After this there was a steady increase in the growth and the OD_{450} value reached a maximum value of 4.2 at 48 h. The biomass was estimated to be a maximum of 2.26 g/L at 48 h, which also coincided with time required to reach the maximum OD_{450} value. Nitrogen concentration decreased from the initial value of 0.503 g/L to 0.333 g/L in 12 h, which further decreased to 0.116 g/L by 27 h and finally decreased to 0.0002 g/L by 48 h. The pH of the culture also showed an increase from 7 to a maximum of 7.4. The yield for P(3HN-co-3HP) was determined to be 2.34% dcw at 9 h, 6.1% dcw at 18 h, 6.57% dcw at 27 h, 18.23% dcw at 36 h and 42.34% dcw at 48 h.

58
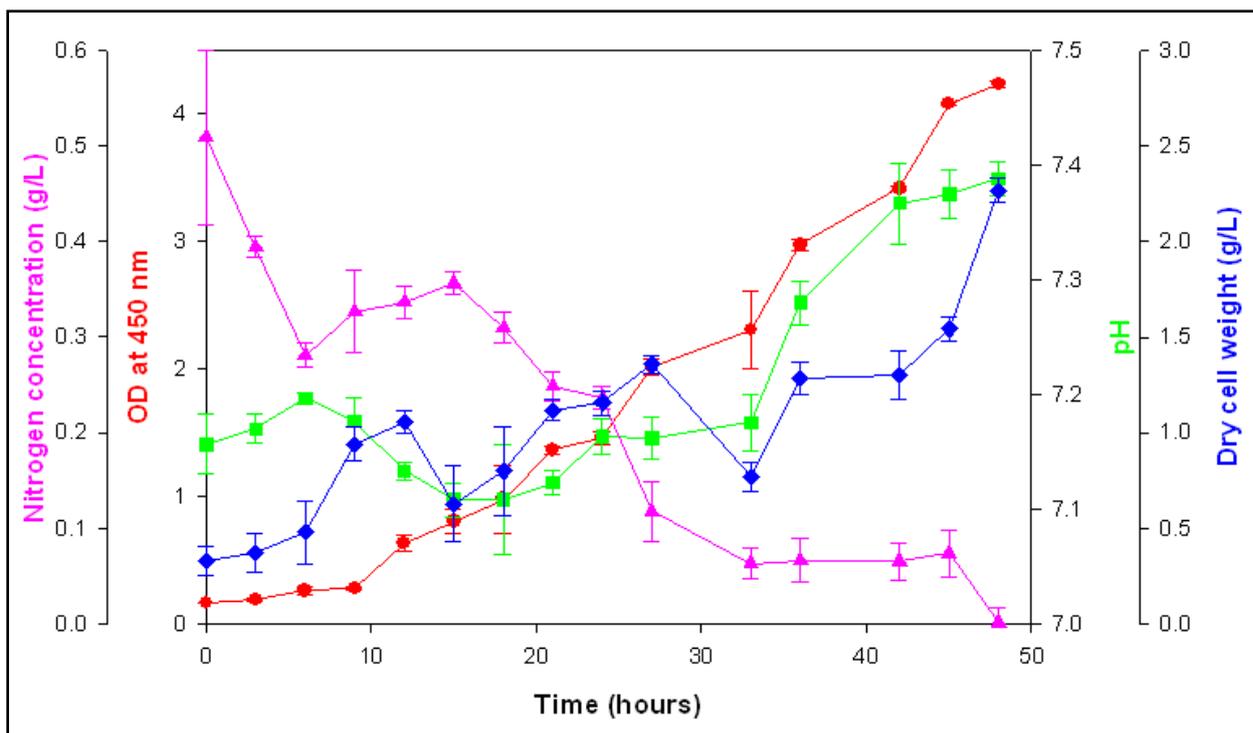
Figure 3.2: *A temporal profile of the fermentation of Pseudomonas mendocina CH50 using sodium nonanoate as the carbon source.* ●— *OD at 450 nm,* ■— *pH,* ◆— *Dry cell weight (g/L),* ▲— *Nitrogen concentration (g/L)*

3.2.2. Characterisation of polymers

Fourier Transform Infrared spectroscopy (FTIR)

Preliminary chemical characterisation of the P(3HO) and P(3HN-co-3HHP) produced using *P.mendocina CH50* was carried out by using ATR-FTIR (Figure 3.3). Presence of characteristic MCL-PHA-specific peaks at 1727.97 cm^{-1} and 1159.15 cm^{-1}, corresponding to the ester carbonyl bond and C-O stretching due to vibration was confirmed by the FTIR spectra of the polymer (Randriamahefa *et al*., 2003). In addition, the peaks at 2956, 2927.41 and 2857.97 cm^{-1} corresponded to the aliphatic C-H group of the polymer backbone while the peak at 3369 cm^{-1} indicated the presence of the hydroxyl group (Sánchez *et al.,* 2003).

(a)
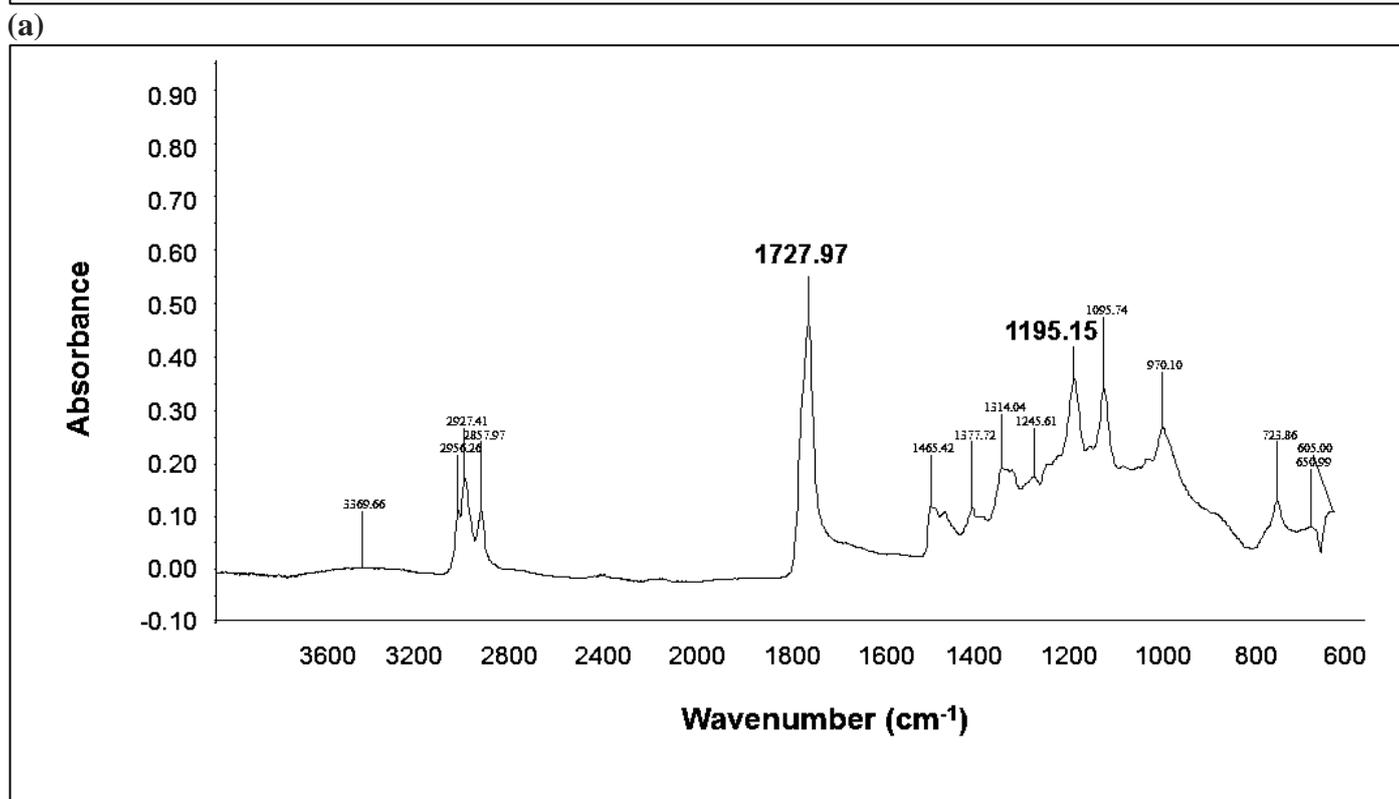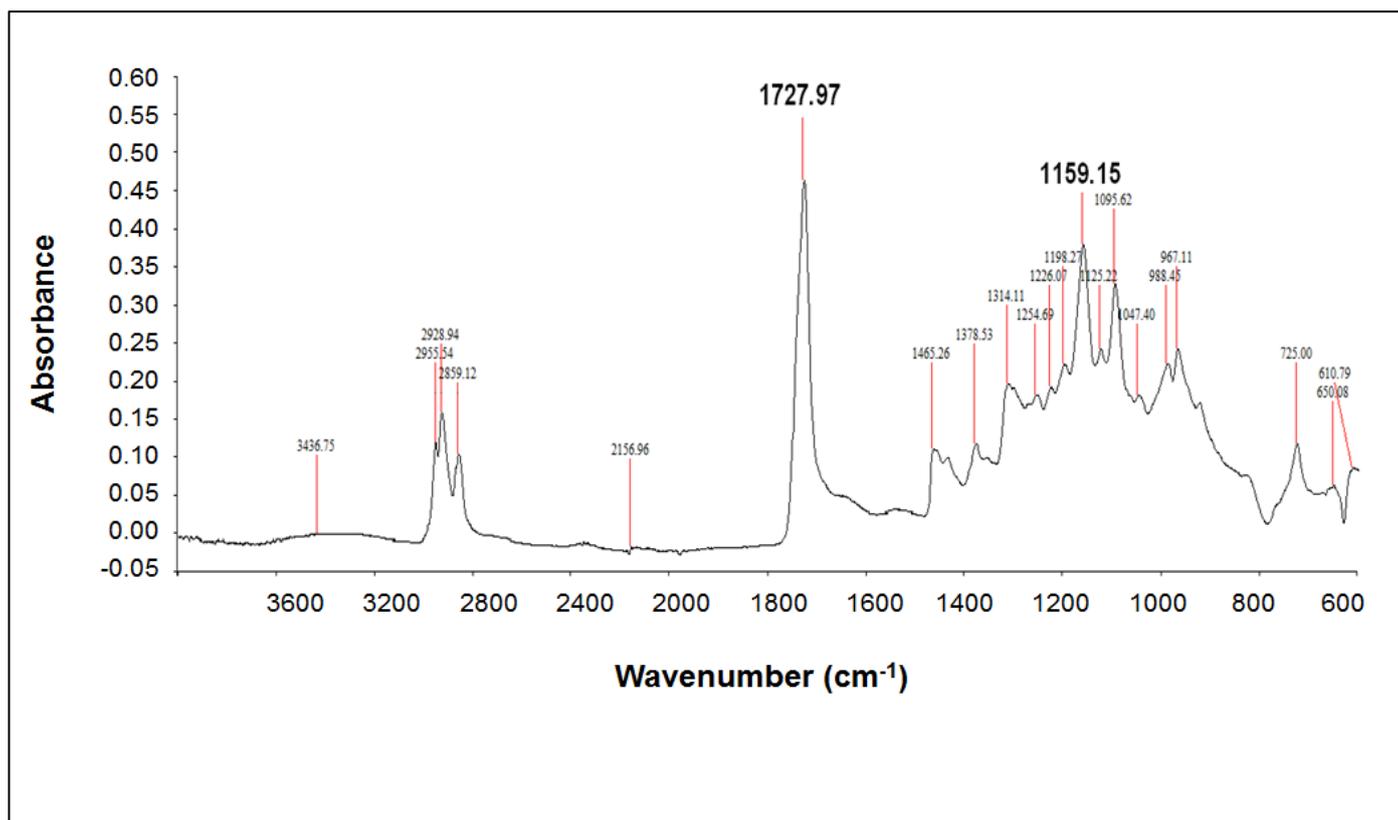
(b)

Figure 3.3: *FTIR spectra of the polymers. (a) P(3HO) and (b) P(3HN-co-3HHP) with major characteristic peaks at 1727 cm^{-1} for ester carbonyl bond and 1159 cm^{-1}C-O vibrational stretching.*

Nuclear Magnetic Resonance spectroscopy (NMR)

The structure of the MCL-PHA obtained from *P.mendocina CH50* when grown using sodium octanoate as the sole carbon source was confirmed using ^{1}H and ^{13}C NMR analysis. These spectra were analysed and the identification of the PHA was carried out by comparing the spectrum obtained with that of the NMR spectra of previously known PHAs. The spectra obtained in this case were identical to that obtained previously for P(3HO) as shown in Rai *et al.,*2010. In the ^{1}H NMR spectrum, five peaks were obtained as there are five different environments for the protons in P(3HO) as seen in Figure 3.4 (a) and (b). The ^{1}H NMR analysis showed the presence of protons bonded to C2 (-CH$_2$ group), C3 (-CH group), C4 (-CH$_2$ group), C5, C6, C7 (-CH$_2$ group) and C8(-CH$_3$ group) with chemical shifts of 2.5, 5.2, 1.6, 1.2 and 0.8 ppm respectively. In the ^{13}C NMR analysis, eight different peaks were obtained corresponding to the eight different environments for the carbon atoms in the molecule. The chemical shift at 169.38 ppm corresponded to C1 (carbon of ester group), 70.82 ppm to C3 (–CH group linked to electronegative oxygen of ester group), 39.08 to C2 (-CH$_2$ group), 23 – 35ppm to C4, C5, C6, C7 (-CH$_2$ groups) and 13.95 ppm to C8 (-CH$_3$). These observations confirmed that the MCL-PHA produced was P(3HO).

The polymer extracted from *P. mendocina CH50* grown in sodium nonanoate was also analysed similarly using the ^{1}H and ^{13}C NMR. The proton spectrum showed five different environments for the hydrogen in the polymer as shown in the Figure 3.5 (a) and (b). These spectra were compared with those seen in Rai *et al*., 2010. The peak at 5.2 ppm corresponded to protons bonded to C3 (-CH group), 2.5 ppm to C2 (-CH$_2$ group), 1.6 ppm to C4 (-CH$_2$ group), 1.2 ppm to C5 and C6 (-CH$_2$ group of 3HHP), C5, C6, C7, and C8 (-CH$_2$ group of 3HN) and 0.8 ppm to C7 (-CH$_3$ group of 3HHP) and C9 (-CH$_3$ group of 3HN). The ^{13}C spectrum, Figure 6(a), showed 10 peaks, corresponding to 10 different environments for the carbon in the extracted polymer. The chemical shift at 169.07 ppm corresponded to C1 (carbon of ester group), 71.01 ppm to C3 (–CH group), 39 to C2 (-CH$_2$ group), 33.5 to C4 (-CH$_2$ group), 32 ppm to C5, (-CH$_2$ group) 28.9 ppm to C6 (-CH$_2$ group of 3HHP), 27 ppm to C6 (-CH$_2$ group of 3HN), 25 ppm to C7 (-CH$_2$ group of 3HN), 22.5 ppm to C8 (-CH$_2$ group of 3HN), 13.5 ppm to C7 (-CH$_3$ group of 3HHP) and C9 (-CH$_3$ group of 3HN). Hence, it was concluded that the monomers present in the polymer were 3-hydroxyheptanoate and 3-hydroxynonanoate. Hence the copolymer produced was P(3HN-co-3HHP).

Hence, the ^{1}H and ^{13}C NMR spectra of the PHAs obtained using sodium octanoate and sodium nonanoate as the sole carbon source confirmed that the PHAs produced were poly(3-hydroxyoctanoate), P(3HO) and poly(3-hydroxynonanoate-co-3-hydroxyheptanoate) (P(3HN-co-3HHP)) .
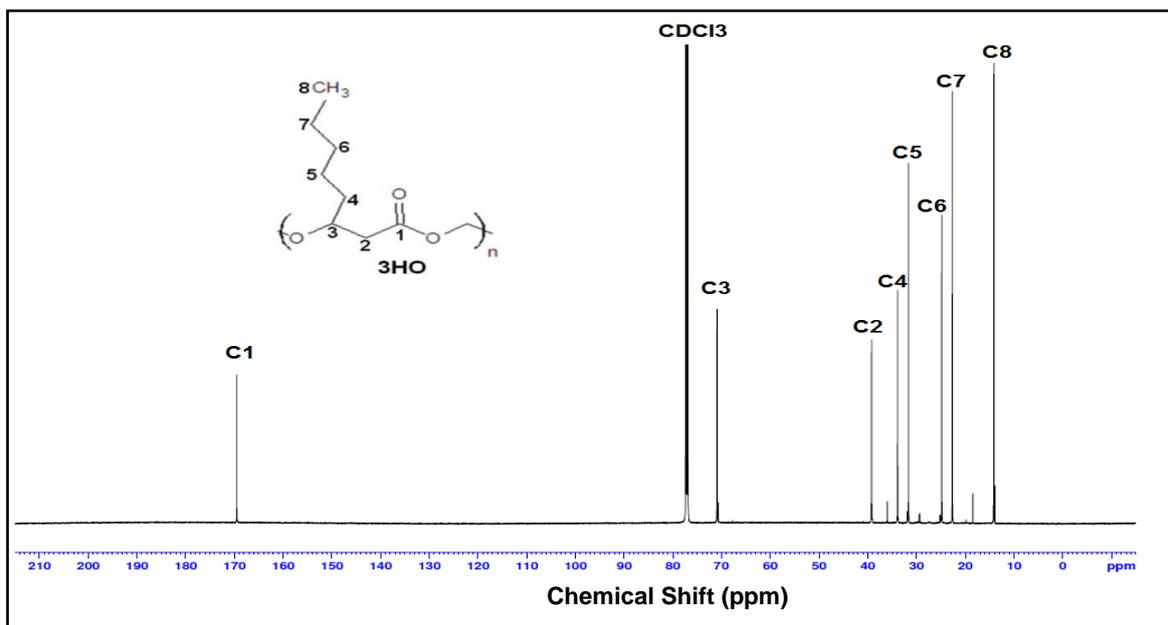
(a)
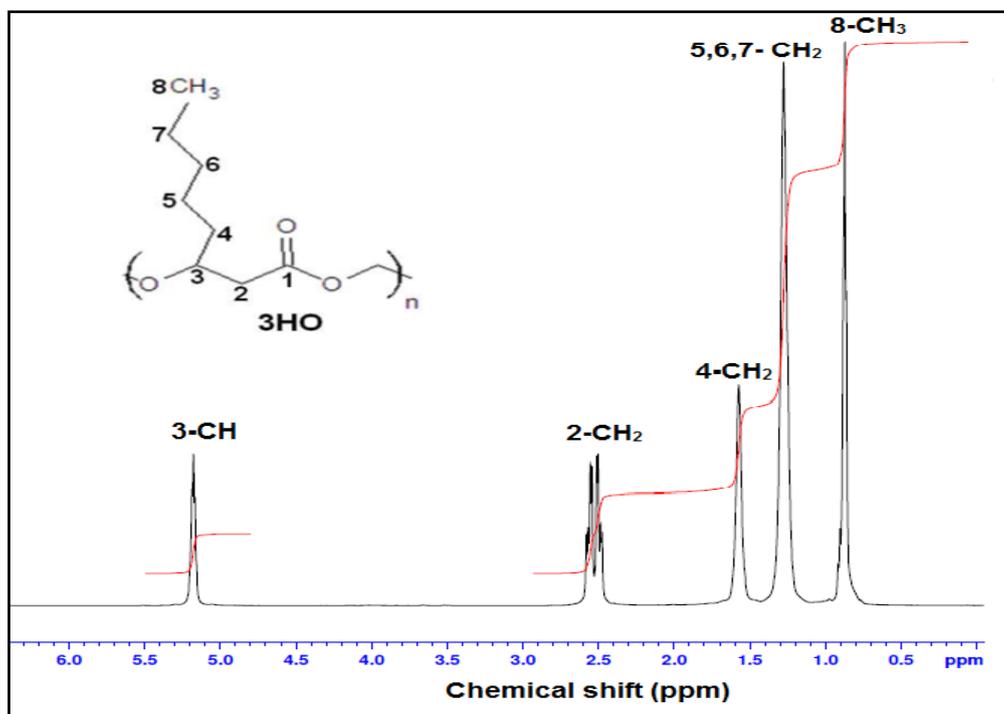
(b)

Figure 3.4: (a) The ^{13}C NMR of P(3HO). (b)The ^{1}H NMR of P(3HO) confirming the polymer to be the homopolymer P(3HO). The structure of P(3HO) is shown as an insert within the spectra.

62
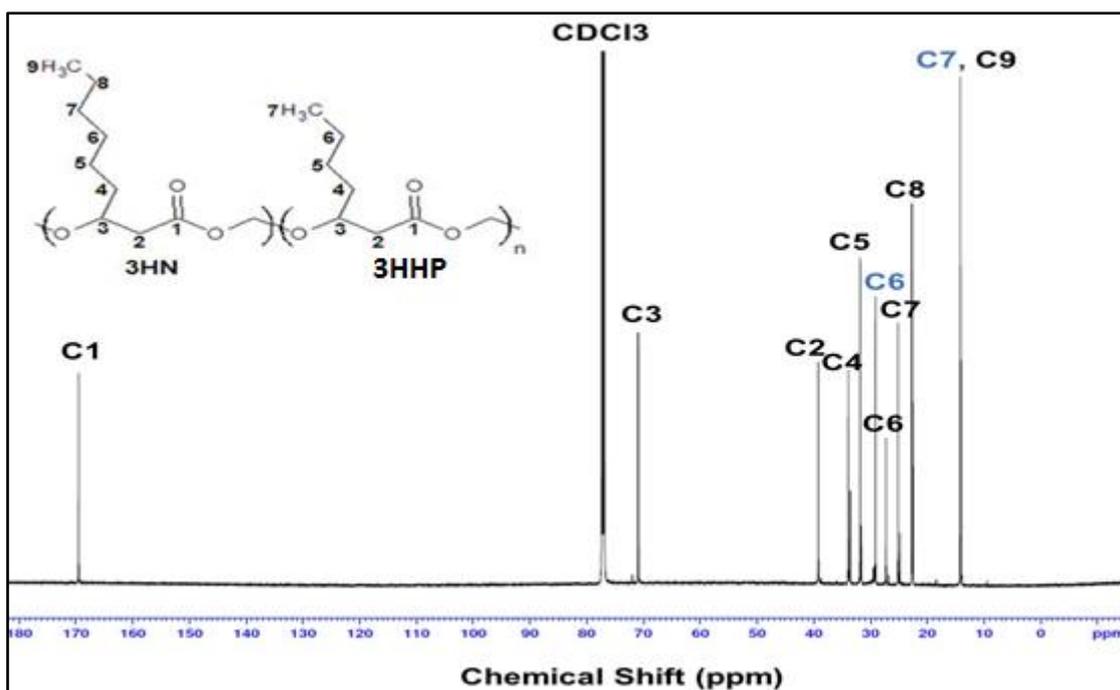
(a)
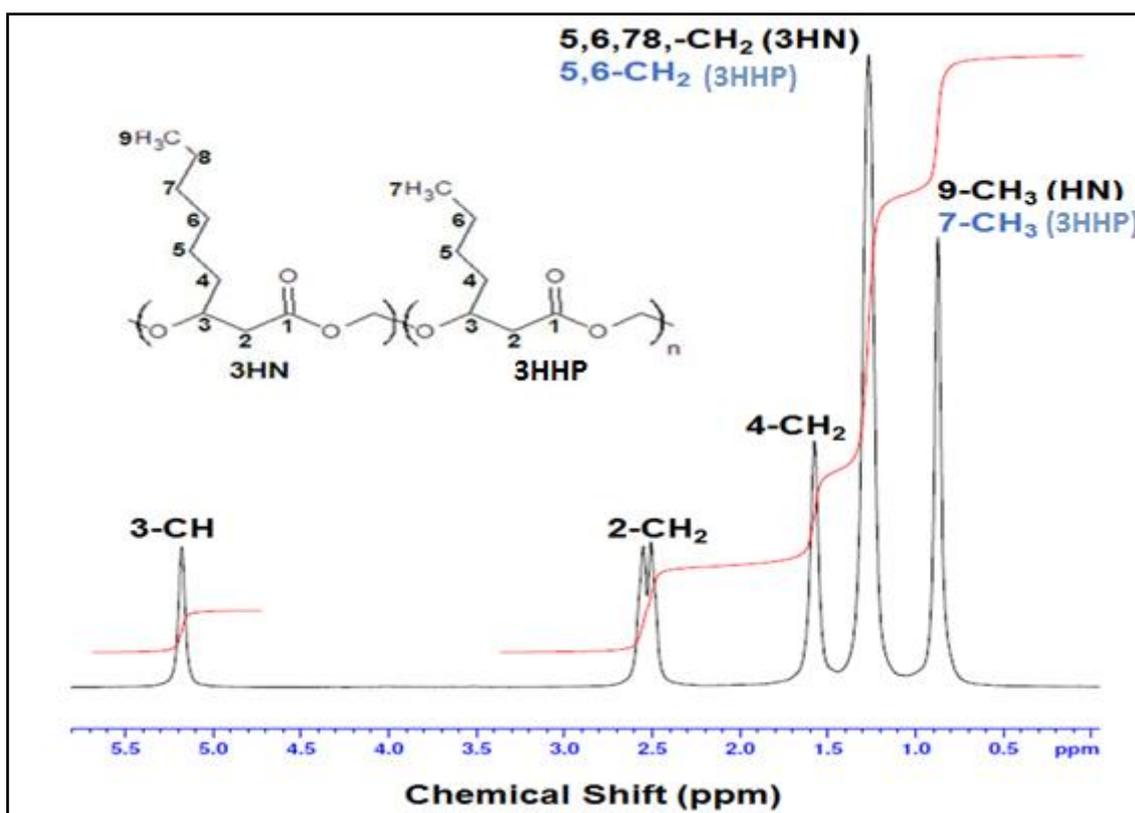
(b)

Figure 3.5: (a) The ^{13}C NMR of P(3HN-co-3HHP). (b)The ^{1}H NMR of P(3HN-co-3HHP) confirming the polymer to be the copolymer P(3HN-co-3HHP). The structure of P(3HN-co-3HHP) is shown as an insert within the spectra

Preparation of neat and blend 2D scaffolds using P(3HO) and P(3HN-co-3HHP) for use as cardiac patches

P(3HO) and P(3HN-co-3HHP) were blended together in different ratios and films were cast in perti dishes using solvent cast technology. These 2D scaffolds were prepared with different ratios of P(3HO) and P(3HN-co-3HHP) which are 100:0, 20:80, 50:50, 80:20 and 0:100, were air dried for 2 weeks and further freeze dried for a week. In this thesis, HO will be used to represent neat P(3HO) scaffolds, HO:HN(20:80) will be used to represent P(3HO):P(3HN-co-3HHP) (20:80) scaffolds, HO:HN(50:50) will be used to represent P(3HO):P(3HN-co-3HHP) (50:50) scaffolds, HO:HN(80:20) is used to represent P(3HO):P(3HN-co-3HHP) (80:20) scaffolds and HN will be used to represent P(3HN-co-3HHP) scaffolds.

Thermal properties of the different polymers

The thermal properties of neat P(3HO) and P(3HN-co-3HHP) were determined using differential scanning calorimetry (DSC) as explained in section 2.4. Differential scanning calorimetry (DSC) determines the heat released or absorbed by the material when it undergoes phase transformation. The material loses its rigid glassy properties and begins to behave as a rubbery polymer at its glass transition temperature, T_g (Sin *et al*., 2012, Liu *et al*., 1995). The T_g and melting temperature, T_m, for the neat polymers and the blends are shown in Table 3.1, Figure 3.6. It can be seen that P(3HO) and P(3HN-co-3HHP) are characterised by low T_g and, therefore, they are in a rubbery state at room and body temperatures. The T_g of P(3HN-co-3HHP) is slightly lower than P(3HO).

The glass transition temperature (T_g) and melting temperature (T_m) values of the P(3HO):P(3HN-co-3HHP) blends were found to be low, around -36.3ºC and -38.8 ºC respectively. Thus blending the homopolymer P(3HO) and copolymer P(3HN-co-3HHP) complicates the stacking of the monomer units. As a result, the free volume increases in polymer blends. The lowest T_g was observed for polymer blends with 50:50 of P(3HO) and P(3HN-co-3HHP) indicating that in this composition stacking is hindered and the largest free volume is achieved. The change in enthalpy (ΔH) at melting was also recorded. The enthalpy change gives an idea about the crystallinity of the substance and hence ΔH is directly proportional to the degree of crystallinity. From the results obtained, due to the high change in enthalpy (ΔH), P(3HO) was found to be the most crystalline material and P(3HO):P(3HN-co-3HHP) (20:80) was the least crystalline. On comparing only the blends, it was observed that with the increase in P(3HO) there was an observed increase in the ΔH and hence also the

degree of crystallinity, where P(3HO):P(3HN-co-3HHP) (20:80) was the least crystalline and P(3HO):P(3HN-co-3HHP) (80:20) was the most crystalline.

Table 3.1: *The T_g and T_m and ΔH values of the neat P(3HO), P(3HO):P(3HN-co-3HHP) (80:20), P(3HO):P(3HN-co-3HHP) (50:50), P(3HO):P(3HN-co-3HHP) (20:80) and neat P(3HN-co-3HHP) .*

Samples	T_g (°C)	T_m (°C)	ΔH (J/g)
P(3HO)	-36.3	59.3	20.3
P(3HO):P(3HN-co-3HHP) (80:20)	-36.6	59.3	17.2
P(3HO):P(3HN-co-3HHP) (50:50)	-38.8	57.8	16.4
P(3HO):P(3HN-co-3HHP) (20:80)	-37.8	55.0	12.0
P(3HN-co-3HHP)	-38.8	57.6	16.0
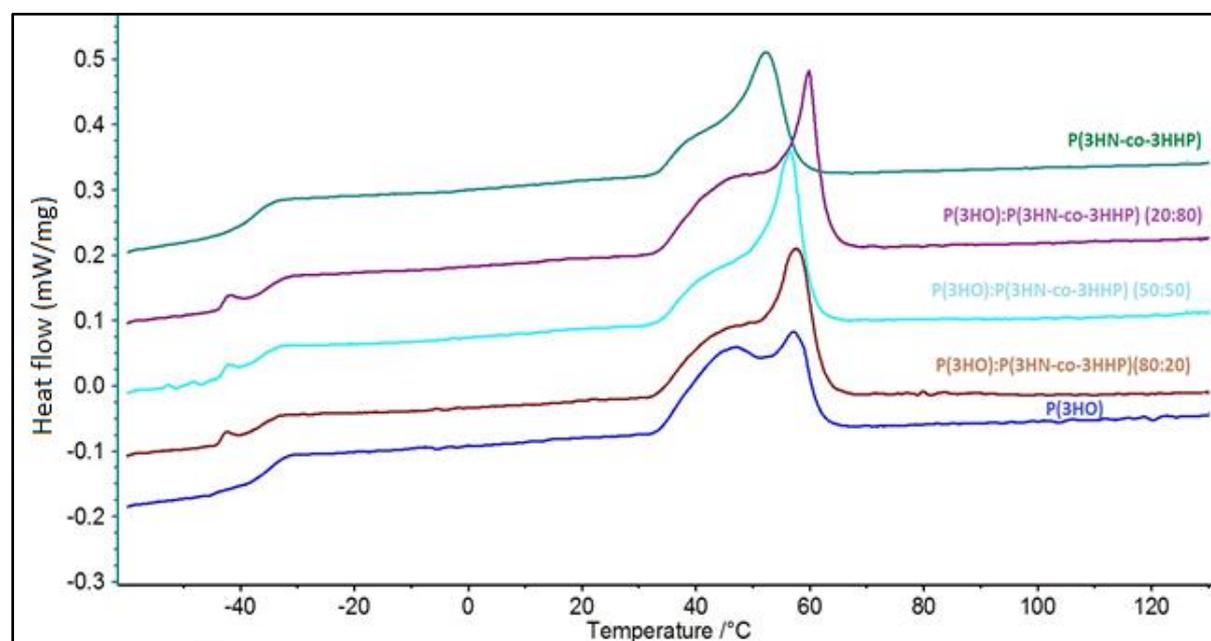
Figure 3.6: *DSC curves of the neat P(3HO), P(3HO):P(3HN-co-3HHP) (80:20), P(3HO):P(3HN-co-3HHP) (50:50), P(3HO):P(3HN-co-3HHP) (20:80) and neat P(3HN-co-3HHP)*

Mechanical Properties

The mechanical properties of the neat and the blend films were measured using the Instron as described in section 2.4. The tensile testing results are summarised in Table 3.2 and Figure 3.7. Both the neat polymers were found to be highly elastomeric in nature with an elongation at break value of around 700%. P(3HO) was found to be more stiff than P(3HN-co-3HHP), but these polymers had similar values of tensile strength. All the three blends were found to be stiffer and less elastomeric materials than the neat polymers with higher Young's modulus values and lower elongation at break values (Table 3.2, Figure 3.7). More than two times increase in stiffness was achieved for P(3HO):P(3HN-co-3HHP) (80:20) as compared to the neat P(3HO). Out of all the scaffolds, the 20:80 blend of P(3HO) and P(3HN-co-3HHP) was found to have the lowest tensile strength and stiffness. These results indicate that by combining and blending the two polymers it is possible to alter the mechanical properties of the neat polymers and achieve a scaffold of desirable mechanical values.

Table 3.2: Mechanical properties of the solvent cast neat polymer and polymer blend scaffolds; including Young's modulus, tensile strength and elongation at break (n=5).

Samples	Young's modulus (E value) (MPa)	Tensile strength (MPa)	Elongation at break (%)
P(3HO)	8.6±1.0	10.4±2.6	700±100
P(3HO):P(3HN-co-3HHP) (80:20)	20.0±1.6	12.0±1.6	440±30
P(3HO):P(3HN-co-3HHP) (50:50)	12.2±0.8	9.7±1.9	500±70
P(3HO):P(3HN-co-3HHP) (20:80)	11.8±1.0	8.3±0.8	510±25
P(3HN-co-3HHP)	5.3±0.5	10.4±1.8	650±60
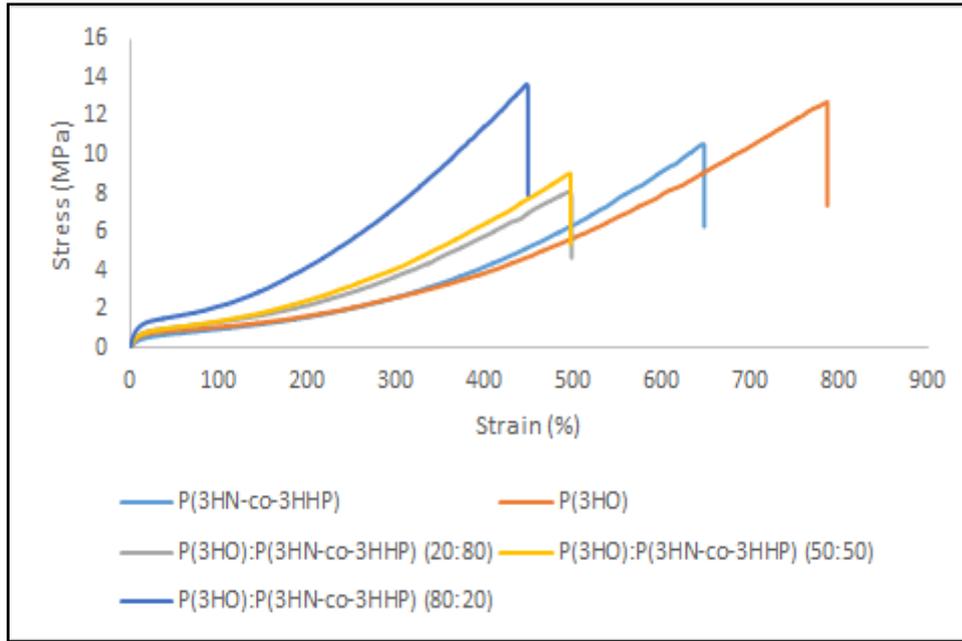
Figure 3.7: *Stress vs Strain graph depicting the mechanical properties of the neat P(3HO), P(3HO):P(3HN-co-3HHP) (80:20), P(3HO):P(3HN-co-3HHP) (50:50), P(3HO):P(3HN-co-3HHP) (20:80) and neat P(3HN-co-3HHP) (n=5)*

Wettability analysis

The surface hydrophilicity / hydrophobicity of the films was determined by measuring the water contact angle of the films (Table 3.3). Polymer films with θ values less than $70°$ are considered to be hydrophilic in nature whereas θ values greater than $70°$ are considered to be hydrophobic in nature (Wang *et al.,* 2008). All the scaffolds had almost similar water contact angle values as shown in Table 3.3.

Table 3.3: *Table depicting water contact angle values (θ) of the neat P(3HO), P(3HO):P(3HN-co-3HHP) (80:20), P(3HO):P(3HN-co-3HHP) (50:50), P(3HO):P(3HN-co-3HHP) (20:80) and neat P(3HN-co-3HHP) films. (n=9).*

Samples	Water contact angle (º)
P(3HO)	101.1±1.5
P(3HO):P(3HN-co-3HHP) (80:20)	100.7±5.0
P(3HO):P(3HN-co-3HHP) (50:50)	94.9±4.6
P(3HO):P(3HN-co-3HHP) (20:80)	99.1±5.6
P(3HN-co-3HHP)	97.7±4.8

Scanning electron microscopy

The surface analysis of the neat and blend films revealed that both neat and blend films had a smooth, uniform and regular surface (Figure 3.8). These results were similar to that of Rai *et al.,* 2011, where P(3HO) films were described to be smooth and without any grooves.
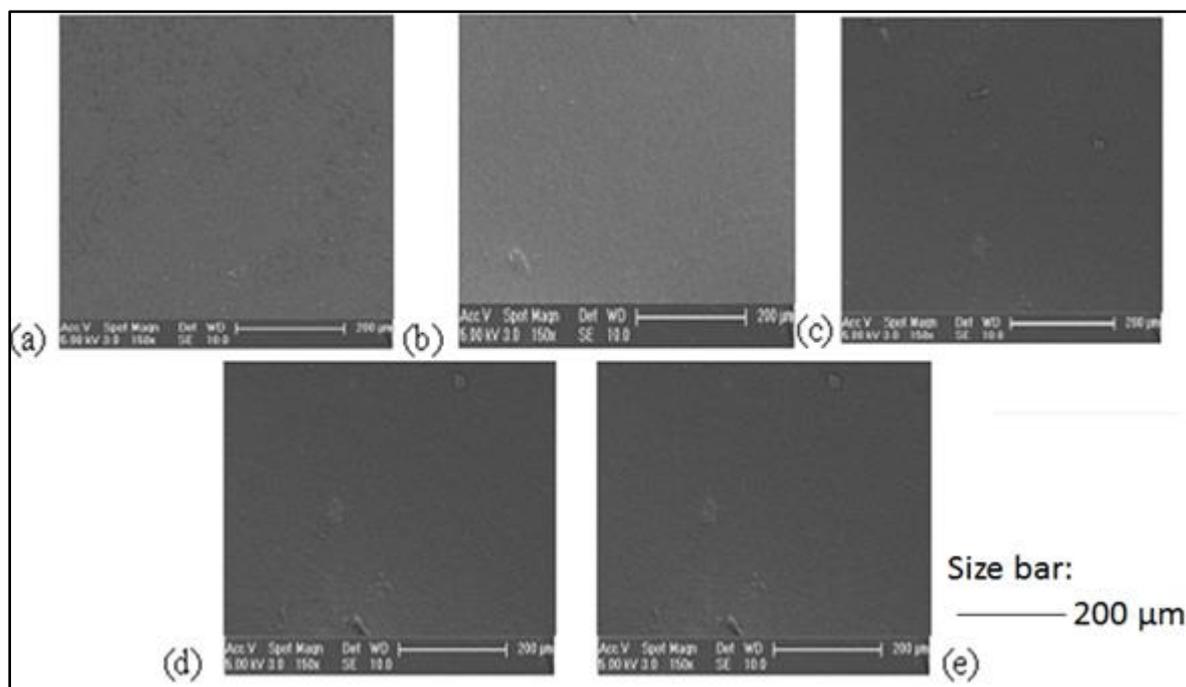
Figure 3.8: *SEM images of the scaffolds: (a) Neat P(3HO) scaffold, (b) Neat P(3HN-co-3HHP) scaffold, (c) P(3HO):P(3HN-co-3HHP) blend (80:20), (d) P(3HO)/P(3N-co-3HHP) blend (50:50) and (e) P(3HO)/P(3N-co-3HHP) blend (20:80).*

3.2.3. *In vitro* degradation study

In vitro degradation study was carried out for the neat and blend P(3HO) and P(3HN-co-3HHP) polymer films. The film strips were cut and immersed in 1 ml of PBS. Measurements at specific time periods of 1, 2 and 3 months. % Water uptake, % weight loss, and pH change were measured.

Water uptake of the degrading films

The film strips were immersed in PBS and the strips were weighed after wiping the excess PBS. The water uptake was measured as explained in section 2.4. The final % water uptake was recorded for a period of 3 months and was observed to increase in the following order (Figure 3.9): P(3HO):P(3HN-co-3HHP) (80:20) 2.5% < P(3HO):P(3HN-co-3HHP) (50:50) 2.88% < P(3HN-co-3HHP) (HN) 2.92% < P(3HO):P(3HN-co-3HHP) (20:80) 3.57% < P(3HO) 4.14%.
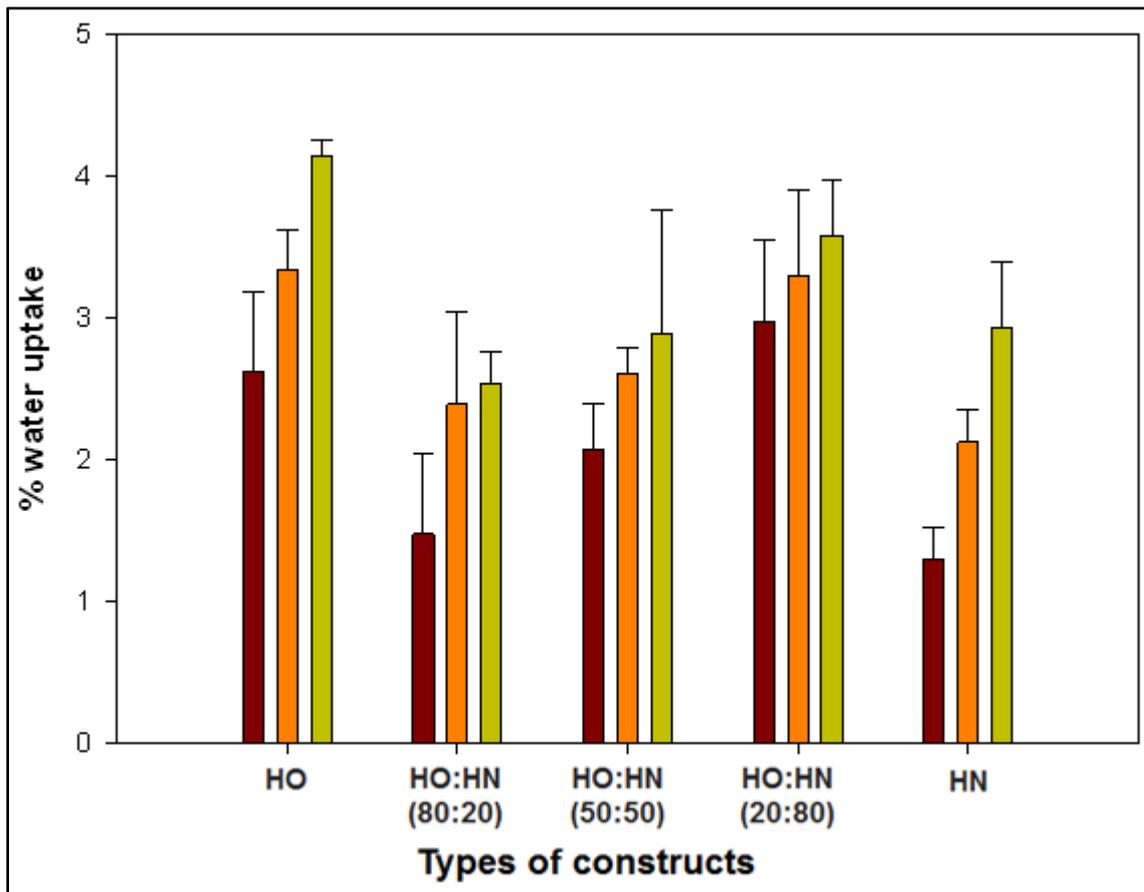
Figure 3.9: *Water uptake by the neat P(3HO), neat P(3HN-co-3HHP), P(3HO):P(3HN-co-3HHP) blend film (80:20), P(3HO):P(3N-co-3HHP) blend film (50:50) and P(3HO):P(3HN-co-3HHP) blend film (20:80) during the degradation study in PBS media for a period of 3 months. (n=3), no significant difference, ANOVA. HO is used to represent the neat P(3HO) scaffolds, HO:HN(20:80) is used to represent P(3HO):P(3HN-co-3HHP) (20:80) scaffolds, HO:HN(50:50) is used to represent P(3HO):P(3HN-co-3HHP) (50:50) scaffolds, HO:HN(80:20) is used to represent P(3HO):P(3HN-co-3HHP) (80:20) scaffolds and HN is used to represent the P(3HN-co-3HHP) scaffolds. This nomenclature will be used in all the figures in this thesis. ▰ represents 1ˢᵗ month, ▰ represents 2ⁿᵈ month and ▰ represents 3ʳᵈ month.*

Weight loss of the degrading films

The wet strips were dried by keeping them in an incubator at 37ºC for 2 days. The weight loss was calculated as mentioned in section 2.4. The final % weight loss observed (Figure 3.10), by the end of 3 months, was observed to decrease in the following order P(3HO):P(3HN-co-3HHP) (20:80) > P(3HO) > P(3HN-co-3HHP) > P(3HO):P(3HN-co-3HHP) (50:50) > P(3HO):P(3HN-co-3HHP) (80:20).
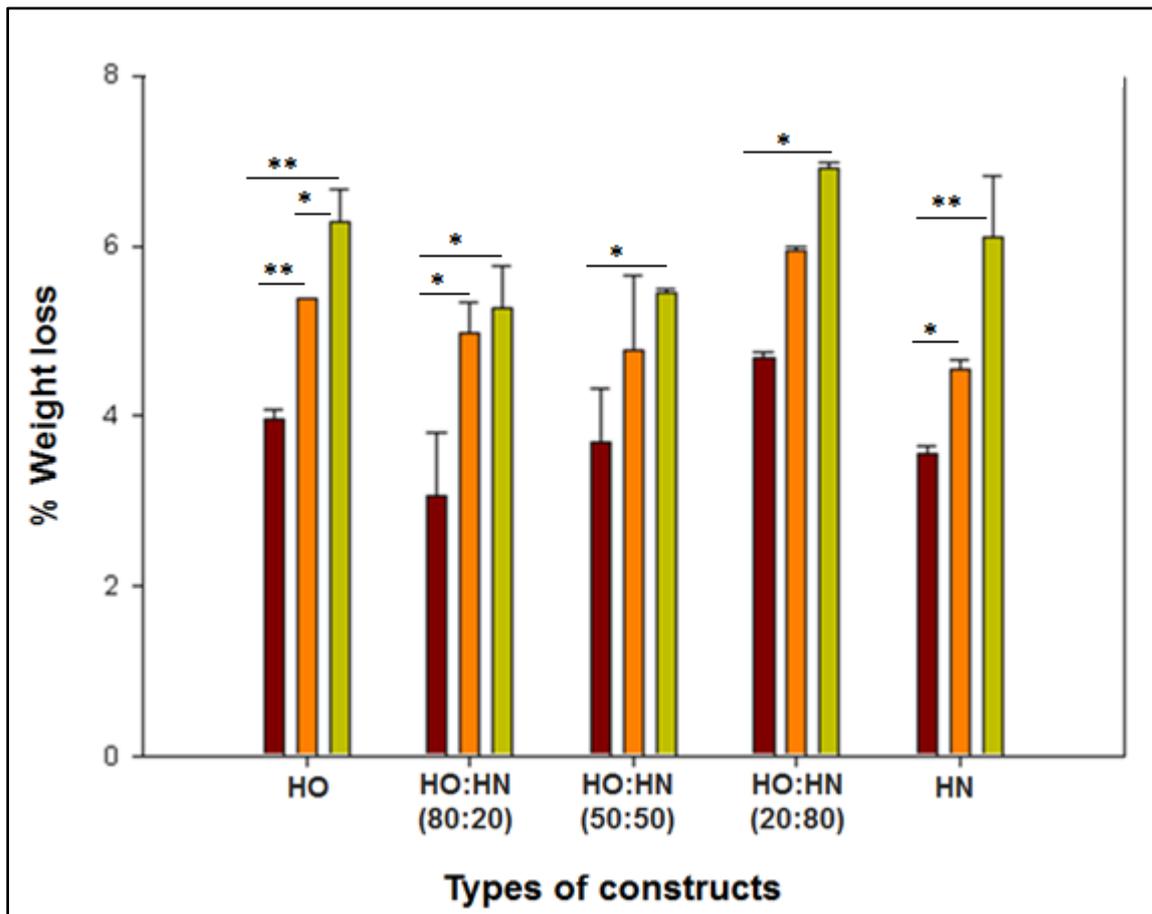
Figure 3.10: *Weight loss by the degrading neat P(3HO) scaffold, P(3HO):P(3HN-co-3HHP) blend scaffold (80:20), P(3HO):P(3HN-co-3HHP) blend scaffold (50:50), P(3HO):P(3HN-co-3HHP) blend scaffold (20:80)and neat P(3HN-co-3HHP), in PBS media for a period of 3 months. (n=3), *p<0.05,**p<0.001, ANOVA.* �represents 1ˢᵗ month,* represents 2ⁿᵈ month and* represents 3ʳᵈ month.*

pH measurements of the degrading films

The pH was also recorded by measuring the pH of PBS at the specified time points of 1, 2 and 3 months as explained in section 2.4. The pH of the media in all the films was observed to decrease in the course of 3 months from 7.4 to around 6.9. All the films recorded a similar final pH of around 6.9 (Figure 3.11).
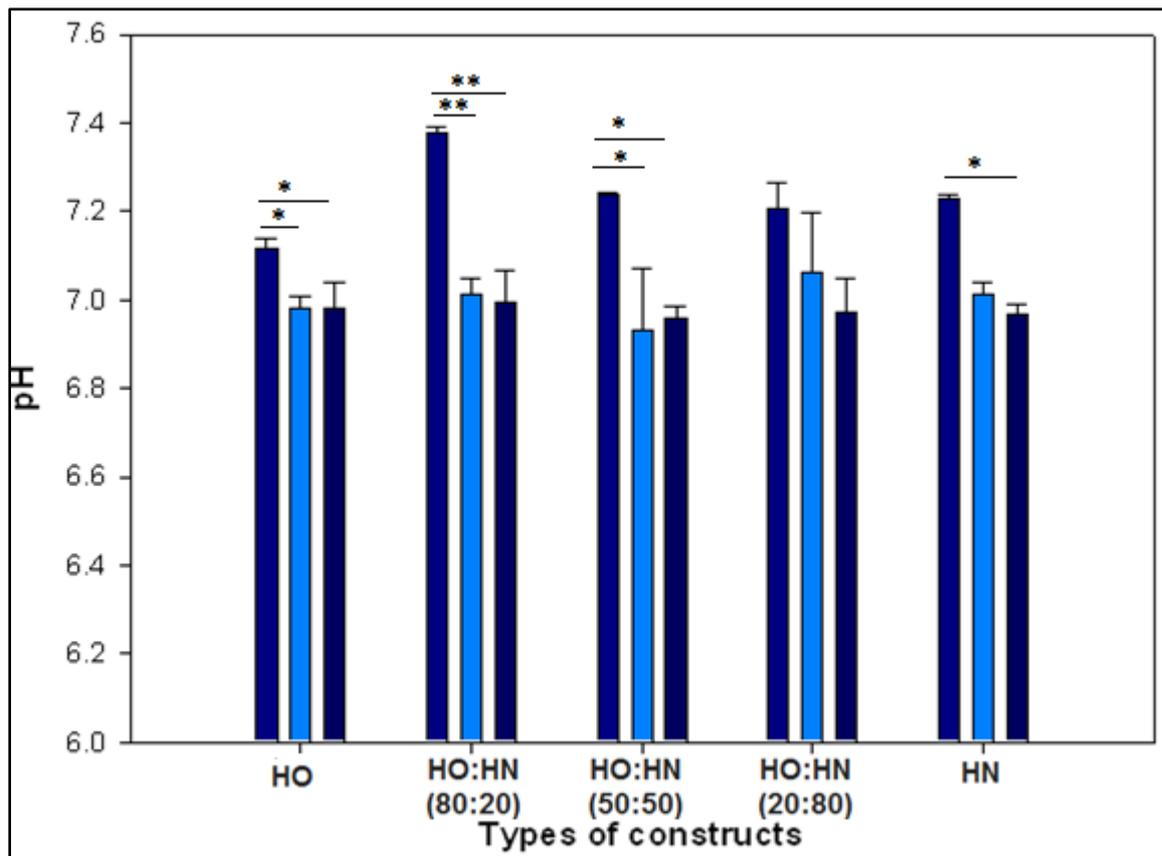
Figure 3.11: *pH measurements of neat P(3HO), P(3HO):P(3HN-co-3HHP) blend scaffold (80:20), P(3HO):P(3HN-co-3HHP) blend scaffold (50:50), P(3HO):P(3HN-co-3HHP) blend scaffold (20:80) and neat P(3HN-co-3HHP) during the degradation study in PBS for a period of 3 months. (n=3), *p<0.05,**p<0.001, ANOVA..* ▬ *represents 1ˢᵗ month,* ▬ represents 2ⁿᵈ month, ▬ represents 3ʳᵈ month.*

3.2.4. *In vitro* biocompatibility study by growing induced pluripotent stem cell derived cardiomyocytes (iPSC-CMs)

The human induced pluripotent stem cell derived cardiomyocytes (hiPSC-CMs) were seeded on coverslips coated with P(3HO), P(3HN-co-3HHP) and the blends of the two polymers. The cells were simultaneously also seeded on 0.1% gelatin which was used as positive control. The cells were analysed on day 14 for various parameters including cell viability using Live/Dead assay, phenotypic analysis (structural similarity as compared to control) by immunofluorescence staining, beating rates, calcium transient analysis, sarcomere length and nuclear density.

Live and dead assay

The live and dead assay was conducted on day 14 on the positive control (gelatin), P(3HO), P(3HN-co-3HHP) and the blend scaffolds (Figure 3.12). The live cells took up the dye and

fluoresced, exhibiting green colour while the dead cells exhibited red colour. It was observed that the cells on both, the gelatin and PHA scaffolds showed large patches of live (green) cells as compared to the dead (red) cells and exhibited uptake of the dye. hiPSC-CMs were cultured for 14 days on the neat and blend films of P(3HO) and P(3HN-co-3HHP). The number of live and dead cells remained unchanged on the scaffolds indicating they were all suitable for cardiac tissue engineering (Figure 3.13).
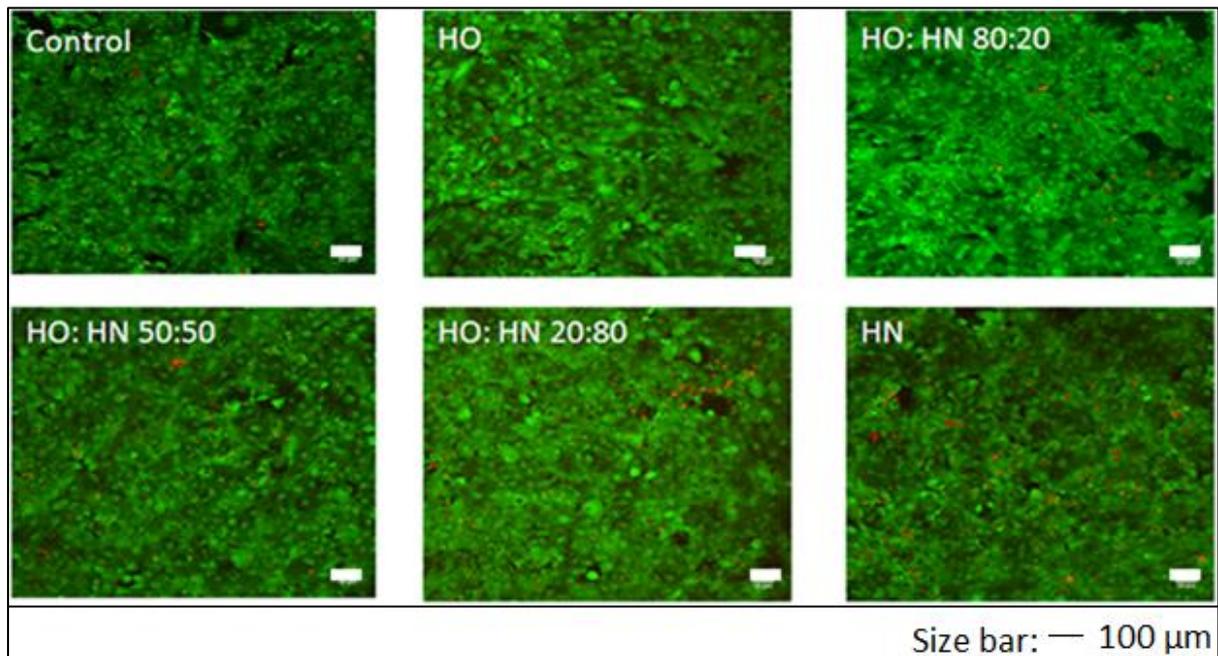
Figure 3.12: *Representative images of hiPSC-CMs on control gelatin, neat P(3HO), P(3HO):P(3HN-co-3HHP) 80:20, P(3HO):P(3HN-co-3HHP) 50:50, P(3HO):P(3HN-co-3HHP) 20:80, neat P(3HN-co-3HHP). The green indicator is Calcein AM that designates live cells and red indicator is Ethidium homodimer-1 that designates dead cells.*
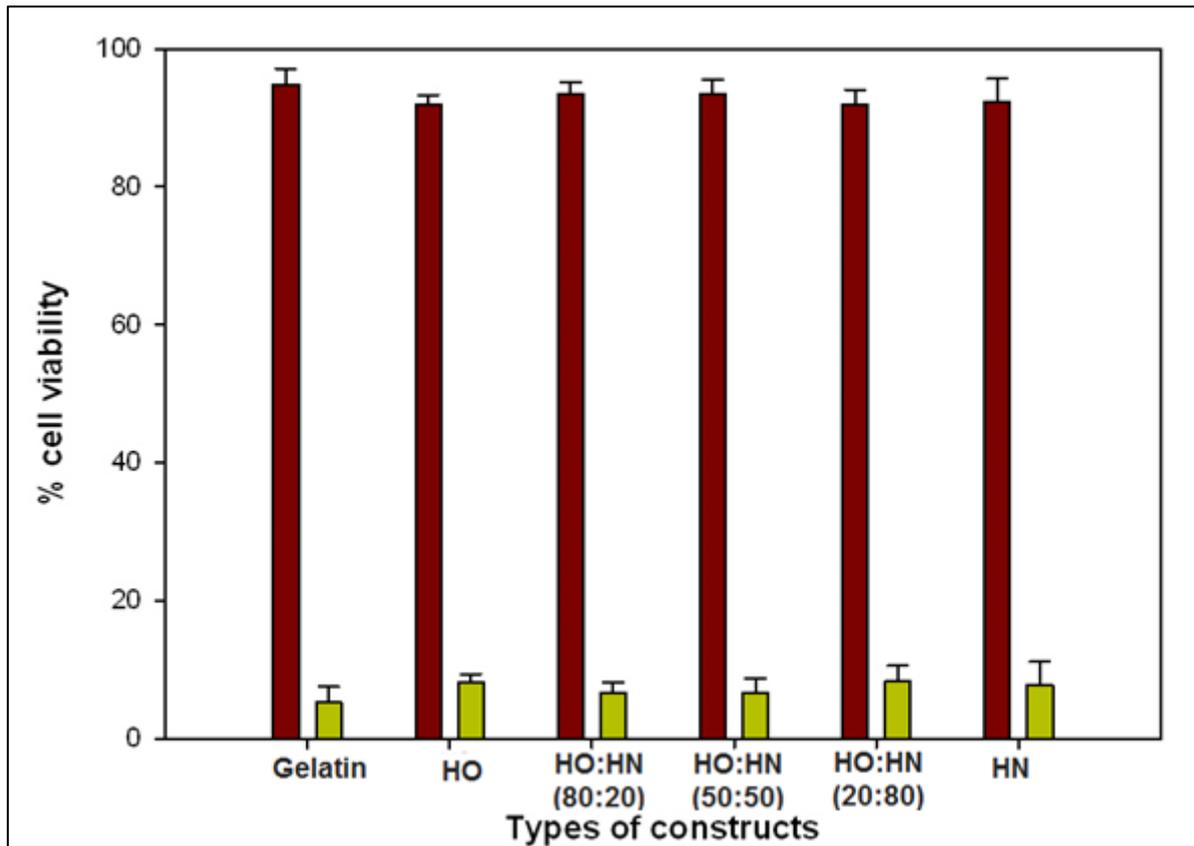
Figure 3.13: *Quantification of the cell viability of live* ▇ *and dead* ▭ *cells on the polymer blends including gelatin as positive control, P(3HO), P(3HO):P(3HN-co-3HHP) (80:20), P(3HO):P(3HN-co-3HHP) (50:50), P(3HO):P(3HN-co-3HHP) (20:80), P(3HN-co-3HHP) (n=6), no significant difference, ANOVA.*

Beat rate measurement

Each polymer blend has a different elasticity, which could impact the hiPSC-CM phenotype, hence beat rate measurements were made. There was a significant increase in the beat rate of hiPSC-CMs cultured on the more elastic P(3HN-co-3HHP) scaffold in comparison to gelatin or P(3HO). The beat rate of cells grown on all the other PHA scaffolds were comparable to that on gelatin, positive control (Figure 3.14).
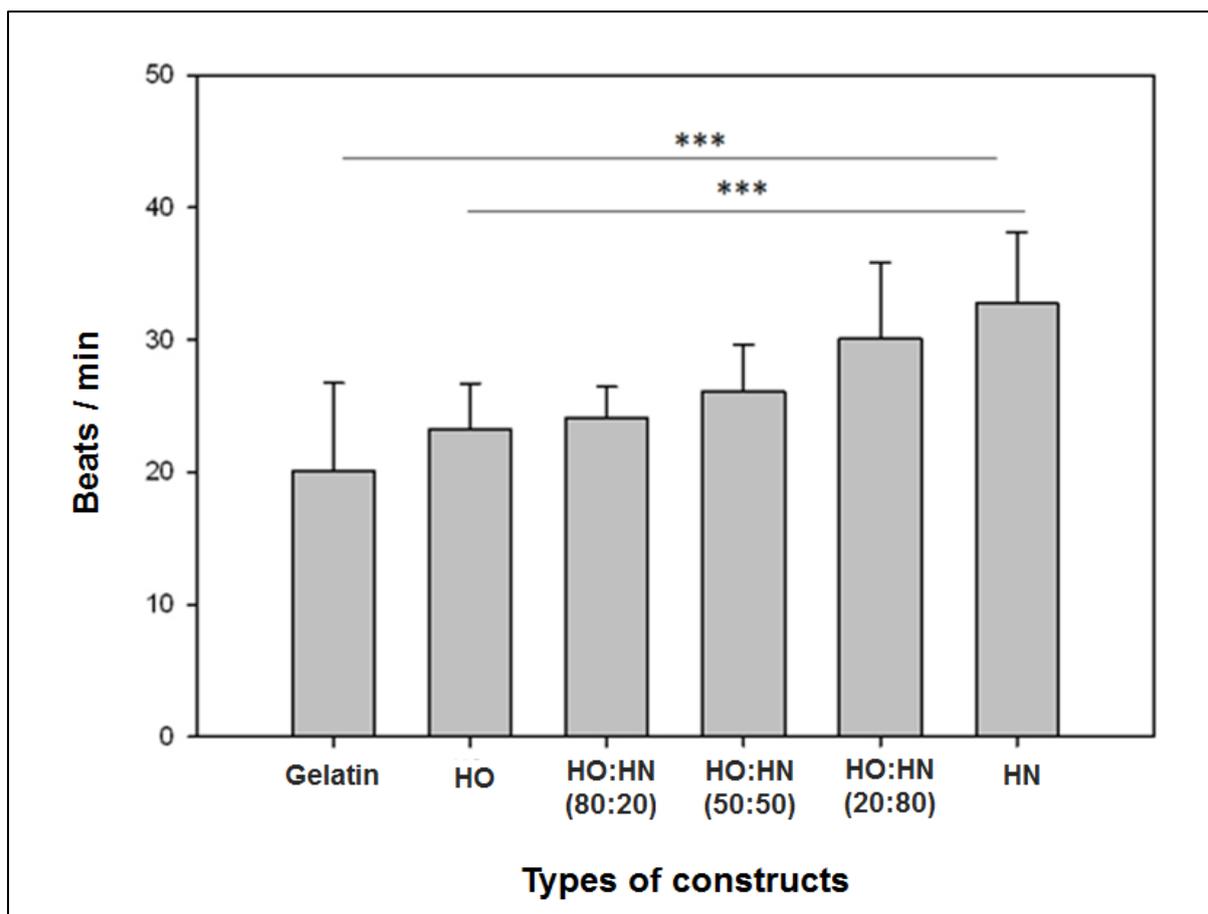
Figure 3.14: *Quantification of the number of beats per minute on the polymer blends including gelatin as positive control, P(3HO), P(3HO):P(3HN-co-3HHP) (80:20), P(3HO):P(3HN-co-3HHP) (50:50), P(3HO):P(3HN-co-3HHP) (20:80), P(3HN-co-3HHP). (n=6, *** p<0.001, ANOVA)*

Calcium transient studies

The effect of calcium transients on the contractions of hiPSC-CM was also studied on all the scaffolds and different parameters were analysed. These experiments were conducted along with Ms. Eleanor Humphrey at National Lung and Heart Institute (NHLI), Imperial College. At 1Hz stimulation, it was observed that there was a significant decrease in the fluorescent amplitude and time to transient peak in hiPSC-CMs cultured on P(3HN-co-3HHP) as compared to gelatin and P(3HO) (Figure 3.15(a)). The time to decay 50% was similar for all the scaffolds and the time to decay 90% was observed to be significantly lower for P(3HO) in comparision with control gelatin. At the 1.5Hz stimulation, the time to transit peak in hiPSC-CMs cultured on P(3HN-co-3HHP) was lower than that observed on control gelatin and P(3HO). Also, the value observed for P(3HO) was lower than that observed on gelatin (Figure 3.15(b)). However, there was no significant change observed in fluorescent amplitude, time to 50% decay and time to 90% decay.
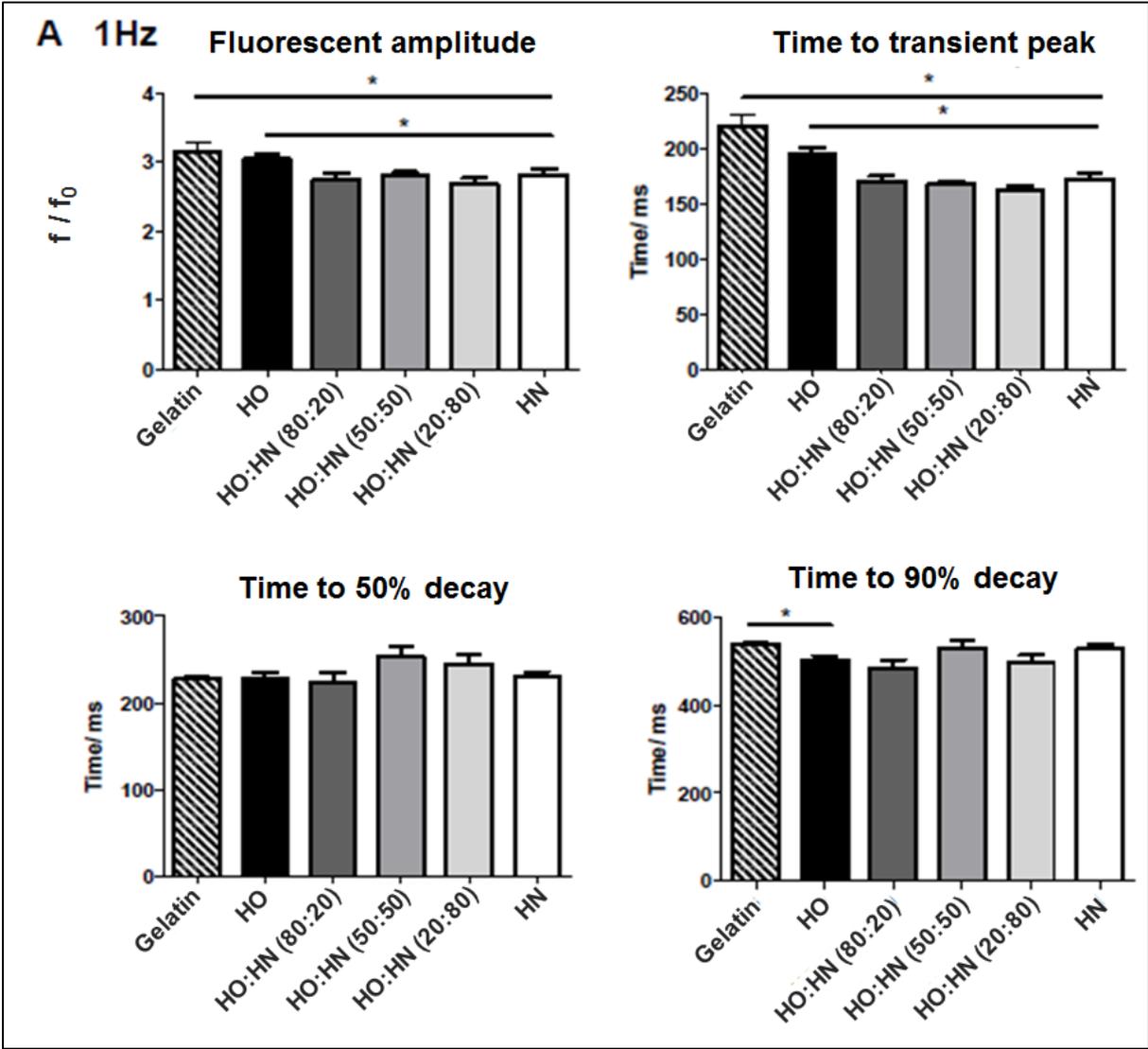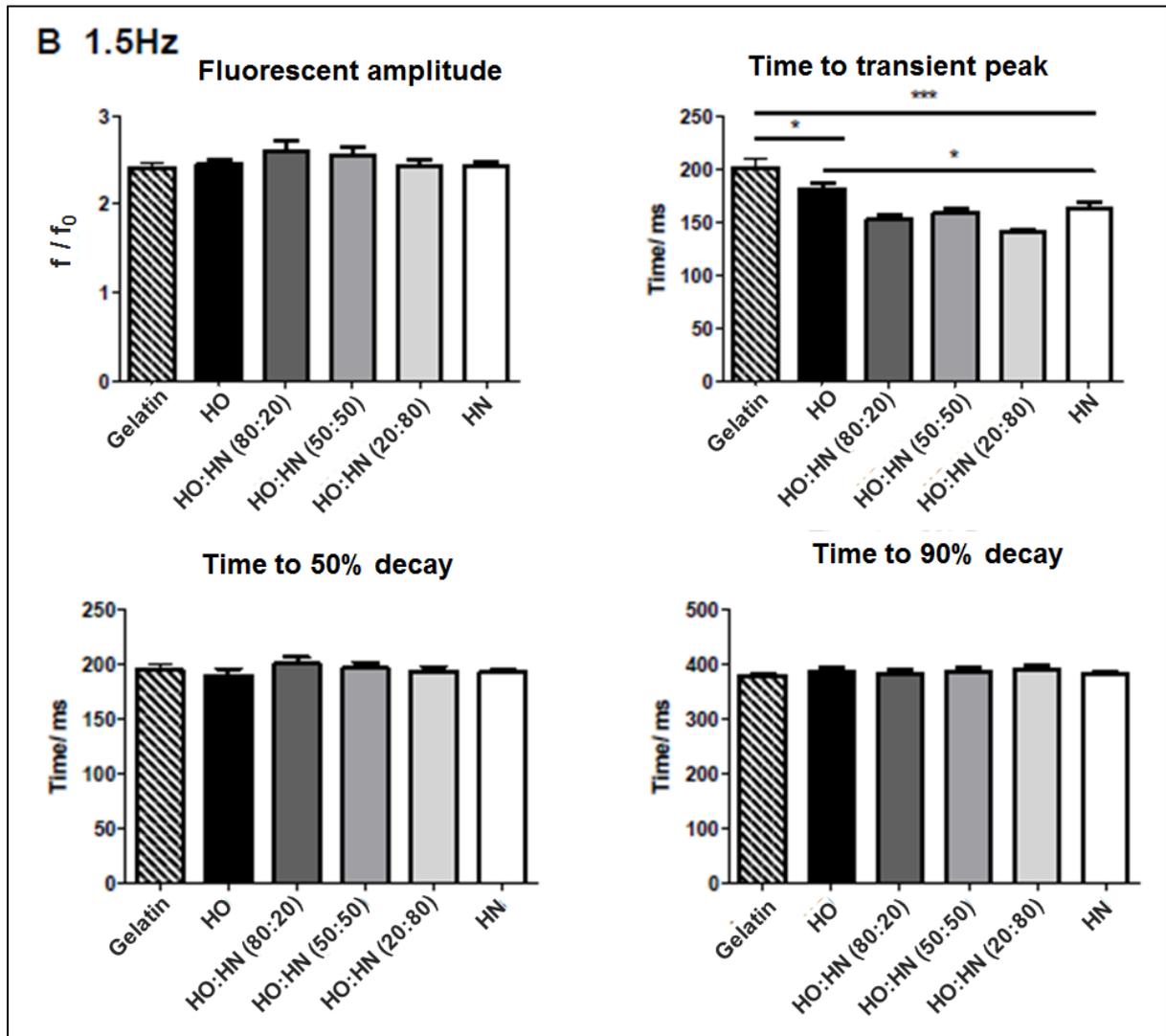
Figure 3.15: *Fluorescence amplitude (f/ f_0), time to peak (T_p), time to 50% decay (T_{50}) and 90% decay (T_{90}) of the calcium transient in cells field stimulated at (A) 1Hz and (B) 1.5 Hz. (n= 6), * p<0.05, *** p<0.001, ANOVA.*

Sarcomere length and nuclei density

The ultrastructure of the cells were analysed by studying the length of the sarcomeres and the nuclei density. This work was also conducted along with Ms. Eleanor Humphrey at National Lung and Heart Institute (NHLI), Imperial College. There was a significant increase in the nuclei density in hiPSC-CMs grown on P(3HN-co-3HHP) compared to gelatin and P(3HO) (Figure 3.16). No significant difference in sarcomere length was observed. The length of the sarcomeres observed in all the scaffolds was around 2µm. (Figure 3.17 and Figure 3.18).
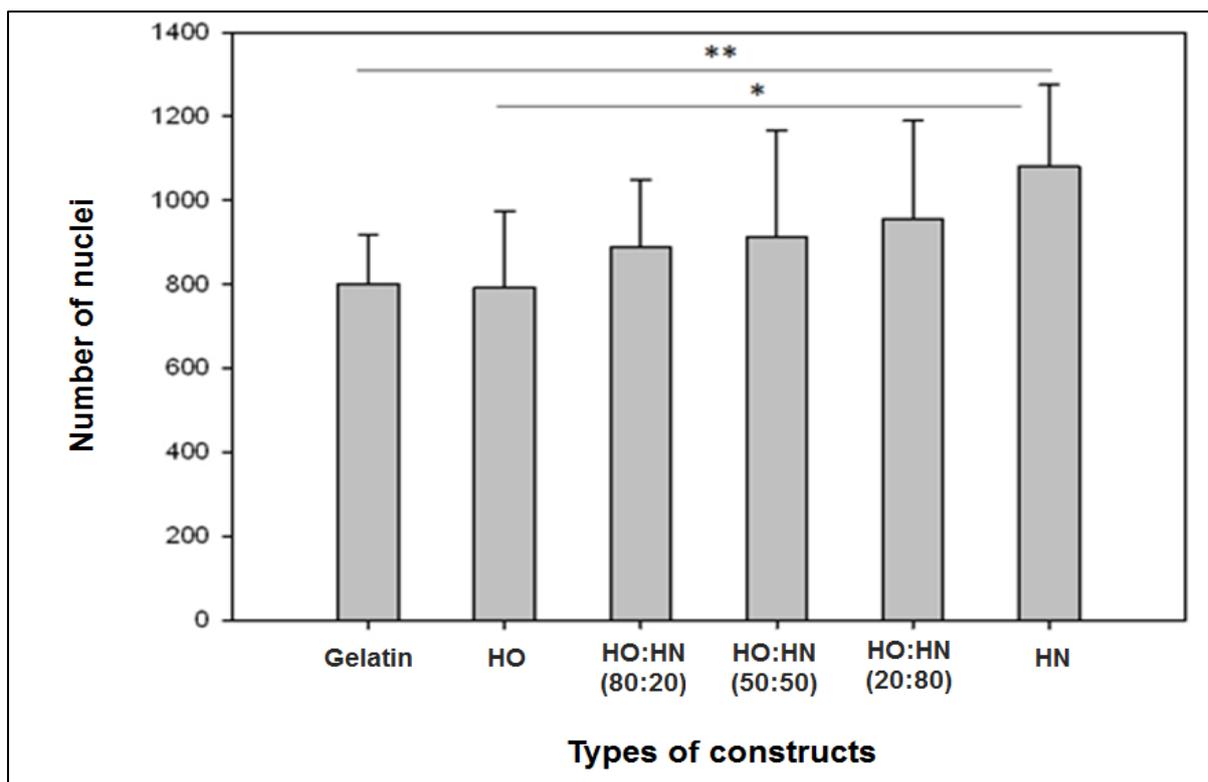
Figure 3.16: *Quantification of the nuclei density in hiPSC-CMs on polymer blends including control, P(3HO), P(3HO):P(3HN-co-3HHP) (80:20), P(3HO):P(3HN-co-3HHP) (50:50), P(3HO):P(3HN-co-3HHP) (20:80), P(3HN-co-3HHP) (n=6, * p<0.05, **p<0.01, ANOVA).*
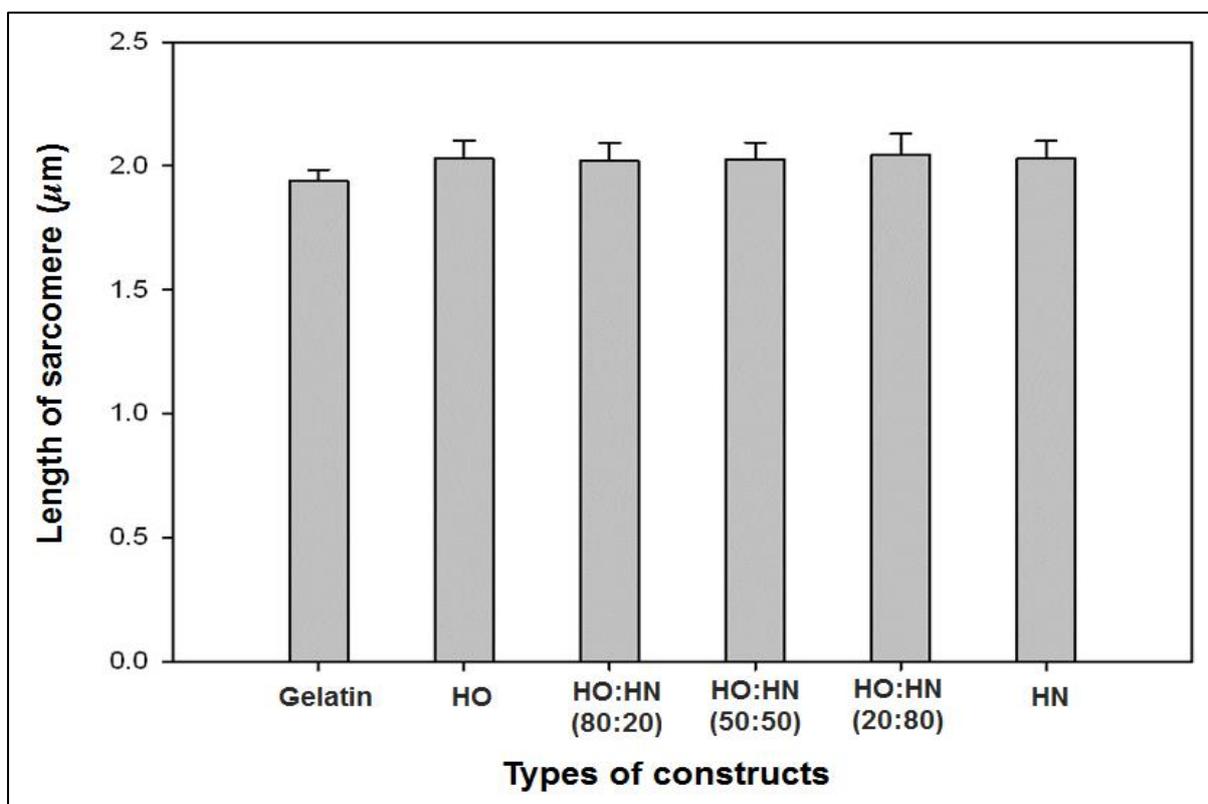
Figure 3.17: *Quantification of the sarcomere length in hiPSC-CMs on polymer blends including control, P(3HO), P(3HO):P(3HN-co-3HHP) (80:20), P(3HO):P(3HN-co-3HHP) (50:50), P(3HO):P(3HN-co-3HHP) (20:80), P(3HN-co-3HHP) (n=6).*
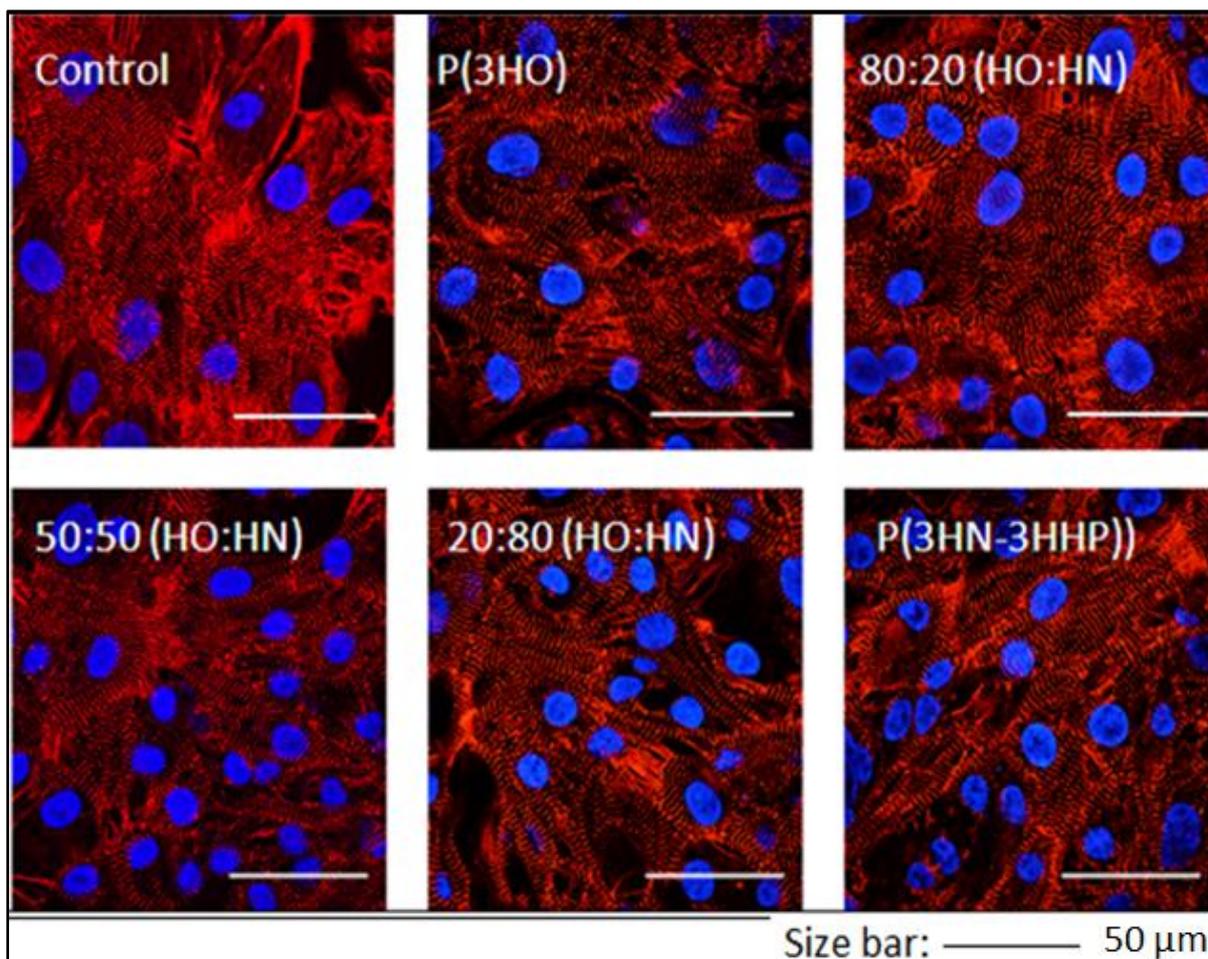
Figure 3.18: *Representative images of hiPSC-CMs on control, P(3HO), P(3HO):P(3HN-co-3HHP) (80:20), P(3HO):P(3HN-co-3HHP) (50:50), P(3HO):P(3HN-co-3HHP) (20:80), P(3HN-co-3HHP). The blue indicator is DAPI for the cell nuclei and red indicator is α-actinin for sarcomeres.*

3.3. Discussion

P. mendocina CH50 was grown in the presence of two different carbon sources i.e. sodium octanoate and sodium nonanoate, and it was found to accumulate different MCL-PHAs which were P(3HO) and P(3HN-co-3HHP) respectively. The two fermentations exhibited a similar trend in the growth profile. The amount of carbon and nitrogen present in the production medium at the beginning of fermentation and also the type of carbon feed provided, plays a crucial role in the type of PHA being produced. In the present study, the bacterium was grown in media with an initial molar ratio of carbon to nitrogen (C/N) of 20 in both the fermentations. The maximum yield of the polymer obtained was approximately 45% dcw in both cases. The C/N ratio is known to play a very important role in the growth and PHA accumulation of PHA-producing bacteria. Studies carried out on *P. stutzeri* 1317 showed that there was an accumulation of 52% dry cell weight of polymer when grown on glucose and ammonium

sulphate at a C/N ratio of 39 (He *et al.*, 1998). In a study conducted by Tian *et al., P. mendocina CH50* strain 0806 was grown in glucose media. It was observed that with increase in the C/N ratio, the PHA formation in the cell was favoured. It was thus concluded that nitrogen limitation was a major factor for the triggering of PHA synthesis (Tian *et al.,* 2000). Hence, these studies showed that in all cases limiting nitrogen concentration favoured polymer accumulation. In this study, for both P(3HO) and P(3HN-co-3HHP) fermentations, the nitrogen concentration was seen to decrease drastically until 48 hrs, leading to nitrogen limiting conditions. This promoted accumulation of polymer and resulted in an increased polymer yield.

Another parameter which was observed in these fermentations was pH. This parameter is known to play an important role in the yield of the polymer which affects both the accumulation and degradation of the polymer. The pH of the culture also showed an increase from 7 to a maximum of 7.8/7.4. A similar increase in pH was found when *Pseudomonas mendocina* was grown on heptanoate, where the pH of the fermentation media increased from 7 to 7.7 (Rai *et al.*, 2011). A study was conducted on *P. aeruginosa S2* where the pH of the fermenter was maintained at 6.8. The performance of the pH-stat fermenter was found to be better as compared to the fed batch process. Hence, pH is one of the most important environmental parameters of PHA fermentation (Chen *et al*., 2007).

It can be seen that P(3HO) and P(3HN-co-3HHP) are characterised by low T_g and, therefore, they are in a rubbery state at room and body temperatures. The T_g of P(3HN-co-3HHP) was slightly lower than P(3HO). The T_g and T_m of polymers are governed by the molecular structure of the polymer. The T_g value of MCL-PHAs are known to decrease with an increase in the number of carbon atoms in the monomeric unit, which in turn leads to an increase in the length of the side chain. The latter leads to poor stacking of the polymer chains (larger free volume) resulting in higher mobility of the polymer chains, leading to lower T_g values (Walle *et al*., 2001). Hence, P(3HO) with a C_8 monomeric unit, is expected to have a higher T_g value that that of P(3HN-co-3HHP), a copolymer of C_7 and C_9 monomeric units, as observed in this study. In a similar study, *P. oleovorans* was grown on n-alkanoates by Gross *et al*. (Gross *et al*., 1989), which led to the production of PHAs with monomers ranging from C_6-C_{10} carbon units. The T_g value of the PHA produced when hexanoate was used as carbon source (T_g = -25ºC) was as predicted, higher than that of the polymer produced using decanoate as the sole carbon source (T_g = -40ºC).

The T_g and T_m values of the P(3HO):P(3HN-co-3HHP) blends were found to be lower as compared to the values for the neat polymers. Thus blending a homo-PHA and the copolymer PHA complicates the stacking of monomer units. As a result, free volume increased in the polymer blends. The lowest T_g was observed for polymer blends with equal amounts of P(3HO) and P(3HN-co-3HHP) indicating that in this composition stacking was hindered and the largest free volume was achieved. When the polymer blend was dominated by one of components free volume decreased and the T_g increased. An important point to note is that all the blends had one value of T_g which indicated that the blends were indeed miscible blends. Similar results were observed when a blend of PVC/PHA was prepared by Hill *et al*. The T_g was found to be lowered with the insertion of oligomeric PHA groups as compared to the polymeric PHA. The presence of a single, composition-dependent T_g in the blends was used to classify the blends as miscible (Hill *et al.*, 1996). MCL-PHAs crystallize very slowly and some copolymers do not crystallize at all, hence, for these polymers no T_m values were observed. Choi *et al*., 1994, observed no T_m when they characterized the polymer produced by *P. citronellois* using heptanoate as the sole carbon source. In this study, however, both the MCL-PHAs and their blends had a characteristic value of T_m. Thus, the thermal properties of PHAs depend on the monomeric units incorporated within the polymer which in turn depends on the carbon source used for their production. These properties are crucial for the processability and hence the applicability of the polymer produced.

The stress-strain curves for neat P(3HO), P(3HN-co-3HHP) and P(3HO):P(3HN-co-3HHP) blends were used to determine the mechanical properties of the polymers. All the scaffolds were elastomeric nature with high elongation at break values, making them all highly suitable for cardiac patch development. However, the neat polymers were slightly more elastomeric in nature than the blends. Stiffness is another important mechanical property for a cardiac patch. Amongst all the scaffolds, the 80:20 blend of P(3HO) and P(3HN-co-3HHP) was found to have the highest Young's modulus value and hence was the stiffest of all the blends. Within the blends an increase in stiffness was observed with increase in P(3HO) content, i.e. the MCL PHA with a smaller pendant group. At the molecular level, large pendant side groups in P(3HN-co-3HHP) make it difficult to have a close packing in a regular three dimensional fashion to form a crystalline array (Preusting *et al.*, 1990; Sánchez *et al.*, 2003). While P(3HO), with small pendant groups, can accommodate easily within the spaces created by the longer side chain, thus creating a packed structure with low mobility of the side chains which increases the stiffness of the blend material (Leceta *et al*., 2015). Finally, tensile strength was the third

mechanical property measured for the different types of scaffolds. The 80:20 blend of P(3HO) and P(3HN-co-3HHP) was also found to have the highest tensile strength. Thus, the strength of the material also increased due to the close stacking of the polymeric side chains in this blend, leading to an increase in the load carrying capacity of the material. These results thus confirm that the blending of P(3HN-co-3HHP) to P(3HO) can be used to predictably change the stiffness and tensile strength of the blends. The mechanical properties of human myocardial tissue include a Young's modulus value of 0.2- 0.5 MPa, elongation at break 100-300% and tensile strength 3-15 KPa. (Watanabe *et al.*, 2006). Hence, the elongation at break of the P(3HO):P(3HN-co-3HHP) (80:20) blend was similar to that of the myocardial tissue. However, the Young's modulus and tensile strength values obtained for these scaffolds in the form of films are not in the range of the myocardial tissue. These values are expected to decrease with the incorporation of porosity within the scaffolds. Further, higher Young's modulus, tensile strength and elongation at break value of the scaffold might have a positive effect on the infarcted heart as after myocardial infarction, the abrupt loss of myocardium triggers ventricular remodelling which includes dilatation, hypertrophy, and the formation of a collagen based scar that increases the load on the infracted region (Martin *et al., 2000*).

All the scaffolds described in this chapter exhibited similar water contact angle values of around 100º, indicating a high degree of hydrophobicity in all the scaffolds. It is expected that the cellular environment around cardiac tissue being hydrophilic, the surface of the scaffold should be hydrophilic in order to allow interaction of various proteins with the scaffold and promote cell attachment. But the *in vitro* interactions of the PHA scaffolds and the cardiomyocytes have been found to be very promising, in fact in some cases out-performing the positive control for cell attachment and viability. Possibly, proteins within the *in vitro* culture conditions bind to the PHA scaffolds in such a manner, that they create a hydrophilic conducive environment for the cellular interaction. This aspect will also be researched in future (Fields *et al.*, 1998; Altankov *et al.*, 1996).

Surface roughness is an important parameter for cell proliferation and differentiation. It is known that increase in surface roughness enhances cell adhesion and proliferation (Deligianni *et al.*, 2000). Hence, further experiments will be conducted to improve the surface roughness of the scaffolds by incorporating porosity, physical and chemical functionalization of the polymer. For example, Rai *et al.,* 2010 demonstrated that there was a change in the surface

topography of the P(3HO)/n-BG composite film due to the addition of nano-bioactive glass (n-BG) particles within the P(3HO) matrix which led to enhanced cell adhesion.

The scaffolds were subjected to *in vitro* degradation in PBS and water uptake, weight loss and pH change were recorded for 3 months. A slow degradation process was observed for all the films. There are several factors which govern the rate of degradation of a polymer including crystallinity, steric hindrance caused due to bulky groups and their stacking behaviour and copolymer composition (Wang *et al.,* 2004, Gijpferich *et al.,* 1996). Water uptake is an important process that speeds up the degradation process. This was found to increase in case of all MCL-PHAs over the period of 3 months. It is extremely difficult to penetrate into the hydrophobic environment of a polymer (Renard *et al.,* 2004). Hence, we observed a very low water uptake in this study, maximum being 4% for P(3HO). This is possibly because P(3HO) has the least bulky pendant group, allowing water absorption by the film surface. Minimum absorption was observed in the case of P(3HO):P(3HN-co-3HHP) (80:20) due to the steric hindrance and close stacking of the side chains. The degradation rate and weight loss of the polymer films is also affected by crystallinity, as mentioned above. The higher the crystallinity of the substance, the slower is the degradation process. The enthalpy of melting (ΔH) is directly proportional to the degree of crystallinity of the polymer. Hence the P(3HO):P(3HN-co-3HHP) (20:80) blend with the lowest value of ΔH, had the lowest crystallinity and hence degraded fastest among all the blends. This blend was also observed to have the lowest T_m. It has been observed, that materials with lower melting temperatures have higher biodegradability (Tokiwa *et al.,* 2004). Hence, based on the combined effects of T_m, crystallinity, hydrophobicity of the alkyl pendant group, steric hindrance and stacking of the copolymer chains, the weight loss in the scaffolds were observed to be in the following order: P(3HO):P(3HN-co-3HHP)(20:80) > P(3HO) > P(3HN-co-3HHP) > P(3HO):P(3HN-co-3HHP)(50:50) > P(3HO):P(3HN-co-3HHP) (80:20). The pH of the media with the degrading films was observed to decrease with time but it was not significantly low. This can be explained as the degrading films release the monomers of the polymer including 3-hydroxyoctanoic acid and 3-hydroxynonanoic acid and 3-hydroxyheptanoic acid. These monomers exist in their acidic form which slightly decreases the pH of the media. A decrease was also observed during the degradation of PLA where the monomer lactic acid were released (Li *et al.,* 2007). However, the decrease of pH observed for PHAs is much lower than that observed for PLA, where the final pH of the media with degrading PLA film had the pH of 1.8 as compared to that of 6.9 for the PHA scaffolds. Hence,

PHAs are considered to be better than PLA for tissue engineering applications (Gijpferich *et al.,* 1996).

In vitro cell culture studies were conducted on the scaffolds using hiPSC-CMs which were seeded on the scaffolds and cell viability and physiology was examined. These studies showed that there were similar number of live cells on all the scaffolds and were comparable to the positive control gelatin. Hence, the PHA scaffolds are indeed promising biomaterials for cardiac tissue engineering. Basnett *et al.,* performed indirect cytotoxicity experiments with P(3HO)/P(3HB) blend films and neat P(3HO) films using human microvascular endothelial cells (HMEC-1). There was no observed cytotoxicity and hence no toxic by-products were released from the films (Basnett *et al*., 2013).

Further to the *in vitro* cell viability, the functioning of the cells was analysed by measuring the beating rate of the cardiomyocytes. Engler *et al.,* 2008 have shown that the culturing of embryonic cardiomyocytes on a series of substrates of different elasticity had a significant effect in the transmission of contractile function and that cells in a rigid matrix are deficient in the assembly of contractile proteins and their beating frequency slows down over time. As a result, the extracellular matrix to which cardiomyocytes attach is a key factor for a highly regulated system such as the heart. It was observed that there was an increase in the beating rate of hiPSC-CMs cultured on P(3HN-co-3HHP) in comparison to the positive control, gelatin. The beat rate observed on all other scaffolds were similar to that on gelatin. This increase in beating rate could be due to immature pacemaker mechanisms in terms of the activity of the hyperpolarisation-activated pacemaker (I_f) or the inward rectifier potassium (I_{K1}) currents, leading to spontaneous activity in the cells (Kim *et al*. 2015). So following on from this result, it is important to study the calcium transients in these cells on the scaffolds.

It has been studied that the increase in intracellular calcium levels lead to an increase in the contraction force which results in a higher contraction amplitude until the calcium levels reached a saturation point and the contraction force declined. This is a continuous process which controls the cardiac contractions (Bers, 2000). In the experiments carried out in this work, there was a decrease in the fluorescence amplitude in the P(3HN-co-3HHP) as compared to the control, gelatin and P(3HO), at a frequency of 1Hz but no difference was observed at 1.5 Hz. The decrease in calcium transient amplitude indicated that there might be a decrease in the cytosolic calcium levels on this scaffold, which suggests that the sarcoplasmic reticulum (SR)

is less developed and so does not release much calcium through the process of calcium-induced calcium release (Dolnikov *et al.* 2006). At 1.5 Hz a significant decrease was observed for the time to transient peak on P(3HN-co-3HHP) and P(3HO) as compared to gelatin. This shorter time to transient peak could also be explained due to the general reduction in cytosolic calcium in the cell (Galie *et al*. 2013). These results showed that the scaffolds did not have an adverse effect on the calcium concentrations, supported the calcium exchange within the cell tubules and promoted contractions.

The length of the sarcomeres and the nuclei density are responsible for the cardiomyocyte contraction and maturation of the cells respectively. Thee parameters were observed on the hiPSC-CMs grown on the different PHA scaffolds. The sarcomere length was observed to be similar on all the scaffolds which was around 2 μm. In adult human myocardium, the length of the sarcomere was observed to be around 2.2 μm while that on immature cardiomyocytes were around 1.65 μm, hence it was concluded that the hiPSC-CMs on the PHA scaffolds exhibited the physiology of adult cardiomyocytes (Bird *et al.,* 2003; Lundy *et al.* 2013). The sarcomeres observed on the PHA scaffolds, did not exhibit anisotropy and were seen to be randomly oriented. The sarcomeres are aligned in the adult native myocardium, enabling them to generate a great force of contraction (Bird *et al.,* 2003). Thus anisotropy is required for efficient functionality of the cardiomyocytes. There was an increase in the nuclei density observed on the P(3HN-co-3HHP) scaffold as compared to the P(3HO) scaffold. Since there were similar number of cells observed on all the scaffolds, it can be suggested that most of the cells on P(3HN-co-3HHP) were binucleated. Adult cardiomyocytes often exhibit binucleation, so it could be suggested that the hiPSC-CMs on P(3HN-co-3HHP) scaffolds were more mature than those on P(3HO) (Olivetti *et al.* 1996; Brodsky *et al.* 1991; Soonpaa *et al.* 1996).

In conclusion, the polymers P(3HO) and P(3HN-co-3HHP) were produced using *Pseudomonas mendocina CH50.* Neat polymer 2D scaffolds and their blends were produced and extensively characterised with respect to their chemical, thermal and mechanical properties. These films have also been proven to be excellent materials for the adhesion and proliferation of human induced pluripotent stem cell derived cardiomyocytes (hiPSC-CMs) and even showed higher biocompatibility than gelatin, the positive control. The sarcomeres observed on the scaffolds, exhibited adult myocardium like characteristics which confirmed that the PHA scaffolds are excellent potential materials for cardiac tissue engineering.

CHAPTER 4

Preparation of random and aligned electrospun fibres

4.1. Introduction

Numerous techniques can be used to generate cell culture scaffolds such as electrospinning and micropatterning which mimic the extracellular matrix and enhance cell attachment. In this study electrospinning was used to generate random and aligned fibres. Electrospinning has received much attention for biomedical applications mainly due to a growing interest in nanotechnologies and their unique material properties. Electrospinning is an established method to create nanoscale polymer fibres with diameter range from 3–5000nm. Nanofibres are suitable to mimic the biological environment because they are in the same scale as biological molecules. In fact, nanomaterials like nanoparticles, nanofibrous morphologies or other complex forms, have been shown to result in improved interaction with cells, for example, selective endocytosis, adhesion and orientation (Kim *et al*., 2006).

In this chapter, random and aligned Poly(3-hydroxyoctanoate)/Poly(3-hydroxynonanoate-co-3-hydroxyheptanoate), P(3HO):P(3HN-co-3HHP), neat and blend electrospun fibres were fabricated, as a potential to be used in cardiac patch development. P(3HN-co-3HHP) was blended with P(3HO) in order to alter P(3HO) properties to further closely mimic that of myocardial tissue. Addition of P(3HN-co-3HHP) provides a tool for the introduction of a subtle variation in material properties, biocompatibility and biodegradation. The solvent cast patches have been previously characterised with respect to their mechanical, thermal and surface microstructural properties as described in Chapter 3. In this Chapter, *in vitro* cytocompatibility of the patches was assessed using human induced pluripotent stem cell-derived-cardiomyocytes, hiPSC-CMs. The electrospun fibre mats provide a substrate which would promote the anisotropy of the hiPSC-CMs, a feature essential to their functionality. A comparative study has been conducted on the cell growth, orientation and function on the random and aligned fibres.

4.2. Results

4.2.1. Fabrication and morphological characterization of electrospun random fibres

Random fibres were electrospun using neat P(3HO) and P(3HN-co-3HHP) and blends in the ratio of 20:80, 50:50, 80:20 respectively. The polymer fibres were electrospun as described in section 2.3. The electrospinning parameters and conditions were optimized for the formation of bead-free smooth and uniform fibres. The fibres were distributed in random directions. The optical images (Figure. 4.1) show the examples of electrospun fibre matrices. (It is very

difficult to image MCL-PHAs using SEM. These polymers have low melting points and melt when bombarded with high energy electron beams) Samples from the same batch were used for seeding the cells. The water contact angle of a scaffold changes with surface topography and the chemical composition of the material in consideration. The water contact angle of the PHA fibres are summarised in Table 4.1. It is known that materials with water contact angles above 70º are hydrophobic in nature while those below are hydrophilic (Wang *et al*., 2008). The water contact angle of all the fibres was observed to be above 100º and so they were all hydrophobic in nature.
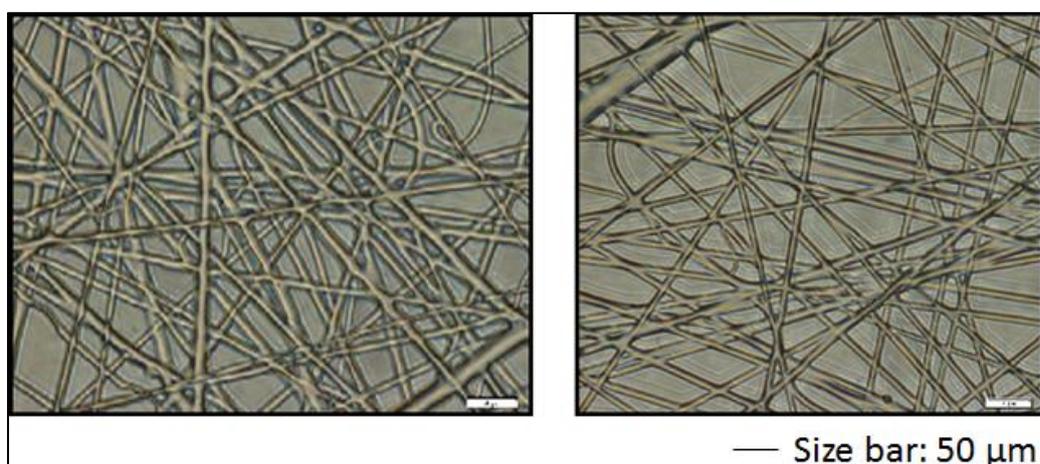
Figure 4.1: *Representative optical images of the electrospun random fibres of the P(3HO), P(3HO):P(3HN-co-3HHP) (80:20). All the other blends P(3HO):P(3HN-co-3HHP) (50:50), P(3HO):P(3HN-co-3HHP) (20:80) and neat P(3HN-co-3HHP) also looked similar.*

Table 4.1: *Table summarising water contact angle values (θ) of the neat P(3HO), P(3HO):P(3HN-co-3HHP) (80:20), P(3HO):P(3HN-co-3HHP) (50:50), P(3HO):P(3HN-co-3HHP) (20:80) and neat P(3HN-co-3HHP) fibres (n=5)*

Samples	Water contact angle (º)
P(3HO)	104.8±3.8
P(3HO):P(3HN-co-3HHP) (80:20)	106.6±9.3
P(3HO):P(3HN-co-3HHP) (50:50)	101.3±3.7
P(3HO):P(3HN-co-3HHP) (20:80)	101.3±3.5
P(3HN-co-3HHP)	101.9±9.7

4.2.2. *In vitro* biocompatibility of hiPSC-CMs on the random fibres

The hiPSC-CMs were grown on the random fibres and live and dead assay was conducted to evaluate the viability of the cells (Figure 4.2). In the random fibre scaffold it was observed that neat P(3HO) and P(3HN-co-3HHP) showed significantly higher cell viability in comparision to all the blend scaffolds. P(3HN-co-3HHP) also showed significantly higher % cell viability as compared to the non-fibrous gelatin (Figure 4.3).
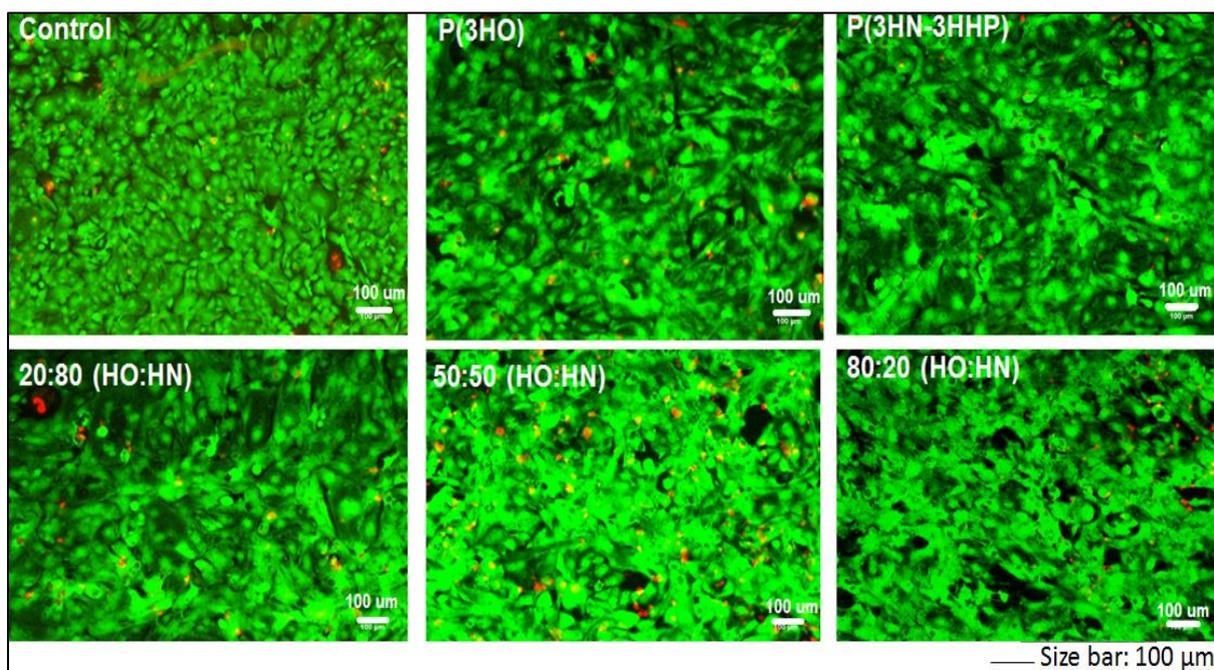
Figure 4.2: *Representative images of live (green) and dead (red) hiPSC-CM cells as grown on the control, gelatin, neat P(3HO), neat P(3HN-co-3HHP), P(3HO):P(3HN-co-3HHP) (20:80), P(3HN-co-3HHP) (50:50), P(3HO):P(3HN-co-3HHP) (80:20) random fibres*
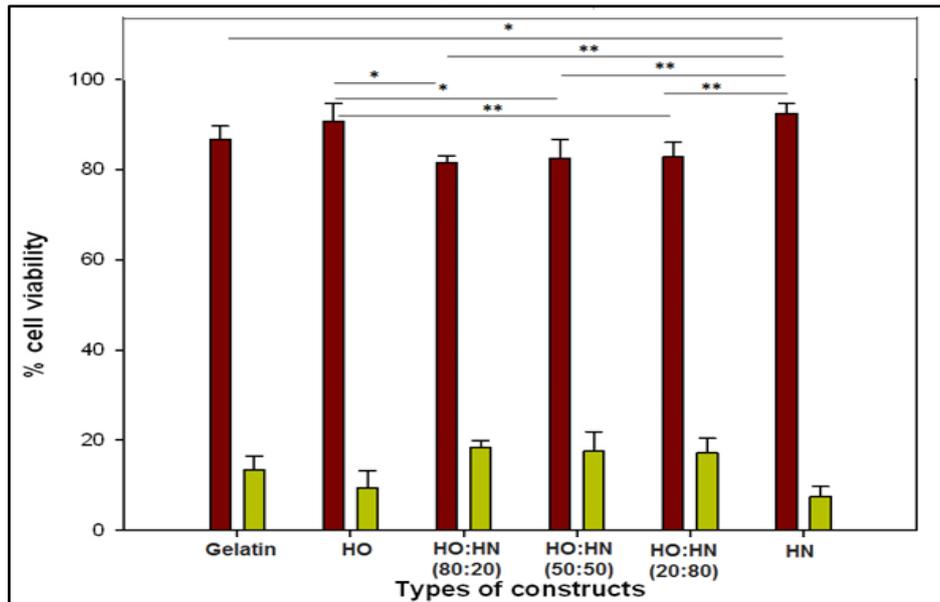
Figure 4.3: *Quantification of the % cell viability of live* � *and dead* ▮ *cells grown on the control, gelatin, neat P(3HO), P(3HO):P(3HN-co-3HHP) (80:20), P(3HO):P(3HN-co-3HHP) (50:50), P(3HO):P(3HN-co-3HHP) (20:80) and neat P(3HN-co-3HHP) random fibres (n=6) *p<0.05, **p<0.001, ANOVA.*

Beat rate analysis

The beat rate of the cells was also measured as described in section 2.4. The beating rates measured are shown in Figure 4.4. All the beating rates were similar to that observed on gelatin. Thus, the beat rate of the cells did not show any anomalous behaviour when compared with that on gelatin, which was used as a positive control.
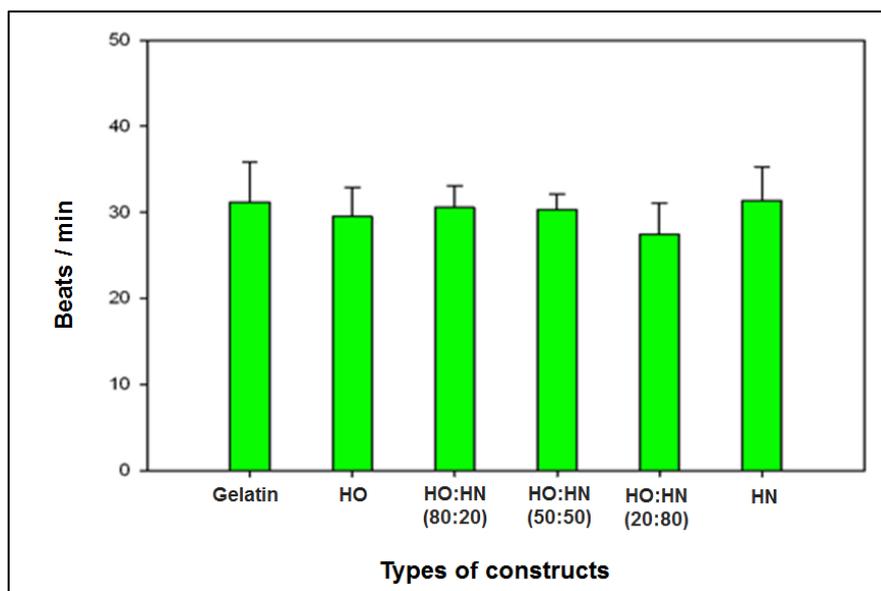
Figure 4.4: *Graph depicting the beat rate of the hiPSC-CMs grown on gelatin, neat P(3HO), P(3HO):P(3HN-co-3HHP) (80:20), P(3HO):P(3HN-co-3HHP) (50:50), P(3HO):P(3HN-co-3HHP) (20:80) and neat P(3HN-co-3HHP) random fibres. (n=6), no significant difference, ANOVA.*

SEM analysis

The SEM analysis was also carried out on the hiPSC-CM cells grown on the scaffold surface in order to observe the surface topography and attachment and proliferation of the cells. The cells were seen to attach and grow on all the different types of PHA fibres including P(3HO), P(3HO):P(3HN-co-3HHP) (80:20), P(3HO):P(3HN-co-3HHP) (50:50), P(3HO):P(3HN-co-3HHP) (20:80) and P(3HN-co-3HHP). (Figure 4.5).
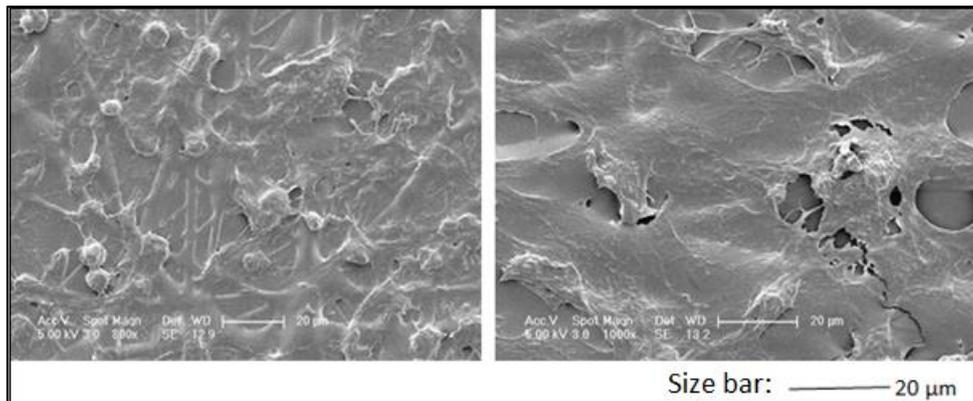
Figure 4.5*: Representative SEM image of the growth and proliferation of the hiPSC-CMs on random PHA fibres.*

Immunofluorescence staining

Immunofluorescence staining was carried out on the cells by staining the filamentous actin (F-actin), myosin heavy chain (MHC) and nuclei. The staining showed the arrangement of the structural proteins (F-actin in green and MHC in red) along with the nuclei (Figure 4.6). The staining on the fibres was very similar to that observed on gelatin. Hence, the phenotypic similarity of the cells was confirmed.
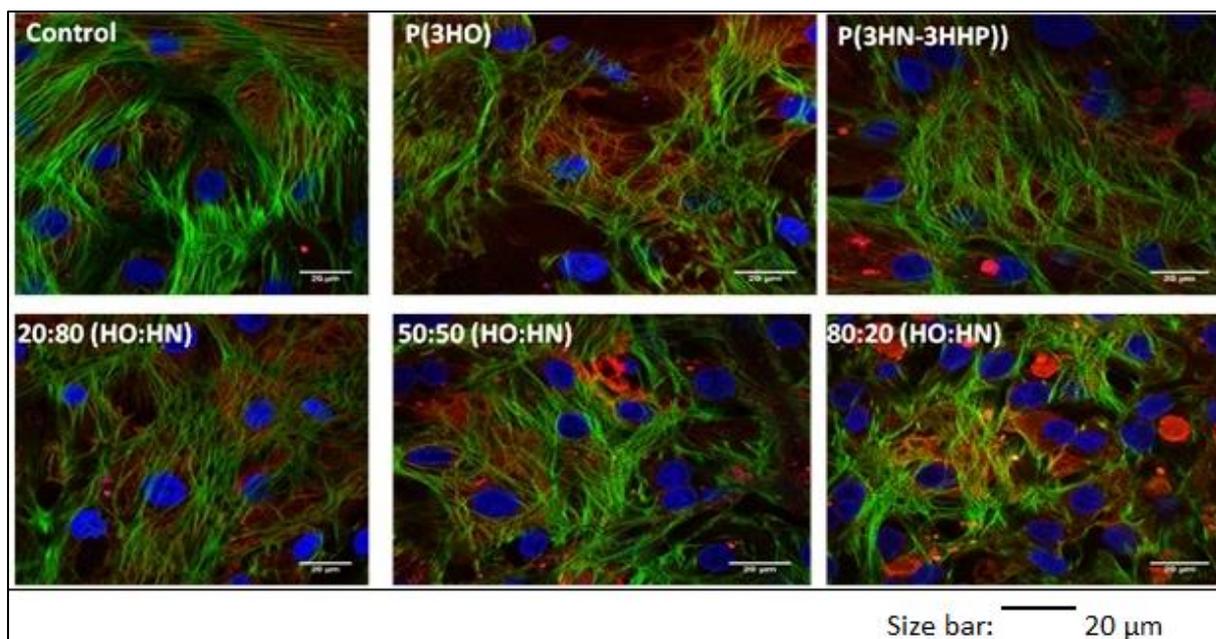
Figure 4.6: *Images of immunofluorescence staining of hiPSC-CMs for various cardiac proteins such as F-actin (green), MHC (red) and nuclei (blue) grown on the positive control, gelatin, neat P(3HO), neat P(3HN-co-3HHP), P(3HO):P(3HN-co-3HHP) (20:80), P(3HO):P(3HN-co-3HHP) (50:50) and P(3HO):P(3HN-co-3HHP) (80:20) random fibres.*

4.2.3. Aligned fibres

Fabrication of aligned fibres of the neat and blend polymers

Fibres of neat P(3HO) and P(3HN-co-3HHP) and blends in the ratio of 20:80, 50:50 and 80:20 were electrospun in an aligned manner on coverslips. The light microscope was used to observe the fibres which looked well aligned (Figure 4.7). A water contact angle study was carried out on the fibres and as shown in the Table 4.2 it was seen that all the fibres had a water contact angle of around 100º which indicated that scaffolds were hydrophobic in nature.
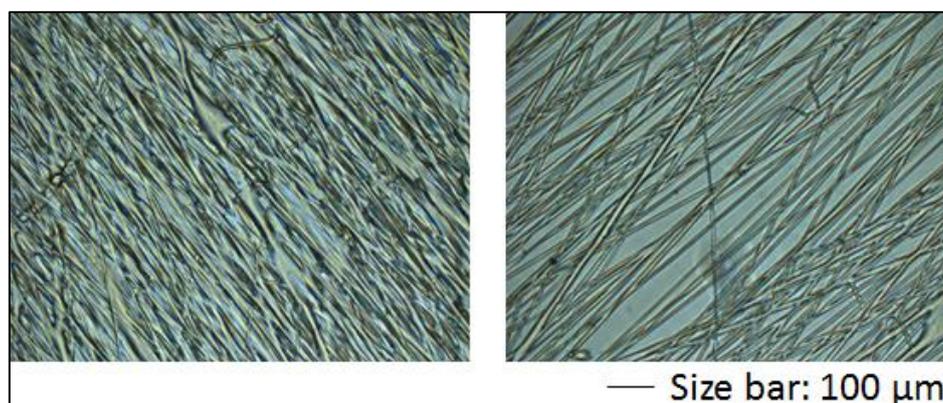
Figure 4.7: *Representative optical images of electrospun P(3HO):P(3HN-co-3HHP) (80:20) and P(3HO):P(3HN-co-3HHP) (50:50) with similar images observed in P(3HO), P(3HO):P(3HN-co-3HHP) (20:80) and neat P(3HN-co-3HHP) aligned fibres.*

91

Table 4.2: *Water contact angle measurement for the P(3HO), P(3HO):P(3HN-co-3HHP) (80:20), P(3HO):P(3HN-co-3HHP) (50:50), P(3HO):P(3HN-co-3HHP) (20:80) and neat P(3HN-co-3HHP) aligned fibres. (n=5)*

Samples	Water contact angle (º)
P(3HO)	101.1±1.9
P(3HO):P(3HN-co-3HHP) (80:20)	100.5±3.5
P(3HO):P(3HN-co-3HHP) (50:50)	95.5±4.0
P(3HO):P(3HN-co-3HHP) (20:80)	99.0±6.0
P(3HN-co-3HHP)	97.5±10.2

***In vitro* biocompatibility and anisotropy of the cells on the aligned fibres**

Live and Dead assay

The live and dead assay was conducted on the hiPSC-CMs grown on the aligned fibres, gelatin, which was used as a positive control and the number of cells were counted. Image of the cells are shown in Figure 4.8. These were further quantified as shown in Figure 4.8. The cell viability on the aligned fibres, unlike on the random fibres indicated that there was no change in the % cell viability on all the scaffolds and were all comparable to the non-fibrous gelatin which was used as a positive control (Figure 4.9).

The cells on the aligned fibres were also seen to be aligned in one direction (Figure 4.8). It was further quantified and the percentage of aligned cells with respect to the total number of fibres was calculated. It was recorded that in P(3HO) around 56% cells, in (P(3HO): P(3HN-co-3HHP)) (80:20) 50% cells, in (P(3HO): P(3HN-co-3HHP)) (50:50) 54% cells, in (P(3HO): P(3HN-co-3HHP)) (20:80) 54% cells and in P(3HN-co-3HHP) 44% cells while in non-fibrous gelatin 14% cells showed a mean deviation of 0º-10º deviation from the fibres (Figure 4.10). The white arrow in Figure 4.7 indicate alignment of cells.
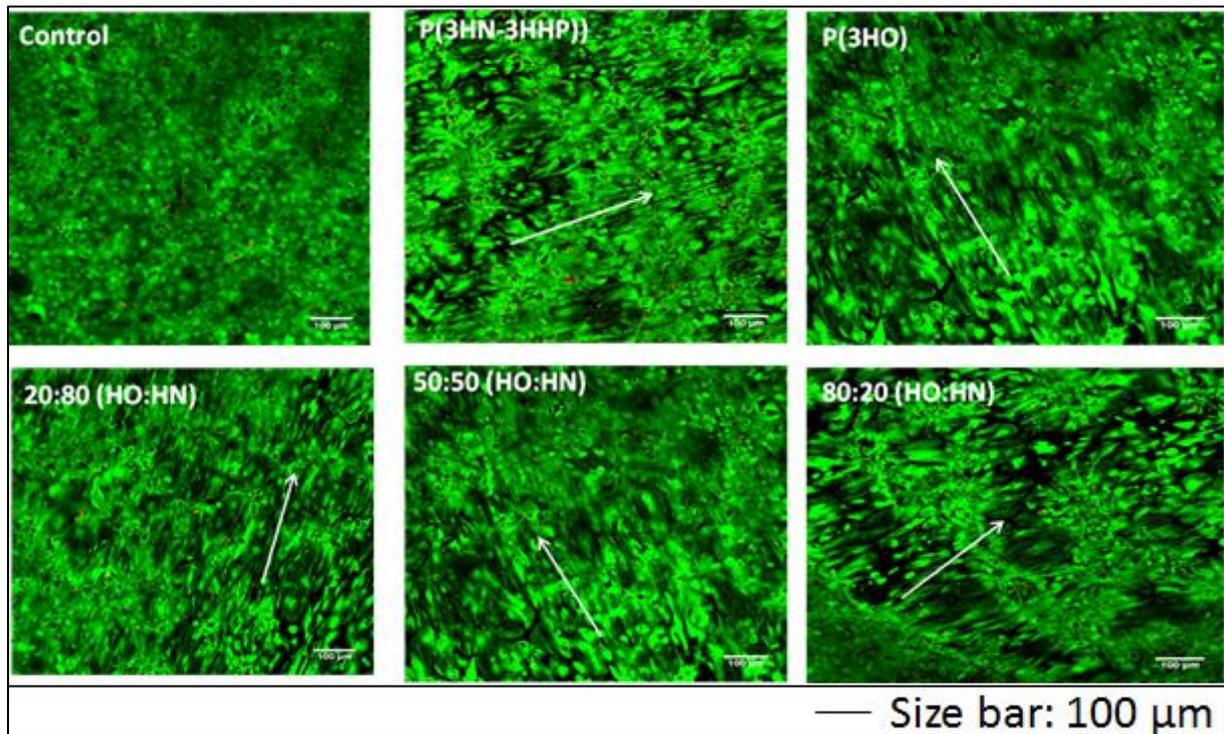
Figure 4.8: *Images showing the live (green) and dead (red) hiPSC-CM cells on the control, gelatin, neat P(3HN-co-3HHP), neat P(3HO), P(3HO):P(3HN-co-3HHP) (20:80), P(3HO):P(3HN-co-3HHP) (50:50) and P(3HO):P(3HN-co-3HHP) (80:20) aligned fibres as positive control. The white arrow shows the alignment of the cells on the individual scaffolds.*
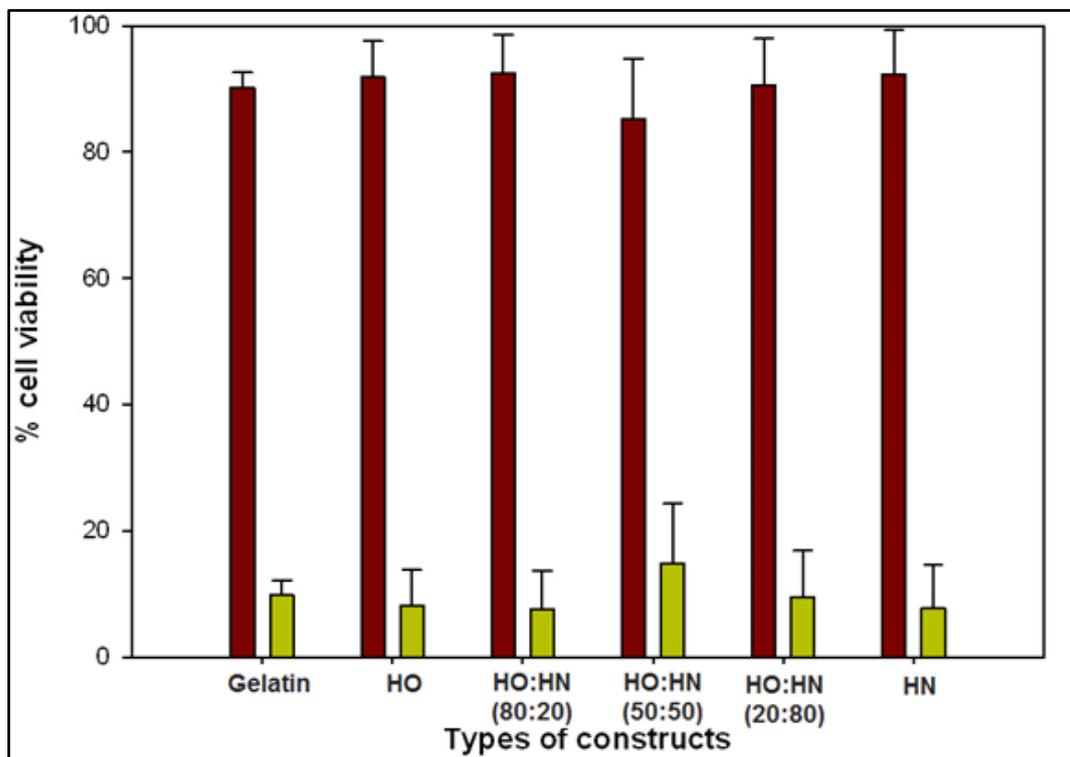
Figure 4.9*: Quantification % cell viability of live* ▰ *and dead* ▰ *cells using the live/dead assay on cells grown on the control, gelatin, neat P(3HO), neat P(3HO):P(3HN-co-3HHP) (80:20), P(3HO):P(3HN-co-3HHP) (50:50) and P(3HO):P(3HN-co-3HHP) (20:80) aligned fibres. (n=6), no significant difference, ANOVA.*
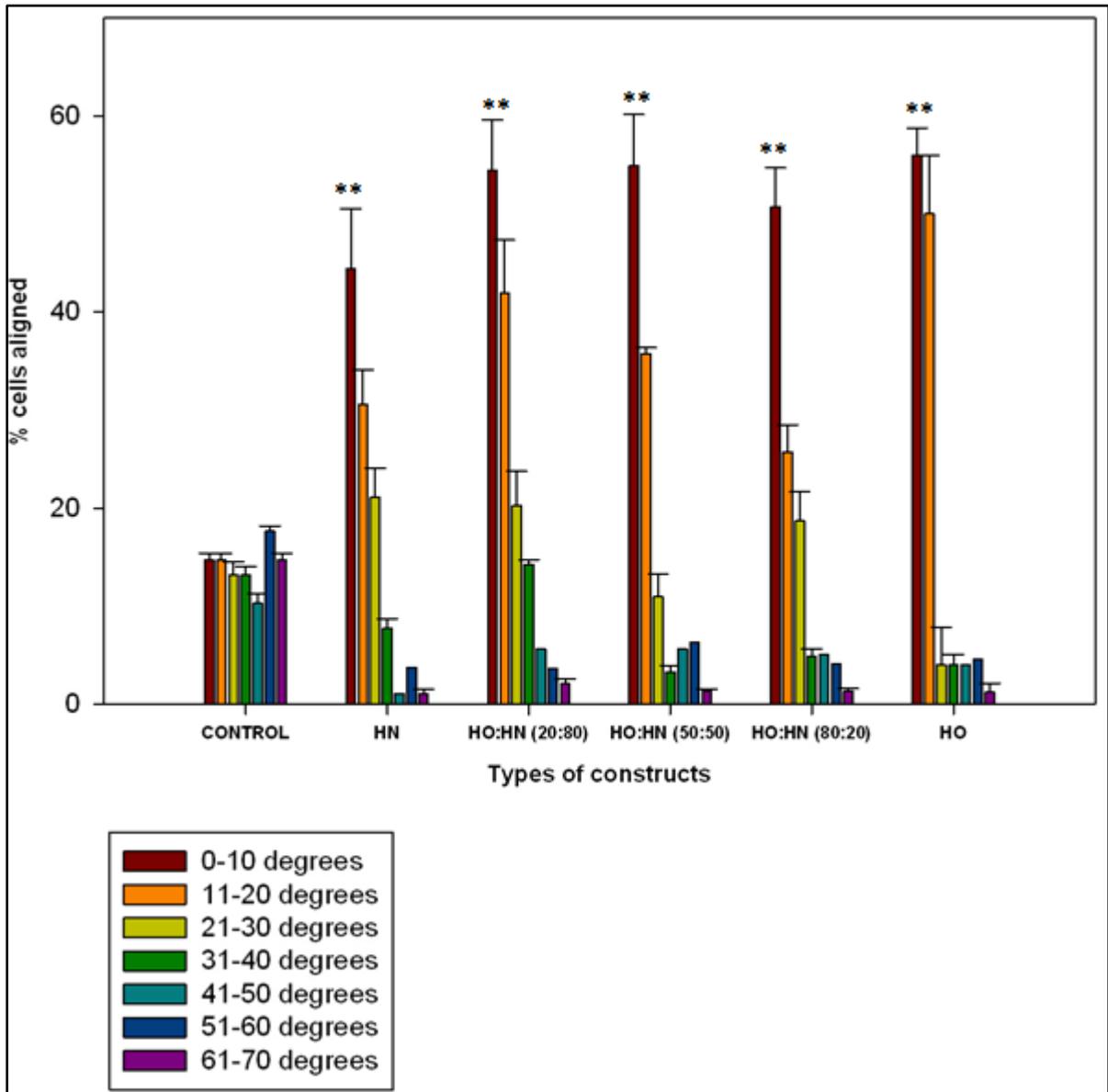
Figure 4.10: *Quantification of the alignment of the cells on non-fibrous gelatin used as control, neat P(3HN-co-3HHP)P(3HO), P(3HO):P(3HN-co-3HHP) (20:80), P(3HO):P(3HN-co-3HHP) (50:50), P(3HO):P(3HN-co-3HHP) (80:20) and neat P(3HO) aligned fibres. (n=6),p<0.001, ANOVA.*

SEM analysis of the cells on the aligned fibres

The surface morphology of the cells was observed by SEM analysis and the anisotropic nature of the cells was observed by cell elongation on the fibres. Further, it was also observed that the cells reached confluence in 14 days and were aligned in a particular direction. The SEM images also confirmed the anisotropy of the cells on the fibres (Figure 4.11).
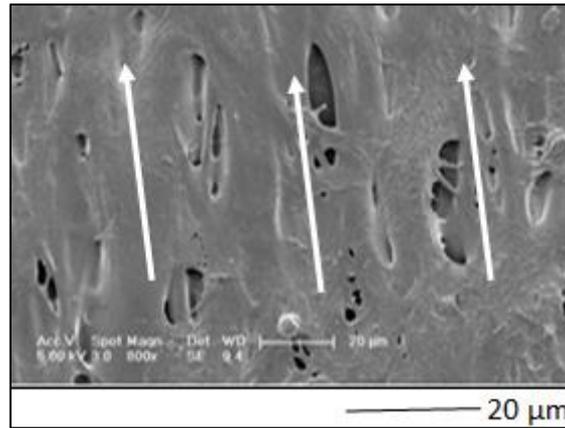
Figure 4.11: Representative image of an SEM micrograph showing the alignment and confluence of the cells on the fibres.

Immunofluorescence staining of the hiPSC-CMs on aligned fibres

The immunofluorescence staining images of the hiPSC-CMs on the aligned fibres show the staining of the F-actin, MHC and nuclei. The images indicate that the cytoskeleton of the cells comprising of the F-actin have been aligned in a particular direction, thus being directed by the scaffold they were seeded on (Figure 4.12). The cells appear to be elongated in the direction of the fibres.
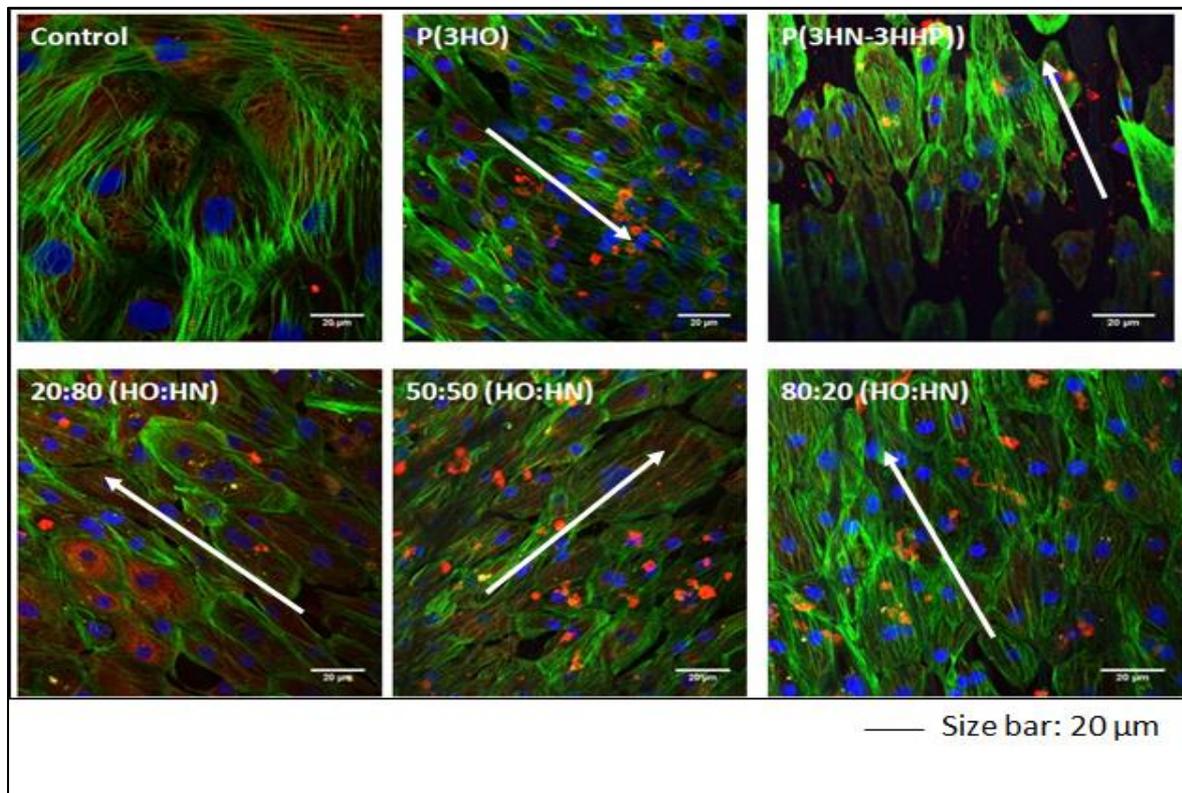
Figure 4.12: Immunofluorescence staining of the cells of hiPSC-CM for various cardiac proteins such as F-actin (green), MHC (red) and nuclei (blue) grown on the different aligned fibres. The white arrows indicate the directionality of the cells grown on the aligned fibres in comparison to the random growth as seen on the non-fibrous gelatin.

95

4.3. Discussion

The extracellular matrix is a complex combination of proteins which serves to enhance cell attachment, survival, migration, proliferation and differentiation. Thus, to provide such structural support, an engineered scaffold should ideally mimic the structure, morphology, chemical and biological signals found in the natural tissue. Electrospinning has been widely used to fabricate the structures and scaffolds which fulfil the above mentioned criteria. In this work, fibrous scaffolds were fabricated by electrospinning neat P(3HO), P(3HN-co-3HHP) and their blends P(3HO):P(3HN-co-3HHP) (80:20), P(3HO):P(3HN-co-3HHP) (50:50), P(3HO):P(3HN-co-3HHP) (20:80). Separate studies were conducted on the random and aligned fibres of the above mentioned compositions. The fibres were electrospun on the coverslips and optical images confirmed the successful formation of the random and aligned fibres. As mentioned before, SEM images could not be observed due to the low melting temperature of the MCL-PHAs, which led to melting of the MCl-PHAs when bombarded with the high energy electron beam. The material characterization including the thermal properties and mechanical properties of the solvent cast polymer films were described in Chapter 3. The mechanical properties of the fibres could not be measured in this study due to the difficulty in removing the fibres from the surface of the coverslips. Few of fibres which were successfully removed from the coverslips were very sticky and were difficult to handle for performing the tensile tests. On the other hand, due to the similarity in the polymer material composition of the fibres with the plain solvent cast films (fabrication explained in Chapter 3), it can be considered that stiffness of the fibres would be in range or lower with that of the plain films. Electrospinning introduces porosity in the fibrous scaffold and porosity tends to decrease the stiffness of the material in comparison to the plain films (Mogosanu *et al.*, 2014).

The wettability analysis of all the fibres were also carried out. The water contact angles, depend on chemical composition and surface topography of the scaffold which hence reflects the hydrophilicity of scaffolds, relating to protein absorption and cell attachment (Wang *et al.* 2008). The water contact angle of the random and aligned fibres were observed to be in the range of 100º-106º. This indicated that the fibrous scaffolds were hydrophobic in nature. It is known that the contact angle measurements of electospun fibres are not accurate quantitative estimates of the degree of hydrophobicity. Due to the surface topography of the fibres and their porosity, it can be stated that the results are purely qualitative as the water drop does not make

full contact with the polymer surface (Kai *et al.*, 2011). Hence the values obtained in this study can be considered to be a qualitative interpretation of the hydrophobicity of the fibres.

In vitro biocompatibility studies were conducted on the random and aligned fibres by seeding hiPSC-CMs and cell viability was performed after 14 days of seeding. On the random fibre scaffolds, a significantly higher cell viability was observed on P(3HN-co-3HHP) and P(3HO) as compared to all the blend scaffolds (P(3HO): P(3HN-co-3HHP) (20:80), P(3HO): P(3HN-co-3HHP) (50:50) and P(3HO): P(3HN-co-3HHP) (80:20)) and P(3HN-co-3HHP) also showed higher cell viability as compared to non-fibrous gelatin. The beating rate were also found to be similar in all the scaffolds and were comparable to the non-fibrous gelatin. Thus it can be confirmed that the random fibre scaffolds resulted in improved cell viability and provided good contractile property as compared to gelatin, which was used as a positive control. In aligned fibrous scaffolds, all the scaffolds exhibited similar cell viability and were all comparable to that of non-fibrous gelatin. The fibrous polymer scaffolds were thus found to have a positive effect on the hiPSC-CM growth. The fibrous polymer scaffolds were thus found to have a positive effect on the hiPSC-CM growth. These results suggest that P(3HO), P(3HN-co-3HHP) and their blends P(3HO):P(3HN-co-3HHP) (80:20), P(3HO):P(3HN-co-3HHP) (50:50), P(3HO):P(3HN-co-3HHP) (20:80) have excellent biocompatibility with the hiPSC-CMs in the form of fibrous scaffolds and hence are suitable materials to be used in cardiac patch applications. On the aligned fibres, the alignment of the cells was also measured in order to observe if there was any directionality and anisotropy directed by the aligned fibres onto the cells. It was observed that around 50-60% cells were aligned with respect to the fibrous scaffold which was not seen in the non-fibrous gelatin which was used as a control. This shows that the cells exhibit anisotropy which is directed due to the alignment of the fibres, as the cells grown on the control non fibrous gelatin show isotropic behaviour. The electrospun fibre scaffolds resemble the fibrous extracellular matrix of the tissue providing an *in vitro* anisotropic resemblance to the cardiac tissue, hence promoting cell growth in an aligned manner. In other studies too, aligned fibres were electrospun and cardiomyocytes were grown to promote anisotropy. For example, in one study, non-woven PLGA aligned fibres were electrospun. Human induced pluoripotent stem cells derived cardiomyocytes were grown on the fibres and highly oriented growth along with anisotropy of rat cardiomyocytes was observed (Khan *et al.,* 2015). Rockwood *et al.*, 2008, also showed highly oriented and anisotropic growth of the cardiomyocytes on the electrospun aligned polyurethane (PU) fibres which also exhibited higher levels of ventricular maturation.

Immunofluorescence studies were also carried out to stain the F-actin, MHC and nuclei of the control, random and aligned fibres of the neat and blend polymers. The staining of the structural proteins of the cell indicated a healthy phenotype for all the cells. The confocal images also showed a directionality of the cells on the aligned fibres and a non-directional growth on the random fibres. The alignment of the cells on the aligned fibres provided a conducive environment to the cells, mimicking the extracellular matrix, hence also enhanced cardiomyocyte maturation and provided better healing to the infarcted tissue and help in functional recovery of the tissue (Kenar *et al.,*2011). In another study, the cardiomyocytes seeded on the aligned scaffolds acquired the structure of the fibres, and organized into aligned tissue. Analysis of cell alignment revealed that contrary to randomly oriented scaffolds, where the cells were not organized, and vast majority of the cells cultured on the aligned scaffolds exhibited organized growth in the direction of the fibres, assembling into an anisotropic tissue (Fiescher *et al.*, 2014).

CHAPTER 5

Production of porous P(3HO) scaffolds

5.1. Introduction

Scaffold permeability is an important parameter in determining cell attachment. It is governed by different parameters which include porosity, pore size and distribution, pore interconnectivity and pore orientation. Thus porosity is a crucial property of a scaffold to be tailored carefully in tissue engineering. A porous scaffold is also important in providing higher surface area for the cells to attach to the scaffold. The interconnectivity of the pores in the scaffold helps in cell penetration, tissue ingrowth, vascularization and nutrient delivery (Chen *et al.*, 2008). The size of the pores is an equally important parameter. Previous speculation regarding cell activity within porous scaffolds has indicated that there exists an optimal pore size, or range for each distinct cell type. Pore size has an influence on cell attachment, as seen with collagen-GAG scaffolds where cell attachment increased with decrease in pore size. This was explained by the fact that a lower specific surface area in scaffolds with a larger mean pore size, resulted in a lower ligand density available for adhesion. In another study conducted on collagen-GAG, porous scaffolds were prepared with different pore sizes ranging from 95.9-150.5 µm. MC3T3 cells were grown on these scaffolds and cell viability studies were conducted. A linear relationship was found between cell attachment and specific surface area and it was thus confirmed that cell viability was governed by the specific surface area available for binding(O'Brien *et al*., 2007).

There are many methods to prepare a porous scaffold, including electrospinning (Demir *et al.*, 2002; Lee *et al.*, 2003), solvent casting/salt leaching (Fromstein *et al.*, 2002) , laser excimer (Doi *et al.,* 1996) and thermally induced phase separation (Saad *et al.*, 1996). Scaffolds prepared by solvent casting/porogen leaching method have the advantage of high level of control on the pore size governed by the size of the salt particles used.

The aim of this study was the preparation of 2D and 3D scaffolds using the MCL-PHA polymer, poly(3-hydroxyoctanoate), P(3HO). This was used to investigate the effect of porosity on the scaffold properties in the context of cardiac tissue engineering. Neat scaffolds were prepared using solvent casting, while the porous scaffolds were prepared using the porogen leaching method, with sucrose of size 250-300 µm as the porogen. The films were characterized with respect to their mechanical properties and surface hydrophilicity/hydrophobicity in order to assess their applicability in cardiac tissue

engineering. Further, *in vitro* biocompatibility studies were also carried out using C2C12 cells on these scaffolds.

5.2. Results

5.2.1. Preparation of 2D porous P(3HO) scaffolds using the porogen leaching method using different salt concentration

5wt % P(3HO) neat and porous scaffolds were prepared. The porous scaffolds had 0.5%, 1% and 1.5% porogen concentration with pore size of 250-300 µm in diameter. Different P(3HO) porous scaffolds were fabricated and compared with the neat P(3HO) constructs.

Mechanical analysis

The mechanical properties of the scaffolds were measured using the Dynamic Mechanical Analyser in the static mode. The Young's modulus, tensile strength and elongation at break for the 5 wt% porous P(3HO) scaffolds with 0.5%, 1.0% and 1.5% porogen concentration were recorded to be significantly low as compared to the 5 wt% neat P(3HO) scaffold (Table 5.1). Thus the porous scaffolds exhibited lower stiffness as compared to the neat P(3HO) scaffolds.

Table 5.1*: Mechanical properties of the solvent cast porous and neat P(3HO) films including Young's modulus, tensile strength and elongation at break (n=5).*

Samples	Young's modulus (E value) (MPa)	Tensile strength (MPa)	Elongation at break (%)
P(3HO)	8.3±0.7	10.1±2.6	674.7±98.5
0.5% porogen P(3HO)	0.46±0.7	2.2±1.2	336±80.2
1% porogen P(3HO)	1.6±1.1	2.2±1.4	345.8±6.3
1.5% porogen P(3HO)	0.46±0.6	1.2±0.5	490.9±54.6

Water contact angle analysis

The surface hydrophilicity/hydrophobicity of the films was determined by measuring the water contact angle of the films. Water contact angle of the P(3HO) neat film was measured as 100.7º while that of the 0.5%, 1.0% and 1.5% porous films were found to be 90.1º, 76.8º and 73.9º respectively (Table 5.2). Hence, there was a decrease in the water contact angle of the porous

film with increasing porogen concentration. The higher surface area on the porous film with respect to that of the neat film, increased accessibility for the water molecules in the former, leading to increased hydrophilicity. Water contact angle measurements indicated a significantly lower water contact angle for the porous P(3HO) film created using 1.5 wt% sucrose as the porogen when compared to the neat P(3HO) film.

Table 5.2: *Water contact angle measurements indicating lower water contact angle for the porous P(3HO) films created using 0.5%, 1.0% and 1.5% porogen as compared to the neat P(3HO) film. (n=5)*

Samples	Water contact angle (º)
P(3HO)	101.1±1.5
0.5% porogen P(3HO)	90.1±1.1
1% porogen P(3HO)	76.8±1.2
1.5% porogen P(3HO)	73.9±0.1

Porosity

The porosity of the porous film was calculated using the equation 2.1 described in Chapter 2 and was found to be 52.29% for the 0.5% porous P(3HO) film, 61.1% for 1.0% porous P(3HO) film and 78.5% for 1.5% porous P(3HO) film.

Scanning Electron Microscopy (SEM)

The surface analysis of the neat and porous films reveal that the neat film has a smooth surface while a porous film has pores scattered on the smooth surface with pore size ranging from 250-300 µm (Figure 5.1).
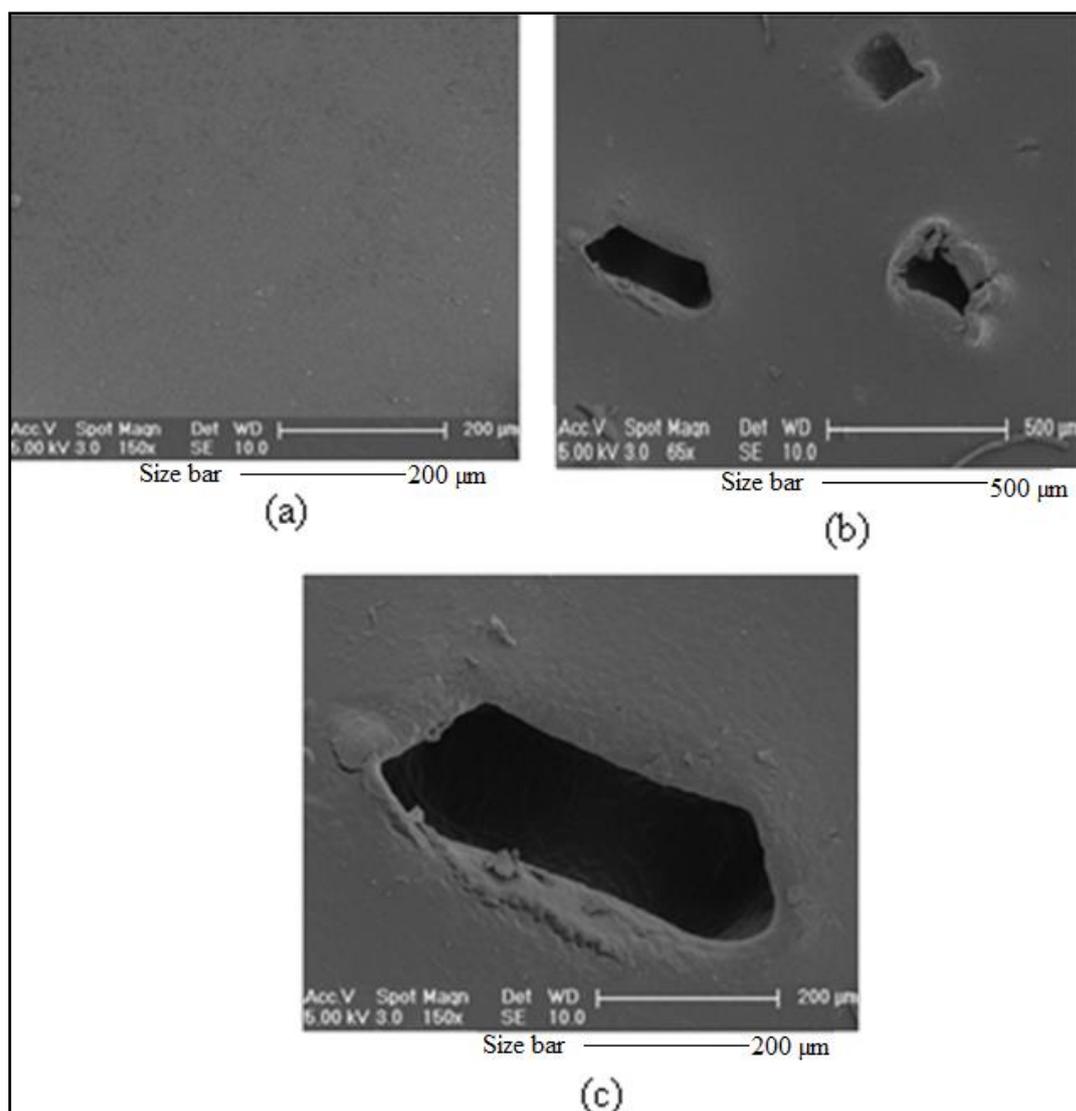
Figure 5.1: *Scanning electron microscopy image of the surface of (a) neat P(3HO) film at 110X. (b) and (c) Porous P(3HO) films at 65X and 150X magnification.*

5.2.2. *In vitro* cytocompatibility study

The C2C12 myoblast cells were grown on the neat and porous films and cell proliferation was observed for 24hrs. The observation showed that the 0.5% porous films exhibited 36.5%, 1% porous films shows 38.5% and 1.5% porous films showed 44.4% cell proliferation as shown in Figure 5.2. SEM images of the porous films with cells show that the cells cover the pores and prefer to grow near them, as shown in Figure 5.3. Hence, the cell proliferation rate was highest in the scaffold with the highest porosity. There was significant increase in the cell proliferation on the 1.5% porous film as compared to the neat P(3HO) film. There was also observed an increase in 0.5% porous film and 1.0% porous film when compared with neat P(3HO) indicating a higher cell proliferation on the porous structures.
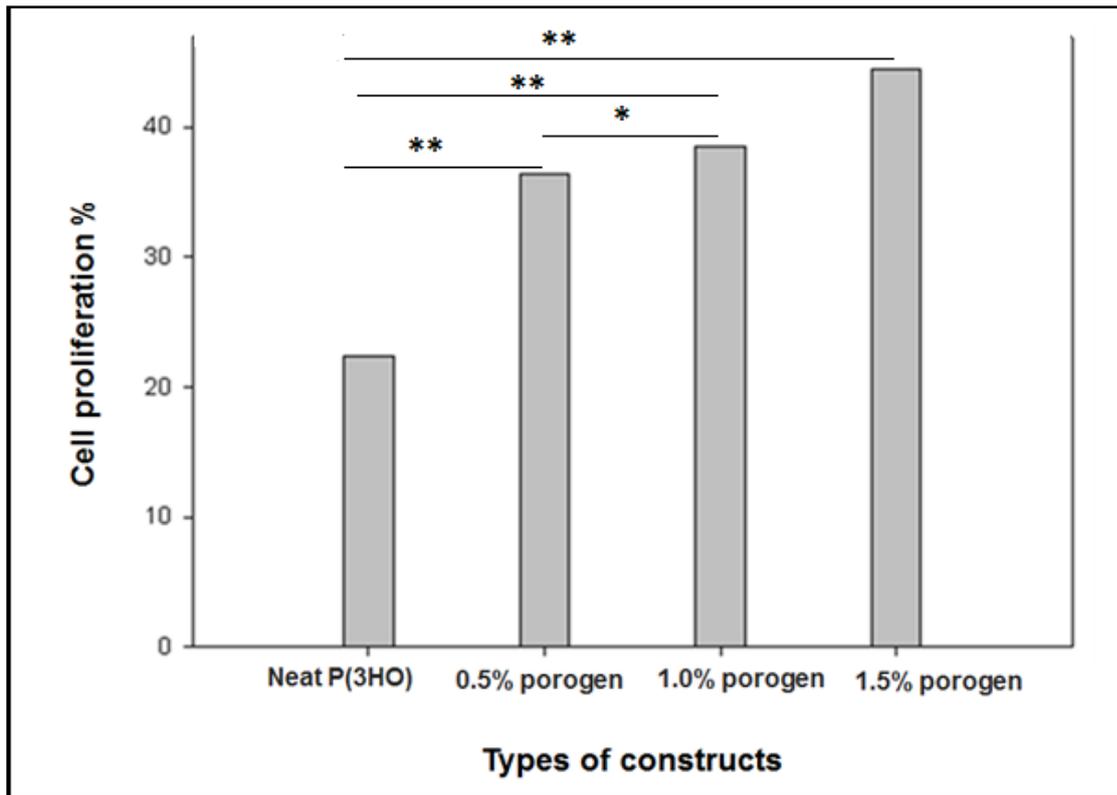
*Figure 5.2: Graph depicting cell proliferation rate of C2C12 myoblast cells grown on different 5wt% neat and porous films after 24 h. (n=3), *p<0.05, **<0.001, ANOVA.*
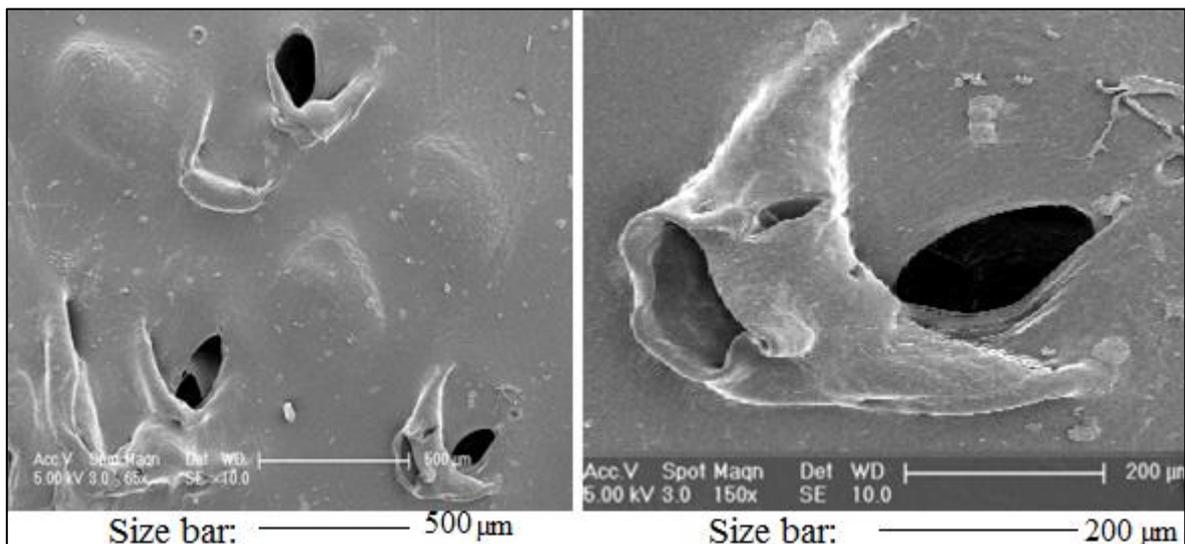
Figure 5.3: SEM images of C2C12 myoblast cells on porous scaffolds as viewed after 24 hr of growth.

Fabrication of 3D porous P(3HO) scaffolds

3D P(3HO) scaffolds were also prepared, as explained in section 2.4. The scaffold was observed to be very soft and spongy due to the porous nature of the scaffold and elastomeric property of the polymer. It was in the shape of a cylinder, 1cm in diameter, 0.5 cm in height.

Scanning electron microscopy study

Scanning electron microscopy of the scaffold showed that the porous scaffold exhibited pore diameters ranging from 250-300 μm. The surface of the scaffold was also observed to have pores with the same dimensions (Figure 5.4(B)). The cross section of the scaffold also revealed proper sized pores formed due to the porogen of diameter 250-300 μm (Figure 5.4(A)).
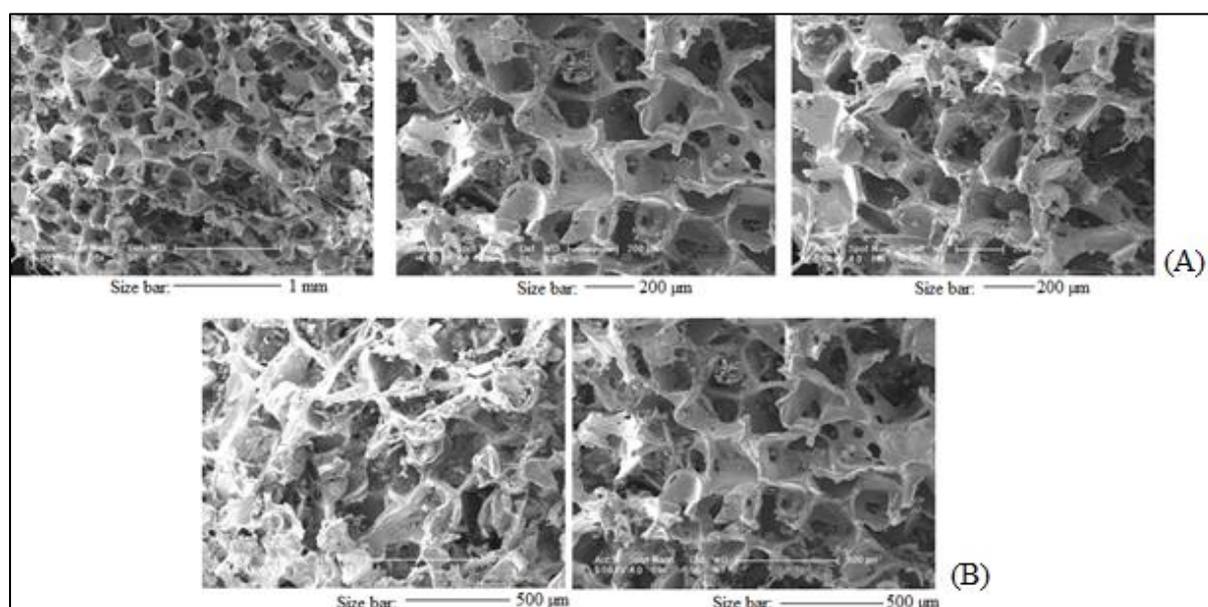
Figure 5.4:*(A) Cross sectional view of the 3D porous P(3HO) scaffold showing well- formed pores within the structure. (B) Surface view of the 3D porous P(3HO) scaffold.*

MicroCT analysis indicating interconnected pores

The microCT analysis was conducted and it was observed that the 3D porous structure had interconnected pores. The microCT video conducted on the 3D structure depicts it passing through the height of the whole scaffold, thus analysing it layer by layer (Figure 5.5). As the video passes through each section of the scaffold it is evident that the pores interconnect the whole scaffold and hence form a well-connected network for the cells to proliferate.

| A | 10sec | B | 15sec | C | 21 sec |
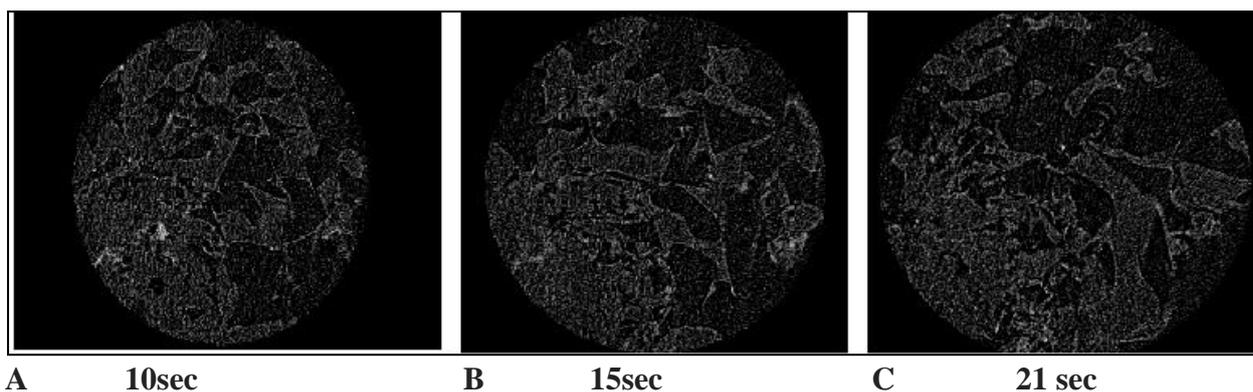
Figure 5.5: Snapshots of the video taken at (A) 10sec (B) 15 sec (C) 21 sec from the microCT of porous scaffold indicating an interconnected porous 3D scaffold. (Complete video provided with the thesis)

Cell culture study on all the porous scaffolds using C2C12 cells

The porous scaffolds were seeded with C2C12 cells and the cell proliferation assay was used to quantify cell proliferation after 2 days. It was analysed that the cell proliferation of the C2C12 cells on the 3D P(3HO) porous scaffold was found to be 99%, a 5 times increase as compared to the 20% cell proliferation observed on the neat P(3HO) scaffold. Figure 5.6 shows SEM images of C2C12 cells grown on neat P(3HO) scaffold and the 3D porous P(3HO) scaffold surface and cross sectional view, where the 3D scaffold exhibited dense cell growth and the cells were seen covering the pores of the scaffold. The white arrows on the image indicate the growth and proliferation of the cells through the pores while covering the porous surface of the scaffold.
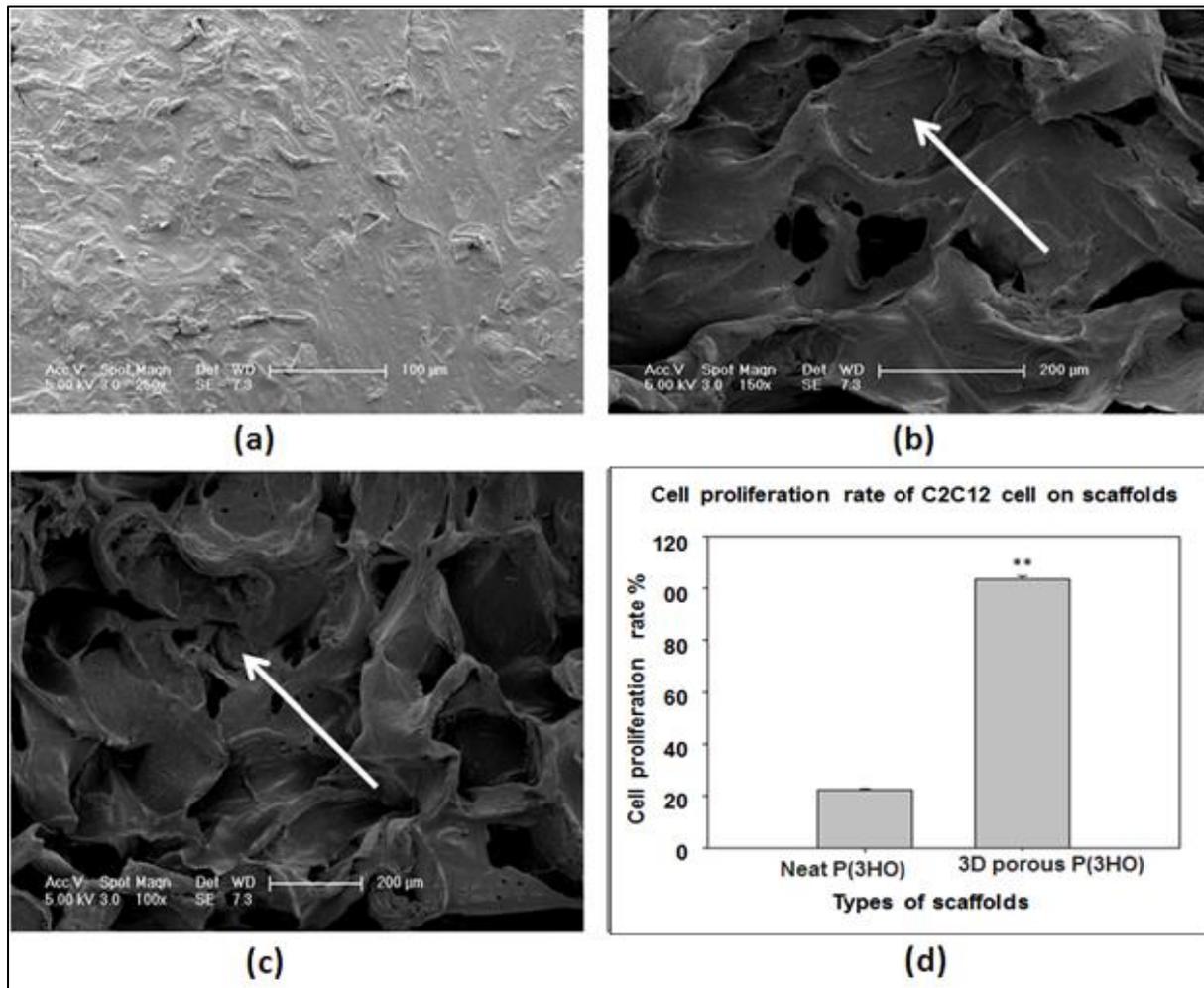
Figure 5.6: *Growth of C2C12 cells on (a) neat P(3HO) film (b) and (c) 3D porous P(3HO) scaffold (d) Cell proliferation assay on the neat and 3D porous P(3HO) scaffolds (n=3) **p<0.01, t-test, unpaired, two-tailed. The white arrows indicate cell migration and proliferation within the pores and are seen to overlap the pores.*

5.3. Discussion

The neat and porous P(3HO) scaffolds were successfully prepared using solvent cast technology. The size of the pores in the porous scaffolds were selected such that they were similar to the size of human myocytes (250-300 µm), allowing the myocytes to infiltrate in to the scaffold and lead to efficient tissue regeneration. In addition, introducing porosity in a scaffold also leads to increased roughness, which is an important property that influences cell adhesion and migration. Hence, in order to obtain a high cell density on the scaffold, the scaffold needs a high surface area and optimal pore architecture in order to accommodate the cells and to provide the required support (Doi and Matsuda, 1997).

The mechanical property of a scaffold is another crucial parameter as it helps to provide support for the adhesion of new cells until new extracellular matrix is synthesized by the cells (Chen *et al.*, 2008) and acts as a support to the diseased organ during regeneration. It is also important for the scaffold to mimic the mechanical property of its host tissue so that its biological functioning is not hindered (Chen *et al.*, 2008).

The mechanical properties of the porous scaffolds were compared to that of the neat P(3HO) scaffold. As expected, the stiffness of the P(3HO) porous scaffold was lower than that of the neat scaffold and the Young's modulus value of the former were in the range of human myocardial tissue, ideal for cardiac tissue engineering. The tensile strength of the porous film was lower in comparison to the neat P(3HO) scaffold and the values measured for the porous scaffolds were also found to be in the range of the myocardial tissue. The elongation at break for the neat scaffold was higher than that of the porous structures. The mechanical properties of the 3D porous P(3HO) scaffold could not be measured in this study and this will be carried out in future. In a similar study carried out by Wang *et al.*, porous scaffolds were prepared using poly(1,8-octanediol-co-citric acid) (POC) and the Young's modulus value was found to decrease with increase in porosity, decreasing from 3.5kPa for 60% porosity to 1.5 kPa for 80% porosity. This was explained by the fact that the pores created large empty spaces in the scaffold which made the structure less stiff and result in a decreased Young's modulus value. Similar studies have also been carried out using poly(glycerol sebacate), where the porous scaffold exhibited a low Young's modulus of 0.28MPa and minimum elongation at break of 267% (Wang *et al.*, 2002). In another study conducted on the effect of collagen in electrospun scaffolds of poly(ester urethane)/collagen blends, it was found that the Young's modulus of the scaffold decreased from 8MPa to 2MPa and the elongation at break increased from 220% to 270%, with scaffolds including 90% collagen (Stankus *et al.*, 2004). Also, scaffolds made of polyester urethane urea were characterised for their use in soft tissue engineering. The tensile strength of the scaffold ranged from 0.97-1.64MPa, while the elongation at break was 214%-294% (Yin *et al.,* 2003). It was also observed that after 2 weeks, due to polymer degradation, the mechanical properties of the scaffold changed with an elongation at break of 150% and a tensile strength of 0.8 MPa.

The surface property of the films is yet another very important factor that governs cell attachment and proliferation on a scaffold, ultimately determining their success in regeneration of the diseased tissue. Biomaterials interact with the biological environment on the surface,

making the characterization of the surface crucial for understanding subsequent biological effects. Water contact angle analysis was conducted on the films and the related static water contact angle measured for the neat and porous P(3HO) films. The water contact angle (θ_{H2O}) is a measure of the hydrophilic or hydrophobic property of a material surface, which is in turn directly related to cell adhesion. Cell adhesion to a surface occurs by adhesion receptors present on the cell that binds to proteins adsorbed on the biomaterial surface and the conformation of these proteins depends on the surface wettability (Lee *et al.*, 2003). Surfaces with θ_{H2O} less than 70° are considered to be hydrophilic and θ_{H2O} greater than 70° are considered to be hydrophobic in nature (Peschel *et al.*, 2008). The water contact angle on the neat P(3HO) film was higher than the porous films. Hence, the P(3HO) neat film was found to be much more hydrophobic than the P(3HO) porous film, which indicated that the porous P(3HO) films have a greater potential as a scaffold as compared to the neat film. It has also been found that hydrophobic films pre-coated with matrix proteins such as laminin, exhibit a lower hydrophobicity and are a better surface for the adhesion of cardiomyocytes. Cardiomyocytes do not attach well on hydrophobic films but attached well on the films precoated with laminin protein (McDevitt *et al.*, 2003). In another study, a composite scaffold was made using poly (lactic-*co*-glycolic acid), poly(DL-lactide-co-caprolactone) and type I collagen. PLGA/PCL polymers are strong but hydrophobic, and hence are not conducive for cell adhesion. Type I collagen was used to coat the surface of the composite to form a modified scaffold which promoted cell proliferation and attachment. The growth of cardiomyocytes and presence of TnI (a marker of contractile protein) on the cardiomyocytes were found to be higher on the composites coated in collagen as compared to the collagen and PLGA controls (Park *et al.*, 2005). Thus, hydrophilic surfaces are considered to be better than hydrophobic surfaces for cell attachment in cardiac tissue engineering. The porosity of the film was also calculated with respect to the neat film. The pores on the films help in cell attachment and provide a higher surface area for the cells to adhere to the surface (Lebourg *et al*., 2008). *In vitro* cell proliferation analysis also confirmed that the increase in porosity promoted cell growth and hence a highest cell proliferation rate was observed on the porous scaffold produced using 1.5% porogen as compared to other porous and neat scaffolds. The SEM image of the porous scaffolds with C2C12 myoblast cells also depicted that the cells preferred to attach on the pores, hence, the presence of the pores increased the cell proliferation rate. The SEM image of the neat P(3HO) scaffold presented a smooth surface. The SEM image of the porous scaffolds revealed pores on the surface which increased the surface area and provided roughness to the scaffold which would help in cell adhesion. With regard to roughness of the surface affecting

the growth of different kinds of cells, researchers have observed that increased surface roughness has a positive effect on cell adhesion (Richert *et al.*, 2008). The result of the neat P(3HO) scaffold was found to be similar to that of Rai *et al.,* 2011, as the neat film was found to be smooth and without any grooves. This film surface was found to be smoother as compared to that of the P(3HB) film.

The scanning electron microscopy of the surface and cross section view of the 3D porous P(3HO) scaffold was found to have pores of diameter 250-300 μm which were formed by the salt leaching. The porosity was evenly distributed throughout the surface and the bulk of the scaffold. The microCT videos which scanned the scaffold through every plane also confirmed a well-connected porosity of the structure. Pok *et al.* (2012) in a similar study, prepared a 3D structure comprising of self-assembled PCL which was sandwiched between a gelatin-chitosan hydrogel which resulted in a porous structure and was used for cardiac tissue engineering. The biocompatibility of this structure was analysed *in vitro* by seeding neonatal rat ventricular rat myocytes (NVRM). A higher rate of cell adhesion and functioning was observed in all the different ratios of gelatin-chitosan with PCL structures as compared to neat PCL scaffolds. This can be explained to be due to the lack of cell binding sites in the neat PCL scaffolds as compared to the higher surface area provided by the 3D sandwich porous structure. In the present study, *in vitro* cytocompatibility with C2C12 was conducted on the scaffold. The cell proliferation study indicated that the 3D porous structure exhibited significantly higher proliferation rate as compared to the 2D neat P(3HO) scaffold. This indicates that the 3D P(3HO) scaffold not only provided support for cell attachment but also promoted a high cell proliferation rate. In a study conducted on *Bombyx mori* silk fibroin scaffold for cardiac tissue engineering, it was also observed that the 3D porous structure provided better support and exhibited higher growth rate for the menstrual blood-derived stem cells (MenSCs) and bone marrow-derived mesenchymal stem cells (BMSCs) (Rahimi *et al.*, 2014).

Hence in this chapter, different 2D and 3D porous P(3HO) scaffolds were studied with respect to their mechanical properties and *in vitro* cytocompatibility with C2C12 cells. A drastically lower stiffness of the 2D porous scaffold was observed as compared to the neat P(3HO) scaffold. The *in vitro* cell compatibility also confirmed a higher cell proliferation rate on the 2D porous scaffolds as compared to the neat structure. The 3D porous structure produced, exhibited a well-connected network of pores within the scaffold which hence provided better attachment and significantly higher cell proliferation rate for the C2C12 cells. These studies

confirmed that porous structures are potentially better scaffolds for cardiac tissue engineering applications.

CHAPTER 6

Modification of the scaffold: Introduction of electrical conductivity; incorporation of peptides and growth factors

6.1. Introduction

Conductive polymers have been useful in a variety of applications including battery technology, photovoltaic devices and biomedical applications. Examples of such polymers include polypyrrole (PPy), polyaniline (PANI). Polyaniline (PANI) is one of the most popular conducting polymers to be used in tissue engineering. Various properties of polyaniline such as good conductivity, low toxicity, better defined electrochemical response as compared to other conducting polymers, make it suitable to be used in tissue engineering applications.

Tissue regeneration is a complex process and involves several promoters/growth factors. Several growth factors such as Vascular Endothelial Growth Factor (VEGF), fibroblast growth factor (FGFs) are required for different essential activities of the cell. Peptides such as RGD are known to enhance cellular adhesion on the scaffold. Hence, incorporation of growth factors and peptides in a scaffold promotes better adhesion and differentiation of the cells on the tissue engineering scaffold. The biocompatibility of the scaffold also depends on its ability to adsorb specific proteins which the cells would interact with, instead of the material alone. Unspecific protein interactions need to be prevented as it can lead to many problems including acute chronic inflammation and fibrous encapsulation. Hence, surface modification of the scaffold in order to enable binding of the desired protein and prevention of non-specific protein binding is desirable. Polymers such as poly(hydroxyethyl methacrylate), poly(acrylamide), poly(N,N-dimethyl acrylamide), dextran, poly(oxazoline) and poly(ethylene glycol) (PEG) have been explored for such applications.

In this chapter, modification of the PHA scaffold has been carried out using two different approaches. The first approach involved the incorporation of electrical conductivity in to the P(3HO) scaffold achieved by blending with PANI followed by analysis of material characteristics and effect on cardiomyocyte proliferation and function. The second approach involved the incorporation of the six-armed star-shaped poly(ethylene oxide-stat-propylene oxide) with isocyanate end groups (NCO-sP(EO-stat-PO) with P(3HO):P(3HN-co-3HHP) (80:20) and its functionalization with RGD, YIGSR peptides and VEGF growth factor. Electrospun fibres of the blend of P(3HO):P(3HN-co-3HHP) (80:20)/modified (NCO-sP(EO-stat-PO) were produced and the effect on cardiomyocyte growth/function was monitored.

6.2. Results

6.2.1. Chemical characterisation of P(3HO):PANI blend films by FTIR

P(3HO):PANI blend films, prepared as described in section 2.4, were dark green coloured and 0.20 cm in thickness. For the chemical characterization of these P(3HO):PANI blend films, FTIR was conducted (Figure 1). It was observed that P(3HO), exhibited the characteristic peaks of 1734 cm^{-1} and 1160 cm^{-1} confirming the carbonyl double bond and the ester C-O stretching respectively. These were also observed in the spectrum of the P(3HO):PANI blend. Additional peaks were observed in the P(3HO):PANI blends at 1035 cm^{-1} indicating the asymmetrical stretching of the sulfonyl group present on the backbone of PANI chains which originated from the camphor sulphonic acid (CSA) and 3235 cm^{-1} which corresponded to the N-H stretching of the aniline group. Other peaks observed were at 2961 cm^{-1} and 2860 cm^{-1} for the alkyl groups. Some other significant peaks indicating the bonding of the CSA with PANI and formation of a blend of P(3HO)-PANI, 1260 cm^{-1} indicated the C-N bond stretching, 1223 cm^{-1} for the C-N vibrational mode, 1010 cm^{-1}, 864 cm^{-1} indicates the asymmetric stretching of the sulfonyl S-O-H group all of which are representative of the emeraldine salt (Mendes *et al*., 2011; Qazi *et al*., 2014).
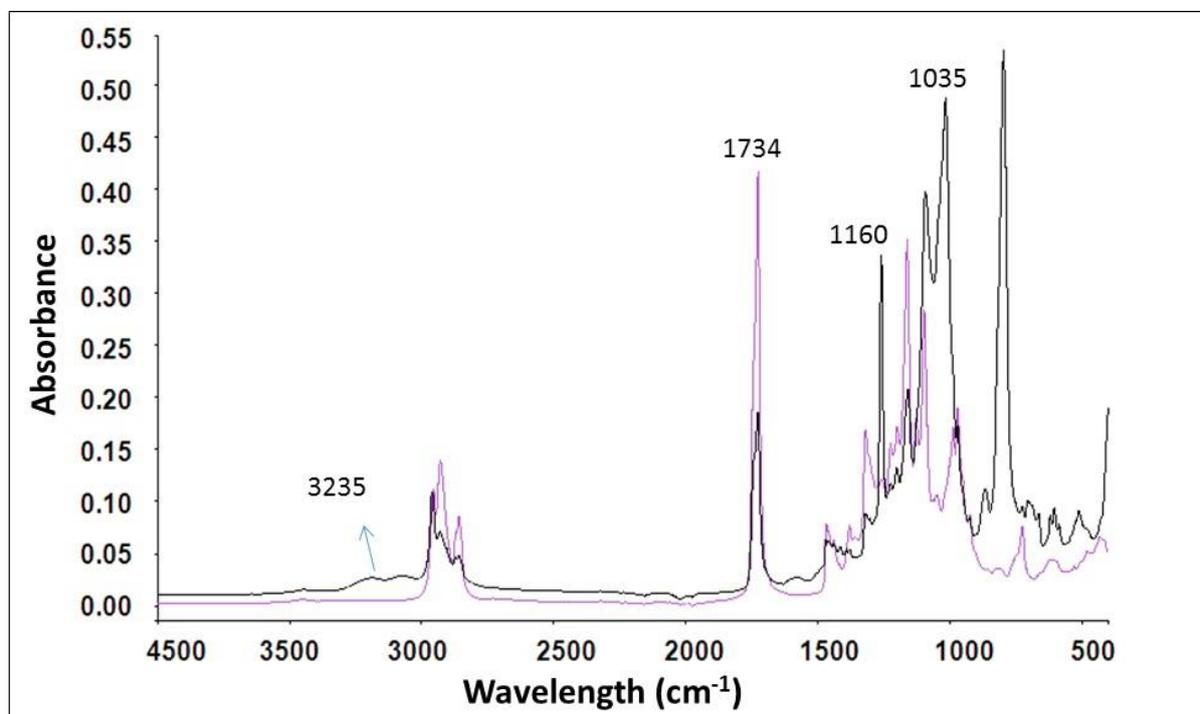
___Figure 6.1:___ *FTIR spectra of P(3HO) (purple line) and P(3HO):PANI scaffold (black line) indicating the important peaks of the spectrum.*

Electrical conductivity

The electrical conductivity of the scaffolds were measured using a multimeter (Figure 6.2). As expected, with the increase in the volume % of PANI, there was a corresponding increase in the electrical conductivity. Also, P(3HO): PANI 30 vol% (the P(3HO)/PANI blend containing 30 vol% of PANI) showed a significantly higher electrical conductivity as compared to the P(3HO):PANI 10 vol%. This showed that all the P(3HO):PANI blends had an inherent electrical conductivity due to the addition of PANI in the blend.
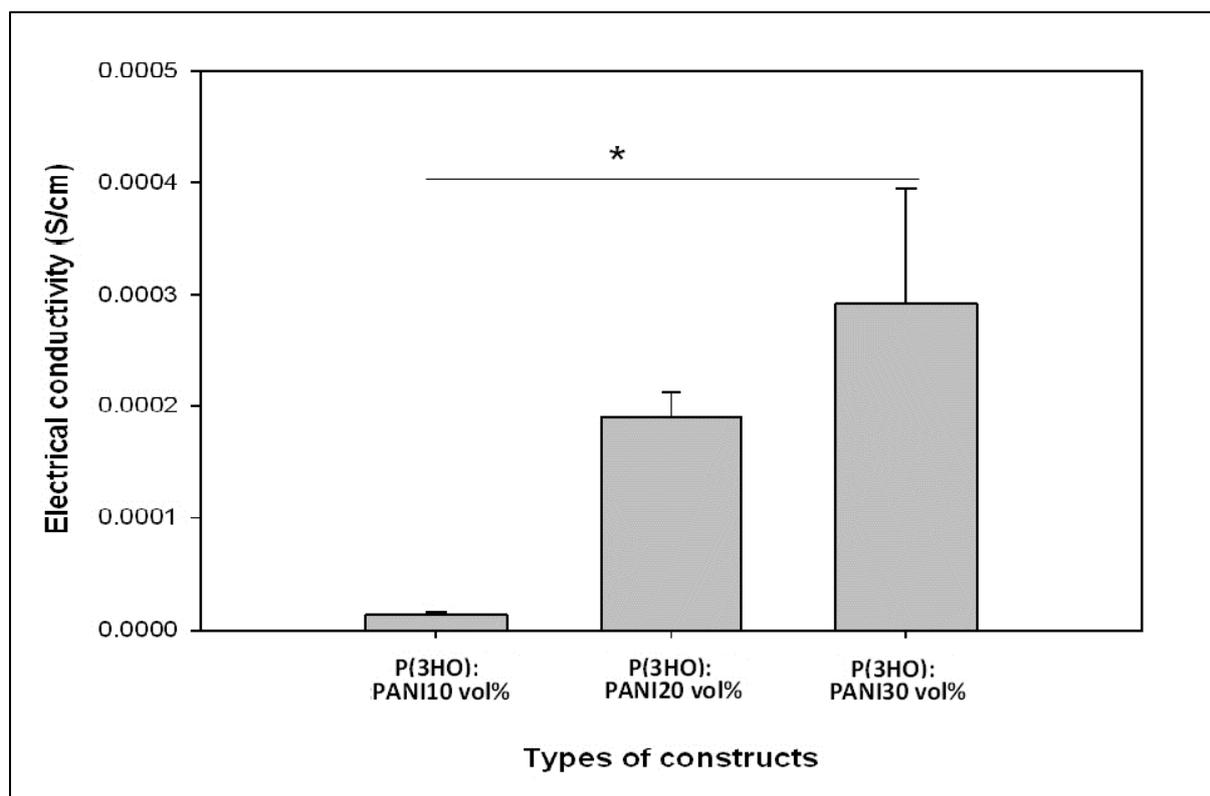
Figure 6.2*: Graph depicting the electrical conductivity of the P(3HO):PANI scaffolds. (n=3, *p<0.05, ANOVA.*

Water contact angle study

The water contact angle of the films with P(3HO):PANI 10 vol%, P(3HO):PANI 20 vol% and P(3HO):PANI 30 vol% were measured and summarised in Table 6.1. This showed that all the scaffolds are slightly hydrophobic in nature as the value is just higher than 70º. There was no significant difference found among the values observed for the P(3HO):PANI blends but it also showed that the introduction of PANI with P(3HO) has significantly reduced the hydrophobicity of neat P(3HO).

Table 6.1: *Water contact angle of the P(3HO):PANI blend scaffolds with 10 vol%, 20 vol%*
and 30 vol% PANI (n=3)

Samples	Water contact angle (º)
P(3HO)	101.1±1.9
P(3HO):PANI 10 vol%	82.1±9.8
P(3HO):PANI 20 vol%	85.3±11.2
P(3HO):PANI 30 vol%	84.4±6.4

Degradation study

The degradation study was also characterized by comparing the % water uptake, % weight loss
and pH change for a period of 30 days and was measured at day 5, day 15 and day 30. The
values were calculated as explained in detail in section 2.4.

The % water uptake was measured on 5, 15 and 30 days as depicted in Figure 6.4, after 30 days
the P(3HO):PANI 20 vol% and P(3HO):PANI 30 vol% showed a gradual and significant
decrease while P(3HO):PANI 10 vol% showed a slight increase. The % weight loss was also
recorded for the scaffolds on day 5, 15 and 30 as shown in Figure 6.5. It was observed that
there was significant increase in % weight loss in P(3HO):PANI 20 vol% and P(3HO):PANI
30 vol% at the end of 30 days while there was a significant decrease observed in P(3HO):PANI
10 vol%.
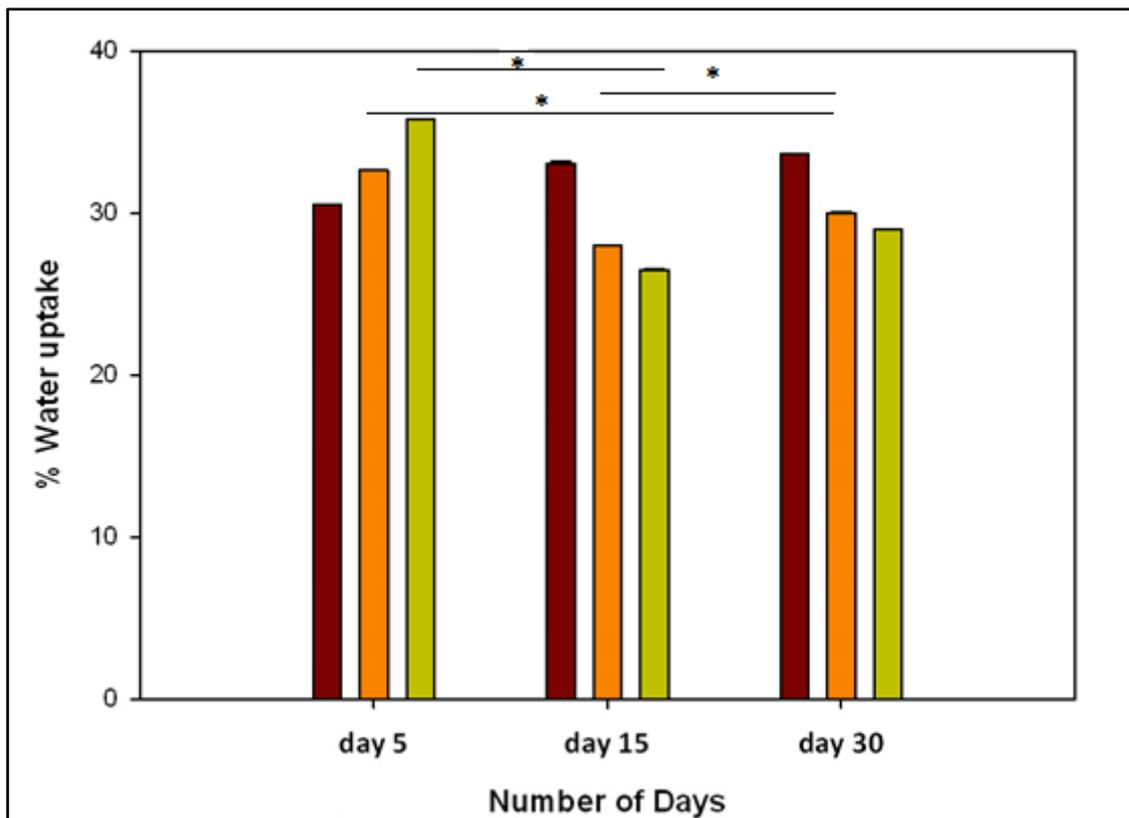
Figure 6.3: *Water uptake % of the P(3HO):PANI blend scaffolds with P(3HO):PANI 10 vol% (brown), P(3HO):PANI 20 vol% (orange), P(3HO):PANI 30 vol% (green) for 5, 15 and 30 days. (n=3),p<0.05, ANOVA.*
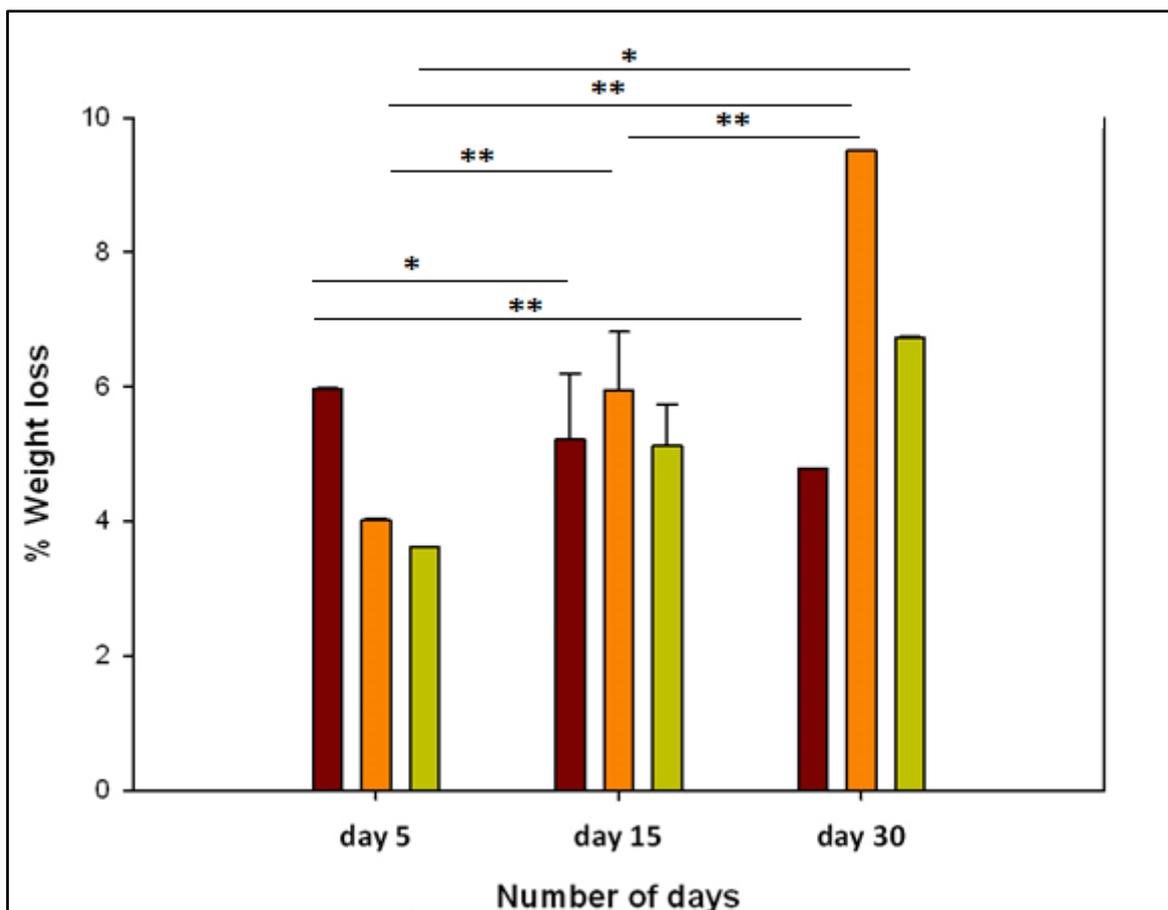
Figure 6.4: *Weight loss % of the P(3HO):PANI blend scaffolds with P(3HO):PANI 10 vol% (brown), P(3HO):PANI 20 vol% (orange), P(3HO):PANI 30 vol% (green) for 5, 15 and 30 day. (n=3), *p<0.05,**p<0.001, ANOVA.*

A pH study was conducted in PBS for a period of 30 days (Figure 6). It was observed that the pH of all the scaffolds i.e. P(3HO):PANI 10 vol% , P(3HO):PANI 20 vol% and P(3HO):PANI 30 vol% significantly decreased from 7.4 to a value of ~6.9 for all the constructs.
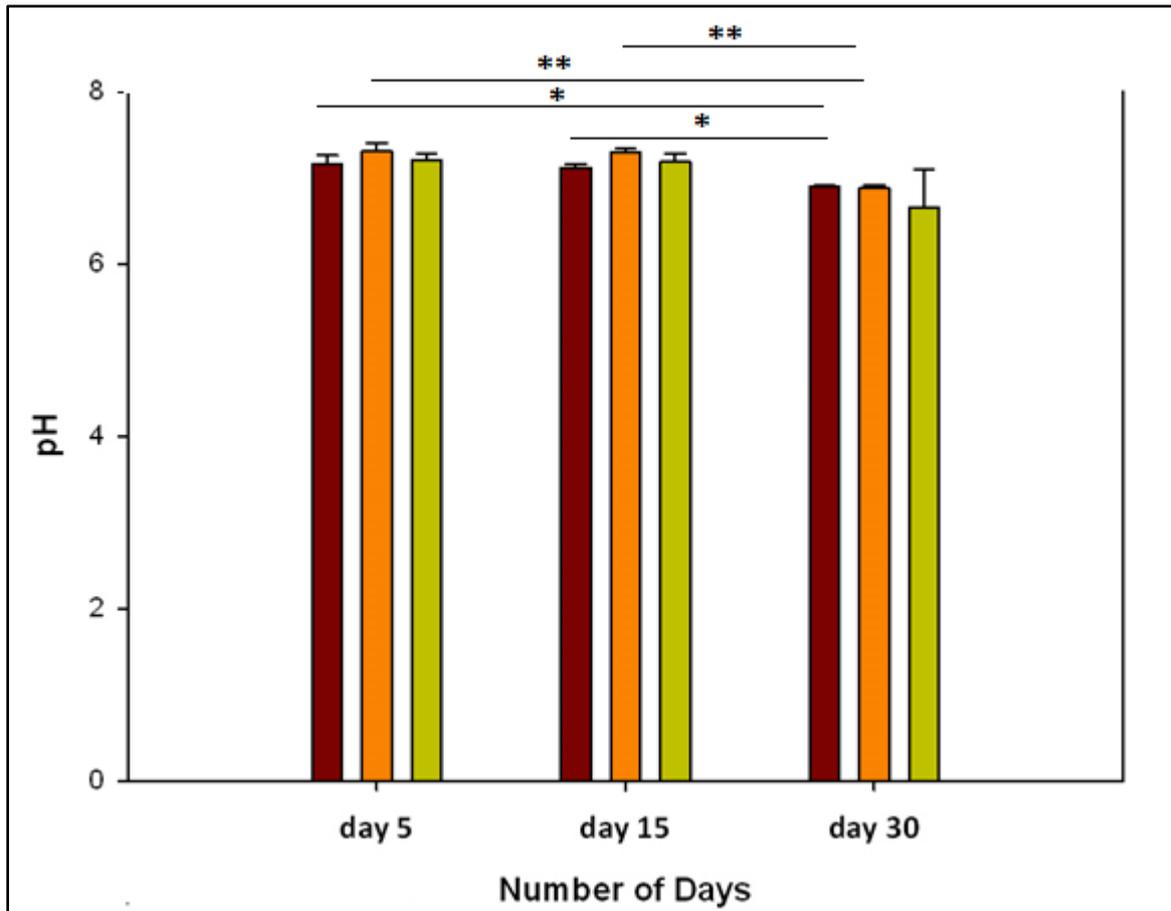
Figure 6.5: *pH profile study of the P(3HO):PANI blend scaffolds with P(3HO):PANI 10 vol% (brown), P(3HO):PANI 20 vol% (orange), P(3HO):PANI 30 vol% (green) for 5, 15 and 30 days.(n=3), *p<0.05,**p<0.001, ANOVA.*

In vitro cell compatibility with the P(3HO): PANI blend scaffolds

The *in vitro* cytocompatibility of the P(3HO):PANI blend scaffolds were tested using Neonatal Ventricular Rat Myocytes (NVRMs). The cells were grown on the scaffolds and a live and dead assay was carried out on day 3 (Figure 6.7 and 6.8). As seen in Figure 6.7, the cells attached and grew well on all the P(3HO):PANI blend scaffolds equally. The higher amount of PANI did not act toxic instead promoted cell attachment and proliferation.
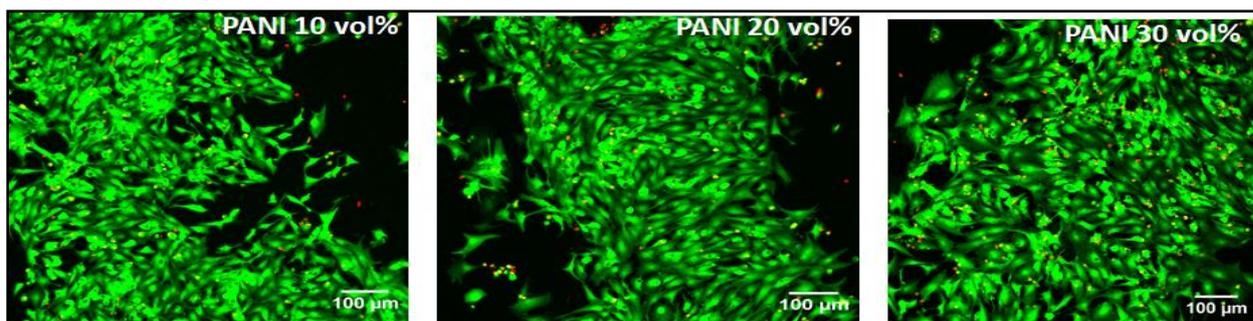
Figure 6.6*: Representative images of live NVRM cells (green) and dead NVRM cells (red) on different P(3HO):PANI blend scaffolds.*
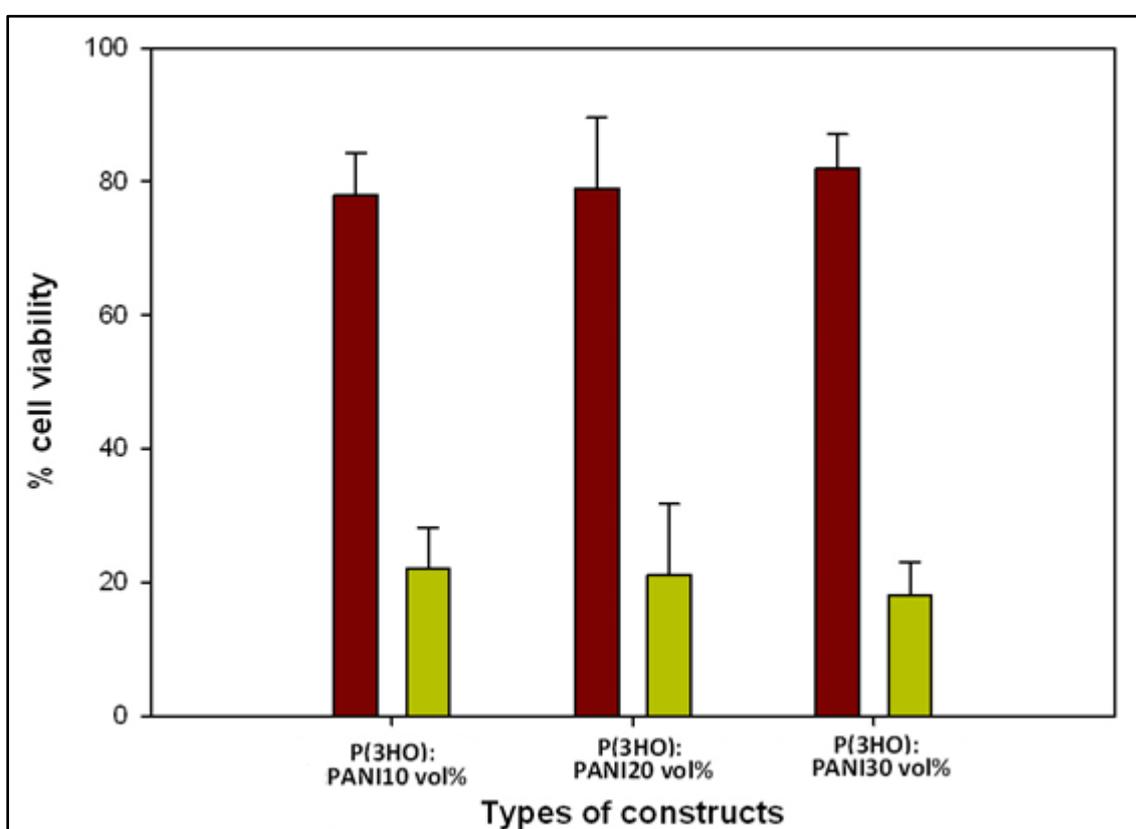
Figure 6.8*: In vitro cell viabiltiy study indicating live NVRM cells (brown) and dead NVRM cells (green) on the P(3HO)/PANI blend scaffolds after conducting a live/dead assay. (n=6), no significant difference ANOVA*

PART 2

6.2.2. P(3HO): P(3HN-co-3HHP) (80:20)/NCO-sP(EO-stat-PO) electrospinning

The polymer solution including a 80:20 blend of P(3HO) and P(3HN-co-3HHP) and NCO-sP(EO-stat-PO), VEGF, RGD and YIGSR were electrospun using the method described in section 2.4. The solutions used were as follows:

- 80:20 blend of P(3HO) and P(3HN-co-3HHP) polymer with only NCO-sP(EO-stat-PO)

- 80:20 blend of P(3HO) and P(3HN-co-3HHP) polymer with NCO-sP(EO-stat-PO) and VEGF

- 80:20 blend of P(3HO) and P(3HN-co-3HHP) polymer with NCO-sP(EO-stat-PO) and RGD and YIGSR

- 80:20 blend of P(3HO) and P(3HN-co-3HHP) polymer with NCO-sP(EO-stat-PO) and VEGF and RGD and YIGSR

Good quality fibres were obtained with no beading (Figure 6.9).

The water contact angle of the fibres obtained were measured as summarised in Table 6.2. There was no significant difference among the scaffolds, however, the scaffolds exhibited significantly lower water contact angles for the P(3HO):P(3HN-co-3HHP) (80:20) fibres with NCO-sP(EO-stat-PO), including RGD,YIGSR peptides and the VEGF growth factor as compared to the neat P(3HO):P(3HN-co-3HHP) (80:20) fibres. This observation indicated the presence of the hydrophilic groups of NCO-sP(EO-stat-PO), RGD,YIGSR and VEGF on the surface of the P(3HO):P(3HN-co-3HHP) (80:20) fibrous scaffolds. Hence, the one step method of functionalisation using NCO-sP(EO-stat-PO) was indeed successful.
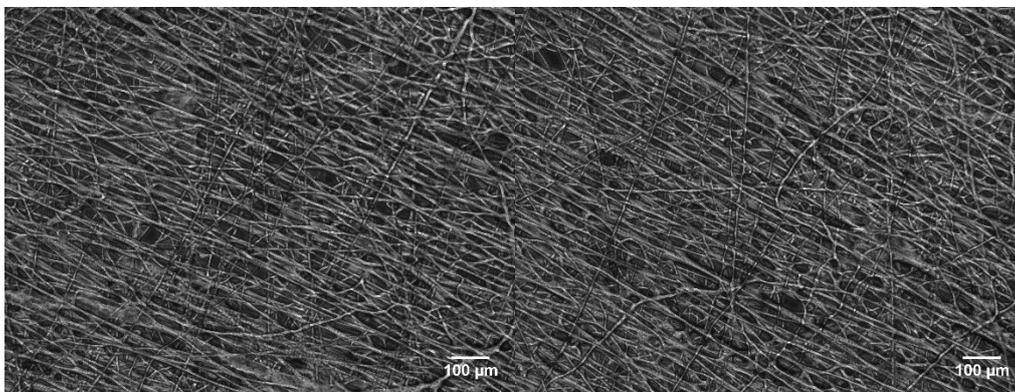
Figure 6.8: *Representative images of electrospun fibres of P(3HO):P(3HN-co-3HHP)(80:20) with NCO-sP(EO-stat-PO),RGD,YIGSR and VEGF.*

Table 6.2: *Table indicating water contact angles of the different constructs including P(3HO):P(3HN-co-3HHP) (80:20) with NCO-sP(EO-stat-PO) VEGF, RGD and YIGSR peptides. (n=5).*

Samples	Water contact angle (°)
P(3HO)/P(3HN-co-3HHP) (80:20) with NCO-sP(EO-stat-PO)	74.7°±2.0
P(3HO)/P(3HN-co-3HHP) (80:20) with NCO-sP(EO-stat-PO) and VEGF	79.7°±3.0
P(3HO)/P(3HN-co-3HHP) (80:20) with NCO-sP(EO-stat-PO), RGD and YIGSR	79.6°±3.5
P(3HO)/P(3HN-co-3HHP) (80:20) with NCO-sP(EO-stat-PO), VEGF, RGD and YIGSR	82.7°±3.4
P(3HO): P(3HN-co-3HHP) (80:20)	100.5±3.5

In vitro cell cytocompatibility with the functionalized fibres

The neonatal ventricular rat myocytes (NVRMs) were grown on the fibres for 3 days. The number of live and dead cells were counted on the fibres and analysed (Figure 6.10). It was observed that the scaffold P(3HO):P(3HN-co-3HHP) (80:20)/NCO-sP(EO-stat-PO) with all the three active molecules including the VEGF growth factor, RGD and YIGSR peptides and P(3HO):P(3HN-co-3HHP) (80:20)/NCO-sP(EO-stat-PO) with two (RGD and YIGSR) additives, exhibited significantly higher number of live cells as compared to that on the P(3HO):P(3HN-co-3HHP) (80:20)/NCO-sP(EO-stat-PO) scaffolds.

.
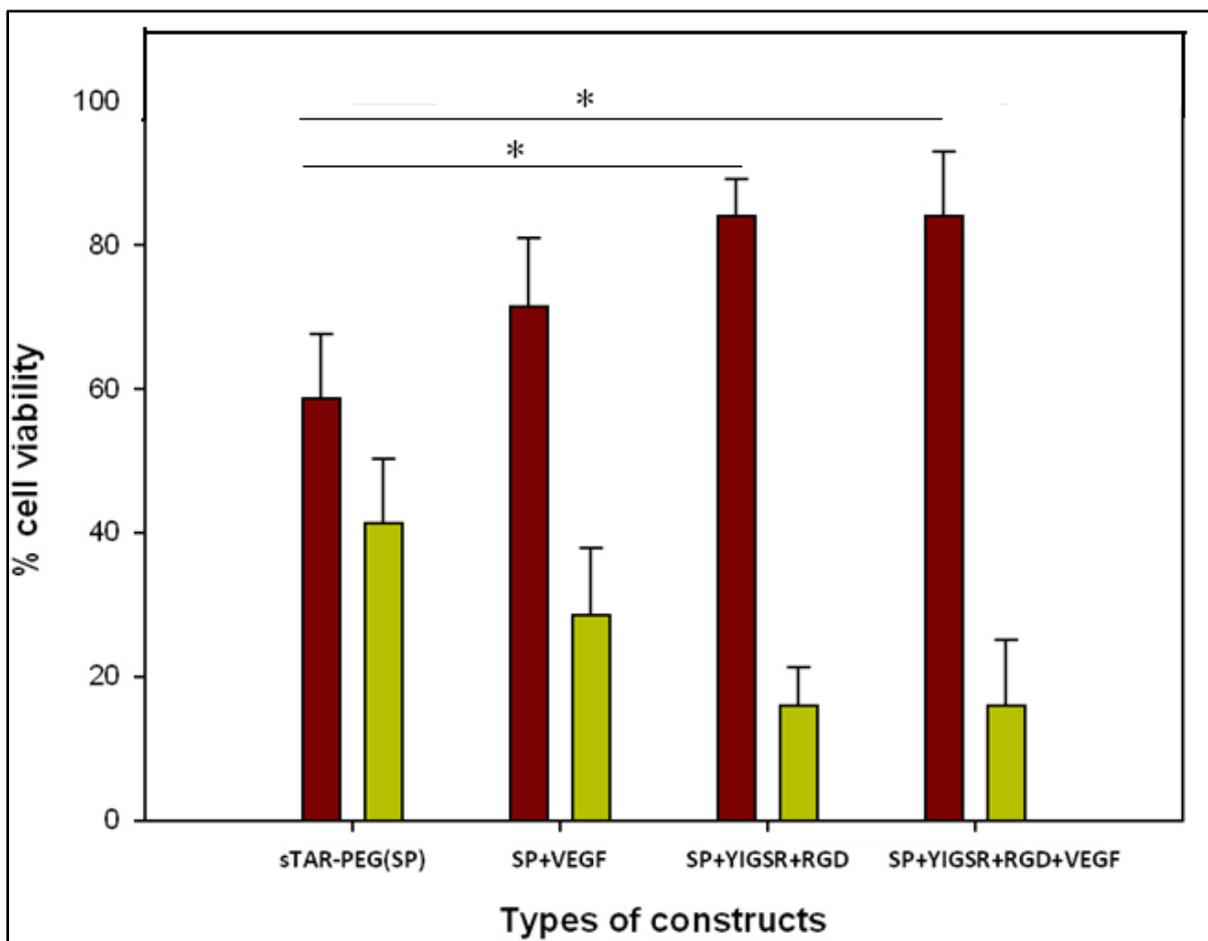
Figure 6.9*: In vitro cell viability showing live cells (brown) and dead cells (green) of NVRMs grown on different scaffolds where (i) star-PEG(SP) indicates P(3HO)/P(3HN-co-3HHP) with NCO-sP(EO-stat-PO) (ii)SP+VEGF indicates scaffolds with P(3HO)/P(3HN-co-3HHP) with NCO- sP(EO-stat-PO) and VEGF (iii) SP+YIGSR+RGD indicates P(3HO)/P(3HN-co-3HHP) with NCO-sP(EO-stat-PO), RGD and YIGSR peptides (iv) SP+YIGSR+ RGD+VEGF indicates P(3HO)/P(3HN-co-3HHP) with NCO-sP(EO-stat-PO), VEGF, RGD and YIGSR. (n=6)*p<0.05. ANOVA*

6.3. Discussion

In this chapter different modifications were performed with the polymers in order to improve their cytocompatibility. In the first part P(3HO) was blended with PANI in different volume % which were 10 vol%, 20 vol% and 30 vol%. The scaffold films were fabricated and dark green coloured films were formed. The confirmation of the incorporation of the PANI was carried out by conducting FTIR of the blend films. Specific peaks were observed involving the presence of sulphonic acid group from CSA and the ester carbonyl double bond from the P(3HO), which confirmed the successful blending of hydrophobic P(3HO) and hydrophilic PANI. This result has also been confirmed by Qazi *et al.*, 2014 where PGS was blended with PANI in different volume %. Hsiao *et al.,* also successfully blended a hydrophobic polymer

PLGA with the hydrophilic PANI and was successful in fabricating aligned fibrous meshes. Neonatal ventricular rat myocytes were grown on these meshes and the cells were seen to align themselves on the fibres with the expression of connexion 43, a gap junction protein. This study showed that PANI was an excellent conducting polymer and could be used to stimulate seeded cardiomyocytes into beating synchronously (Hsiao *et al.*, 2013)

The electrical conductance of the scaffold is one of the major desirable attributes of a scaffold to be used for cardiac tissue engineering. In a study conducted by Roberts-Thomson *et al.* the conductivity of the native myocardium was founded to be in the range of 0.0016 S cm^{-1} longitudinally to $5x10^{-5}$ S cm^{-1} transversally. In this work the P(3HO):PANI blends showed values of conductivity ranging from 1.38 x10^{-5} S cm^{-1} - $2.92x10^{-4}$ S cm^{-1}. These values were found to be in the range found in literature for other polymer blends. In a study by Qazi *et al.*, PANI-PGS blend films were fabricated with 15 vol%, 20 vol%, 25 vol% and 30 vol% of PANI and electrical conductivities of $1.4x10^{-5}$, $2.8x10^{-5}$, $1.7x10^{-4}$ and $1.03x10^{-3}$ S cm^{-1} respectively were measured after 4 days (Qazi *et al.*, 2014). In another study blend and coaxial fibrous mats of poly(L-lactide-co-ε-caprolactone) (PLCL) and PANI were electrospun with different ratios of (PLCL/PANI) ranging from of 0, 15 and 30% of PANI content. Neat PLCL fibres did not show detectable conductivity. While the incorporation of PANI into PLCL fibres significantly increased the conductivity according to the amount of PANI; from 0.160 ± 0.046 S/cm for the PLCL/PANI-15 fibres to 0.296 ± 0.064 S/cm for the PLCL/PANI-30 fibres (Jun *et al.*, 2009).

The water contact angle of the scaffolds were measured in order to observe the wettability of the films with the incorporation of PANI in P(3HO). In this study it was observed that the static water contact angle of the PANI blended scaffolds decreased significantly as compared to the neat P(3HO) scaffold. Hence, as expected, the incorporation of PANI in P(3HO), made the blend more hydrophilic. This was also observed in a study conducted on Co_3O_4 and PANI, where the core shell structure was fabricated using PANI which formed the shell and the core comprised Co_3O_4 and PANI-Co_3O_4 nanocomposites were formed. It was observed that the water contact angle of the PANI coated composite was 48.88º as compared to the neat Co_3O_4 which was 67.74º (Hai *et al.,* 2016). In a similar study conducted on polyvinyl alcohol (PVA)/PANI films, it was observed that the films with higher thickness of PANI exhibited lower contact angles and hence lower hydrophobicity. This was explained to be due to an increase in the porosity and hydrophilicity of the PANI coated films (Patil *et al.*, 2011). In another study a mixed matrix of polyethersulfone (PES) with PANI-co-MWCNTs

(polyanilinie-co-multi walled carbon nanotubes) composite nanoparticles were used to produce a nanofiltration membrane. Different amounts of the PANI-co-MWCNT composite nanoparticles were used with a constant concentration of PES. It was observed that with increasing concentration of the PANI-co-MWCNT in the composite, the water contact angle decreased from 69.43º for the scaffold with no particles to 43.76º for scaffolds with 1% PANI-co-MWCNT nanoparticles. Thus the results showed that with an increase in PANI-co-MWCNT concentration, there was an increase in the hydrophilicity of the membrane. The addition of PANI makes the scaffold porous in nature allowing access to water molecules, lowers the contact angle, thus resulting in a higher apparent hydrophilicity of the scaffolds (Bagheripour *et al.*, 2016). The lowering of the water contact angle enables various growth factors to interact and support cell proliferation.

In vitro degradation was also carried out for a duration of 30 days and samples were analysed at day 5, 15 and 30. There was a gradual and significant decrease in the % water uptake observed in P(3HO):PANI 20 vol% and P(3HO):PANI 30 vol% and an increase observed in P(3HO):PANI 10 vol% over the period of 30 days. Due to the higher PANI content in scaffolds with 20 vol% and 30 vol%, they absorbed more water in the initial days of the experiment and became saturated earlier over the course of time while in scaffold with 10 vol% PANI, the water was absorbed gradually and hence an increase was observed. The % weight loss was also measured and with P(3HO):PANI 20 vol% and P(3HO):PANI 30 vol% , a significant increase was measured while with P(3HO):PANI 10 vol% blend, a decrease in the % weight loss was observed. This could be explained in conjunction with the % water uptake. As the P(3HO):PANI 20 vol% and P(3HO):PANI 30 vol% had a higher % water uptake during the course of the experiment, they exhibited a higher weight loss during this period due to enhanced hydrolytic degradation and loss of the absorbed water. The P(3HO):PANI 10 vol% had a gradual increase in the water uptake, hence the weight loss was not initially enhanced and in turn a decrease in the weight loss was observed. A lower pH was observed for all the scaffolds. This lowering of the pH can be explained by the leaching of the CSA dopant from the scaffolds as a result of the degradation. This was also observed by Qazi *et al*. (2014) where the pH of PGS/PANI constructs dropped from 7.4 to ~ 6.9 after 30 days, in an in vitro degradation study.

Cell compatibility is an important desirable property for a scaffold, in order to be suitable for tissue engineering applications. In this work, NVRM cells were seeded on the P(3HO): PANI blend scaffolds and it was observed that the number of live cells increased with the increase in

PANI volume content. This study thus demonstrated that the NVRMs proliferated well on the P(3HO):PANI blend scaffolds and the scaffolds did not leach out any toxic by-product for the whole duration of the experiment i.e. 3 days. A study conducted by Qazi *et al.* (2014), showed a higher cytocompatibility and cell proliferation of the C2C12 cells on the PANI-PGS scaffolds. Jun *et al*. (2009) also conducted cell compatibility studies by seeding C2C12 cells on the PLCL/PANI scaffolds and cell proliferation was observed for 8 days with the formation of myotubes. In another study conducted on the PCL/PANI scaffolds, human mesenchymal stem cells (hMSC) were grown resulting in a cardiac tissue like growth. The cell survival test was investigated by using the MTT colorimetric assay. Immunoassay studies using antibodies specific for sarocomeric α-actinin also confirmed the interaction of the cells with PANI/PCL (Borriello *et al*., 2011).

The NCO-sP(EO-stat-PO) (poly(ethylene oxide-stat -propylene oxide) with isocyanate end groups) is a hexameric molecule which has been used in the functionalization of the polymers with various peptides and has been found to be highly effective. In this work, NCO-sP(EO-stat-PO) was electrospun with a blend of P(3HO) and P(3HN-co-3HHP) in the ratio of 80:20. The optical images of the fibres indicated successful electrospinning of the fibres. There have been various studies which have used NCO-sP(EO-stat-PO) and combined with other polymers and peptides to form scaffolds for tissue engineering applications. In a study poly(D,L-lactide-co-glycolide) (PLGA) was combined with NCO-sP(EO-stat-PO) in acetone and the resulting solution was used for electrospinning. The fibres were then functionalized with the peptide Gly-Arg-Gly-Asp-Ser (GRGDS) and cell adhesion studies were carried out by seeding human dermal fibrobasts. Higher number of adherent cells were observed on the scaffold with peptide functionalization and the overall survival rate was found to be above 88%. The wettability of the fibres were also recorded. It was observed that the PLGA fibres had a contact angle of 120º but the PLGA/NCO-sP(EO-stat-PO) fibres absorbed the water droplet within seconds thus showing the highly hydrophilic nature of the fibres with the additive (Grafahrend *et al*., 2010). Similar results were observed in this study where the water contact angle of P(3HO):P(3HN-co-3HHP) scaffold was around 100º but with the functionalisation of the RGD, YIGSR and VEGF using NCO-sP(EO-stat-PO) on the polymer, a significantly lower water contact angle was observed ranging from 74.6 º (P(3HO):P(3HN-co-3HHP)/ NCO-sP(EO-stat-PO)), 79.6º (with RGD and YIGSR), 79.7º (with VEGF) and 82.7º (with both peptide and VEGF). The cell compatibility on the scaffolds were also analysed by growing NVRMs onto the functionalized fibres and deducing the cell viability on the fibres. The NCO-sP(EO-stat-PO)

star additive rendered the PHA to be hydrophilic in nature. The surface segregation of the hydrophilic PEO based hydrophilic molecule within the hydrophobic polymer groups provides a conducive surface for interaction of cells (Grafahrend *et al*., 2010). The % cell viability was highest on the P(3HO):P(3HN-co-3HHP) (80:20)/ NCO-sP(EO-stat-PO) functionalized with VEGF, RGD and YIGSR and was found to be significantly higher as compared to the P(3HO):P(3HN-co-3HHP) (80:20)/ NCO-sP(EO-stat-PO). The cells on P(3HO):P(3HN-co-3HHP) (80:20)/ NCO-sP(EO-stat-PO) functionalized with RGD and YIGSR also showed higher cell viability as compared to the P(3HO):P(3HN-co-3HHP) (80:20)/ NCO-sP(EO-stat-PO) scaffold. This can be explained as the peptides and the growth factors interact positively with the cells and hence promote cell adhesion and proliferation. The NCO-sP(EO-stat-PO)) does not have any impact on the structure of the peptides and hence the adhesive peptides interact with their corresponding integrins without any hindrance (Fiedler *et al*., 2011).

CHAPTER 7

Conclusions and Future work

7.1. Conclusion

Polyhydroxyalkanoates (PHAs), in recent times have gained a lot of attention in medical applications due to their biodegradability and biocompatibility. In cardiac tissue engineering, there is need for a material which can give support to the infarct region along with help in reviving the heart tissue. For this purpose, in this project mcl PHAs, P(3HO) and P(3HN-co-3HHP) were used for the fabrication of a suitable cardiac patch. Different 2D and 3D scaffolds were fabricated using neat P(3HO), P(3HN-co-3HHP) and their blends. To increase the patch efficiency, a conducting polymer, polyaniline was incorporated in order to enhance the electrical performance of the patch. Also, in order to promote cell adhesion and angiogenesis, RGD peptide, YIGSR peptide and VEGF were introduced in to the scaffold.

In the first part of the project, P(3HO) and P(3HN-co-3HHP) polymers were synthesised using *Pseudomonas mendocina CH50* using MSM media, sodium octanoate and sodium nonanoate as the carbon source respectively, with nitrogen being the limiting factor. The bacteria were successfully cultured and the purified polymers were successfully extracted. The growth profile of the two fermentations were obtained. The maximum polymer content of the P(3HO) and P(3HN-co-3HHP) extracted after 48 hrs was measured to be 45.76% dry cell weight and 42.34% dry cell weight respectively. The preliminary structure of the polymers, expected to be mcl-PHAs were confirmed using FTIR. Final confirmation of the structure of the polymers were carried out by ^{13}C and ^{1}H NMR spectroscopy.

Five weight percent 2D neat scaffolds were fabricated using neat P(3HO), P(3HN-co-3HHP) and their blends in the ratio of 20:80 (P(3HO):P(3HN-co-3HHP)), 50:50 (P(3HO):P(3HN-co-3HHP)) and 80:20 (P(3HO):P(3HN-co-3HHP)) by solvent casting technology. The scaffolds were examined to be hydrophobic in nature along with smooth and plain surface topography. These scaffolds were assessed as possible candidates for cardiac patch development. One of the important aspects of a cardiac patch is its biodegradability. *In vitro* degradation studies suggested there was an increase in % water uptake and % weight loss along with a small decrease in pH in all the scaffolds over a period of 3 months. It is also highly important for the material to have biocompatibility with the seeded cells (Chen *et al*., 2008). The cardiac patch ideally is seeded with suitable cells and is implanted onto the infarct cardiac tissue. *In vitro* biocompatibility was compared among the films by seeding them with human induced pluripotent stem cell derived cardiomyocytes (hiPSC-CM). The live and dead assay showed

that all the scaffolds showed a comparable % cell viability with the positive control, gelatin. The material was biocompatible with the hiPSC-CM cells and hence promoted cell growth on the polymers, thus indicating that they were all suitable for cardiac patch development. The beating rate also indicated that the hiPSC-CM cells were viable and actively beating on all the scaffolds and gelatin but a significantly higher beat rate was measured on the neat P(3HN-co-3HHP) scaffold. This result confirmed that there were no deleterious effects caused by the polymer on the contractile properties of the cardiomyocytes. To study this in further detail, calcium transients were analysed which is an essential parameter for regulating cardiac contractions. The calcium transients analysed on all hiPSC-CMs which were grown on the PHA scaffolds were found to be comparable to the calcium transients when these were grown on gelatin. There was a decrease in the fluorescence amplitude in the P(3HN-co-3HHP) as compared to gelatin at a stimulation frequency of 1Hz but no difference was observed at a stimulation frequency of 1.5 Hz. The sarcomere length of the cardiomyocytes grown on all the constructs were found to be around 2µm which is comparable to that of the adult human myocardium. This confirmed that the cells grown on the films exhibited properties of adult cardiomyocytes. The nuclei density was found to be highest on the neat P(3HN-co-3HHP) scaffold.

In another part of the study, random aligned fibres were successfully electrospun using P(3HO), P(3HN-co-3HHP) and their blends in the ratio of 20:80 P(3HO):P(3HN-co-3HHP), 50:50 P(3HO):P(3HN-co-3HHP) and 80:20 P(3HO):P(3HN-co-3HHP). The fibres were hydrophobic in nature. The mechanical properties of the fibres could not be measured since they had a sticky texture and were difficult to handle on their own. *In vitro* biocompatibility of the fibres were analysed by growing hiPSC-CM cells on the electrospun sheets. The cells were found to be viable on the electrospun sheets and the beat rate was also comparable to the healthy cells. The live and dead assay showed a highest % cell viability was on the P(3HN-co-3HHP) scaffold for random fibres, while for aligned fibres all the scaffolds exhibited similar % cell viability. Cardiomyocytes exhibit anisotropy *in vivo*, so the cells on the scaffold should also be able to align themselves in order to exhibit maximum functionality. Hence, an ideal scaffold structure should be able to guide and support cellular alignment (Rockwood *et al.,* 2008). A quantification of alignment was conducted on the cells grown on the aligned fibres and in all the fibrous scaffolds, around 50% of the cells, while in non-fibrous gelatin 14% cells, showed a mean deviation of 0º-10º from the control line. This showed that the cells exhibited anisotropy which was directed due to the alignment of the fibres, as the cells grown on the non-fibrous gelatin show

isotropic behaviour. Thus, 50% of the cells exhibited anisotropy which was influenced because of the aligned fibrous scaffold.

In the next part of the study, 2D and 3D porous scaffolds were fabricated using P(3HO). The 2D porous films had a significantly lower Young's modulus value as compared to neat P(3HO), an important parameter to be considered for cardiac patch development. The hydrophilicity of the porous P(3HO) scaffolds produced using 0.5%, 1.0% and 1.5% porogen increased significantly as compared to the neat P(3HO) film. It was not possible to measure the water contact angle on the 3D P(3HO) scaffold as the water would not form a drop on the scaffold instead would fill in the pores of the scaffold. The *in vitro* cytocompatibility study on porous scaffolds with C2C12 myoblast cells indicated a significant increase in cell proliferation rate with increase in porogen concentration, confirming the positive role of porosity in cell attachment and proliferation.

Electrical conductivity plays a crucial part in the initiation of contraction in heart tissue, hence it is an added benefit to the scaffold to have intrinsic electrical conductivity when used as a cardiac patch. In this project, polyaniline was used as the conducting polymer. Polyaniline was synthesised and was successfully doped with camphor sulphonic acid (CSA). Different amounts of PANI were blended with P(3HO) and the solvent cast films were successfully produced. The films were characterised using FTIR and it was confirmed that polyaniline was successfully incorporated in all the P(3HO) films. All the blended films were measured to be electrically conductive. The *in vitro* degradation of all the films were studied and a decrease in % water uptake was observed in P(3HO):PANI 20 vol% and 30 vol% while an increase in % water uptake was observed in P(3HO):PANI 10 vol% after a 30 day period. An increase in % weight loss was observed in P(3HO):PANI 20 vol% and 30 vol% while a decrease in % weight loss was observed in P(3HO):PANI 10 vol% after a 30 day period. A small decrease in pH was observed in all the films after a 30 day period. The *in vitro* cytocompatibility of the blend films was analysed using NVRMs and the presence of a large number of viable cells was confirmed by the live/dead assay, confirming cytocompatibility of the P(3HO): PANI blends.

In the final part of the project, surface functionalisation of the scaffolds was carried out by incorporating the RGD and YIGSR peptides along with the growth factor VEGF using NCO-sP(EO-stat-PO) on 80:20 (P(3HO):P(3HN-co-3HHP)) polymer blend electrospun fibres. Hence, a one-step method of surface functionalisation was successfully achieved using the

NCO-sP(EO-stat-PO) with 80:20 (P(3HO):P(3HN-co-3HHP)) blend. There was an increase in hydrophilicity of these fibres as compared to the non-functionalised fibres confirming the presence of the peptides/protein on the surface of the fibres. The *in vitro* cytocompatibility of these fibres showed that the highest cell viability was observed on the fibres functionalised with RGD, YIGSR peptide and the VEGF growth factor, exhibiting an additive activity of the three factors.

7.2. Future work

Based on the research and results carried out in this study the following areas could be further investigated for an optimal cardiac patch development:

- MCL-PHAs have been used for soft tissue engineering but the use of P(3HO) which is a homopolymer and P(3HN-co-3HHP) is novel in the field of cardiac patch development. Production of P(3HN-co-3HHP) with 42% dcw yield has been described in this project but it would be good to study the optimisation of the production of P(3HN-co-3HHP) from *Pseudomonas mendocina CH50*. This can be achieved by changing the fermentation conditions including pH of the media, C/N ratio and stirrer speed for increasing the yield of the polymers. These would have an impact on the growth of the cells and would promote polymer accumulation. Response surface analysis could be used to study the different fermentation conditions.

- Alignment and porosity are important parameters that a scaffold should have for its application in cardiac tissue engineering applications. In this work, P(3HO) and P(3HN-co-3HHP) and their blends have been fabricated into aligned fibres fabricated using electrospinning. There are many other techniques being used for the fabrication of aligned scaffolds. It would be interesting to achieve 3D aligned scaffolds using 3D printing technology. Porosity was also studied in this work by using porogen leaching technology and solvent casting. Freeze drying is another alternative technique which has shown to induce porosity including aligned porosity in various other elastomeric polymers. Hence, it would be a good study to fabricate 3D porous scaffolds using this technique (Frydrych *et al*., 2013) in the future.

- As scaffolds with inherent electrical conductivity is an important property for a cardiac patch, PANI was blended with P(3HO) to form conducting scaffolds. To mimic the extracellular matrix of the cardiomyoctes, further optimisation of these scaffolds could

be brought about by blending and electrospinning polyaniline with P(3HO) and P(3HN-co-3HHP) and produce aligned fibrous conducting scaffolds.

- The use of the additive NCO-sP(EO-stat-PO) for surface functionalisation of the scaffold in a one step process was proven to be a very simple and convenient process. The use of this additive could be further investigated for the generation of highly bioactive scaffold structures and its impact on cell adherence and viability. The use of RGD and YIGSR peptides was observed to increase cell attachment and proliferation. The combined use of RGD, YIGSR and VEGF could be further investigated by varying the concentration of the active molecules and determining an optimal concentration.

- Continuing with this work, further detailed study could be conducted on attachment, growth and alignment of hiPSC-CMs and NVRMs on the P(3HO) based cardiac patches by including an in depth analysis of the various known genetic markers linked to the process of cardiac differentiation.

- Along with an *in vitro* study, an *in vivo* study is essential to confirm the compatibility of the material with the infarcted heart tissue. The interaction of the surrounding tissues with the scaffold material will be an essential step forward in understanding of the *in vivo* functionality of the developed cardiac patch.

- Based on latest research in cardiac tissue engineering, the combination of bioprinting of gelatin methacryloyl (GelMA), microfluids and endothelial stem cells has been explored in an endothelial-myocardium-on-a-chip platform (Zhang *et al.,* 2016). This could provide an enabling technology for the development of next-generation human organ models for the diseased and infarcted myocardium. In relation to this work, studies could be conducted with the elastomeric P(3HO)/P(3HN-co-3HHP) polymers to enable the formation of an perfusion network on the chip with the help of the bioprinted polymer, endothelial cells and stem cells which could in future be used to treat the infarcted heart.

REFERENCES

- Akaraonye, E., Filip, J., Safarikova, M., Salih, V., Keshavarz, T., Knowles, J.C. and Roy, I., 2016. P (3HB) Based Magnetic Nanocomposites: Smart Materials for Bone Tissue Engineering. Journal of Nanomaterials, 2016, pp.1-14.

- Akaraonye, E., Moreno, C., Knowles, J.C., Keshavarz, T. and Roy, I., 2012. Poly (3-hydroxybutyrate) production by Bacillus cereus SPV using sugarcane molasses as the main carbon source. Biotechnology journal, 7(2), pp.293-303.

- Altankov, G., Grinnell, F. and Groth, T., 1996. Studies on the biocompatibility of materials: Fibroblast reorganization of substratum-bound fibronectin on surfaces varying in wettability. *Journal of biomedical materials research*, *30*(3), pp.385-391.

- Athira, K.S., Sanpui, P. and Chatterjee, K., 2014. Fabrication of Poly (Caprolactone) Nanofibers by Electrospinning. Journal of Polymer and Biopolymer Physics Chemistry, 2(4), pp.62-66.

- Bagdadi, A.V., Safari, M., Dubey, P., Basnett, P., Sofokleous, P., Humphrey, E., Locke, I., Edirisinghe, M., Terracciano, C., Boccaccini, A.R. and Knowles, J.C., 2016. Poly (3-hydroxyoctanoate), a promising new material for cardiac tissue engineering. Journal of Tissue Engineering and Regenerative Medicine, doi: 10.1002/term.2318.

- Bagheripour, E., Moghadassi, A. and Hosseini, S.M., 2016. Preparation of mixed matrix PES-based nanofiltration membrane filled with PANI-co-MWCNT composite nanoparticles. Korean Journal of Chemical Engineering, 33(4), pp.1462-1471.

- Basnett, P., Ching, K.Y., Stolz, M., Knowles, J.C., Boccaccini, A.R., Smith, C., Locke, I.C., Keshavarz, T. and Roy, I., 2013. Novel Poly (3-hydroxyoctanoate)/Poly (3-hydroxybutyrate) blends for medical applications. Reactive and Functional Polymers, 73(10), pp.1340-1348.

- Bedada, F.B., Wheelwright, M. and Metzger, J.M., 2016. Maturation status of sarcomere structure and function in human iPSC-derived cardiac myocytes. Biochimica et Biophysica Acta (BBA)-Molecular Cell Research, 1863(7), 1829-1838.

- Bendrea, A.D., Cianga, L. and Cianga, I., 2011. Review paper: progress in the field of conducting polymers for tissue engineering applications. Journal of biomaterials applications, 26(1), pp.3-84.

- Bergmann O, Zdunek S, Felker A, Salehpour M, Alkass K, Bernard S (2015) Dynamics of cell generation and turnover in the human heart. Cell 161:1566–1575

- Bers, D.M., 2000. Calcium fluxes involved in control of cardiac myocyte contraction. Circulation research, 87(4), pp.275-281.

- Bird, S.D., Doevendans, P.A., Van Rooijen, M.A., de la Riviere, A.B., Hassink, R.J., Passier, R. and Mummery, C.L., 2003. The human adult cardiomyocyte phenotype. Cardiovascular research, 58(2), pp.423-434.

- Borriello, A., Guarino, V., Schiavo, L., Alvarez-Perez, M.A. and Ambrosio, L., 2011. Optimizing PANi doped electroactive substrates as patches for the regeneration of cardiac muscle. Journal of Materials Science: Materials in Medicine, 22(4), pp.1053-1062.

- Brodsky, V.Y., Chernyaev, A.L. and Vasilyeva, I.A., 1992. Variability of the cardiomyocyte ploidy in normal human hearts. Virchows Archiv B, 61(1), pp.289-294.

- Byrom, D., 1994. Plastics from microbes: microbial synthesis of polymers and polymer precursors.(pp. 5-33). Munich: Hanser.

- Camelliti, P., Borg, T.K. and Kohl, P., 2005. Structural and functional characterisation of cardiac fibroblasts. Cardiovascular research, 65(1), pp.40-51..

- Capulli, A. K., L. A. MacQueen, Sean P. Sheehy, and K. K. Parker. "Fibrous scaffolds for building hearts and heart parts." Advanced drug delivery reviews 96 (2016): 83-102.

- Castro-Ferreira, R., Fontes-Carvalho, R., Falcão-Pires, I. and Leite-Moreira, A.F., 2011. The role of titin in the modulation of cardiac function and its pathophysiological implications. Arquivos brasileiros de cardiologia, 96(4), pp.332-339.

- CDI, 2013. iCell Cardiomyocytes user's guide. Cellular Dynamics International, Inc

- Cesca, F., Limongi, T., Accardo, A., Rocchi, A., Orlando, M., Shalabaeva, V., Di Fabrizio, E. and Benfenati, F., 2014. Fabrication of biocompatible free-standing nanopatterned films for primary neuronal cultures. RSC Advances, 4(86), pp.45696-45702.

- Chen, G., Zhang, G., Park, S. and Lee, S., 2001. Industrial scale production of poly (3-hydroxybutyrate-co-3-hydroxyhexanoate). Applied microbiology and biotechnology, 57(1-2), pp.50-55.

- Chen, G.Q. and Wu, Q., 2005. The application of polyhydroxyalkanoates as tissue engineering materials. Biomaterials, 26(33), pp.6565-6578.

- Chen, G.Q. and Wu, Q., 2005. The application of polyhydroxyalkanoates as tissue engineering materials. Biomaterials, 26(33), pp.6565-6578.

- Chen, G.Q., 2010. Plastics completely synthesized by bacteria: polyhydroxyalkanoates. In Plastics from bacteria (pp. 17-37). Springer Berlin Heidelberg.

- Chen, Q.Z., Harding, S.E., Ali, N.N., Lyon, A.R. and Boccaccini, A.R., 2008. Biomaterials in cardiac tissue engineering: ten years of research survey. Materials Science and Engineering: R: Reports, 59(1), pp.1-37.

- Chen, S.Y., Wei, Y.H. and Chang, J.S., 2007. Repeated pH-stat fed-batch fermentation for rhamnolipid production with indigenous Pseudomonas aeruginosa S2. Applied microbiology and biotechnology, 76(1), pp.67-74.

- Choi, M.H. and Yoon, S.C., 1994. Polyester biosynthesis characteristics of Pseudomonas citronellolis grown on various carbon sources, including 3-methyl-branched substrates. Applied and environmental microbiology, 60(9), pp.3245-3254.

- Chu, P.K., Chen, J.Y., Wang, L.P. and Huang, N., 2002. Plasma-surface modification of biomaterials. Materials Science and Engineering: R: Reports, 36(5), pp.143-206.

- Coulombe, K.L., Bajpai, V.K., Andreadis, S.T. and Murry, C.E., 2014. Heart regeneration with engineered myocardial tissue. Annual review of biomedical engineering, 16, pp.1-28.

- De Smet, M.J., Eggink, G., Witholt, B., Kingma, J. and Wynberg, H., 1983. Characterization of intracellular inclusions formed by Pseudomonas oleovorans during growth on octane. Journal of Bacteriology, 154(2), pp.870-878.

- Deligianni, D.D., Katsala, N.D., Koutsoukos, P.G. and Missirlis, Y.F., 2000. Effect of surface roughness of hydroxyapatite on human bone marrow cell adhesion, proliferation, differentiation and detachment strength. Biomaterials, 22(1), pp.87-96.

- Demir, M.M., Yilgor, I., Yilgor, E.E.A. and Erman, B., 2002. Electrospinning of polyurethane fibers. Polymer, 43(11), pp.3303-3309.

- Do Young Kim, H.W.K., Chung, M.G. and Rhee, Y.H., 2007. Biosynthesis, modification, and biodegradation of bacterial medium-chain-length polyhydroxyalkanoates. The Journal of Microbiology, pp.87-97.

- Doi, K., Nakayama, Y. and Matsuda, T. 1996. Novel compliant and tissue-permeable microporous polyurethane vascular prosthesis fabricated using an excimer laser ablation technique. Journal of Biomedical Materials Research, 31 (1), 27–33

- Dolnikov, K., Shilkrut, M., Zeevi-Levin, N., Gerecht-Nir, S., Amit, M., Danon, A., Itskovitz-Eldor, J. and Binah, O., 2006. Functional properties of human embryonic stem cell–derived cardiomyocytes: intracellular Ca2+ handling and the role of sarcoplasmic reticulum in the contraction. Stem cells, 24(2), pp.236-245.

- Dubey, P., Boccaccini, A. and Roy, I., 2014. Novel cardiac patch development using biopolymers and biocomposites. Lightweight Materials from Biopolymers and Biofibers Chapter 10, pp 159–175

- Dufresne, A. and Vincendon, M., 2000. Poly (3-hydroxybutyrate) and poly (3-hydroxyoctanoate) blends: morphology and mechanical behavior. Macromolecules, 33(8), pp.2998-3008.

- Eder, A., Vollert, I., Hansen, A. and Eschenhagen, T., 2016. Human engineered heart tissue as a model system for drug testing. Advanced drug delivery reviews, 96, pp.214-224.

- Engler, A.J., Carag-Krieger, C., Johnson, C.P., Raab, M., Tang, H.Y., Speicher, D.W., Sanger, J.W., Sanger, J.M. and Discher, D.E., 2008. Embryonic cardiomyocytes beat best on a matrix with heart-like elasticity: scar-like rigidity inhibits beating. Journal of cell science, 121(22), pp.3794-3802.

- Fiedler, J., Groll, J., Engelhardt, E., Gasteier, P., Dahmen, C., Kessler, H., Moeller, M. and Brenner, R.E., 2011. NCO-sP (EO-stat-PO) surface coatings preserve biochemical properties of RGD peptides. studies, 3, p.4.

- Fleischer, S., Shapira, A., Regev, O., Nseir, N., Zussman, E. and Dvir, T., 2014. Albumin fiber scaffolds for engineering functional cardiac tissues. Biotechnology and bioengineering, 111(6), pp.1246-1257.

- Francis, G.S., 2001. Pathophysiology of chronic heart failure. The American journal of medicine, 110(7), pp.37-46.

- Fromstein, J.D. and Woodhouse, K.A., 2002. Elastomeric biodegradable polyurethane blends for soft tissue applications. Journal of Biomaterials Science, Polymer Edition, 13(4), pp.391-406.

- Frydrych, M. and Chen, B., 2013. Large three-dimensional poly (glycerol sebacate)-based scaffolds–a freeze-drying preparation approach. Journal of Materials Chemistry B, 1(48), pp.6650-6661.

- Galie, P.A., Khalid, N., Carnahan, K.E., Westfall, M.V. and Stegemann, J.P., 2013. Substrate stiffness affects sarcomere and costamere structure and electrophysiological function of isolated adult cardiomyocytes. Cardiovascular Pathology, 22(3), pp.219-227.

- Göpferich, A., 1996. Mechanisms of polymer degradation and erosion. Biomaterials, 17(2), pp.103-114.

- Grafahrend, D., Heffels, K.H., Beer, M.V., Gasteier, P., Möller, M., Boehm, G., Dalton, P.D. and Groll, J., 2011. Degradable polyester scaffolds with controlled surface chemistry

combining minimal protein adsorption with specific bioactivation. Nature materials, 10(1), pp.67-73.

- Gross, R.A., DeMello, C., Lenz, R.W., Brandl, H. and Fuller, R.C., 1989. The biosynthesis and characterization of poly (β-hydroxyalkanoates) produced by Pseudomonas oleovorans. Macromolecules, 22(3), pp.1106-1115.

- Guillemette, M.D., Park, H., Hsiao, J.C., Jain, S.R., Larson, B.L., Langer, R. and Freed, L.E., 2010. Combined technologies for microfabricating elastomeric cardiac tissue engineering scaffolds. Macromolecular bioscience, 10(11), pp.1330-1337.

- Guimard, N.K., Gomez, N. and Schmidt, C.E., 2007. Conducting polymers in biomedical engineering. Progress in Polymer Science, 32(8), pp.876-921.

- Hai, Z., Gao, L., Zhang, Q., Xu, H., Cui, D., Zhang, Z., Tsoukalas, D., Tang, J., Yan, S. and Xue, C., 2016. Facile synthesis of core–shell structured PANI-Co_3O_4 nanocomposites with superior electrochemical performance in supercapacitors. Applied Surface Science, 361, pp.57-62.

- Halami, P.M., 2008. Production of polyhydroxyalkanoate from starch by the native isolate Bacillus cereus CFR06. World Journal of Microbiology and Biotechnology, 24(6), pp.805-812.

- Hall, J.E., 2016. Guyton and Hall textbook of medical physiology.

- Hanson J, Huxley HE (1953) Structural basis of the cross-striations in muscle. Nature 172:530–532

- Haywood, G.W., Anderson, A.J. and Dawes, E.A., 1989. A survey of the accumulation of novel polyhydroxyalkanoates by bacteria. Biotechnology letters, 11(7), pp.471-476.

- He, W., Tian, W., Zhang, G., Chen, G.Q. and Zhang, Z., 1998. Production of novel polyhydroxyalkanoates by Pseudomonas stutzeri 1317 from glucose and soybean oil. FEMS microbiology letters, 169(1), pp.45-49.

- Heeger, A.J., MacDiarmid, A.G. and Shirakawa, H., 2000. The Nobel Prize in Chemistry. The Royal Swedish Academy of Sciences.

- Hersel, U., Dahmen, C. and Kessler, H., 2003. RGD modified polymers: biomaterials for stimulated cell adhesion and beyond. Biomaterials, 24(24), pp.4385-4415.

- Hill, A.J., Zipper, M.D., Tant, M.R., Stack, G.M., Jordan, T.C. and Shultz, A.R., 1996. A free volume approach to the mechanical behaviour of miscible polycarbonate blends. Journal of Physics: Condensed Matter, 8(21), p.3811.

- Hirano, Y., Okuno, M., Hayashi, T., Goto, K. and Nakajima, A., 1993. Cell-attachment activities of surface immobilized oligopeptides RGD, RGDS, RGDV, RGDT, and YIGSR toward five cell lines. Journal of Biomaterials Science, Polymer Edition, 4(3), pp.235-243.

- Hsiao, C.W., Bai, M.Y., Chang, Y., Chung, M.F., Lee, T.Y., Wu, C.T., Maiti, B., Liao, Z.X., Li, R.K. and Sung, H.W., 2013. Electrical coupling of isolated cardiomyocyte clusters grown on aligned conductive nanofibrous meshes for their synchronized beating. Biomaterials, 34(4), pp.1063-1072.

- Humpolicek, P., Kasparkova, V., Saha, P. and Stejskal, J., 2012. Biocompatibility of polyaniline. Synthetic Metals, 162(7), pp.722-727.

- Huxley HE (1953) Electron microscope studies of the organisation of the filaments in striated muscle. Biochim Biophys Acta 12:387–394

- Hyakutake, M., Saito, Y., Tomizawa, S., Mizuno, K. and Tsuge, T., 2011. Polyhydroxyalkanoate (PHA) synthesis by class IV PHA synthases employing Ralstonia eutropha PHB− 4 as host strain. Bioscience, biotechnology, and biochemistry, 75(8), pp.1615-1617.

- Ikada, Y., 2011. Tissue engineering: fundamentals and applications (Vol. 8). Academic Press.

- Jia, W., Gungor-Ozkerim, P.S., Zhang, Y.S., Yue, K., Zhu, K., Liu, W., Pi, Q., Byambaa, B., Dokmeci, M.R., Shin, S.R. and Khademhosseini, A., 2016. Direct 3D bioprinting of perfusable vascular constructs using a blend bioink. Biomaterials, 106, pp.58-68.

- Jin, J., Jeong, S.I., Shin, Y.M., Lim, K.S., Lee, Y.M., Koh, H.C. and Kim, K.S., 2009. Transplantation of mesenchymal stem cells within a poly (lactide-co-ε-caprolactone) scaffold improves cardiac function in a rat myocardial infarction model. European journal of heart failure, 11(2), pp.147-153.

- Jun, I., Jeong, S. and Shin, H., 2009. The stimulation of myoblast differentiation by electrically conductive sub-micron fibers. Biomaterials, 30(11), pp.2038-2047.

- Kabilan, S., Ayyasamy, M., Jayavel, S. and Paramasamy, G., 2012. Pseudomonas sp. as a source of medium chain length polyhydroxyalkanoates for controlled drug delivery: perspective. International journal of microbiology, 2012.

- Kai, D., Prabhakaran, M.P., Jin, G. and Ramakrishna, S., 2011. Guided orientation of cardiomyocytes on electrospun aligned nanofibers for cardiac tissue engineering. Journal of Biomedical Materials Research Part B: Applied Biomaterials, 98(2), pp.379-386.

- Kai, D., Prabhakaran, M.P., Jin, G. and Ramakrishna, S., 2011. Polypyrrole-contained electrospun conductive nanofibrous membranes for cardiac tissue engineering. Journal of Biomedical Materials Research Part A, 99(3), pp.376-385.

- Kehat, I. and Molkentin, J.D., 2010. Molecular pathways underlying cardiac remodeling during pathophysiological stimulation. Circulation, 122(25), pp.2727-2735.

- Kenar, H., Kose, G.T. and Hasirci, V., 2010. Design of a 3D aligned myocardial tissue construct from biodegradable polyesters. Journal of Materials Science: Materials in Medicine, 21(3), pp.989-997.

- Kenar, H., Kose, G.T. and Hasirci, V., 2010. Design of a 3D aligned myocardial tissue construct from biodegradable polyesters. Journal of Materials Science: Materials in Medicine, 21(3), pp.989-997.

- Khan, M., Xu, Y., Hua, S., Johnson, J., Belevych, A., Janssen, P.M., Gyorke, S., Guan, J. and Angelos, M.G., 2015. Evaluation of changes in morphology and function of human induced pluripotent stem cell derived cardiomyocytes (HiPSC-CMs) cultured on an aligned-nanofiber cardiac patch. PloS one, 10(5), p.e0126338.

- Kharaziha, M., Shin, S.R., Nikkhah, M., Topkaya, S.N., Masoumi, N., Annabi, N., Dokmeci, M.R. and Khademhosseini, A., 2014. Tough and flexible CNT–polymeric hybrid scaffolds for engineering cardiac constructs. Biomaterials, 35(26), pp.7346-7354.

- Kierszenbaum, A.L. and Tres, L., 2015. *Histology and cell biology: an introduction to pathology*. Elsevier Health Sciences.

- Kim, J.J., Yang, L., Lin, B., Zhu, X., Sun, B., Kaplan, A.D., Bett, G.C., Rasmusson, R.L., London, B. and Salama, G., 2015. Mechanism of automaticity in cardiomyocytes derived from human induced pluripotent stem cells. Journal of molecular and cellular cardiology, 81, pp.81-93.

- Kim, T.G. and Park, T.G., 2006. Biomimicking extracellular matrix: cell adhesive RGD peptide modified electrospun poly (D, L-lactic-co-glycolic acid) nanofiber mesh. Tissue engineering, 12(2), pp.221-233.

- Knollmann, B.C. and Roden, D.M., 2008. A genetic framework for improving arrhythmia therapy. Nature, 451(7181), pp.929-936.

- Kofidis, T., Akhyari, P., Boublik, J., Theodorou, P., Martin, U., Ruhparwar, A., Fischer, S., Eschenhagen, T., Kubis, H.P., Kraft, T. and Leyh, R., 2002. In vitro engineering of heart muscle: artificial myocardial tissue. The Journal of thoracic and cardiovascular surgery, 124(1), pp.63-69.

- Kolesky, D.B., Truby, R.L., Gladman, A., Busbee, T.A., Homan, K.A. and Lewis, J.A., 2014. 3D bioprinting of vascularized, heterogeneous cell-laden tissue constructs. Advanced materials, 26(19), pp.3124-3130.

- Krupnick, A.S., Kreisel, D., Engels, F.H., Szeto, W.Y., Plappert, T., Popma, S.H., Flake, A.W. and Rosengard, B.R., 2002. A novel small animal model of left ventricular tissue engineering. The Journal of heart and lung transplantation, 21(2), pp.233-243.

- Laizzo P (2009). Handbook of Cardiac Anatomy, Physiology, and Devices. Springer.

- Langer R, Vacanti J .1993. Tissue engineering. Science. 260: 920-926.

- Lebourg, M., Serra, R.S., Estellés, J.M., Sánchez, F.H., Ribelles, J.G. and Antón, J.S., 2008. Biodegradable polycaprolactone scaffold with controlled porosity obtained by modified particle-leaching technique. Journal of Materials Science: Materials in Medicine, 19(5), pp.2047-2053.

- Leceta, I., Peñalba, M., Arana, P., Guerrero, P. and De La Caba, K., 2015. Ageing of chitosan films: Effect of storage time on structure and optical, barrier and mechanical properties. European Polymer Journal, 66, pp.170-179.

- Lee, H.C., Smith, N., Mohabir, R. and Clusin, W.T., 1987. Cytosolic calcium transients from the beating mammalian heart. Proceedings of the National Academy of Sciences, 84(21), pp.7793-7797.

- Lee, K.H., Kim, H.Y., Ryu, Y.J., Kim, K.W. and Choi, S.W., 2003. Mechanical behavior of electrospun fiber mats of poly (vinyl chloride)/polyurethane polyblends. Journal of Polymer Science Part B: Polymer Physics, 41(11), pp.1256-1262.

- Lee, V.K., Kim, D.Y., Ngo, H., Lee, Y., Seo, L., Yoo, S.S., Vincent, P.A. and Dai, G., 2014. Creating perfused functional vascular channels using 3D bio-printing technology. Biomaterials, 35(28), pp.8092-8102.

- Leor, J. and Cohen, S., 2004. Myocardial tissue engineering: creating a muscle patch for a wounded heart. Annals of the New York Academy of Sciences, 1015(1), pp.312-319.

- Leor, J., Aboulafia-Etzion, S., Dar, A., Shapiro, L., Barbash, I.M., Battler, A., Granot, Y. and Cohen, S., 2000. Bioengineered cardiac grafts a new approach to repair the infarcted myocardium?. Circulation, 102(suppl 3), pp.Iii-56.

- Leor, J., Amsalem, Y. and Cohen, S., 2005. Cells, scaffolds, and molecules for myocardial tissue engineering. Pharmacology & therapeutics, 105(2), pp.151-163.

- Li, Z., Lin, H., Ishii, N., Chen, G.Q. and Inoue, Y., 2007. Study of enzymatic degradation of microbial copolyesters consisting of 3-hydroxybutyrate and medium-chain-length 3-hydroxyalkanoates. Polymer Degradation and Stability, 92(9), pp.1708-1714.

- Limongi, T., Tirinato, L., Pagliari, F., Giugni, A., Allione, M., Perozziello, G., Candeloro, P. and Di Fabrizio, E., 2017. Fabrication and Applications of Micro/Nanostructured Devices for Tissue Engineering. Nano-Micro Letters, 9(1), p.1.

- Liu, J., Jean, Y.C. and Yang, H., 1995. Free-volume hole properties of polymer blends probed by positron annihilation spectroscopy: miscibility. *Macromolecules*, *28*(17), pp.5774-5779.

- Liu, Y., Lu, J., Xu, G., Wei, J., Zhang, Z. and Li, X., 2016. Tuning the conductivity and inner structure of electrospun fibers to promote cardiomyocyte elongation and synchronous beating. Materials Science and Engineering: C, 69, pp.865-874.

- Luklinska, Z.B. and Schluckwerder, H., 2003. In vivo response to HA-polyhydroxybutyrate/polyhydroxyvalerate composite. Journal of microscopy, 211(2), pp.121-129.

- Lundy, S.D., Zhu, W.Z., Regnier, M. and Laflamme, M.A., 2013. Structural and functional maturation of cardiomyocytes derived from human pluripotent stem cells. Stem cells and development, 22(14), pp.1991-2002.

- Martin, D.P., Rizk, S., Ahuja, A. and Williams, S.F., Tepha, Inc., 2014. Polyhydroxyalkanoate Medical Textiles and Fibers. U.S. Patent Application 14/276,708.

- Martin, D.P., Rizk, S., Ho, K. and Williams, S.F., Tepha, Inc., 2012. Medical devices containing melt-blown non-wovens of poly-4-hydroxybutyrate and copolymers thereof. U.S. Patent 8,287,909.

- Matsuda, T., 1997. Significance of porosity and compliance of microporous, polyurethane-based microarterial vessel on neoarterial wall regeneration. Journal of biomedical materials research, 37(4), pp.573-584.

- McDevitt, T.C., Woodhouse, K.A., Hauschka, S.D., Murry, C.E. and Stayton, P.S., 2003. Spatially organized layers of cardiomyocytes on biodegradable polyurethane films for myocardial repair. Journal of Biomedical Materials Research Part A, 66(3), pp.586-595.

- Mendes, L.C., Falco, A.P.S., Pinho, M.S. and Marques, P.O., 2011. Sulfonated polyaniline: influence of sulfonation routes on its thermal and structural characteristics. Materials Research, 14(4), pp.466-471.

- Meng, S., Rouabhia, M. and Zhang, Z., 2011. Electrical stimulation in tissue regeneration. INTECH Open Access Publisher.

- Misra, S.K., Mohn, D., Brunner, T.J., Stark, W.J., Philip, S.E., Roy, I., Salih, V., Knowles, J.C. and Boccaccini, A.R., 2008. Comparison of nanoscale and microscale bioactive glass on the properties of P (3HB)/Bioglass® composites. Biomaterials, 29(12), pp.1750-1761.

- Mogosanu, D.E., Verplancke, R., Dubruel, P. and Vanfleteren, J., 2016. Fabrication of 3-dimensional biodegradable microfluidic environments for tissue engineering applications. Materials & Design, 89, pp.1315-1324.

- Molkentin, J.D., Lu, J.R., Antos, C.L., Markham, B., Richardson, J., Robbins, J., Grant, S.R. and Olson, E.N., 1998. A calcineurin-dependent transcriptional pathway for cardiac hypertrophy. Cell, 93(2), pp.215-228.

- Mordwinkin, N.M., Burridge, P.W. and Wu, J.C., 2013. A review of human pluripotent stem cell-derived cardiomyocytes for high-throughput drug discovery, cardiotoxicity screening, and publication standards. Journal of cardiovascular translational research, 6(1), pp.22-30.

- Narkis, M., Haba, Y., Segal, E., Zilberman, M., Titelman, G.I. and Siegmann, A., 2000. Structured electrically conductive polyaniline/polymer blends. Polymers for Advanced Technologies, 11(8-12), pp.665-673.

- Nelson, T.J., Martinez-Fernandez, A., Yamada, S., Perez-Terzic, C., Ikeda, Y. and Terzic, A., 2009. Repair of acute myocardial infarction by human stemness factors induced pluripotent stem cells. Circulation, 120(5), pp.408-416.

- Nomura, C.T. and Taguchi, S., 2007. PHA synthase engineering toward superbiocatalysts for custom-made biopolymers. Applied microbiology and biotechnology, 73(5), pp.969-979.

- O'Brien, F.J., Harley, B.A., Waller, M.A., Yannas, I.V., Gibson, L.J. and Prendergast, P.J., 2007. The effect of pore size on permeability and cell attachment in collagen scaffolds for tissue engineering. Technology and Health Care, 15(1), pp.3-17.

- Olivey, H.E. and Svensson, E.C., 2010. Epicardial–myocardial signaling directing coronary vasculogenesis. Circulation Research, 106(5), pp.818-832.

- Orlova, Y., Magome, N., Liu, L., Chen, Y. and Agladze, K., 2011. Electrospun nanofibers as a tool for architecture control in engineered cardiac tissue. Biomaterials, 32(24), pp.5615-5624.

- Ota, T., Sawa, Y., Iwai, S., Kitajima, T., Ueda, Y., Coppin, C., Matsuda, H. and Okita, Y., 2005. Fibronectin-hepatocyte growth factor enhances reendothelialization in tissue-engineered heart valve. The Annals of thoracic surgery, 80(5), pp.1794-1801.

- Ozawa, T., Mickle, D.A., Weisel, R.D., Koyama, N., Ozawa, S. and Li, R.K., 2002. Optimal biomaterial for creation of autologous cardiac grafts. Circulation, 106(12 suppl 1), pp.I-176.

- Park, H., Radisic, M., Lim, J.O., Chang, B.H. and Vunjak-Novakovic, G., 2005. A novel composite scaffold for cardiac tissue engineering. In Vitro Cellular & Developmental Biology-Animal, 41(7), pp.188-196.

- Patil, D.S., Shaikh, J.S., Dalavi, D.S., Kalagi, S.S. and Patil, P.S., 2011. Chemical synthesis of highly stable PVA/PANI films for supercapacitor application. Materials Chemistry and Physics, 128(3), pp.449-455.

- Patra, C., Boccaccini, A.R. and Engel, F.B., 2015. Vascularisation for cardiac tissue engineering: the extracellular matrix. Thrombosis and haemostasis, 113(3), pp.532-547.

- Peschel, G., Dahse, H.M., Konrad, A., Wieland, G.D., Mueller, P.J., Martin, D.P. and Roth, M., 2008. Growth of keratinocytes on porous films of poly (3-hydroxybutyrate) and poly (4-hydroxybutyrate) blended with hyaluronic acid and chitosan. Journal of Biomedical Materials Research Part A, 85(4), pp.1072-1081.

- Pham, Q.P., Sharma, U. and Mikos, A.G., 2006. Electrospinning of polymeric nanofibers for tissue engineering applications: a review. Tissue engineering, 12(5), pp.1197-1211.

- Philip, S., Keshavarz, T. and Roy, I., 2007. Polyhydroxyalkanoates: biodegradable polymers with a range of applications. Journal of Chemical Technology and Biotechnology, 82(3), pp.233-247.

- Pinto AR, Ilinykh A, Ivey MJ, Kuwabara JT, D'Antoni ML, Debuque R (2016) Revisiting cardiac cellular composition. Circ Res 118:400–409

- Pok, S., Myers, J.D., Madihally, S.V. and Jacot, J.G., 2013. A multilayered scaffold of a chitosan and gelatin hydrogel supported by a PCL core for cardiac tissue engineering. Acta biomaterialia, 9(3), pp.5630-5642.

- Pons, J., Huang, Y., Takagawa, J., Arakawa-Hoyt, J., Ye, J., Grossman, W., Kan, Y.W. and Su, H., 2009. Combining angiogenic gene and stem cell therapies for myocardial infarction. *The journal of gene medicine*, *11*(9), pp.743-753.

- Povolo, S., Toffano, P., Basaglia, M. and Casella, S., 2010. Polyhydroxyalkanoates production by engineered Cupriavidus necator from waste material containing lactose. Bioresource technology, 101(20), pp.7902-7907.

- Preusting, H., Nijenhuis, A. and Witholt, B., 1990. Physical characteristics of poly (3-hydroxyalkanoates) and poly (3-hydroxyalkenoates) produced by Pseudomonas oleovorans grown on aliphatic hydrocarbons. Macromolecules, 23(19), pp.4220-4224.

- Qazi, T.H., Rai, R. and Boccaccini, A.R., 2014. Tissue engineering of electrically responsive tissues using polyaniline based polymers: a review. Biomaterials, 35(33), pp.9068-9086.

- Qazi, T.H., Rai, R., Dippold, D., Roether, J.E., Schubert, D.W., Rosellini, E., Barbani, N. and Boccaccini, A.R., 2014. Development and characterization of novel electrically conductive PANI–PGS composites for cardiac tissue engineering applications. Acta biomaterialia, 10(6), pp.2434-2445.

- Qu, X.H., Wu, Q., Liang, J., Zou, B. and Chen, G.Q., 2006. Effect of 3-hydroxyhexanoate content in poly (3-hydroxybutyrate-co-3-hydroxyhexanoate) on in vitro growth and differentiation of smooth muscle cells. Biomaterials, 27(15), pp.2944-2950.

- Quinteros, R., Goodwin, S., Lenz, R.W. and Park, W.H., 1999. Extracellular degradation of medium chain length poly (β-hydroxyalkanoates) by Comamonas sp. International journal of biological macromolecules, 25(1), pp.135-143.

- Rahimi, M., Mohseni-Kouchesfehani, H., Zarnani, A.H., Mobini, S., Nikoo, S. and Kazemnejad, S., 2014. Evaluation of menstrual blood stem cells seeded in biocompatible Bombyx mori silk fibroin scaffold for cardiac tissue engineering. Journal of biomaterials applications, 29(2), pp.199-208.

- Rai, R., 2010. Biosynthesis of polyhydroxyalkanoates and its medical applications (Doctoral dissertation, University of Westminster).

- Rai, R., Boccaccini, A.R., Knowles, J.C., Mordon, N., Salih, V., Locke, I.C., Moshrefi-Torbati, M., Keshavarz, T. and Roy, I., 2011. The homopolymer poly (3-hydroxyoctanoate) as a matrix material for soft tissue engineering. Journal of Applied Polymer Science, 122(6), pp.3606-3617.

- Rai, R., Keshavarz, T., Roether, J.A., Boccaccini, A.R. and Roy, I., 2011. Medium chain length polyhydroxyalkanoates, promising new biomedical materials for the future. Materials Science and Engineering: R: Reports, 72(3), pp.29-47.

- Randriamahefa, S., Renard, E., Guérin, P. and Langlois, V., 2003. Fourier transform infrared spectroscopy for screening and quantifying production of PHAs by Pseudomonas grown on sodium octanoate. Biomacromolecules, 4(4), pp.1092-1097.

- Ravichandran, R., Sundarrajan, S., Venugopal, J.R., Mukherjee, S. and Ramakrishna, S., 2010. Applications of conducting polymers and their issues in biomedical engineering. Journal of the Royal Society Interface, 7(Suppl 5), pp.S559-S579.

- Ravichandran, R., Venugopal, J.R., Sundarrajan, S., Mukherjee, S., Sridhar, R. and Ramakrishna, S., 2013. Expression of cardiac proteins in neonatal cardiomyocytes on PGS/fibrinogen core/shell substrate for Cardiac tissue engineering. International journal of cardiology, 167(4), pp.1461-1468.

- Rehm B . 2003. Polyester synthases: natural catalysts for plastics. Biochem. J. 376: 15–33.

- Renard, E., Walls, M., Guérin, P. and Langlois, V., 2004. Hydrolytic degradation of blends of polyhydroxyalkanoates and functionalized polyhydroxyalkanoates. Polymer degradation and Stability, 85(2), pp.779-787.

- Richardson, T.P., Peters, M.C., Ennett, A.B. and Mooney, D.J., 2001. Polymeric system for dual growth factor delivery. Nature biotechnology, 19(11), pp.1029-1034.

- Richert, L., Vetrone, F., Yi, J.H., Zalzal, S.F., Wuest, J.D., Rosei, F. and Nanci, A., 2008. Surface nanopatterning to control cell growth. Advanced Materials, 20(8), pp.1488-1492.

- Roberts-Thomson, K.C., Kistler, P.M., Sanders, P., Morton, J.B., Haqqani, H.M., Stevenson, I., Vohra, J.K., Sparks, P.B. and Kalman, J.M., 2009. Fractionated atrial electrograms during sinus rhythm: relationship to age, voltage, and conduction velocity. Heart Rhythm, 6(5), pp.587-591.

- Robinson, K.A., Li, J., Mathison, M., Redkar, A., Cui, J., Chronos, N.A., Matheny, R.G. and Badylak, S.F., 2005. Extracellular matrix scaffold for cardiac repair. Circulation, 112(9 suppl), pp.I-135.

- Rockwood, D.N., Akins, R.E., Parrag, I.C., Woodhouse, K.A. and Rabolt, J.F., 2008. Culture on electrospun polyurethane scaffolds decreases atrial natriuretic peptide expression by cardiomyocytes in vitro. Biomaterials, 29(36), pp.4783-4791.

- Rnjak-Kovacina, J. and Weiss, A.S., 2011. Increasing the pore size of electrospun scaffolds. Tissue Engineering Part B: Reviews, 17(5), pp.365-372.

- Saad, B., Matter, S., Ciardelli, G., Neuenschwander, P., Suter, U.W., Uhlschmid, G.K. and Welti, M., 1996. Interactions of osteoblasts and macrophages with biodegradable and highly porous polyesterurethane foam and its degradation products. Journal of biomedical materials research, 32(3), pp.355-366.

- Saito, T., Tomita, K., Juni, K. and Ooba, K., 1991. In vivo and in vitro degradation of poly (3-hydroxybutyrate) in pat. *Biomaterials*, *12*(3), pp.309-312.

- Salick, M.R., Napiwocki, B.N., Sha, J., Knight, G.T., Chindhy, S.A., Kamp, T.J., Ashton, R.S. and Crone, W.C., 2014. Micropattern width dependent sarcomere development in human ESC-derived cardiomyocytes. Biomaterials, 35(15), pp.4454-4464.

- Sánchez, R.J., Schripsema, J., da Silva, L.F., Taciro, M.K., Pradella, J.G. and Gomez, J.G.C., 2003. Medium-chain-length polyhydroxyalkanoic acids (PHA mcl) produced by Pseudomonas putida IPT 046 from renewable sources. European Polymer Journal, 39(7), pp.1385-1394.

- Sevastianov, V.I., Perova, N.V., Shishatskaya, E.I., Kalacheva, G.S. and Volova, T.G., 2003. Production of purified polyhydroxyalkanoates (PHAs) for applications in contact with blood. Journal of Biomaterials Science, Polymer Edition, 14(10), pp.1029-1042.

- Shachar, M., Tsur-Gang, O., Dvir, T., Leor, J. and Cohen, S., 2011. The effect of immobilized RGD peptide in alginate scaffolds on cardiac tissue engineering. Acta biomaterialia, 7(1), pp.152-162.

- Shadrin, I.Y., Khodabukus, A. and Bursac, N., 2016. Striated muscle function, regeneration, and repair. Cellular and Molecular Life Sciences, 1-28.

- Shijun, X., Junsheng, M., Jianqun, Z. and Ping, B., 2016. *In vitro* three-dimensional coculturing poly3-hydroxybutyrate-co-3-hydroxyhexanoate with mouse-induced pluripotent stem cells for myocardial patch application. Journal of biomaterials applications, 30(8), pp.1273-1282..

- Shishatskaya, E.I., Volova, T.G. and Gitelson, I.I., 2002, March. *In vivo* toxicological evaluation of polyhydroxyalkanoates. In Doklady Biological Sciences Vol. 383, No. 1, pp. 109-111.

- Shishatskaya, E.I., Volova, T.G., Puzyr, A.P., Mogilnaya, O.A. and Efremov, S.N., 2004. Tissue response to the implantation of biodegradable polyhydroxyalkanoate sutures. Journal of Materials Science: Materials in Medicine, 15(6), pp.719-728.

- Shum-Tim, D., Stock, U., Hrkach, J., Shinoka, T., Lien, J., Moses, M.A., Stamp, A., Taylor, G., Moran, A.M., Landis, W. and Langer, R., 1999. Tissue engineering of autologous aorta using a new biodegradable polymer. The Annals of thoracic surgery, 68(6), pp.2298-2304.

- Siemann, U., 2005. Solvent cast technology–a versatile tool for thin film production. In Scattering Methods and the Properties of Polymer Materials (pp. 1-14). Springer Berlin Heidelberg.

- Silva, A.C., Rodrigues, S.C., Caldeira, J., Nunes, A.M., Sampaio-Pinto, V., Resende, T.P., Oliveira, M.J., Barbosa, M.A., Thorsteinsdóttir, S. and Nascimento, D.S., 2016. Three-

dimensional scaffolds of fetal decellularized hearts exhibit enhanced potential to support cardiac cells in comparison to the adult. *Biomaterials*, *104*, pp.52-64.

- Sin, M.C., Tan, I.K.P., Annuar, M.S.M. and Gan, S.N., 2012. Thermal behaviour and thermodegradation kinetics of poly (vinyl chloride) plasticized with polymeric and oligomeric medium-chain-length poly (3-hydroxyalkanoates). *Polymer degradation and stability*, *97*(11), pp.2118-2127.

- Smith, I.O., Liu, X.H., Smith, L.A. and Ma, P.X., 2009. Nanostructured polymer scaffolds for tissue engineering and regenerative medicine. Wiley Interdisciplinary Reviews: Nanomedicine and Nanobiotechnology, 1(2), pp.226-236.

- Sodian, R., Hoerstrup, S.P., Sperling, J.S., Daebritz, S., Martin, D.P., Moran, A.M., Kim, B.S., Schoen, F.J., Vacanti, J.P. and Mayer, J.E., 2000. Early in vivo experience with tissue-engineered trileaflet heart valves. Circulation, 102(suppl 3), pp.Iii-22.

- Sodian, R., Loebe, M., Hein, A., Martin, D.P., Hoerstrup, S.P., Potapov, E.V., Hausmann, H., Lueth, T. and Hetzer, R., 2002. Application of stereolithography for scaffold fabrication for tissue engineered heart valves. Asaio Journal, 48(1), pp.12-16.

- Soonpaa, M.H., Kim, K.K., Pajak, L., Franklin, M. and Field, L.J., 1996. Cardiomyocyte DNA synthesis and binucleation during murine development. The American journal of physiology, 271(5 Pt 2), pp.H2183-9.

- Stankus, J.J., Guan, J. and Wagner, W.R., 2004. Fabrication of biodegradable elastomeric scaffolds with sub-micron morphologies. Journal of Biomedical Materials Research Part A, 70(4), pp.603-614.

- Stejskal, J. and Gilbert, R.G., 2002. Polyaniline. Preparation of a conducting polymer (IUPAC technical report). Pure and Applied Chemistry, 74(5), pp.857-867.

- Stock, U.A., Wiederschain, D., Kilroy, S.M., Shum-Tim, D., Khalil, P.N., Vacanti, J.P., Mayer, J.E. and Moses, M.A., 2001. Dynamics of extracellular matrix production and turnover in tissue engineered cardiovascular structures. Journal of cellular biochemistry, 81(2), pp.220-228.

- Sun, J., Dai, Z., Zhao, Y. and Chen, G.Q., 2007. In vitro effect of oligo-hydroxyalkanoates on the growth of mouse fibroblast cell line L929. Biomaterials, 28(27), pp.3896-3903.

- Sutton M and Sharpe N (2000). Left Ventricular Remodeling After Myocardial Infarction: Pathophysiology and Therapy. Circulation. 101: 2981-2988.

- Taylor, G., 1969, December. Electrically driven jets. In Proceedings of the Royal Society of London A: Mathematical, Physical and Engineering Sciences (Vol. 313, No. 1515, pp. 453-475). The Royal Society.

- Thull, R., 2001. Surface functionalization of materials to initiate auto-biocompatibilization in vivo. Materialwissenschaft und werkstofftechnik, 32(12), pp.949-952.

- Tian, W., Hong, K., Chen, G.Q., Wu, Q., Zhang, R.Q. and Huang, W., 2000. Production of polyesters consisting of medium chain length 3-hydroxyalkanoic acids by Pseudomonas mendocina 0806 from various carbon sources. Antonie van Leeuwenhoek, 77(1), pp.31-36.

- Tokiwa, Y. and Calabia, B.P., 2004. Review degradation of microbial polyesters. Biotechnology letters, 26(15), pp.1181-1189.

- Vacanti, C.A., 2006. History of tissue engineering and a glimpse into its future. Tissue engineering, 12(5), pp.1137-1142.

- Valappil, S.P., Boccaccini, A.R., Bucke, C. and Roy, I., 2007. Polyhydroxyalkanoates in Gram-positive bacteria: insights from the genera Bacillus and Streptomyces. Antonie Van Leeuwenhoek, 91(1), pp.1-17.

- Valappil, S.P., Misra, S.K., Boccaccini, A.R. and Roy, I., 2006. Biomedical applications of polyhydroxyalkanoates, an overview of animal testing and in vivo responses. Expert Review of Medical Devices, 3(6), pp.853-868.

- Van der Walle, G.A.M., De Koning, G.J.M., Weusthuis, R.A. and Eggink, G., 2001. Properties, modifications and applications of biopolyesters. In Biopolyesters (pp. 263-291). Springer Berlin Heidelberg.

- Volova, T.G., 2004. Polyhydroxyalkanoates--plastic materials of the 21st century: production, properties, applications. Nova publishers.

- Wang, F. and Guan, J., 2010. Cellular cardiomyoplasty and cardiac tissue engineering for myocardial therapy. Advanced drug delivery reviews, 62(7), pp.784-797.

- Wang, X., Berggren, M. and Inganäs, O., 2008. Dynamic control of surface energy and topography of microstructured conducting polymer films. Langmuir, 24(11), pp.5942-5948.

- Wang, Y., Ameer, G.A., Sheppard, B.J. and Langer, R., 2002. A tough biodegradable elastomer. Nature biotechnology, 20(6), pp.602-606.

- Wang, Y.W., Mo, W., Yao, H., Wu, Q., Chen, J. and Chen, G.Q., 2004. Biodegradation studies of poly (3-hydroxybutyrate-co-3-hydroxyhexanoate). Polymer degradation and stability, 85(2), pp.815-821.

- Wang, Y.W., Wu, Q. and Chen, G.Q., 2005. Gelatin blending improves the performance of poly (3-hydroxybutyrate-co-3-hydroxyhexanoate) films for biomedical application. Biomacromolecules, 6(2), pp.566-571.

- Wang, Y.W., Wu, Q., Chen, J. and Chen, G.Q., 2005. Evaluation of three-dimensional scaffolds made of blends of hydroxyapatite and poly (3-hydroxybutyrate-co-3-hydroxyhexanoate) for bone reconstruction. Biomaterials, 26(8), pp.899-904.

- Watanabe, S., Shite, J., Takaoka, H., Shinke, T., Imuro, Y., Ozawa, T., Otake, H., Matsumoto, D., Ogasawara, D., Paredes, O.L. and Yokoyama, M., 2006. Myocardial stiffness is an important determinant of the plasma brain natriuretic peptide concentration in patients with both diastolic and systolic heart failure. European heart journal, 27(7), pp.832-838.

- Weber, K.T. and Brilla, C.G., 1991. Pathological hypertrophy and cardiac interstitium. Fibrosis and renin-angiotensin-aldosterone system. Circulation, 83(6), pp.1849-1865.

- Wise, D.L., 1998. Electrical and Optical Polymer Systems: Fundamentals: Methods, and Applications. CRC Press.

- Witholt, B. and Kessler, B., 1999. Perspectives of medium chain length poly (hydroxyalkanoates), a versatile set of bacterial bioplastics. Current opinion in biotechnology, 10(3), pp.279-285.

- Wu, Q., Wang, Y. and Chen, G.Q., 2009. Medical application of microbial biopolyesters polyhydroxyalkanoates. Artificial Cells, Blood Substitutes, and Biotechnology, 37(1), pp.1-12.

- Wu, S., Liu, Y.L., Cui, B., Qu, X.H. and Chen, G.Q., 2007. Study on Decellularized Porcine Aortic Valve/Poly (3-hydroxybutyrate-co-3-hydroxyhexanoate) Hybrid Heart Valve in Sheep Model. Artificial Organs, 31(9), pp.689-697.

- Xing, Y., Lv, A., Wang, L., Yan, X., Zhao, W. and Cao, F., 2012. Engineered myocardial tissues constructed in vivo using cardiomyocyte-like cells derived from bone marrow mesenchymal stem cells in rats. Journal of biomedical science, 19(1), p.1.

- Yang, M.C., Chi, N.H., Chou, N.K., Huang, Y.Y., Chung, T.W., Chang, Y.L., Liu, H.C., Shieh, M.J. and Wang, S.S., 2010. The influence of rat mesenchymal stem cell CD44 surface markers on cell growth, fibronectin expression, and cardiomyogenic differentiation on silk fibroin–hyaluronic acid cardiac patches. Biomaterials, 31(5), pp.854-862.

- Yin, Y., Ye, F., Cui, J., Zhang, F., Li, X. and Yao, K., 2003. Preparation and characterization of macroporous chitosan–gelatin/β-tricalcium phosphate composite scaffolds for bone tissue engineering. Journal of Biomedical Materials Research Part A, 67(3), pp.844-855.

- Yoon, J.J., Song, S.H., Lee, D.S. and Park, T.G., 2004. Immobilization of cell adhesive RGD peptide onto the surface of highly porous biodegradable polymer scaffolds fabricated by a gas foaming/salt leaching method. Biomaterials, 25(25), pp.5613-5620.

- Young, J.B. and Mills, R.M., 2004. Clinical management of heart failure. Professional Communications.

- Zhang, T., Maier, L.S., Dalton, N.D., Miyamoto, S., Ross, J., Bers, D.M. and Brown, J.H., 2003. The δC isoform of CaMKII is activated in cardiac hypertrophy and induces dilated cardiomyopathy and heart failure. Circulation research, 92(8), pp.912-919.

- Zhang, Y.S., Arneri, A., Bersini, S., Shin, S.R., Zhu, K., Goli-Malekabadi, Z., Aleman, J., Colosi, C., Busignani, F., Dell'Erba, V. and Bishop, C., 2016. Bioprinting 3D microfibrous scaffolds for engineering endothelialized myocardium and heart-on-a-chip. *Biomaterials*, *110*, pp.45-59.

- Zhao, K., Deng, Y., Chen, J.C. and Chen, G.Q., 2003. Polyhydroxyalkanoate (PHA) scaffolds with good mechanical properties and biocompatibility. Biomaterials, 24(6), pp.1041-1045.

- Zhao, K., Deng, Y., Chen, J.C. and Chen, G.Q., 2003. Polyhydroxyalkanoate (PHA) scaffolds with good mechanical properties and biocompatibility. *Biomaterials*, *24*(6), pp.1041-1045.

- Zheng, Z., Bei, F.F., Tian, H.L. and Chen, G.Q., 2005. Effects of crystallization of polyhydroxyalkanoate blend on surface physicochemical properties and interactions with rabbit articular cartilage chondrocytes. Biomaterials, 26(17), pp.3537-3548.

- Zimmermann, W.H. and Eschenhagen, T., 2003. Cardiac tissue engineering for replacement therapy. Heart failure reviews, 8(3), pp.259-269.

- Zwi, L., Caspi, O., Arbel, G., Huber, I., Gepstein, A., Park, I.H. and Gepstein, L., 2009. Cardiomyocyte differentiation of human induced pluripotent stem cells. Circulation, 120(15), pp.1513-1523.

APPENDIX

Publications

Dubey, P., Boccaccini, A. and Roy, I., 2014. Novel cardiac patch development using biopolymers and biocomposites. Lightweight Materials from Biopolymers and Biofibers Chapter 10, pp 159–175

Bagdadi, A.V., Safari, M., Dubey, P., Basnett, P., Sofokleous, P., Humphrey, E., Locke, I., Edirisinghe, M., Terracciano, C., Boccaccini, A.R., Knowles, J.C., 2016, Harding S and Roy I. Poly (3-hydroxyoctanoate), a promising new material for cardiac tissue engineering. Journal of Tissue Engineering and Regenerative Medicine.

Mouriño, V., Cattalini, J.P., Roether, J.A., Dubey, P., Roy, I. and Boccaccini, A.R., 2013. Composite polymer-bioceramic scaffolds with drug delivery capability for bone tissue engineering. Expert opinion on drug delivery, 10(10), pp.1353-1365.

Conference publications

Dubey P, Bagdadi A, Harding S, Knowles J, Boccaccini AR, Edirisinghe M and Roy I. 2013, "Production of medium chain length Polyhydroxyalkanoates (mcl-PHAs) for the development of Cardiac Patches" In proceedings of UK Society of Biomaterials (UKSB), Birmingham, UK

Dubey P, Ravi S, Bagdadi A, Harding S, Knowles J, Boccaccini AR and Roy I, 2014. "Poly(3-hydroxyoctanoate), a Novel Natural Material for Cardiac Tissue Engineering" In proceedings of Joint BHF Regenerative Medicine centres meeting, London, UK.

Dubey P, Ravi S, Bagdadi A, Knowles J, Boccaccini AR, Stevens M, Harding Sand Roy I. 2014."Novel cardiac patch development for cardiac tissue engineering using Poly(3-hydroxyoctanoate)" In proceedings of International Symposium of Bio Polymers, Santos, Brazil.

Dubey P, Humphrey E, Harding S, Terracciano C, Stevens M and Roy I, 2015. "Development of Cardiac Patches Using Medium Chain Length Polyhydroxyalkanoates" In proceedings of BSCR joint annual conference, Glasgow, UK.

Dubey P, Humphrey E, Harding S, Terracciano C and Roy I. 2015. "Development of cardiac patches using medium chain length polyhydroxyalkanoates" In proceedings of UK Society of Biomaterials (UKSB), Belfast, North Ireland.